GEODYNAMIC EVOLUTION OF THE SOUTHERN CHEWORE INLIERS, ZIMBABWE : EVIDENCE FOR 1.4 GA MARGINAL BASIN CRUST

Simon Paul Johnson

A Thesis Submitted for the Degree of PhD
at the
University of St Andrews

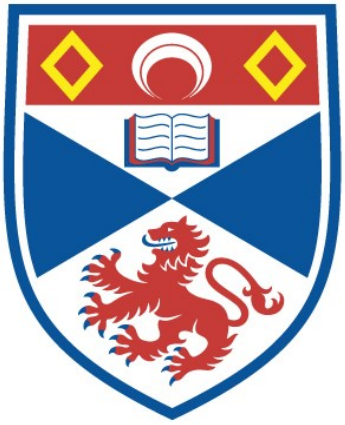

1999

GEODYNAMIC EVOLUTION OF THE SOUTHERN CHEWORE INLIERS, ZIMBABWE : EVIDENCE FOR 1.4 Ga MARGINAL BASIN CRUST.

Simon Paul Johnson

Submitted in the partial fulfilment
of the degree of Doctor of Philosophy.
December 1998.

Crustal Geodynamics Group
School of Geography and Geosciences
University of St Andrews
Scotland.

Project Supervisor : Dr. G. J. H. Oliver.

ProQuest LLC.
789 East Eisenhower Parkway
P.O. Box 1346
Ann Arbor, MI 48106 – 1346

I Simon Paul Johnson hereby certify that this thesis has been composed by myself, that it is a record of my own work and that it has not been accepted in partial or complete fulfilment of any other degree or professional qualification.

Signed.....Date.....4/12/98.....

I was admitted to the Faculty of Science of the University of St Andrews under the Ordinance General No. 12 on *1st December 1995* and as a candidate for the Degree of Ph.D. in *December 1996.*

Signed.....Date.....

I hereby certify that the candidate has fulfilled the conditions of the Resolution and Regulations appropriate to the degree of Ph.D.

Signed.....Date.....4/12/98.....

Copyright

Unrestricted

In submitting this thesis to the University of St Andrews I understand that I am giving permission for it to be made avaliable for use in accordance with the regulations of the University Library for the time being in force, subject to any copyright vested in the work not being affected thereby. I also understand that the title and abstract will be published, and that a copy of the work may be made and supplied to any bona fide library or research worker.

Abstract

This thesis reports the detailed study of 150 km^2 of a newly discovered ophiolite terrane in the Chewore Inliers of northern Zimbabwe. It is apparently the oldest dated ophiolite (*senso stricto*) in Africa.

Field and laboratory investigation of the the Ophiolite Terrane (OT) shows that it comprises three distinct lithological groups. The Maunde Ophiolite Group is comprised of back - arc ophiolite - type assemblages, namely :- meta - mafic volcanics, sheeted meta - mafic dykes, meta - gabbro, meta - mafic cumulates and serpentinites. The Kaourera Island - Arc Group is comprised of a silica and potassium variable suite of extrusive volcanic lithologies which represent a tectonically excised island - arc complex. The Kadunguri Whiteschists are comprised of chemically restricted whiteschists which are characterised by the equilibrium assemblage of talc and kyanite and unusual yoderite + kyanite + chlorite + talc + dravite + hematite assemblages.

The Ophiolite Terrane has had a single period of crustal thickening with a NNE - SSW shortening direction. This event is characterised by high shear strains with the development of non - coaxial intrafolial shear folds, an axial planar cleavage and an extension lineation which is parallel to the intrafolial fold hinges. Tectonic transport was directed obliquely toward the NNE. Associated clockwise metamorphism peaked within the upper amphibolite facies at 700°C and 10 kbar. The high pressure, moderate temperature Kadunguri Group whiteschists record peak metamorphic *PT's* of between 13 and 21 kbar and 550 - 650°C with the production of the second natural occurrence of the mineral yoderite.

A plagiogranite sheet within the ophiolite has been SHRIMP dated at 1393 ± 22 Ma (Oliver *et al.*, 1998) and is interpreted to be the age of the ophiolite.

Investigation of the terranes to the north of the OT by Goscombe *et al.*, (1998) reveal a previous, high *T*, low *P*, anti - clockwise, local granulite facies tectono - metamorphic cycle (M_1) which is not recognised within the OT. All terranes are variably overprinted by the main clockwise *PTt* path, amphibolite facies, crustal thickening event (M_2). The M_1 cycle has been U / Pb SHRIMP dated from zircons within the Granulite Terrane at 943 ± 34 Ma (Goscombe *et al.*, 1998) and interpreted to represent crustal extension associated with continental break up of Rodinia. Zircon overgrowths within the Granulite Terrane date the M_2 cycle at 524 ± 16 Ma. The lack of M_1 metamorphism and associated fabrics within the OT and the similarity in early M_2 structures between all terranes indicate that juxtaposition of the Chewore terranes occurred during the earliest part of the M_2 cycle i.e., at 524 ± 16 Ma.

The plethora of Pan - African radiometric ages (*c.* 520 - 530 Ma) throughout the Zambezi Belt suggests that the belt containing the OT represents a complex east to west trending suture zone which divides West Gondwana into a 'northern' (Congo Craton) and 'southern' (Zimbabwe Craton) component. The Zimbabwe and Congo Cratons were therefore ultimately juxtaposed during the Pan - African Orogeny.

Acknowledgements.

The support and assistance of the following people or institutions are gratefully acknowledged:-

The Welch and Irvine bequests to Geosciences at St Andrews University, for funding both fieldwork and maintenance for this study.

Dr Grahame Oliver for his dedicated support, open office, advice and patience in the supervision of this thesis.

My family, especially my mother for their undying support and encouragement.

Sarah for keeping up my spirits up while putting together the final draft.

Colin Donaldson, Ed Stephens and Ian Alsop for their helpful discussions.

Donald Herd for his help with the microprobe analyses, Angus Calder for his assistance and help in the preparation of the fused discs for XRF analyses and Andy Mackie for the production of thin and probe sections.

The National Parks of Zimbabwe for allowing me access the Chewore Safari Area in the Zambezi Valley.

The Research Council of Zimbabwe for issuing me a permit to allow me to conduct research in Zimbabwe.

The University Of Zimbabwe for the use of their vehicle, computer facilities and participation in undergraduate field trips and their introduction to Zimbabwean Geology.

Prof. T. Blenkinsop for his fruitful discussion, monetary assistance and help in the logistics of the project.

Prof. H. Munyanyiwa and Drs. P. Dirks, H. Jelsma, K. Walsh and D. Shoko for their fruitful discussions.

All the technical staff at the University of Zimbabwe for their help and assistance in the production of photographic slides, thin sections, crushing and heavy mineral separation.

All the staff at Sable Lodge, Selous Ave, Harare (especially Robert the chef and George) who treated me not like a paying customer but as a friend and guest of the establishment. Thanks also go to the many friends I have made in Harare.

Lastly but not least all the game scouts from Mkanga Field station of the Chewore Safari Area who invited me with open arms and treated me as a long lost friend. Special thanks go to Enias 'Francis' Dzingira who is my dear friend who has keen eyes and always a good story to tell. Thanks also go to the other scouts who accompanied me in the field : Joseph Ndlovu, Shadreck Chickwangani and Nicolas Mapfumo and to my two field assistants Gillian Lee and Rex Chaukura.

Contents

List of Figures

List of Tables

Chapter One

Introduction.

1.1 Background.

The Chewore Inliers are a group of isolated horsts situated within the Zambezi Valley of northern Zimbabwe and are part of the Late Proterozoic, transcontinental, Pan - African orogenic system that links the Damara Belt of western Africa, the Lufillian Arc of central Africa and the north - south trending Mozambique Belt in eastern Africa (Fig 1.1). This east - west trending orogenic system separates the Zimbabwe Craton from the Congo Craton.

1 : 50,000 scale, reconnaissance mapping of the Chewore Inliers by the Zimbabwe Geological Survey has led to the recognition of three major, thrust bound terranes, namely the 'Granulite', 'Quartzite' and 'Gneiss' Terranes (Both, 1991, 1992 and Goscombe *et al.*, 1994, 1997, 1998), (Fig. 1.2 and 1.3). Sub - division of each terrane into a formal lithostratigraphy has not yet been made. The Granulite Terrane consists of mafic to felsic, granulite facies gneisses which are interpreted by Goscombe *et al.*, (1994) to have no compositional equivalents within the neighbouring terranes. The Quartzite Terrane is comprised entirely of amphibolite facies grade meta - quartzites and the Gneiss Terrane by quartzo - feldspathic gneisses with amphibolitic and minor pelitic assemblages. However, fieldwork for this study, based in the southeastern region of the Gneiss Terrane (outlined area in Fig. 1.3) has identified all the elements of an ophiolite suite in accordance with the criteria set down by the Geological Society of America, Penrose Conference on Ophiolites (Anon, 1972). This ophiolite is interpreted as part of a distinct thrust bound terrane which has been named in this study and in Oliver *et al.*,

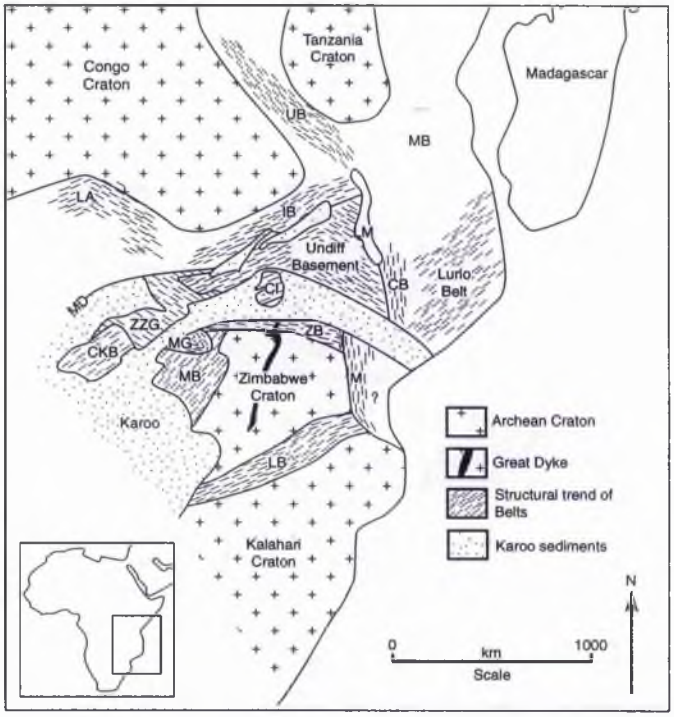

Fig.1.1 Location of the Chewore Inliers in relation to the tectonic belts of Sub - Saharan Africa. Abbreviations :- MB - Mozambique Belt; CB - Coube Belt; CI - Chewore Inliers; MD - Mwembeshi Dislocation; LA - Lufilian Arc; ZZG - Zambian Zambezi Group; CKB - Choma Kalomo Block; MG - Makuti Group; MB - Magondi Belt; M - Manica Belt; ZB - Zambezi Belt.

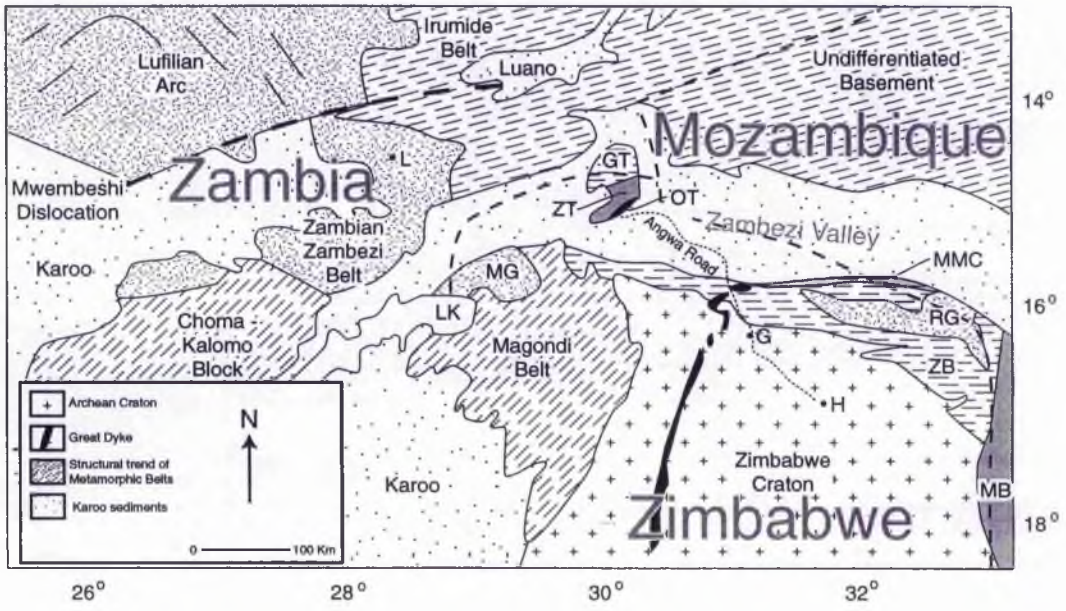

Fig. 1.2 Location of the Chewore Inliers in relation to the surrounding tectonic belts . Key :- GT, ZT and OT are the components within the Southern Chewore Inliers. LK - Lake Kariba ; MG - Makuti Group; MMC - Mavhuradonna Metamorphic Complex; RG - Rushinga Group; ZB - Zambezi Belt; MB - Manica Belt; G- Guruve; H - Harare and L - Lusaka.

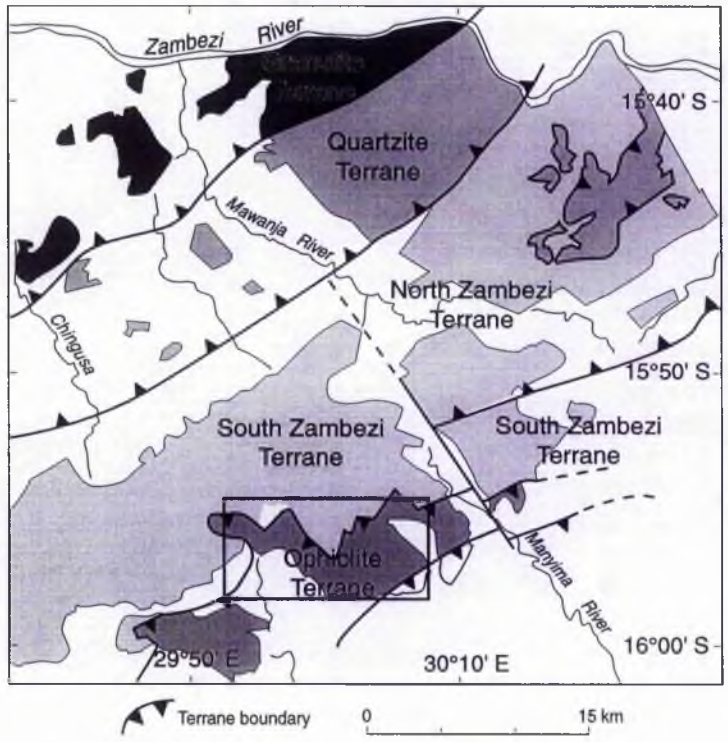

Fig. 1.3. Geological terranes of the Chewore Inliers after Goscombe *et al.*, 1994, 1998. Box outlines the position of Fig. 1.4.

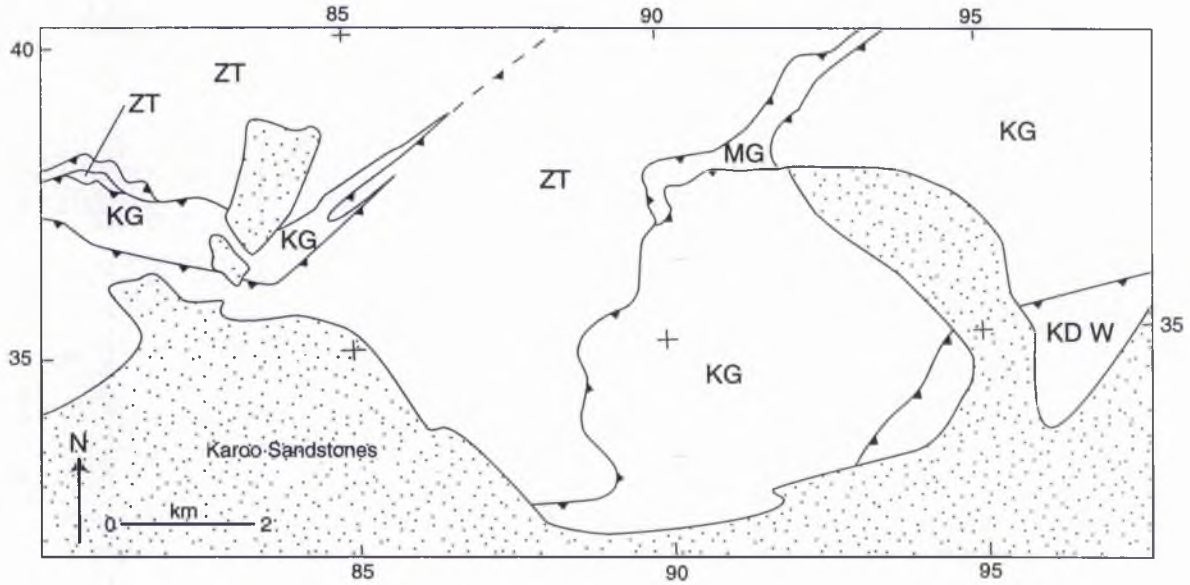

Fig. 1.4 Sketch map of the major mapping groups within the Ophiolite Terrane. For detailed geology refer to map inserts 1, 2 and 3.Abbreviations :- KD W - Kadunguri Whiteschists; KG - Kaourera Island - Arc Group; MG - Maunde Ophiolite Group; ZT - Zambezi Terrane.

(1998), as the Ophiolite Terrane (Fig. 1.3). Recognition of the Ophiolite Terrane has led to the sub - division of the Gneiss Terrane into the Zambezi (quartz - feldspathic gneisses) and Ophiolite Terranes (meta - mafic to meta - ultramafic lithologies) (Goscombe *et al.*, 1997, 1998).

1.2 Aims.

The aims of the research were to:-

1) Produce a 1 : 10 000 scale map of the Ophiolite Terrane together with more detailed 1 : 5000 scale maps of the critical areas around the Maunde and Kaourera River which contain the type sections for the ophiolite, island - arc and whiteschist lithologies.

2) Document the various lithologies within the Ophiolite Terrane and to set up an informal lithostratigraphy.

3) Compare the lithostratigraphy and whole - rock major and trace element geochemistry of the Maunde Ophiolite Group with Phanerozoic ophiolites and examples from differing, present - day tectonic settings to test the hypothesis that this group represents a dismembered ophiolite.

4) Compare the lithostratigraphy and whole - rock major and trace element geochemistry of the Kaourera Island - Arc Group with present day island - arc systems to test the hypothesis that this group represents a dismembered island - arc complex.

5) To document the metamorphic assemblages, whole - rock major and trace element geochemistry and compositions of important mineral phases such as yoderite, within the Kadunguri Whiteschists.

6) To present a new U / Pb SHRIMP zircon age for a plagiogranite sheet within the Maunde Group.

7) To produce a regional tectono - metamorphic synthesis to illustrate the geodynamic evolution of the Ophiolite Terrane, Chewore Inliers and surrounding tectonic belts.

1.3 Logistics.

The Southern Chewore Hills are remotely situated in the Chewore Safari Area of the Mid - Zambezi Valley. Entrance to the Safari Area is strictly by permit only, this can be acquired by means of a research application through the National Parks Headquarters in Harare and the acquisition of a research permit from the Research Council of Zimbabwe.

The Chewore Safari Area is reached by the main Angwa corrugated road from Guruve. From the safari area scout camp, the field area is reached by numerous, variably upheld hunter tracks and off - road, cross country driving. A four wheel drive Land Rover or 'Backkie' is essential.

The remoteness of the field area meant that bush camping was conducted for a period of several weeks at a time and all the food, fuel and water had to be carried in and managed at base camp for the duration.

Fieldwork was conducted during the dry season from June to Sept when temperatures are at their lowest (*c.* 25° C). During the late dry season and early wet season temperatures rise to over 50° C. Since the field area is situated within a safari area, big game such as elephant, lion, buffalo and

leopards are a hazard. This hazard combined with the remoteness of the area meant that a National Park game scout with a two way radio and automatic rifle and a local field assistant were essential.

The Geology Department of the University of Zimbabwe aided in the application for the research and National Park permits. They also kindly provided logistical support, camping equipment, rock cutting, crushing and heavy mineral separation facilities, computing and mail facilities and a four wheel drive Backkie.

1.4 Style of Thesis.

The thesis is aimed to be presented in a logical manner so that each chapter is virtually self - contained. Each chapter starts with an introduction, presents the data, is followed by interpretation and discussion and finishes with a set of conclusions. Many plates have been placed at the end of each chapter.

The thesis contains six main chapters. The first describes and sets up an informal lithostratigraphy for the Ophiolite Terrane. The second presents the geochemical analysis of the main mapping formations in an attempt to constrain a tectonic environment of formation. This is followed by chapters outlining the tectono - metamorphic evolution of the Ophiolite Terrane (metamorphism, structure and radiometric age determinations). The thesis is concluded with a discussion on the tectonic setting and evolution of the Ophiolite Terrane, Chewore Inliers and a regional synthesis.

Chapter Two

Lithostratigraphy.

2.1 Introduction.

The aims of this chapter are :-

1) To document the various lithologies of the Ophiolite Terrane.

2) To organise the ophiolite and island - arc lithologies into an informal lithostratigraphy based on the stratigraphical procedure recommended by Whittaker *et al.*, (1994).

3) Briefly describe the lithological characteristics of the surrounding Zambezi Terrane.

Since both the ophiolite and island - arc groups previously contained a structured organisation of lithologies, an attempt will be made to construct an informal lithostratigraphy; however, the whiteschist and gneiss units show no evidence for such an organisation. These will be described and subdivided on the basis of their mineralogy. The recommendations in Whittaker *et al.*, (1994) for the naming of lithostratigraphic units indicate that each lithotype should have a proper name chosen where applicable from a distinctive geographical feature near a characteristic section, which is ideally the type section. However, within the Southern Chewore Hills, especially within the region of the Ophiolite Terrane, there is a lack of named geographical features. There are more lithostratigraphic formations than geographical names. Therefore, features such as streams and small hilltops have been informally named in this study. All new informal names are illustrated on map inserts 1, 2 and 3. Appendix A is a list of the samples collected. It gives the map reference of the

locality, a brief sample description and the mapping formation to which it belongs. Map references are from the 1 : 50 000 scale topographic sheets (Anon, 1989).

2.2 The Maunde Ophiolite Group.

The various lithotypes that comprise the Maunde Ophiolite Group are best observed along an 800 m section of the Maunde River between MR [9105 3770] and MR [9167 3765] (map insert 2a, b) which is classified here as the type section for the group. Each formation crops out as a south - easterly dipping, thrust bounded unit. Since all formations are in tectonic contact it is impossible to determine their relative ages and thus the type section will be described as a structural section from the top to bottom i.e., an east to west traverse along the Maunde river (Fig. 2.1).

2.2.1 Nzou Meta - Greywacke Formation.

This formation is characterised by meta - sedimentary lithologies. The type section crops out within the Maunde River at the most easterly extent of the type section, adjacent to the informally named Nzou stream, starts at MR [9113 3713]. The approximate thickness of the formation is 25 m. The outcrop is imbricated (on the metre scale) with each imbricate slice dipping toward the south east.

Grey Member.

At MR [9113 3713] this member is variable in colour from pale blue to pale brown, fine grained (Plate. 2.1 a) and comprised of quartz, plagioclase, biotite, muscovite, calcite, epidote and opaque metallic minerals (sample [SJ 100.1] and Appendix B). The assemblage is dominated by quartz and plagioclase and the subordinate phyllosilicate portion is dominated by biotite. A

penetrative foliation (section 5.4) is defined by the alignment of the phyllosilicates and a tectonic lineation by thin, granoblastic aggregations of quartz and plagioclase which occur as upto 1 cm long lenses, the long axes of which are parallel to the lineation (Plate. 2.1 a and b). A 1 to 5 mm thick, disrupted, foliation parallel band of metallic ore is surrounding with a corona of green oxide (Plate. 2.1 c). The green colouration indicates the presence of oxidised copper and suggests that the metallic band itself is a cuprous ore.

Within thin section this member is observed to be laminated on the millimetre scale. Laminations are defined by the variable proportion of biotite between 5 and 10% and are interpreted to represent original sedimentary layering i.e., S_0. The S_0 is parallel to the main S_2 foliation (section 5.4).

Dark Member.

At MR [9113 3713] this member is dark blue to black in colour, fine grained and comprised predominantly of biotite and chlorite with subordinate muscovite, quartz, plagioclase, epidote, calcite and opaque minerals (sample [SJ 202] and Appendix B). Spherical, 2 to 5 mm diameter, quartz, muscovite and chlorite aggregations are randomly distributed throughout this member and comprise upto 10% of the rock (Plate. 2.1 d). Both biotite and chlorite form 2 mm long tabular crystals which are aligned to define a crenulated, schistose fabric.

This member occurs as semi - continuous (upto 1.5m long, 20 cm thick), isolated lenses within the Grey Member (Fig. 2.1). Contacts between the two are sharp except at the tips of the pelite lenses where a gradation into the Grey Member occurs over the distance of a few centimetres.

2.2.2 *Mvuu Meta - Mafic Volcanic Formation.*

This formation is characterised predominantly by fine grained amphibolites. The base of the section starts at MR [9165 3770], adjacent to the informally

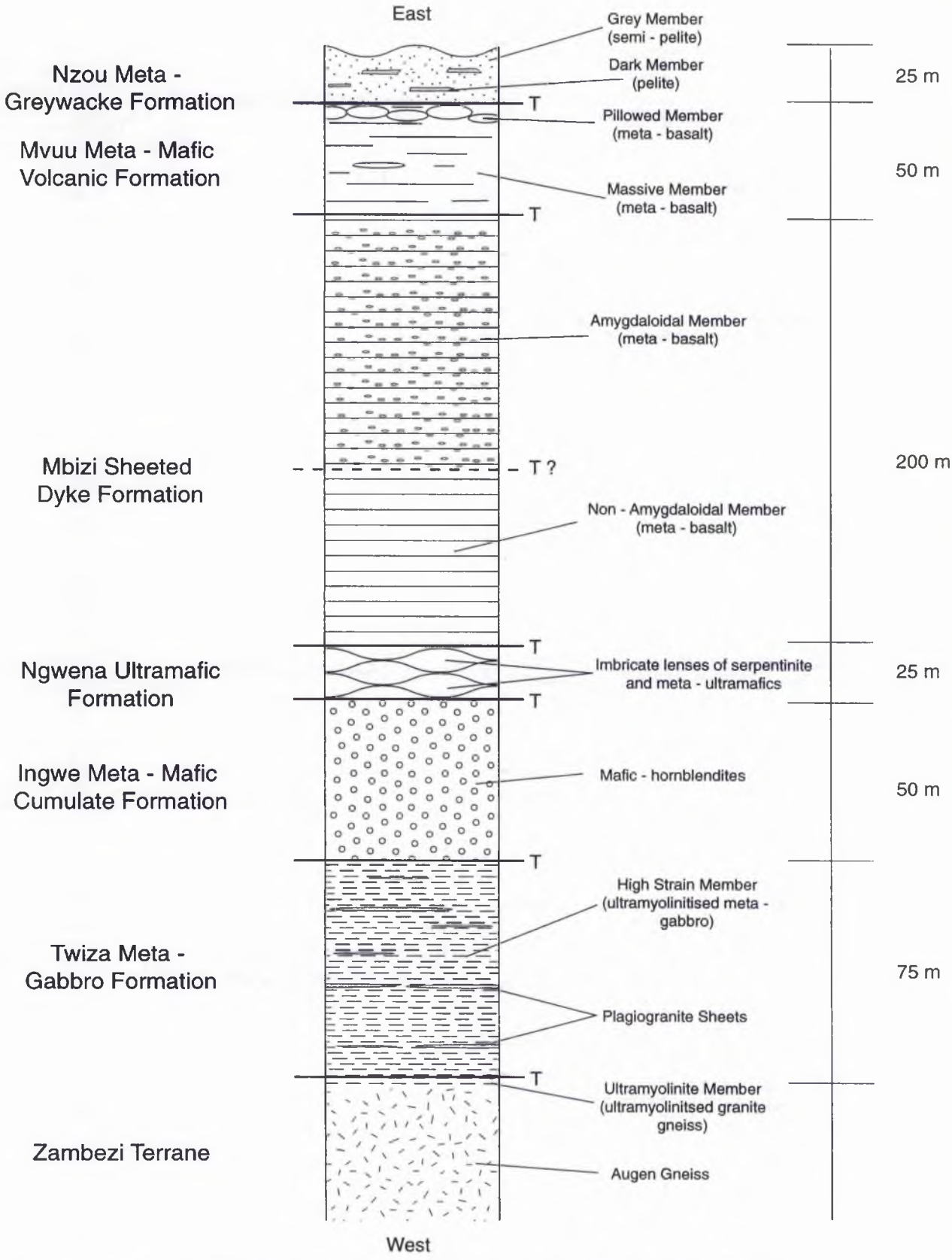

Fig. 2.1 Tectono - stratigraphic column of the type section of the Maunde Ophiolite Group which crops out along the Maunde River. T = Tectonic Boundary.

named Mvuu Stream. This formation is structurally located below the Nzou Meta - Greywacke Formation. Both top and base contacts are interpreted to be tectonic. The formation is approximately 50 m thick.

Massive member.

At MR [9167 3763] this member is pale blue, very fine grained has a massive appearance and is mineralogically and texturally homogenous (Plate. 2.2 a). It is comprised of hornblende, plagioclase, quartz, epidote, sphene and chlorite (sample [SJ 203] and Appendix B). No opaque metallic minerals occur within the specimen. Hornblende dominates the assemblage as parallel, less than 0.5 mm long, bladed crystals which define a weak foliation. Seriticised plagioclase and quartz occur as upto 4 mm long lenses which are aligned with the long axes of the hornblende blades to produce a weakly defined L_2 lineation (section 5.4).

Pillowed Member.

This member is grass green in colour, contains upto 30 %, pale yellow, irregular shaped, 2 - 15 mm long epidote and calcite filled amygdales and displays distinctive, metre scale, 'pillowed' outcrop profiles (Plate. 2.2 b, c and d). At the type section (MR [9165 3770]), 5 individual 'pillows' are evident (Plate. 2.3). The main portion of the member is fine grained and comprised predominantly of anhedral to mildly tabular, randomly oriented epidote and zoisite with minor hornblende, sphene and calcite (sample [SJ 100.3] and Appendix B). Plagioclase, quartz and opaque metallic minerals are not present. The amygdales contain large (upto 2 mm long), acicular, radial epidote crystals and minor, anhedral calcite. A poorly developed tectonic fabric is developed from the alignment of amphibole blades (section 5.4).

The top and base of the Pillowed Member are marked by a 20 - 60 mm thick, darkly coloured, fine grained band (Plate. 2.2 b and c) which contains

less than 1 mm, elongate, epidote filled amygdales and a poorly developed tectonic fabric. Hornblende dominates the assemblage as upto 3 mm long, tabular, weakly aligned to randomly oriented crystals with minor plagioclase, quartz, epidote and sphene (sample [SJ 100.4] and Appendix B). Due to subsequent shear dominated deformation (D_2, see section 5.4), minor modification of the pillow structures makes it impossible to determine the 'way up' of the structures.

The Massive Member comprises upto 95 % of the formation. The Pillowed Member crops out as variably deformed, isolated or trains of pillows upto 30 cm thick within the Massive Member.

2.2.3 Mbizi Sheeted Dyke Formation.

This formation is characterised by planar bounded, predominantly amygdaloidal amphibolites. The type section begins at MR [9158 3779] which is adjacent to the informally named Mbizi Stream. The approximate thickness of this formation is 200 m. Both the base and top contacts are interpreted to be tectonic.

Amygdaloidal Member

At MR [9148 3780] this member is very fine grained, dark grey to black and contains upto 60% , irregular, elongate, leucocratic amygdales (Plate. 2.2 e). The fine grained matrix is comprised predominantly of aligned, upto 4 mm long, tabular hornblende with minor, interstitial quartz and plagioclase (sample [SJ 208.2] and Appendix B). Randomly distributed, 0.5 mm diameter, anhedral, opaque metallic minerals are abundant. The amygdales are prolate, 10 to 20 mm long, sub - parallel to the tectonic fabric (section 5.4), comprised of plagioclase, quartz and more rarely epidote. The proportion of amygdales varies between 30 and 60 % but is on average only 30 to 35 %. The variable

concentrations are contained within sharp, foliation sub - parallel boundaries creating amygdaloidal rich and poor bands of between 10 and 100 cm thick. Each band can be traced laterally throughout the extent of the outcrop (i.e., 10 to 20 m) and is interpreted to represent multiple dyke contacts.

Non - Amygdaloidal Member

At MR [9147 3780] this member is dark grey to black in colour and occurs as both fine and medium grained, parallel sided, 20 - 50 cm thick units (Plate. 2.2 f). Both are comprised predominantly of aligned, euhedral, tabular and diamond shaped hornblende with minor, interstitial, granoblastic quartz and plagioclase (sample [SJ 101.1] and Appendix B). Randomly distributed, 0.5 mm diameter opaque minerals and sphene comprise less than 5 % of the specimen. Epidote is not recorded. A variably developed tectonic fabric is sub - parallel to the sharp, straight contacts between the fine and medium grained units (section 5.4). The contacts are sharp (Plate. 2.4 a); however, at MR [9150 3780] a 30 cm thick, fine grained unit is observed to grade (from 0.25 mm to less than 0.1 mm grain size) over a distance of 10 mm, towards the contact with a medium grained unit (Plate. 2.4 b) and is traceable along the length of the outcrop (i.e., 2 m). This is interprted to be a relict, chilled margin. Contacts between fine and medium, fine and fine (Plate. 2.4 c) or medium and medium grained units are all evident within the outcrop and are interpreted to represent multiple dyke contacts i.e., a sheeted dyke complex.

The top and base of the formation are obscured by recent river deposits but are assumed to be tectonic in origin. The parallel sided Amygdaloidal and Non - Amygdaloidal Members dip moderately and steeply toward the south - east. The Non - Amygdaloidal member crops out within the structural base of the formation i.e., to the west, where both fine and medium grained units are equally represented. A two metre gap in outcrop marks the boundary

between the two members. Both are similarly oriented on either side of this contact and it is not known whether they are in tectonic or stratigraphic contact.

2.2.4 Ngwena Ultramafic Formation.

This formation is characterised by metamorphosed ultrabasic rocks. The type section occurs along the Maunde River between MR [9116 3765] (base) and [9117 3765] (top) at the bottom of the informally named Ngwena Stream. The approximate thickness of the formation is 25 m. Both the base and top contacts are interpreted to be tectonic.

Tremolite Member.

At MR [9116 3765] this member is very fine grained, pale grey and weathers to smooth, rounded outcrops due to its soft nature (Plate. 2.4 d). Tremolite predominates the assemblage as both 1 - 2 mm porphyroblasts with dusty, opaque inclusions and as 1 - 4 mm long, aligned, tabular and diamond shaped crystals (sample [SJ 213 A] and Appendix B). Chlorite lenses upto 10 mm long are predominant and contain less than 1 mm, randomly oriented chlorite blades and 0.5 mm diameter rutile crystals. Irregular shaped, 1mm diameter chromites are randomly distributed throughout the specimen. The member contains a weakly defined, penetrative foliation and lineation (section 5.4). At MR [9124 3786] a small outcrop contains upto 60 mm 'books' of bottle green clinochlore (Plate. 2.4 e) which comprises *c.* 5 % of the outcrop and is randomly distributed and is oriented sub - parallel to the foliation.

Layered Tremolite Member.

At MR [9115 3766] this member has a similar field appearance to the Tremolite Member. It is pale grey and very fine grained, but contains an increased opaque mineral content (upto 20 %). The opaque minerals are

concentrated into lensoid aggregates which contain upto 70 % opaques. These aggregates form thin (< 5 mm), elongate (upto 60 mm) trains which are parallel to the weakly defined foliation (Plate. 2.4 f). The main fine grained portion of the member is comprised predominantly of tremolite which occurs as both 1 - 2 mm porphyroblasts with dusty opaque inclusions and as very fine grained, less than 0.1 mm, aligned, tabular crystals (sample [SJ 213 C] and Appendix B). Chlorite forms upto 10 mm long, lenses with less than 1 mm long, randomly oriented chlorite blades and fine, irregular shaped rutile crystals. Small amounts of chromite are also randomly disseminated throughout the rock. The opaque rich lenses are comprised of both 1mm, irregular shaped opaque ores and 1 - 2 mm diameter, tremolite porphyroblasts with dusty opaque rich inclusions.

Serpentinite Member.

At MR [9115 3767] this member is dark blue with pale blue patches, very fine grained (Plate. 2.5 a), contains a weak tectonic fabric (section 5.4) and is comprised of *either* very fine grained serpentine and upto 2 mm diameter or chromite with minor, fine grained talc, rutile and tremolite or very fine grained serpentine and tremolite with fine grained disseminated opaque minerals or as tremolite porphyroblasts with dusty opaque mineral inclusions set within a very fine grained talc and tremolitic matrix (sample [SJ 213 F] and Appendix B). Upto 2 mm wide veins of less than 0.5 mm long, acicular, radial serpentine cut through the various mineral assemblages.

The most distinctive Ngwena Ultramafic Formation lithotype occurs as an isolated block of float at MR [9165 3770]. This lithology has yet to be identified in - situ and thus cannot be described as a member. Important textural characteristics however, warrant its description. It is comprised of two distinct components: a very fine grained, dark blue matrix comprised of

less than 0.1 mm long, serpentine and / or tremolite and 1 to 2 mm tremolite porphyroblasts with dusty opaque mineral inclusions. The second component is comprised of upto 60 mm long, isolated, black lenses which contain 1 to 2 mm wide anastamosing fractures which are orthogonal to the long axis of the pod and filled with fine grained talc and serpentine. The pods do not form trains or pseudo - bands but are randomly distributed and comprise upto 60 % of the specimen (Plate. 2.5 b). The pods are equigranular, coarse grained with individual crystals reaching upto 3 mm diameter and comprised of serpentine and tremolite. Dihedral angles between all the crystals approach 120°. The serpentine, although very fine grained, occurs within large (2 to 3 mm), hexagonal, straight sided areas which may represent relict, igneous, euhedral to subhedral olivine crystals which have been replaced by serpentine. These areas also contain thin (less than 0.5 mm) bands of opaque minerals which cross - cut the relict crystal shape in many random orientations. These opaques can comprise upto 50 % of the relict crystal. The tremolite crystals are 2 to 3 mm in dimension, subhedral to anhedral and display straight crystal edges. They contain a high proportion (*c.* 40 %) of very finely disseminated chromite. The edges of most of these crystals are mantled in a 0.5 mm thick rim of fine grained talc and opaque free tremolite which is in optical continuity with the larger crystal (Plate. 2.5 c). The pods are cross - cut by upto 2 mm wide, anastamosing bands of randomly oriented less than 0.5 mm long, tabular talc crystals.

The type locality of the formation contains many imbricate lenses, each of which is comprises a different member. All of the contacts, including the structural top and base of the formation are interpreted to be tectonic. All of the other known outcrops of this formation outside the type locality are comprised entirely of the Tremolite Member.

2.2.5 Ingwe Meta - Mafic Cumulate Formation.

This formation is characterised by granular, hornblende dominant lithologies. The type starts in the Maunde River at MR [9115 3768] at the base of the informally named Ingwe Stream. The approximate thickness of the formation is 50 m. The structural top and base are interpreted to be tectonic.

This formation is dark to bottle green, friable and occurs as topographically low, rounded outcrops. It is comprised of upto 70 %, dark green, 1 to 2 mm long, augen shaped, hornblende porphyroblasts which are randomly distributed throughout the rock. The porphyroblasts seldom touch and are separated by a fine grained bottle to dark green, platy to tabular hornblende dominant matrix which displays a tectonic fabric (Plate. 2.5 d). The hornblende porphyroblasts contain abundant epidote and sphene inclusions which are either randomly distributed or occur as trains of parallel inclusions that are at an angle to the surrounding foliation trend. The matrix is comprised of upto 1.5 mm long, tabular, aligned hornblende laths with minor clusters of less than 0.5 mm long, tabular zoisite crystals and variable opaque mineral contents (samples [SJ 105.5], [SJ 214 F] and Appendix B).

2.2.6 Twiza Meta - Gabbro Formation.

This formation is characterised by various meta - gabbroic and related lithologies. Since all members are not observed at a single outcrop a type locality will be described for each member.

Massive Member.

The type locality for this member is at MR [9115 3768] where it crops out as a 1 m wide, 2m long imbricate slice within the Ingwe Meta - Mafic Cumulate Formation. It is medium to coarse grained and displays a gabbroic texture. It is comprised of dark green, 1 - 2 mm long, flattened, oblate hornblende

porphyroblasts set within a fine grained matrix of plagioclase, sphene and epidote (Plate. 2.5 e). The alignment of the equidimesional x - y axes of the oblate porphyroblasts gives the rock a coarse foliation (section 5.4). There is no tectonic lineation present. The matrix is comprised of less than 0.5 mm long, aligned, hornblende laths and upto 1 mm long, irregular shaped, randomly oriented plagioclase crystals. Epidote occurs as very fine grained, aligned inclusions within the hornblende porphyroblasts which lie at an angle to the aligned hornblende laths within the matrix. Sphene occurs a less than 0.1 mm long, randomly distributed, irregular shaped crystals. There are no opaque minerals present (sample [SJ 213 Hb] and Appendix B).

Layered Tremolite Member.

The type locality for the Layered Tremolite Member is at MR [9010 3705]. This member is similar in appearance to the Massive Member but differs due to a gross, centimetre scale, parallel banding created by a variable hornblende porphyroblast content (Plate. 2.6 a and b). The alignment of the oblate porphyroblasts create a coarse foliation which is parallel to the gross - scale banding. Porphyroblast - rich bands contain upto 90 % porphyroblasts, are generally 10 - 20 mm thick and are laterally extensive along the length of the outcrop. The porphyroblast bands which contain normal proportions of porphyroblasts (70%) predominate and range in thickness from 10 mm to 1 m. The transition between the two is gradational such that the proportion of porphyroblasts increase or decrease over a distance of 10 - 20 mm. It is interpreted that this banding represents an original, layered igneous texture such as density grading. If one porphyroblast rich and one porphyroblast normal band are classified as a single cycle then the Layered Tremolite Member on average displays 4 or 5 cycles per metre.

High Strain Member.

The type locality of the High Strain Member is at MR [9111 3771]. This member is predominantly dark grey to black, fine grained and contains 10 to 40 mm thick, coarser grained, leucocratic, parallel and sub - parallel bands (Plate. 2.6 c and d). The margins of these leucocratic bands are sharp and display a reduction in grain size across a distance of less than 1 mm. At the type locality the bands comprise less 5 % of the outcrop and are randomly spaced, whereas at MR [9105 3785], a 3 m outcrop contains upto 50 % leucocratic, coarser grained material (Plate. 2.6 e). Grain size reduction at this locality occurs over a distance of upto 5 mm. The main fine grained portion is comprised predominantly of aligned, tabular hornblende with minor plagioclase. Irregular shaped, less than 0.1 mm long, sphene and epidote are randomly distributed throughout the specimen. There is a variable opaque mineral concentration (sample [SJ 215 B], [SJ 215 G] and Appendix B). The coarser grained, leucocratic portion is mineralogically bimodal and comprised of flattened, elongate, 5 to 10 mm long aggregations of hornblende and plagioclase. The hornblende laths are aligned and define a tectonic fabric which is sub - parallel to the margins of the bands (Plate. 2.6 c). This member is interpreted to be a deformed version of the Massive Member.

Plagiogranite Sheets.

At MR [9110 3771] the Plagiogranite Sheets occur within the High Strain Member as clean, white to pale cream, medium grained, equigranular, sugary textured, upto 30 cm thick, foliation sub - parallel dykes (Plate. 2.6 f). These plagiogranites also occur as thin veinlets within the Massive and Layered Tremolite Members (Plate. 2.7 a). It is comprised predominantly of equigranular, 1 to 2 mm diameter quartz and plagioclase, both which occur in equal proportions. Minor phases which comprise less than 0.5 % of the specimen include tabular biotite crystals (sample [SJ 106.1] and Appendix B)

which are randomly distributed throughout the specimen are aligned to give the member a very weak tectonic fabric and irregular, randomly distributed, less than 0.5 mm diameter opaque minerals. Sample [SJ 106.1] was selected for SHRIMP zircon dating (see chapter 6).

The Massive Member comprises the majority of outcrops of the Twiza Meta - Gabbro Formation while the Layered Tremolite Member is mapped as single, isolated outcrops surrounded by the Massive Member. The High Strain Member crops out only between MR [9111 3771] and [9101 3771] where it is juxtaposed against granitic gneisses of the Zambezi Terrane. The contacts between the Twiza and surrounding formations are poorly exposed and are assumed to be tectonic. However, at MR [9115 3768] an igneous contact is observed between the Massive Member and the Medium Grained Member of the Ingwe Meta - Mafic Cumulate Formation (Plate. 2.5 e). The outcrop is an imbricate slice, 1 m wide and 2 m long and comprised of coarse grained meta - gabbro to the east and medium grained hornblendite to the west. The two are observed to sharply grade into one another over a distance of less than 2 mm. The 1 to 2 mm long hornblende crystals within the meta - gabbro occur without loss of grain size, shape or distribution, within the hornblendite. The plagioclase dominant matrix within the meta - gabbro grades over a distance of 5 mm into a hornblende dominant matrix within the hornblendite. This zone of grading is relatively sharp and straight along the length of the outcrop. The two are interpreted to be in igneous contact.

2.2.7 Discussion.

The Maunde Ophiolite Group consists of a series of meta - sedimentary, meta - mafic and meta - ultramafic formations which may or may not represent an ophiolite complex. In this discussion, the lithostratigraphy of both 'ophiolites', *senso stricto* (Anon, 1972) and the Maunde Ophiolite Group will be compared.

The term ophiolite, as defined at the Geological Society of America, Penrose Conference on ophiolites in 1972, refers to a distinctive assemblage of mafic to ultramafic rocks consisting of the following lithostratigraphic units occurring in the following sequence from base to top :- Ultramafic complex, Gabbro complex, Mafic Sheeted Dyke complex and a Mafic Volcanic complex. Other associated rock types include podiform chromite deposits within the Ultramafic complex and an overlying pelagic sedimentary sequence. Sub - divisions and lithostratigraphic variations within each complex differ with the particular ophiolite being studied. Since the Troodos Ophiolite in Cyprus has been well documented and because the lithostratigraphy is well known (Geological Survey Department Nicosia, 1987), the lithostratigraphic sub - divisions in Troodos will be used (see Fig. 2.2) to test the hypothesis that this group represents an ophiolite, albeit metamorphosed and dismembered.

Ultramafic complex.

The Ultramafic complex (anon, 1972), consists of variable proportions of harzburgite (olivine + orthopyroxene), lherzolite (olivine + clinopyroxene + orthopyroxene) and dunite (olivine) which may be serpentinised, contain variable proportions of chromite and contain a penetrative tectonic fabric. Such lithologies are evident within the Troodos Massif, along with podiform chromite deposits (Geological Survey Department Nicosia, 1987). The meta - ultramafic formation of the Maunde Ophiolite Group, namely the Ngwena Ultramafic Formation is comparable with this complex. All the members of the Ngwena Ultramafic Formation contain greater than 90 % mafics (i.e., < 10 % quartz and plagioclase) with variable chromite concentrations and thus based on the IUGS subcommission recommendations given in Le Maitre (1989), can be classified as ultramafic rocks. Alteration of the original igneous mineralogy by amphibolite grade metamorphism (section 4.3) makes it difficult to classify each member according to the IUGS subcommission

recommendations (Le Maitre, 1989). Whole rock geochemical analysis (section 3.2.4) indicates that both major and trace element concentrations are similar to those in other ophiolite complexes.

Gabbro complex.

Coleman (1977) describes the gabbro complex as a large part of the ophiolite sequence that has been derived by fractional crystallisation of a mafic magma to produce a sequence of ultramafic to leucocratic rocks. The sequence at Troodos usually displays a crude layering with ultramafic cumulate rocks such as wherlites (olivine + clinopyroxene) and pyroxenites (clinopyroxene + orthopyroxene) at the base, grading upward into increasingly feldspar - rich gabbroic rocks such as layered and massive gabbros and finally into irregular, small and discontinuous zones of plagiogranite (Fig. 2.2).

The mafic cumulate rocks are represented by the Ingwe Meta - Mafic Cumulate Formation which is characterised by porphyroblast dominant hornblendites. If the porphyroblasts are interpreted as relict igneous crystals which display their original size, shape and distribution, then this formation can be considered as a metamorphosed mafic - cumulate. The formation displays adcumulus textures since the relict crystals do not touch. The lack of plagioclase or relict plagioclase and the similar composition of inter - cumulus and cumulus phases indicate that although metamorphosed, the original cumulate assemblage was dominated by a mafic mineralogy such as pyroxenes (clino and/ or orthopyroxene).

Although metamorphosed, the Massive, Layered and High Strain Members of the Twiza Meta - Gabbro Formation are interpreted to be meta - gabbros since they display relict gabbroic textures and are composed predominantly of plagioclase and a meta - mafic mineral. The comparison between the Layered Tremolite Member and the layered gabbro is obvious

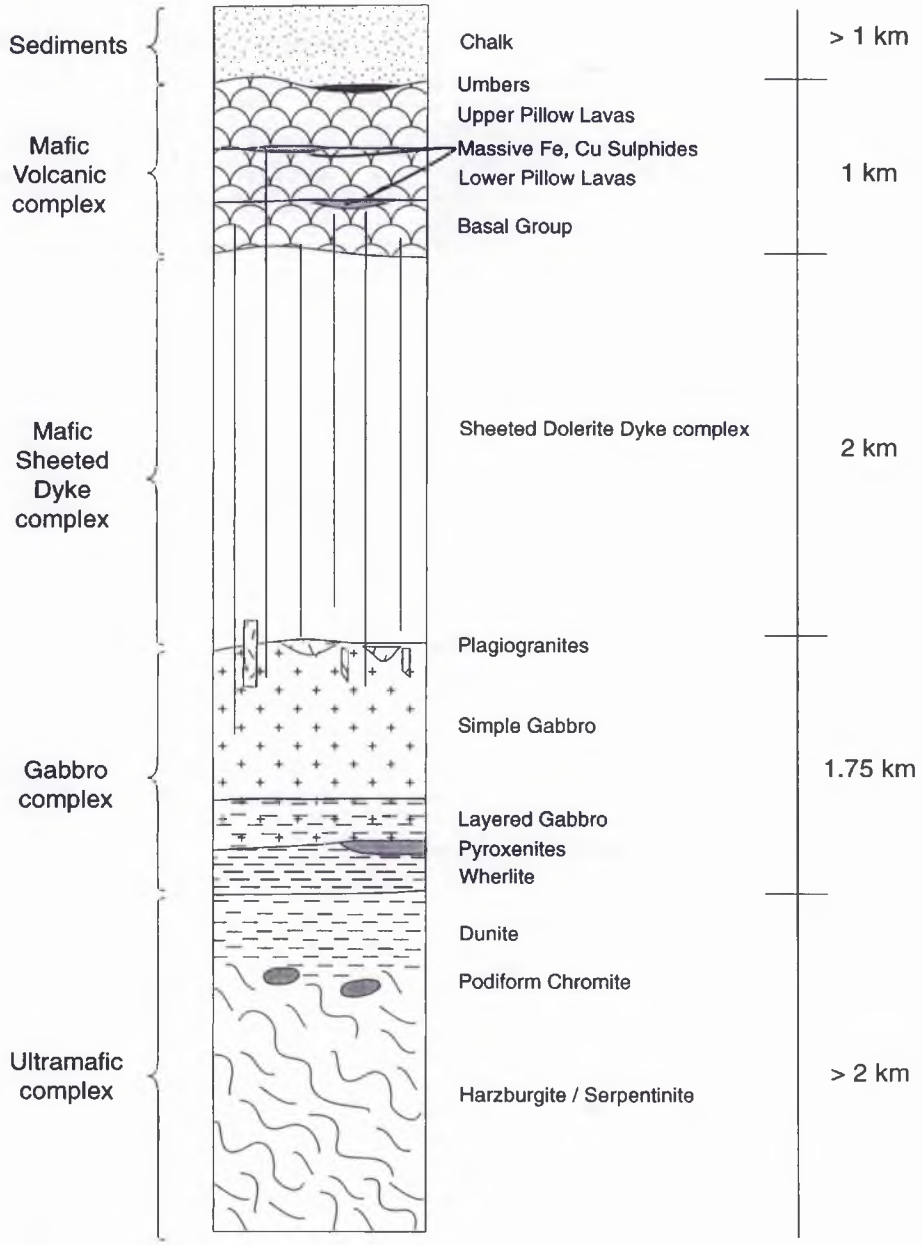

Fig. 2.2 Lithostratigraphic sequence of the Troodos Ophiolite Complex (after Geological Survey Department Nicosia, 1987).

since both display rhythmic, density layering. Cryptic layering which is also associated with fractional crystallisation of a mafic magma (Coleman, 1977) is difficult to demonstrate since the Layered Tremolite Member has been metamorphosed. The Massive and High Strain Member may be compared to the simple gabbro since both display (or are interpreted to have once displayed) massive textures. The irregular, small and discontinuous zones of plagiogranite are evident throughout all members of the formation, especially within the High Strain Member which when compared to Troodos may suggest that it was located much higher in the sequence than the other members. Most of the contacts between the Twiza and Ingwe Meta - Mafic Cumulate Formations are assumed to be tectonic; however, an igneous contact between the Massive Member and the Ingwe Meta - Mafic Cumulate Formation (Plate. 2.5 e) indicates that the two lithologies are related by crystal settling within a magma chamber.

Mafic Sheeted Dyke complex.

In Troodos this complex comprises essentially 100 %, parallel sided, 5 cm - 5 m thick, dolerite dyke swarms which act as feeders for the overlying pillows and volcanics and extend down into the underlying gabbro. The Mbizi Sheeted Dyke Formation comprises amygdaloidal and non - amygdaloidal, parallel sided, upto 50 cm thick, meta - doleritic rocks. The parallel nature of the dykes and the textural preservation of relict chilled margins suggests that this is a dyke complex. No oblique to orthogonal cross cutting relations are observed suggesting that the dykes were fed parallel to the dyke margins and thus do not represent a sill complex.

Mafic Volcanic complex.

This complex is characterised by mafic pillow basalts, massive flows, thin sheet flows, breccias and hyaloclastites (Coleman, 1977). Within the Troodos

Ophiolite, the pillow basalts have been commonly divided into two groups (Upper and Lower Pillow Lavas), based on their original igneous mineralogy and composition (Geological Survey Department Nicosia, 1987). The Upper Pillow Lavas are dominantly olivine and pyroxene - phyric with picritic zones while the Lower Pillow Lavas are dominated by aphyric oversaturated basaltic lavas. Since the Maunde Ophiolite Group has been metamorphosed and the original igneous mineralogy altered the sub - division of any of the possible correlative formations of this group based on this principle is unfeasible. The Basal Group of the Troodos Ophiolite lithostratigraphy is characterised as a mixed, transition group comprising both sheeted dykes and pillow lavas.

The Mvuu Meta - Mafic Volcanic Formation is characterised by deformed, massive and pillowed meta - basalts. The presence of the Pillowed Member is direct evidence for subaqueous volcanic eruption and thus the extrusive nature of at least part of this formation. The Massive Member is mineralogically and texturally homogeneous throughout the formation. This is due in part to deformation (section 5.4) but possibly reflects its original igneous nature. This member represents a series of massive or thin sheet flows. The relatively minor proportion of pillow lavas compared to massive meta - basalts within this formation is a reflection of both deformation and the limited extent of outcrop.

Sediments

The overlying sedimentary succession as defined at the Penrose Conference should typically include ribbon cherts, thin shale interbeds and minor limestones (Coleman, 1977). In reality, the make up of the overlying sedimentary succession will depend on the tectonic setting of the ophiolite. If the ophiolite represents oceanic crust formed at mid ocean ridges, i.e., below the carbonate compensation depth, then ribbon cherts will be predominant.

The interpretation of most modern ophiolite analogues suggest that they have formed within a back arc spreading ridge (Wilson, 1989) and are thus characterised by relatively shallow water sediments. The Troodos ophiolite is overlain by thin, lenticular umbers and a thick succession of chalk and limestones (Geological Survey Department Nicosia, 1987).

The meta - sedimentary Nzou Meta - Greywacke Formation is characterised by pelitic and semi - pelitic lithologies indicating a dominant, terrestrial derived input to the original sedimentary system. The presence of calcite suggets that deposition was not below the carbonate compensation depth indicating a shallow water origin analogous to deposition within a back arc rather than a mid ocean ridge setting.

In comparing the lithostratigraphy of typical ophiolites (Anon, 1972) with the Maunde Ophiolite Group, a direct comparison with ophiolites can be made. The term ophiolite, defined during the Penrose Conference, indicates that it is the distinctive assemblage of the mafic to ultramafic rocks which define an ophiolite and not the presence of one or a few members of the ophiolite assemblage. Every complex of the ophiolitic assemblage can be correlated with a Maunde Ophiolite Group formation. Although tectonised, the order of the formations within the type section (Fig. 2.3) are such that the base to top order of the ophiolite stratigraphy has been preserved. These observations altogether suggest that the Maunde Ophiolite Group, although metamorphosed and deformed, represents a dismembered ophiolite complex.

2.3 The Kaourera Island - Arc Group

The Kaourera Island - Arc Group consists of a series of meta - volcanic and meta - pelitic rocks which comprise the majority of the Ophiolite Terrane. The greatest diversity of formations within this group crop out along the Kaourera

River between MR [9175 3760] and MR [8992 3685] and although this section does not contain all of the Kaourera Island - Arc Group formations, it is classified as the type section. A lack of way - up structures and possible repetition of lithologies by thrusting make it difficult to interpret the way - up and relative ages of formations within the group. It is also possible that lithologies are repeated within the primary igneous stratigraphy. Formations within this group are based on composition and therefore rock units belonging to the same formation within different parts of the section are not necessarily identical in age.

2.3.1 Nhema Amphibolite Formation.

This formation predominates within the type section at MR [9164 3700] and is repeated many times within the sequence. Due to a lack of outcrop, it is unclear as to whether this repetition is due to thrusting or whether it represents an original igneous stratigraphy. The formation is between 25 and 150 m in thickness.

Biotite Member.

The type locality of this member is at MR [9164 3700] at the base of the informally named Nhema Stream, where it crops out as a darkly coloured, fine grained, texturally homogeneous, biotite rich rock (Plate. 2.7 b). The specimen is dominated by elongate, parallel, upto 1 mm long biotite crystals which envelop less than 1 mm long lenses of quartz and plagioclase. Epidote and opaque metallic minerals are less than 0.5 mm diameter, irregular and randomly distributed within both the biotite rich and quartz and plagioclase rich portions (specimen [SJ 219] and Appendix B). The alignment of the platy minerals define a strong, planar, tectonic fabric (section 5.4).

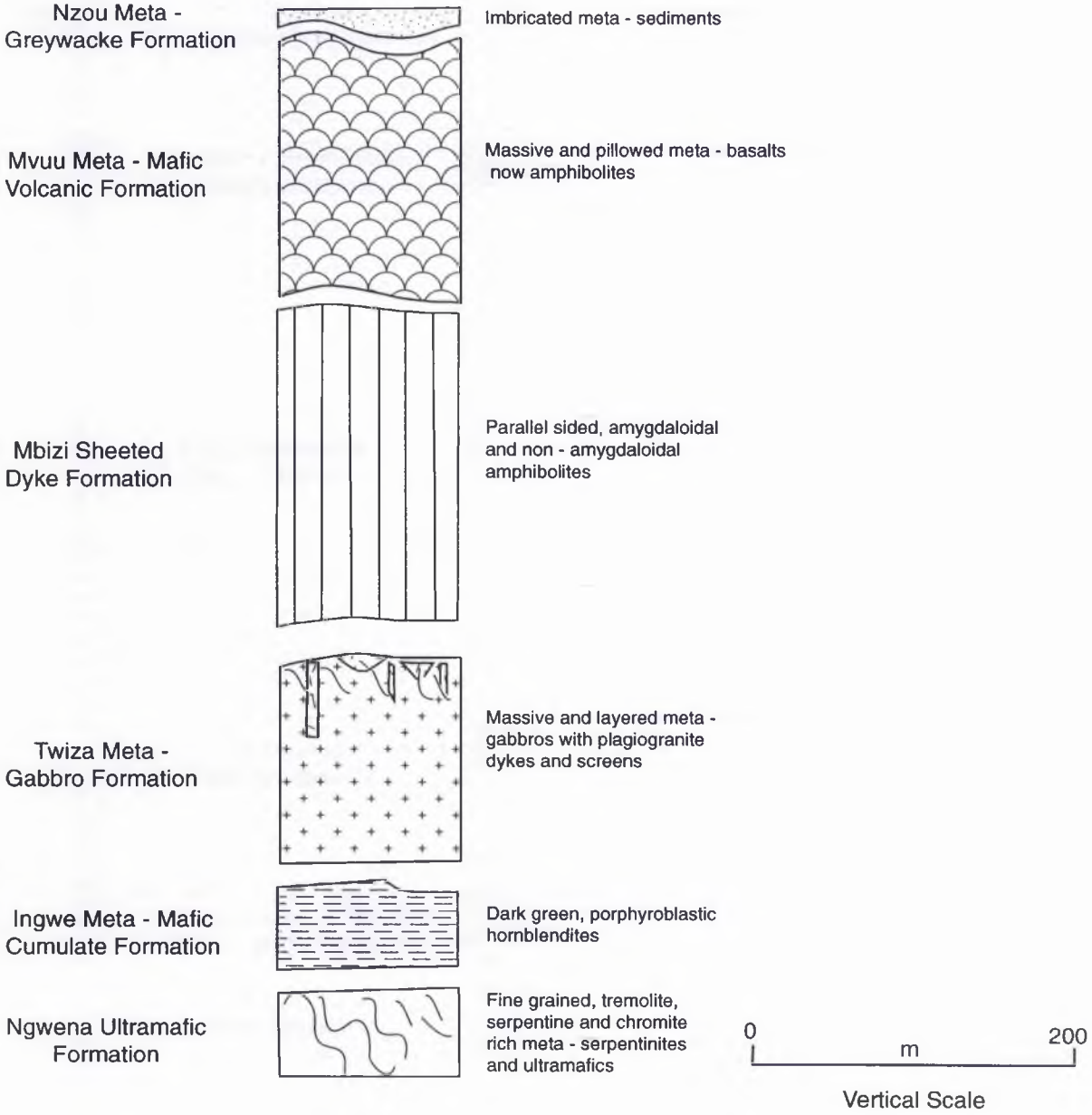

Fig. 2.3 Reconstructed lithostratigraphic section through the Maunde Ophiolite Group. Compare this figure with the lithostratigraphic section of the Troodos Ophiolite in Fig. 2.2.

Garnet Member.

The type locality of this member is at MR [9161 3732] where it crops out as a darkly coloured, fine grained biotite - and garnet - rich rock. The garnet porphyroblasts are upto 4 mm diameter, randomly distributed and comprise upto 10 % of the total rock volume. The matrix is dominated by less than 1 mm long, tabular biotite and chlorite plates which wrap around the garnet porphyroblasts and millimetre scale lenses of plagioclase and quartz. Epidote forms predominantly euhedral, upto 0.5 mm long, tabular crystals (specimen [SJ 110] and Appendix B) which are aligned parallel to the tectonic fabric (section 5.4).

Granular Textured Member.

This member outcrops within the type section at MR [9125 3730] as a dark green, granular textured rock comprising upto 4 mm diameter, spherical, hornblende porphyroblasts, which comprises upto 70 % of the rock (Plate. 2.7 c). The porphyroblasts are evenly distributed and generally do not touch and contain fine grained, randomly distributed inclusions of epidote and plagioclase. They are separated by a pale yellow to white, fine grained matrix which is comprised of less than 0.5 mm long, tabular hornblende crystals and an anhedral, granoblastic aggregation of fine grained quartz and plagioclase (specimen [SJ 287] and Appendix B). The hornblende laths are aligned to form a tectonic fabric (section 5.4).

The Biotite Member predominates in this formation. The Garnet and Granular Textured Members crop out as small, rare, isolated outcrops surrounded by the Biotite Member. Unfortunately no direct contacts have been observed and thus it is unclear whether they share primary or tectonic contacts.

2.3.2 Bere Amphibolite Formation.

The type locality of this formation begins at MR [9133 3739] where it crops out at the base of the informally named Bere Stream. Like the Nhema Amphibolite Formation this lithology is repeated many times within the section. Thicknesses range from 20 to 150 m. The contacts with other lithologies are obscured and it is unclear whether this formation is in igneous or tectonic contact with the other formations.

This lithology is fine grained, displays a distinctive pale green colour and contains a weak tectonic foliation. The specimen contains upto 20 %, irregular shaped, oblate, upto 15 mm long, white and pale yellow epidote and quartz filled amygdales (Plate. 2.7 d) indicating an igneous origin. The amygdales are randomly distributed throughout the member. The matrix is comprised of very fine grained epidote and hornblende. The epidote predominates as less than 0.1 mm diameter, equigranular grains whilst the hornblende occurs as randomly oriented and distributed, less than 0.5 mm long tabular crystals. The irregular shaped amygdales are comprised of both granoblastic, 1 mm diameter quartz crystals and upto 3 mm long, radially arranged epidote crystals (specimen [SJ 285] and Appendix B).

2.3.3 Gondo Meta - Felsic Volcanic Formation.

The type locality of this formation begins at MR [9116 3723] where it crops out at the base of the informally named Gondo Stream. Again this formation is repeated many times within the section. Lithological thicknesses range from 25 to 100 m.

Mharapara Member

This member is the predominant lithology within this formation. The type locality is at MR [9116 3723] where it is very fine grained (less than 0.1 mm diameter) and pale grey in colour. It is comprised predominantly of very fine

grained quartz and plagioclase but also contains rare, upto 2 mm in length, euhedral, tabular, simple twinned plagioclase crystals which are oriented sub - parallel with the tectonic foliation (section 5.4). These randomly distributed crystals contain abundant epidote inclusions. The margins display minor subgrain development and grain size reduction. They are interpreted as relict, igneous phenocrysts. Muscovite and biotite comprise less than 15 % of the specimen, are evenly distributed, tabular, less than 0.5 mm long and are aligned to producing a weakly developed tectonic fabric (sample [SJ 226] and Appendix B). Centimetre scale colour variations due to a variation in proportion of plagioclase within the matrix gives the specimen a banded appearance in hand specimen (Plate. 2.7 e).

Gora Member.

The type locality is at MR [9143 3714] where it crops near the base of the informally named Gora Stream. This formation has only been mapped at the type locality but due to its distinctive lithology and texture its has been classified as a formation. The unit thickness is less than 25 m. It is unclear as to whether this formation is in tectonic or igneous contact with the surrounding Nhema Amphibolite Formation.

At the type locality, this member crops out as four, 1 to 1.5 m wide bodies which display convex tops and concave bases which are interpreted to be pillow lavas (Plate. 2.7 f) indicating the extrusive igneous nature of this formation. The rock is pale yellow, fine grained and contains dark green, upto 2 mm long, tabular hornblende which is randomly distributed and moderately aligned forming a weak tectonic fabric (section 5.4). The hornblende laths comprises upto 15 % of the specimen. The matrix is predominated by equigranular, granoblastic quartz and plagioclase with minor, fine grained and irregular shaped epidote and opaque metallic minerals (specimen [SJ 229] and Appendix B).

Fura Member.

The type locality of this member is at MR [9163 3740] where it crops out near the base of the informally named Fura Stream. This formation has only been mapped at the type locality but due to its distinct lithology it has been classified as a formation. The unit thickness is less than 10 m. It is unclear as to whether the formation is in tectonic or igneous contact with the surrounding Nhema Amphibolite Formation.

This member is very fine grained, pale cream to yellow in colour, displays a concoidal fracture when broken and is banded on a millimetre scale. The bands are defined by a variation in colour (pale pastel yellows and creams) are parallel and are laterally non - persistent (Plate. 2.8 a). A penetrative tectonic fabric is not evident within this member. Plagioclase dominates the assemblage but epidote, quartz, opaque minerals and biotite are also present (sample [SJ 220] and Appendix B). The millimetre scale banding is reflected by both a variable epidote content and plagioclase crystal size. The epidote occurs as very fine grained, less than 0.1 mm, equigranular crystals which are variably distributed. Epidote - rich bands contain upto 40% epidote while the epidote - poor bands contain only 15% . Where the epidote content is high, the grain size of the other minerals such as plagioclase and quartz is very small (less than 0.1 mm) and equigranular. Within the epidote poor bands, the grain size of the plagioclase laths range from 0.5 mm to 2 mm long and display no preferred orientation. Grain size reduction and change in epidote content at the margins of the bands is gradual over a distance of between 0.1 to 0.5 mm. Less than 0.1 mm long, tabular biotite laths are randomly distributed throughout the specimen and are weakly aligned with the banding.

2.3.4 Bhumi Semi - Pelite Formation.

This formation does not crop out in the type section along the Kaourera River. The type section is to the northwest, below the summit of the informally named Bhumi Hill (map insert 1a, b). Both top MR [9298 3880] and base boundaries MR [9310 3950] are interpreted to be tectonic in origin. The maximum thickness of the formation is approximately 100 m.

Coarse Member.

The type locality of this member is at MR [9280 3920] where it crops out within a small stream section as an isolated, 4 m wide, 5 m long outcrop. The specimen is a garnet rich semi - pelite. The garnet porphyroblasts are deep red, upto 10 mm in diameter, are randomly distributed and comprise upto 10 % of the specimen (Plate 2.8 b). The matrix is comprised predominantly of upto 2 mm long chlorite blades, quartz, plagioclase muscovite and opaque minerals (sample [SJ 370] and Appendix B). The quartz and plagioclase are concentrated within millimetre scale parallel but discontinuous bands which alternate with the phyllosilicate rich bands. A penetrative tectonic fabric which wraps around the individual garnet porphyroblasts pronounces this banding (section 5.4). No original sedimentary structures are evident.

Fine Member.

The type locality of this member is at MR [9380 3995]. This specimen is finer grained than the Coarse Member, is pale brown to beige in colour and dominated by quartz and muscovite (sample [SJ 378] and Appendix B). Garnet porphyroblasts are less than 0.5 mm in diameter, are randomly distributed and comprise less than 5 % of the specimen. Oriented muscovite laths with minor chlorite wrap around individual garnet porphyroblasts and quartz and plagioclase lenses producing a tectonic fabric (section 5.4).

The Coarse Member dominates the formation but is generally highly weathered, soft and thus poor in outcrop. The Fine Member only crops out at the type locality. It is difficult to tell whether the two members are in tectonic or stratigraphic contact since they are not seen within the same outcrop. The orientation of the banding and tectonic fabric is coherent between both outcrops suggesting that the Fine Member might represent a higher strain version of the Coarse Member.

2.3.5 Kamuyu Amphibolite Formation.

This formation comprises the majority of the Kaourera Island - Arc Group within the Kamuyu, Kanhungwa and Chitumbi regions. The type section is defined at MR [8195 3680]. The formation is predominated by the Banded Member which is repeated by ductile, shear dominated thrusting (section 5.4) to a maximum thickness of 3 km. The Calc - Silicate Member comprises a single outcrop of less than 1 m thick.

Banded Member.

The type locality is at MR [8195 3680] which outcrops below the summit of Kamuyu Hill. Within the Chitumbi region this member is interleaved with imbricate slices of the Gondo Meta - Felsic Volcanic Formation and granite gneisses of the Zambezi Terrane (Map insert 1a, b). Boundaries are interpreted to be tectonic (section 5.4).

This member is fine to medium grained, dark brown to black in colour and has a bimodal, banded appearance. The melanocratic bands predominate and are comprised of aligned, less than 1 mm long tabular hornblende laths, minor plagioclase, sphene, epidote, opaque minerals and very rarely biotite. The leucocratic bands are on average 1 to 2 mm thick, discontinuous and comprise upto 20 % of the total rock volume. Thicker (upto 5 mm thick) leucocratic bands are more laterally persistent (upto 5 m long). Equigranular,

granoblastic, plagioclase, quartz, epidote and minor hornblende is identified within these layers (sample [SJ 67] and Appendix B). The transition between the two mineralogically distinct bands is gradational with respect to mineral proportions rather than grain size. Although the leucocratic bands comprise only 20 % of the rock, their distribution may be either, equally spaced or more rarely, concentrated into banded leucocratic - rich layers (Plate 2.8 c) which may by upto 20 cm thick. Garnet porphyroblasts are very rarely evident, mainly as very small, less than 0.5 mm porphyroblasts which are invariably selvaged with plagioclase.

Calc - Silicate Member.

The type locality of this member is at MR [8221 3650] where it crops out as a less than 1m thick unit. Both boundaries are unexposed and the way up of the unit is unknown. The Banded Member occurs on either side of each boundary. The member is continuous along the length of the outcrop (*c.* 3m) but it is unclear whether the unit is lensoid or laterally continuous.

In hand specimen this member is predominantly leucocratic and contains aligned, lensoid aggregates of hornblende, garnet and epidote. The mafic aggregates are upto 20 mm long, 5 mm wide and comprise upto 25 % of the specimen. Garnet porphyroblasts are randomly distributed and range in size from 1 to 5 mm diameter. The leucocratic matrix is comprised of very fine grained (less than 0.1 mm) plagioclase and epidote (sample [SJ 134], Appendix B and D).

2.3.8 Discussion.

The Kaourera Island - Arc Group is compositionally very varied. It is comprised of meta - mafic, muscovite and biotite - rich meta - intermediate and quartz / plagioclase dominant lithologies. The amygdaloidal nature of the Bere Amphibolite Formation, the pillow lavas of the Gora Member and

the relict igneous plagioclase phenocrysts within the Mharapara Member all indicate the igneous and extrusive nature of some formations within this group. The presence of muscovite and biotite within these lithologies indicates that they are alkali enriched. Such a varied suite of alkalic, mafic to felsic igneous and extrusive lithologies can be found within an island arc environment. The comparison of this group to a suite of island arc rocks by lithology alone is inconclusive and thus analysis of the major and trace element geochemistry of this group is needed (section 3.3).

2.4 The Kadunguri Whiteschists

The Kadunguri Whiteschists are situated on the south - eastern margin of the Ophiolite Terrane and are characterised by compositionally restricted, high pressure metamorphosed lithologies which are dominated by either talc and kyanite, gedrite and kyanite or quartz and kyanite (Section 4.3.2). The whiteschists are centred on Kadunguri Hill, MR [9619 3498], after which they are named. The lack of primary sedimentary or igneous structures makes it difficult to interpret the way up of the units. It is unclear whether each unit is in tectonic or stratigraphic contact. All lithologies strike generally east to west and dip moderately toward the south (Map insert 3a, b). The lithologies will be described as a structural section from the structural base to top.

2.4.1 *Phlogopite Whiteschists.*

This formation crops out within the informally named Tsoko Stream. The type section is between MR [9625 3547] (base) and MR [9625 3519] (top). It occurs at the most northerly extent of the whiteschists and is at the structural base of the group where it is in tectonic contact with Kaourera Island - Arc Group meta - basalts (section 5.4). Outcrop of this lithology is extremely poor. Two varieties of Phlogopite Whiteschist have been identified, both of which

are characterised by quartz and kyanite dominant lithologies. The Talc - Phlogopite Whiteschist predominates with the Kyanite - Phlogopite Whiteschist being restricted to a single outcrop. The maximum thickness of the formation is 200 m.

Talc - Phlogopite Whiteschist.

The type locality for this member is at MR [9618 3532] where it is pale in colour, displays a granular texture and individual minerals are 2 to 3 mm in diameter. The specimen is dominated by equigranular quartz and pale green kyanite crystals which are tabular, upto 2 cm long but on average 1 cm long, are randomly oriented and distributed. Dravite occurs as a deep red, irregular shaped, 1 to 10 mm diameter, randomly distributed minor phase along with irregular shaped, upto 1 cm long hematite crystals. Phlogopite and talc blades occurs between the quartz grains (sample [SJ 479], Appendix B). They are weakly aligned to produce a weak foliation.

Kyanite - Phlogopite Whiteschist.

At MR [9654 3531], a very coarse grained quartz and kyanite rock crops out. It is comprised of irregular shaped quartz crystals upto 2 cm diameter and elongate, acicularly arranged, green kyanite crystals which reach upto 50 cm in length. The kyanite crystals comprise roughly 40 % of the member and are randomly distributed throughout the outcrop (Plate 2.8 d).

2.4.2 *Quartz - Whiteschists.*

The type section for these whiteschists are at MR [9657 3529] (base) and MR [9685 3482] (top) and centred on the informally named Shamwari Stream which runs off the northern side of Kadunguri Hill toward the east. The lithology is dominated by the Quartz - Whiteschists (Unfoliated), (Map insert 3a, b). The maximum thickness of this formation is 1 km.

Quartz - Whiteschists (Foliated).

The type locality for this unit is at MR [9675 3492] where it crops out as a white, very soft, soapy, foliated but weakly lineated rock which is comprised predominantly of aligned talc laths which gives the rock a schistose fabric (Plate. 2.8 e). Randomly distributed within this talc dominant rock are less than 0.5 mm long kyanite laths which are aligned parallel to the fabric, 1 to 2 mm granular quartz, less than 1 mm diameter, semi - spherical dravite and minor, irregular shaped sometimes elongate, hematite crystals (sample [SJ 124] and Appendix B), which are oriented parallel to the foliation. The tectonic foliation is nearly always crenulated and occasionally a transposed crenulation cleavage is evident. A tectonic lineation is rare but when present is defined by quartz aggregates and the alignment of the long axis of elongate minerals. No chlorite has been identified within this member.

Quartz - Whiteschists (Unfoliated).

This unit has a large outcrop extent (map insert 3a, b) and is texturally and mineralogically homogeneous throughout. The type locality is MR [9664 3492]. This unit is again white in colour but has a granular appearance with individual minerals upto 2 to 3 mm diameter. On inspection of the mineralogy, talc, quartz, kyanite, hematite and dravite are once again evident (sample [SJ 482] and Appendix B). The talc crystals are tabular, generally less than 0.5 mm long, and randomly distributed throughout the specimen. The dravite and hematite are both upto 1.5 mm diameter, randomly oriented and irregularly shaped, while the quartz crystals are irregular shaped but upto 3 mm diameter. The kyanite is semi - tabular, less than 0.5 mm long and is randomly oriented and distributed. The slightly coarser grained nature of and the random orientation of all of the minerals is responsible for the specimens granular appearance. No chlorite has been identified within this specimen.

2.4.3 *Yoderite Whiteschist.*

This unit crops out at a single locality (MR [9662 3494]) as many small (< 35 cm), scattered, in - situ blocks within a 12 x 3 m area, roughly defining an ellipsoid pod (Fig. 2.4). The lithology is very coarse grained with individual minerals upto 4 cm long which are randomly oriented. Chlorite dominates the assemblage as upto 2 cm diameter, randomly oriented plates which occur in stable contact with upto 1 mm long, tabular talc laths. Pale blue to green kyanite crystals are arranged in radiating masses, often upto 4 cm long; hematite forms large (upto 2.5 cm), euhedral, tabular to hexagonal crystals which aggregate together into randomly oriented clusters of upto 5 cm diameter. Dravite occurs as upto 1 cm diameter, ruby red, irregular shaped masses and an interstitial, pale green, less than 5 mm diameter mineral which all occur randomly distributed and oriented throughout the specimen (sample [SJ 128], Appendix B, C and D) (Plate. 2.9). No quartz has been identified either as individual crystals or as inclusions within other minerals. This is the second occurrence in nature of the mineral yoderite

2.4.4 *Gedrite Whiteschist*

The type locality of this unit is at MR [9652 3439]. This litholohy is bimodal in terms of its mineralogy and textures. The main portion is pale blue to pale green in colour, very fine grained and contains radially arranged, acicular, upto 2 cm long, pale yellow gedrite porphyroblasts (Plate. 2.10 c). The pale blue matrix contains a fine grained (less than 0.5 mm), granoblastic, equigranular assemblage of kyanite, quartz and gedrite and upto 1 mm diameter, deep red, randomly distributed dravite crystals (specimen [SJ 125] and Appendix B, C and D). The acicular gedrite porphyroblasts comprise upto 60 % of this portion. The minor portion is comprised of very fine grained, equigranular hematite, quartz and kyanite which occur as millimetre to decimetre scale, parallel bands. These bands comprise upto 60 % of the

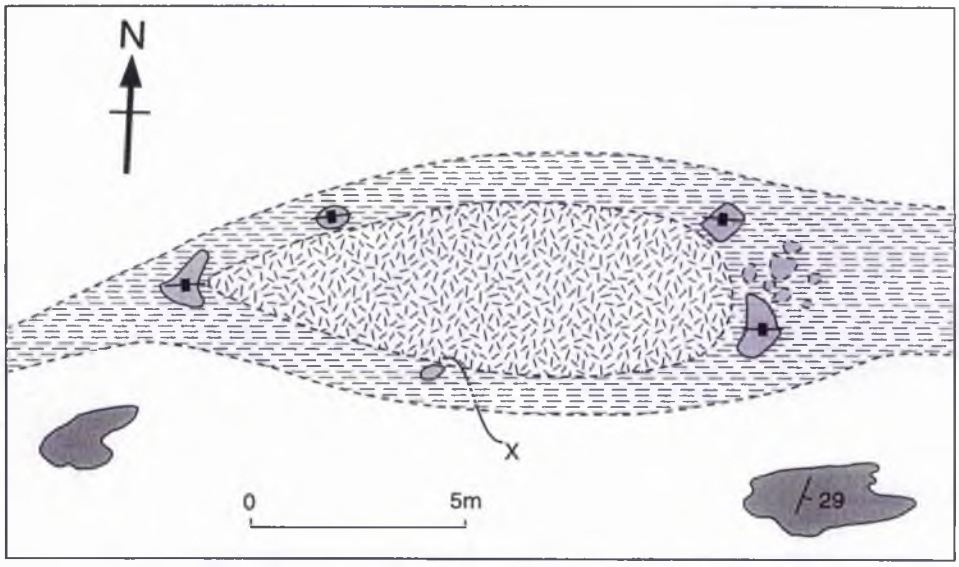

Quartz Whiteschist (Foliated). Fine grained, talc + kyanite + quartz rocks. Strong foliation and lineation to the north of the yoderite - bearing pod, grading into random fabrics 5 - 10m south of the pod. Shaded areas represent outcrop.

Quartz - Hematite Sheets. Contains parallel sided, steeply oriented quartz + hematite veins >1 cm wide, giving the unit a banded appearance. Banding is parallel to the long axis of the yoderite - bearing pod. Shaded areas represent: (solid lines) - outcrop and (dashed lines) - float.

Yoderite Whiteschist. Mineral phases are coarse grained and randomly oriented.

S1 foliation.

Trend of vertical/steep quartz + hematite banding.

Fig. 2.4 Sketch map of the Yoderite Whiteschist and surrounding lithologies. The Yoderite Whiteschist occurs as many small (<35 cm) scattered blocks within the ellipsoid region. Position X marks a small exposure where the boundary between the Yoderite Whiteschist and the Quartz - Hematite Sheets can be pinpointed to within 20 cm. Sample [SJ 128] was collected from the centre of the area.

specimen but on average comprise only 30 % (Plate. 2.10 d). The kyanite crystals are tabular, less than 0.5 mm long and aligned parallel to the margins of the body, although this does not impart a tectonic fabric on this portion. The margins of both portions, texturally and mineralogically grade into one another over a distance of 1 to 2 mm. In a rare occurrence at MR [9579 3348] the banded portion of this unit is not evident (Plate. 2.10 c). The banding is continuous on the metre scale.

2.4.5 *Minor Lithologies.*

Quartz - Hematite Sheets.

This unit crops out as a 1 to 5 m thick band that surrounds the Yoderite Whiteschist and separates the Foliated from the Unfoliated Qtz Whiteschists. Exposure of this lithology is extremely poor and encountered mainly as float. The type locality is at MR [9634 3510]. This unit is bimodal in appearance. The main body is fine grained, dark grey in colour and equigranular. The specimen contains an equal proportion of less than 0.5 mm diameter, quartz and hematite with minor, very fine grained, randomly oriented, tabular, less than 0.5 mm long kyanite laths. This body is cross cut by predominantly parallel sided, coarse grained, semi continuous bands of hematite and quartz or hematite, quartz and kyanite. These bands can comprise upto 50 % of the total rock volume. Individual hematite crystals are tabular and can be upto 8 cm long but are on average 1 to 2 cm long. The quartz and kyanite crystals are generally anhedral with a maximum size of 1 cm (Plate. 2.8 f). At one locality, MR [9662 3494] the coarse hematite, quartz and kyanite banding takes the form of an anastamosing network suggesting that this is not a primary igneous or sedimentary feature (Plate. 2.10 a) but possibly of metasomatic origin (section 4.2).

Qtz - Dravite Sheets.

This lithology is restricted in outcrop. The type is at MR [9643 3436] where it crops out as metre scale, lenses within the Unfoliated Qtz - Whiteschists. Large, upto 6 cm long, sub - tabular, deep red, randomly oriented and distributed dravite crystals are common (Plate. 2.10 b). The lenses are highly fractured and annealed with quartz and pale grey chlorite.

Qtz - Hematite Sheets.

At MR [9582 3322] the Gedrite Whiteschist is cut by many cross cutting, 1 to 5 cm thick quartz rich bands. The individual quartz crystals are irregular in shape, very coarse grained (upto 4 cm) and highly fractured. Tabular, upto 8 cm long hematite crystals are randomly oriented and distributed throughout this member (Plate. 2.10 e). Contacts with the Gedrite Whiteschist are sharp and although these bands are not parallel, most are straight and continuous on the decimetre scale.

The Foliated Quartz Whiteschists crop out at the northern extent of the formation and contains a tectonic foliation and weak lineation. These aligned tectonic fabrics grade over a distance of 10 to 20 m, into the random fabrics of the Unfoliated Quartz Whiteschists. Along this 10 to 20 m thick zone occurs a discontinuous train of metre scale lenses of the Qtz - Hematite Sheets. Unfortunately outcrop is poor and no actual contacts between any lithologies are visible. The Yoderite Whiteschist also crops out within this zone and itself is surrounded by the Qtz - Hematite Sheets. In - situ outcrops of this unit in this contact zone are rare but a small exposure on the southern margin pinpoints the boundary of the Yoderite Whiteschist and the Qtz - Hematite Sheets to within 20 cm (Fig. 2.4). Neither unit changes in character towards this contact, and the examination of nearby float, suggests that, both rock types are discrete members and do not texturally or mineralogically grade into one another.

The margins of the Qtz - Dravite Sheets are once again poorly exposed. The mineral composition and lack of any strong tectonic features in the adjacent areas surrounding this unit suggests that this unit may be metasomatic in origin (section 4.3.2).

2.4.6 *Discussion.*

The Kadunguri Whiteschists are characterised by a very restricted mineralogy, including talc, kyanite, dravite, hematite and either quartz or chlorite. The outcrop within this area is poor and relationship of the formations which each other is thus poorly understood. They may be either in tectonic contact or may represent an original sedimentary or layered igneous stratigraphic succession (section 5.4).

The presence of talc and kyanite together in chemical equilibrium within the same rock assemblage, was first recognised by Schreyer in 1973 who termed this assemblage 'whiteschist'. This assemblage is restricted to rocks with an unusual bulk chemistry (Schreyer, 1977) consisting of only MgO - Al_2O_3 - SiO_2 - Fe_2O_3 and H_2O (section 4.3.2). The origin of such chemically restricted rocks is still unclear (Fockenburg & Schreyer, 1994; McKie, 1959; Vrána & Barr, 1972; Bodenlos, 1955 and Johnson & Oliver, 1998) and the discrimination of their origin from the lithostratigraphy alone is difficult. Talc and kyanite, along with dravite, hematite and / or chlorite, volumetrically comprise the majority of the Shamwari and Tsoko Formations which themselves, volumetrically dominate the group. In terms of square kilometres, the outcrop extent of the Kadunguri 'whiteschist' Group is in the order of 3 km^2 (map insert 1a, b). However, interpretation of aeromagnetic maps (Anon, 1992) indicates that this group continues under the Karoo cover with an extent near 10 km^2. Since most whiteschist occurrences are restricted to sedimentary horizons such as those of Sar e Sang in Afghanistan (Kulke & Schreyer, 1973) or as localised outcrops such as those in Zambia (Vrána &

Barr, 1972), the Kadunguri Whiteschists is perhaps the largest outcrop of 'whiteschist' anywhere in the world.

The second natural occurrence of the mineral yoderite within the Yoderite Member of the Shamwari Group also indicates that this member is of an unusual bulk chemistry. It is a metamorphic indicator of high pressure and moderate temperature (Fockenburg & Schreyer, 1994), both of these points will be pursued in chapter 4.

2.5 The Kanhungwa Gneisses

The Kanhungwa Gneisses are named after Kanhungwa Hill (MR [8510 3690]) where this lithology was studied and contains all of the rocks studied within the Zambezi Terrane. It is characterised by granitic augen gneisses with very minor, smaller scale, laterally discontinuous, granitic members. Since there is a lack of map scale variations and that these units belong to a separate tectono - metamorphic terrane to the Ophiolite Terrane all of the rocks are classified into a single mapping unit.

Augen Gneiss.

This lithology volumetrically comprises 99.9 % of the mapping unit. The type locality starts at MR [8555 3725]. Throughout the region it is mineralogically very homogeneous and varies only slightly in its texture. The lithology is very coarse grained and displays an augen gneissic texture. Upto 60 % of the total rock volume is comprised of augens, 80 % of which are pale pink in colour, range in size between 1 to 10 cm in length, are generally tabular in shape and are comprised of potassic feldspar (Plate. 2.11 a). Dimensions of the feldspar augens are generally prolate with x : y : z dimensions ranging between 1 : 3 : 5 and 1 : 2 : 8 but at MR [8495 3650] an L tectonite with dimensions of 1 : 1 : 25 was observed. Minor, pale cream and colourless plagioclase and quartz

augens are also evident. The matrix is dark, coarse grained, biotite rich with minor plagioclase, muscovite, tourmaline and quartz. Alignment of the biotites produce a crude tectonic fabric which wrap around individual feldspar augens. Elongation and recrystallisation of the feldspar augens and the aggregation of quartz into ribbon grains defines a tectonic lineation. Textural variations are due to the volumetric proportion and the x : y : z dimensions of the feldspar augens. In one extreme this unit can comprise upto 60 % augens with dimensions ranging from 1 to 10 cm in length and x : y : z ratios of 1 : 3 : 5, while in the other can comprise less than 50 % augens, range in size from 0.5 to 4 cm in length with x : y : z ratios of 1 : 2 : 8. All the intermediate variations exist.

Ultramyolinite Gneiss.

This unit is very limited in extent of outcrop but is best observed at its type locality along the Maunde River at MR [9104 3757]. The unit is extremely fine grained, pale pink to yellow in colour, very hard and breaks with a concoidal fracture (Plate. 2.11 b). Very fine grained microcline, plagioclase, biotite, muscovite and quartz are present (specimen [SJ 107] and Appendix B). Millimetre scale bands of monomineralic microcline or plagioclase and quartz produce colour variations which describe parallel and semi - continuous bands (upto 15 cm long) in outcrop.

Aplites.

This unit crops out at MR [8080 3725] as three, 5 to 60 cm thick, fine grained, foliated and lineated, meta - aplitic intrusions. The units are leucocratic, with individual granoblastic minerals of microcline, plagioclase, quartz, biotite and muscovite occurring upto 2 to 3 mm in length. All the minerals are oblate and aligned to produce a foliation which is at an angle to the margins of each body. A weak lineation is produced by the alignment of quartz rods and

recrystallised feldspar. These units occur within the Augen Gneiss Member where contacts between the two are sharp (Plate. 2.11 c). There is an immediate reduction in grain size and change in mineralogical proportions at contacts between the two.

Tonalite Gneiss.

This unit crops out at MR [8150 3840] as a 5 m diameter, pale cream, leucocratic, granular rock containing 10 mm long, irregular shaped, melanocratic lenses and 5 mm long lenses of fine grained, granular quartz (Plate. 2.11 d). The leucocratic portion is comprised of equigranular potassic feldspar with minor quartz and plagioclase. The melanocratic lenses which are moderately aligned to produce a poorly defined fabric, are comprised of tabular, aligned hornblende and less than 0.1 mm diameter, granular epidote crystals.

A lack of exposure at the margins of this body make it impossible to interpret whether it is tectonic or primary igneous in origin. The similarity in mineralogy in terms of the leucocratic portion may suggest that this is also felsic igneous body.

Discussion.

This mapping unit is characterised predominantly by a very coarse grained, potassic feldspar rich, leucocratic augen gneiss. The protolith was a potassic feldspar, megacrystic granite which has undergone a variable proportion of simple shear dominated deformation (see chapter 5). In fact such a rock has been described from the Zambezi Belt in Zambia by Hanson *et al.*, (1994) where it also crops out as a very coarse grained, potassic feldspar rich, augen gneiss.

The Ultramyolinite Gneiss is an extremely myolinitised version of the Augen Gneiss. At the type locality it crops out in juxtaposition with the High

Strain Member of the Twiza Meta - Gabbro Formation. The Maunde Ophiolite Group and the Kanhungwa Gneisses are interpreted to be allocthonous and thus this boundary is tectonic. When examining outcrops progressively away from this contact towards the Augen Gneiss, the progressive coarsening of augens is evident. Variations in augen size and dimensions might be interpreted to be strain related. The extreme grain size reduction is related to ductile deformation during the juxtaposition of the Maunde Ophiolite Group and the Kanhungwa Gneisses (section 5.4).

2.6 Conclusions

It is concluded that : -

1) the Maunde Ophiolite Group is comprised of a lithostratigraphy similar to that within Phanerozoic ophiolite complexes.

2) the Kaourera Island - Arc Group is comprised of a lithostratigraphy that is similar to that evident within island - arc complexes.

3) the Kadunguri Whiteschists are comprised of chemically and mineralogically restricted lithotypes of whiteschist compositions.

4) the Kanhungwa Gneisses of the Zambezi Terrane are comprised of granitic augen gneiss interpreted to represent variably deformed potassic, megacrystic granites.

Plate 2.1

a) Looking east. Compass clinometer is 10 cm long. At MR [9167 3765] the fine grained Grey Member of the Nzou Meta - Greywacke Formation is foliated and contains 0.5 to 1 cm long lenses of plagioclase and quartz. The lineation direction trends from left to right.

b) Looking south. Compass clinometer is 20 cm long. At MR [9167 3762] the Grey Member contains a strong lineation, here defined by the predominant quartz and plagioclase lenses.

c) Looking west. Pencil is 8 cm long. At MR [9170 3765] the Grey Member contained a 5 mm thick, disrupted band of metallic ore, which is coronered by a halo of green oxide (possible copper oxide).

d) North is to the top of the page. Pencil is 15 cm long. At MR [9167 3762] both the Dark (darker coloured band that trends from top right to bottom left) and Grey Members of the Nzou Meta - Greywacke Formation crop out. The foliation is parallel to the sharp and straight contacts between the two. The Dark Member contains upto 5 mm diameter quartz, muscovite and chlorite aggregates.

a)

b)

c)

d)

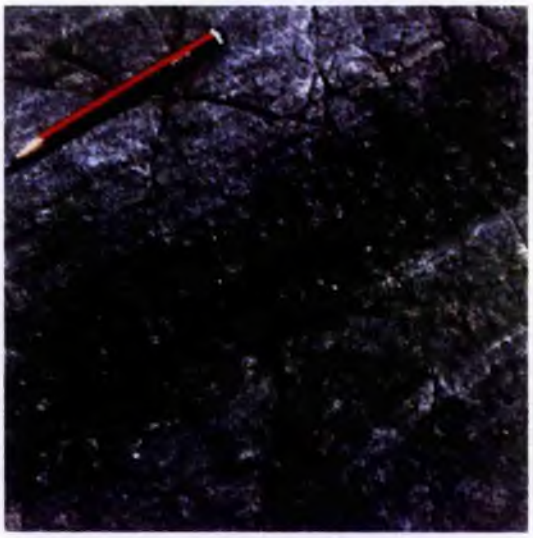

Plate 2.2

a) Looking south. Notebook is 20 cm in length. At MR [9165 3770] the south easterly dipping Massive Member is evident. Although mineralogically homogeneous a weak tectonic fabric and strong decimetre scale partings are evident.

b) Looking south. Hand lens is 6 cm in length. MR [9165 3770]. The base and top of each pillow is marked by a 20 to 60 mm thick, darkly coloured band. Both contain a poor foliation which is moderately developed within the underlying Massive Member.

c) Looking south. Width of view is roughly 45 cm. MR [9165 3770]. The Pillowed Member contains upto 30 % , pale yellow, epidote and plagioclase filled amygdales. In this example they are predominantly spherical and less than 5 mm diameter. The dark coloured selvage can be seen at the bottom left of the picture.

d) Looking south. Hand lens is 6 cm in length. MR [9165 3770]. In this example of the Pillowed Member the amygdales are more irregularly shaped and slightly flattened.

e) Looking north east. Pen is 15 cm long. At MR [9158 3779] the Amygdaloidal Member of the Mbizi Sheeted Dyke Formation crops out. These sheeted dykes contain upto 60 %, elongate leucocratic lenses. The main body is amphibolitic and contains a strong foliation and lineation.

f) Looking south east. Hammer is 50 cm long. At MR [9150 3780] the planar bounded Non - Amygdaloidal Member of the Mbizi Sheeted Dyke Formation crops out. The plate displays several planar bounded, parallel sided, 20 to 50 cm thick, dyke bodies trending from the top right to bottom left of the picture. The sheeted dyke margins are parallel and no cross - cutting features are evident.

a)

b)

c)

d)

e)

f)

Plate 2.3 : Looking south east. Width of view is roughly 12 metres. A photo montage and outline sketch of the Pillowed Member at MR [9165 3770]. Here five individual pillows are evident. The Massive Member (base of picture) dips toward the south east.

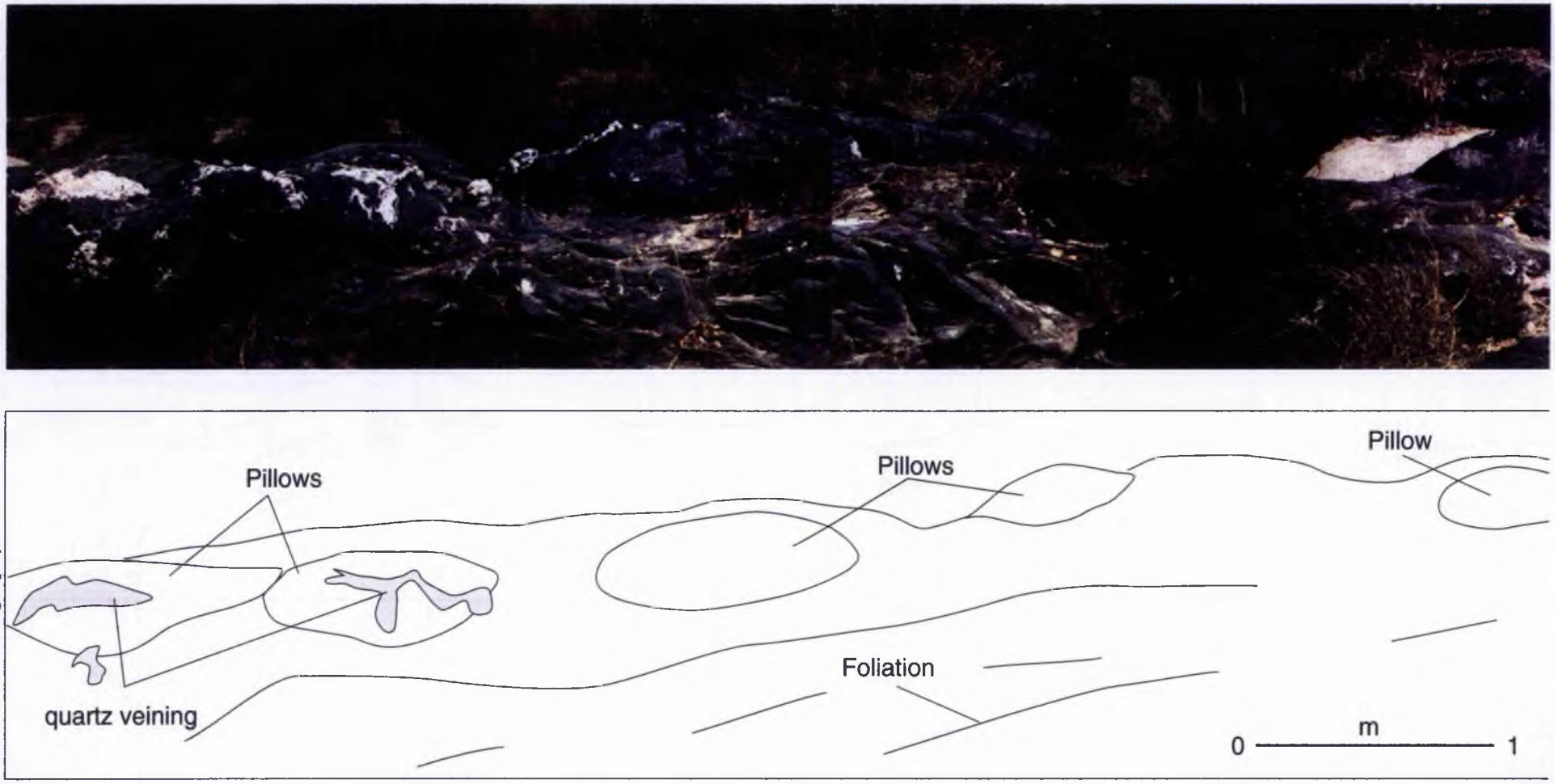
Pillows
Pillows
Pillow
quartz veining
Foliation
0
m
1

Plate 2.4

a) Looking north east. Hammer is 50 cm long. MR [9150 3780]. Close up view of the sharp contact between the fine and coarser grained units that comprise the sheeted dyke complex (Non - Amygdaloidal Member). A tectonic foliation is evident in both units, which is sub - parallel to the contact.

b) Looking north. Pencil is 7 cm long. MR [9150 3780]. Close up view of the contact between a fine and a medium grained dyke. The fine unit (on the left of the picture) is seen to gradually become finer over a distance of 10 mm, towards the medium unit, the contact of which is marked by the leucocratic vein.

c) Looking north east. Compass is 10 cm long. MR [9150 3780]. Sharp, straight contacts are evident between five, fine grained dykes within the sheeted dyke complex.

d) Looking north. Compass is 20 cm long. At MR [9117 3765] the Tremolite Member of the Ngwena Ultramafic Formation crops out. The member is pale grey, very fine grained, soft and weathers to smooth, rounded outcrops.

e) Looking east. Diameter of hand lens is 1.5 cm. At MR [9124 3786] the Tremolite Member contains upto 60 mm diameter 'books' of bottle green clinochlore which are randomly distributed and oriented within the outcrop.

f) Looking east. Hand lens is 3 cm long. Two metres to the west (left) of Plate 2.4 d, the Layered Tremolite Member is present. This has a similar field appearance to the Tremolite Member but contains less than 5 mm thick, lensoid aggregations of chromite (dark trains running top left to bottom right of picture).

a)

b)

c)

d)

e)

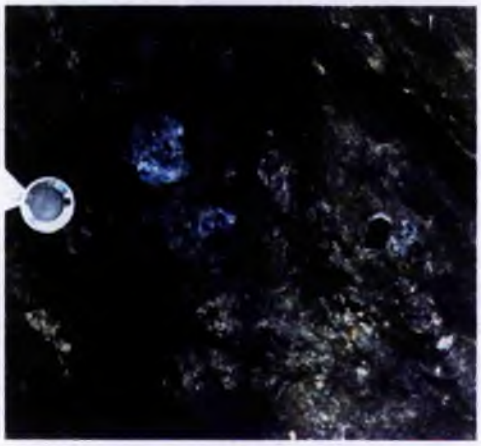

f)

Plate 2.5

a) Looking south west. Closed compass is 10 cm long. MR [9124 3786]. The fine grained, Serpentinite Member is evident. The compass is sitting on the contact between the serpentine rich Serpentinite Member and a 5 cm thick patch of white, granular, soft carbonate.

b) Looking south. Lens cap is 50 mm diameter. At MR [9116 3766] a 2 m diameter block of float (podiform lithotype) is comprised of a very fine grained, dark blue matrix, similar to the Serpentinite Member (Plate. 2.5 a) and upto 60 mm long lenses of chromite rich serpentine and tremolite. The pods are fractured and filled with talc (white mineral).

c) PPL sketch of micro - textures within the podiform lithotype of the Ngwena Ultramafic Formation. Note the tremolite porphyroblasts (Tr) with abundant chromite inclusions and the mantling tremolite and talc rims which are in optical continuity with the porphyroblasts which are interpreted to pseudomorph relict igneous clinopyroxene crystals. The interstitial areas are comprised of randomly oriented, very fine grained serpentine, which is cross - cut by randomly oriented trains of chromite. These serpentinite rich areas are interpreted to be relict olivine crystals. The line drawing is a sketch of the photomicrograph showing the boundaries of the original crystals. Scale bar is 2 mm in length.

d) Looking north west. Compass is 10 cm long. At MR [9114 3770] the Ingwe Meta - Mafic Cumulate Formation crops out. The formation is comprised of upto 5 mm diameter amphibole porphyroblasts. The plate shows a 20 cm thick band of coarse, 4mm diameter porphyroblasts which grade into the main body with 2 mm diameter porphyroblasts.

e) Looking east. Compass dial is 4 cm diameter. At MR [9115 3768] an imbricate slice containing the Ingwe Meta - Mafic Cumulate Formation (sample [SJ 213 Ha]) to the north west (top left of picture) and the Massive Member of the Twiza Meta - Gabbro Formation (sample [SJ 213 Hb]) to the south east (bottom right). The boundary is sharp (see text for details).

a)

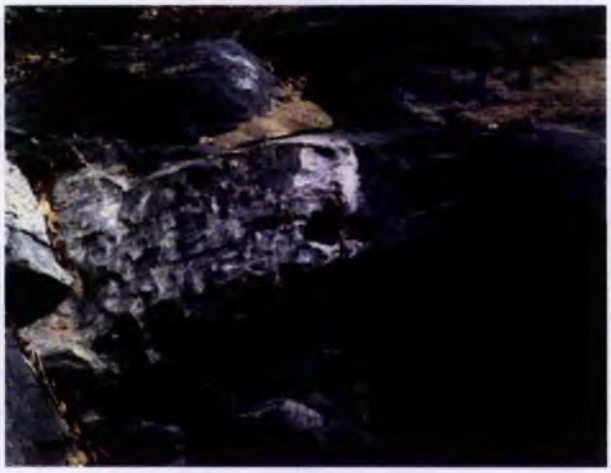

b)

c)

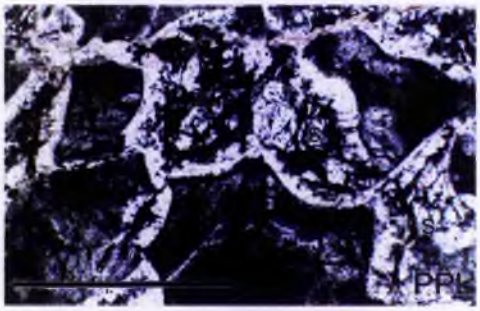

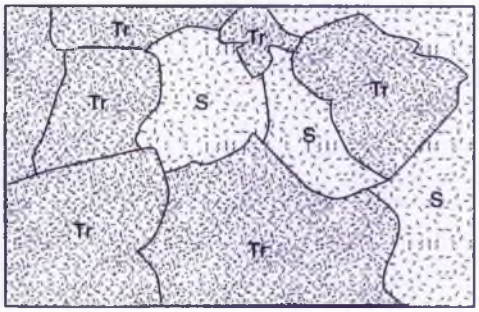

d)

e)

Plate 2.6

a) Looking north. Compass is 10 cm long. At MR [9010 3705] the Layered Member of the Twiza Meta - Gabbro Formation crops out. This member contains hornblende - rich (upto 90 %) bands upto 5 mm thick (top of outcrop) which are repeated several times within the outcrop.

b) Looking north west. Pencil is 10 cm long. At MR [8990 3687] the Layered Member of the Twiza Meta - Gabbro Formation crops out. Rhythmic layering, upto 10 cm thick is repeated several times within the outcrop.

c) Looking north. Compass is 10 cm long. At MR [9111 3771] the High Strain Member of the Twiza Meta - Gabbro Formation crops out. A coarser grained, leucocratic band cross cuts the tectonic fabric.

d) Looking north. Width of view is 2 metres. An overview of the High Strain Member of the Twiza Meta - Gabbro Formation at MR [9111 3771]. The fine grained portion is cut by continuous, upto 15 cm thick leucocratic coarser grained bands (right of picture) and discontinuous, boudinaged plagiogranite sheets (left of picture).

e) Looking north. Compass is 10 cm long. At MR [9105 3785] the High Strain Member of the Twiza Meta - Gabbro Formation contains upto 50 %, coarser grained material.

f) Looking west. Compass is 10 cm long. At MR [9111 3771] a 15 cm thick, foliation parallel, boudinaged, plagiogranite body crops out within the High Strain Member of the Twiza Meta - Gabbro Formation.

a)

b)

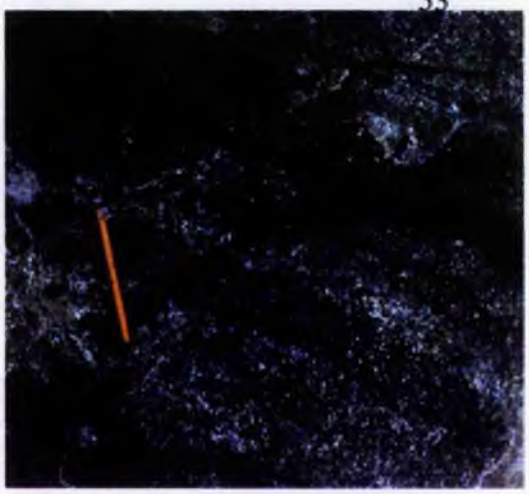

c)

d)

e)

f)

Plate 2.7

a) Looking north west. Width of view is 50 cm. At MR [8990 3687] a network of fine grained plagiogranite veins crops out within the Massive Member of the Twiza Meta - Gabbro Formation.

b) Looking north east. Hammer is 50 cm long. At MR [9164 3742] the Biotite Member of the Nhema Amphibolite Formation crops out. The member is darkly coloured, fine grained and contains a strong tectonic fabric. Minor leucocratic lenses and layers are sub - parallel to the fabric.

c) Looking east. Pencil is 8 cm long. At MR [9125 3730] the Granular Member of the Nhema Amphibolite Formation crops out. The member contains upto 70 %, 4 mm diameter, dark green hornblende porphyroblasts set within a leucocratic, quartz and plagioclase matrix.

d) Looking north. Pencil is 10 cm long. At MR [9133 3739] the Bere Amphibolite Formation crops out. The specimen is fine grained, green and contains 15 mm, oblate to irregular quartz and epidote filled amygdales.

e) Looking north east. Pencil is 8 cm long. At MR [9116 3723] the Mharapara Member of the Gondo Meta - Felsic Volcanic Formation crops out. The member is very fine grained, leucocratic and displays centimetre scale banding created by from the variable proportion of plagioclase within the matrix.

f) Looking south west. Width of view is 2 metres. At MR [9143 3714] the Gora Member of the Gondo Meta - Felsic Volcanic Formation crops out. The outcrop displays four leucocratic, pillow bodies.

a)

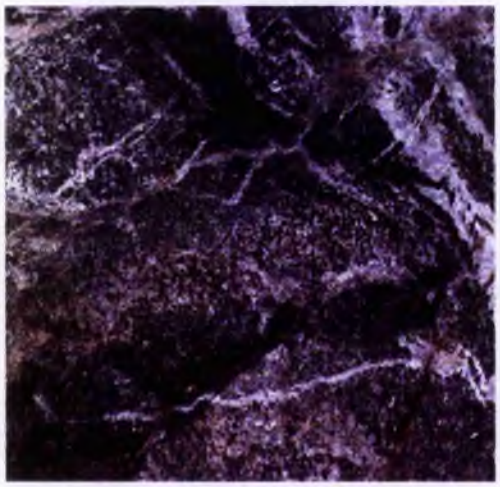

b)

c)

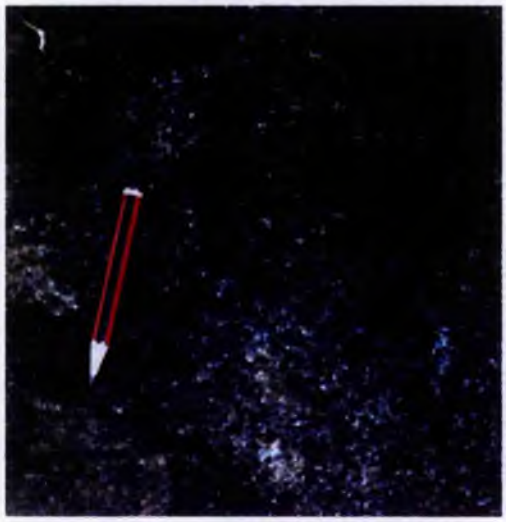

d)

e)

f)

Plate 2.8

a) Looking east. Compass is 10 cm long. At MR [9163 3740] the Fura Member of the Gondo Meta - Felsic Volcanic Formation crops out. This member is very fine grained, leucocratic and contains millimetre scale colour variations which define semi - continuous bands.

b) Looking north. Width of view is 1 metre. At MR [9280 3920] the Coarse Member of the Bhumi Semi - Pelite Formation crops out. The member is semi - pelitic in composition and contains upto 10 mm diameter, randomly distributed garnet porphyroblasts.

c) Looking north. The AK 47 attack rifle is 1 metre long. At MR [8195 3680] the Banded Member of the Kamuyu Amphibolite Formation crops out. The member is predominantly melanocratic but contains upto 20 %, 1 to 2 mm thick leucocratic bands that are parallel to the tectonic foliation.

d) Looking north. Pencil is 15 cm long. At MR [9654 3531] the Kyanite - Phlogopite Whiteschist crops out. Radially arranged, pale green, upto 50 cm long kyanite laths are randomly distributed within a coarse grained quartz matrix.

e) Looking north east. Lens cap is 50 mm in diameter. At MR [9654 3511] the Foliated Quartz Whiteschist Member crops out. The talc schist is crenulated. Randomly oriented, upto 5 cm long, pale blue tabular aggregates of kyanite overprints this fabric.

f) Looking north. Pencil is 10 cm long. At MR [9634 3510] Quartz - Hematite Bands crop out. Steeply oriented, parallel, coarse grained bands of hematite, kyanite and quartz cut through the main fine grained quartz and hematite body.

a)

b)

c)

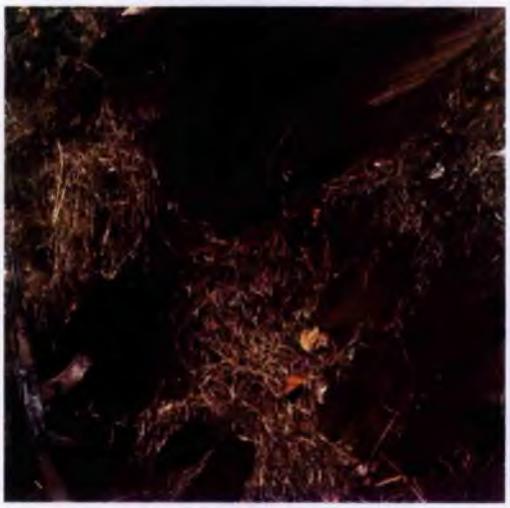

d)

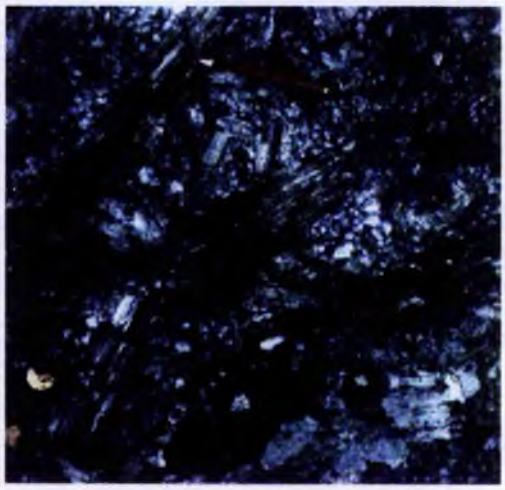

e)

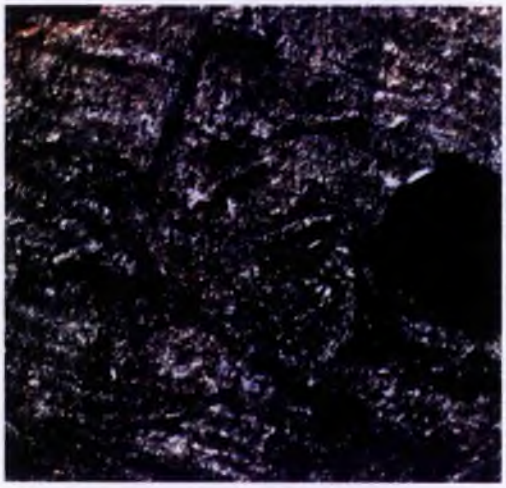

f)

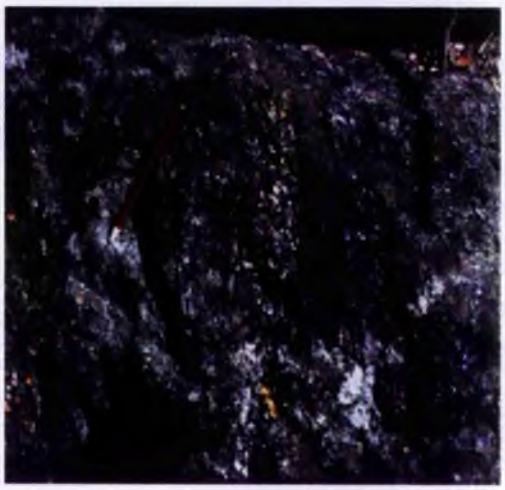

Plate. 2.9 : Photograph of thin section [SJ 128] Yoderite Whiteschist. Note the coarse grain size and random orientation of all mineral phases. The rock is comprised of chlorite (Chl), talc (Tlc), kyanite (Ky), yoderite (Y), hematite (Hem) and dravite (Dr). The positions of Plates. 4.1 a, c and d are illustrated. Scale bar is 5mm in length.

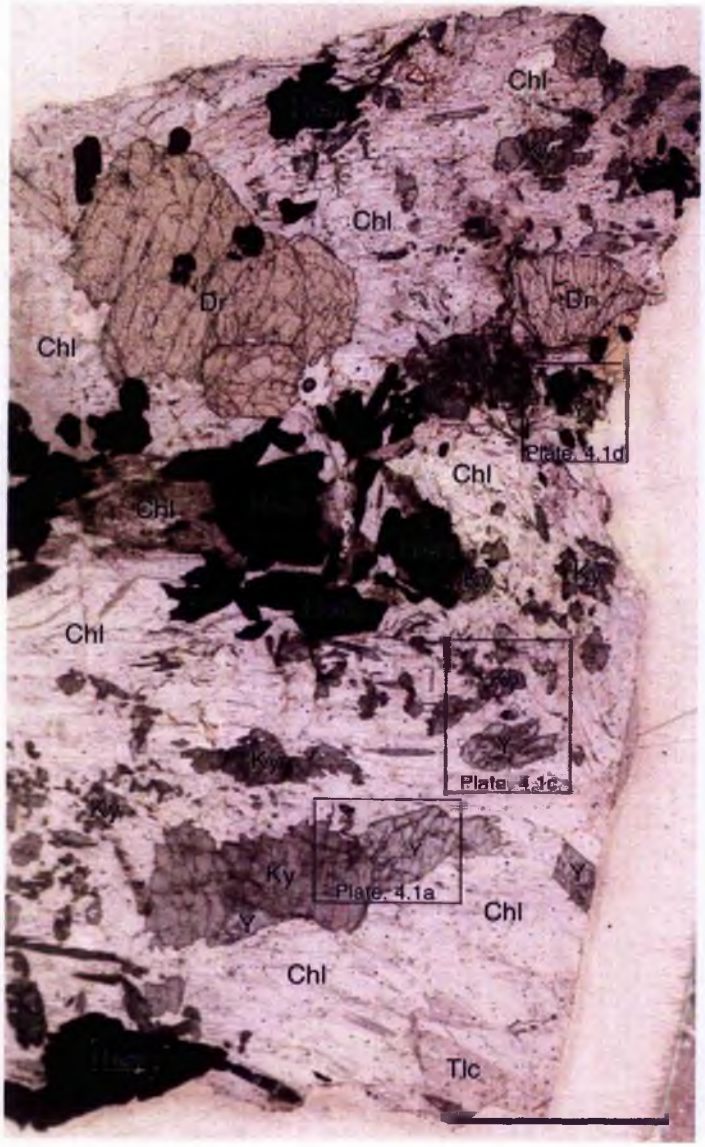
Chl
Chl
Dr
Dr
Chl
Plate 4.1d
Chl
Chl
Chl
Ky
Y
Plate 4.1c
Ky
Ky
Plate 4.1a
Y
Y
Chl
Chl
Tlc

Plate 2.10

a) Looking north. Pencil is 15 cm long. At MR [9662 3494] Quartz - Hematite Bands crop out. Coarse grained, hematite, quartz and kyanite (dark bands) form an anastamosing network of veins within the fine grained hematite and quartz main body.

b) Looking north. Pencil is 6 cm long. At MR [9643 3436] Quartz - Dravite Sheets crop out. It is comprised of quartz with upto 6 cm long, deep red, randomly distributed and oriented dravite crystals.

c) Looking north. Pencil is 6 cm long. At MR [9579 3348] the Gedrite Whiteschist crops out. The specimen is comprised predominantly of rosettes of acicular, radially arranged gedrite crystals. This specimen does not contain the quartz and hematite banding which is present at most other localities.

d) Looking north. Hammer is 50 cm long. At MR [9652 3439] Gedrite Whiteschist crops out. The outcrop is banded due to 1 to 30 cm thick, parallel bands of very fine grained quartz and hematite rock.

e) Looking north east. The pen is 15 cm long. At MR [9582 3322] the Quartz - Hematite Sheets crop out. The specimen contains quartz and upto 4 cm long, tabular, randomly oriented hematite crystals.

a)

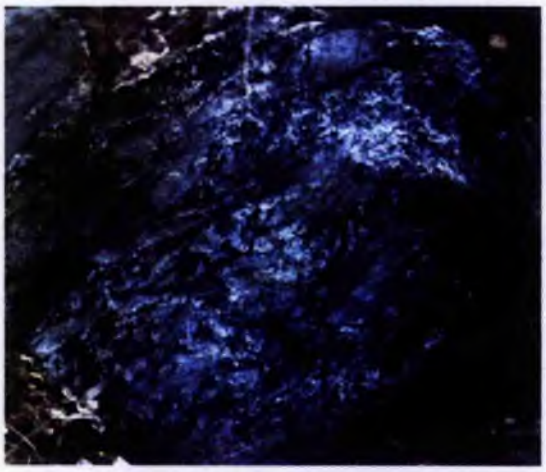

b)

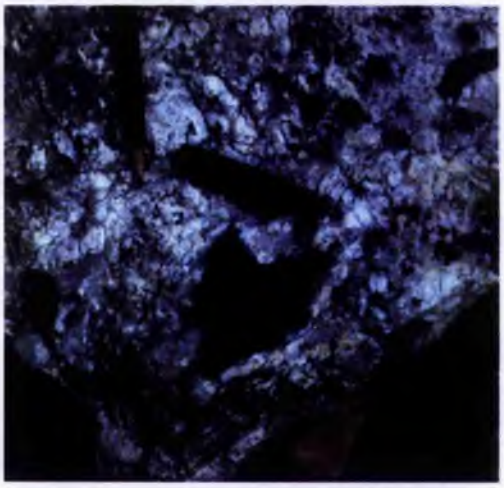

c)

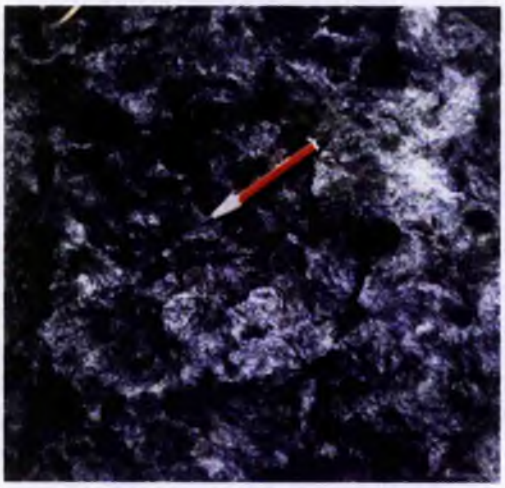

d)

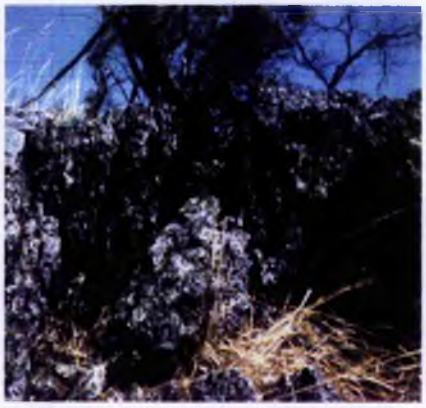

e)

Plate 2.11

a) Looking north. Compass is 10 cm long. At MR [8555 3725] the Augen Gneisses Member crop out. Towards the bast of the picture an 8 cm long, tabular potassic feldspar augen is evident.

b) Looking north west. Width of view is 20 cm. At MR [9104 3757] the Ultramyolinite Gneiss is evident. The very fine scale bands are due to variations is plagioclase and quartz.

c) Looking south. Pencil is 8 cm long. At MR [8080 3725] the Aplite Gneiss crops out. At the base of the picture the Augen Gneiss is evident. The contact between the two is sharp, straight and cross cuts the tectonic fabric.

d) Looking north. Compass is 10 cm long. At MR [8150 3840] the Tonalite Gneiss crops out. The member is predominantly leucocratic but contains dark green lenses of hornblende and epidote.

a)

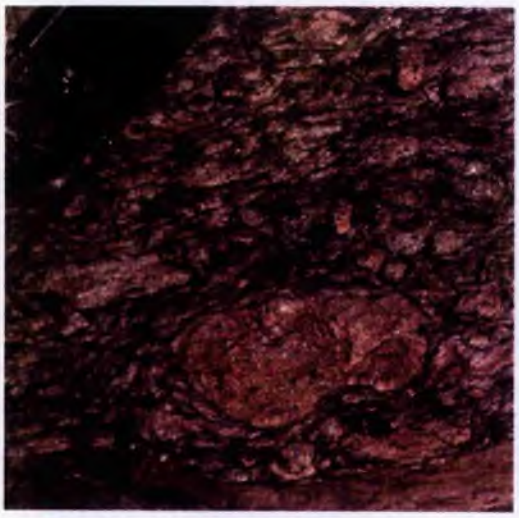

b)

c)

d)

Chapter Three

Geochemistry.

3.1 Introduction.

The aims of this chapter are :-

1) To document the whole rock major and trace element geochemistry of the meta - igneous formations of the Ophiolite Terrane.

2) To see if there are geochemical links or trends between the lithological formations.

3) To assess the geochemical characteristics of each formation and to interpret a tectonic environment of formation.

4) To test the hypothesis that the Maunde Ophiolite Group represents a relict ophiolite complex and that the Kaourera Island - Arc Group represents a relict island - arc complex.

3.2 The Maunde Ophiolite Group.

In the previous chapter (section 2.2), the various lithostratigraphic units of the Maunde Ophiolite Group were compared with those observed within ophiolite complexes (such as the Troodos Ophiolite) and a good correlation was established. In this section the whole rock, major and trace element geochemistry of these units will be analysed to test this hypothesis.

3.2.1. Meta - basalts.

The meta - volcanic and sheeted intrusive complexes (Mvuu Meta - Volcanic and Mbizi Sheeted Dyke Formations) of the Maunde Ophiolite Group consist of epidote amphibolite grade (section 4.3.1) meta - basalts. The whole rock

major and trace element analyses are given in Appendix C. The Harker variation diagram of total alkalis verses silica (TAS), (Fig. 3.1 a) is the standard plot for classifying terrestrial volcanic rocks (Le Maitre, 1989). The volcanic section of the Ophiolite Terrane, the Mvuu Meta - Mafic Volcanic Formation, consists of sub - alkalic basalts; the central, grass green, amygdaloidal portion of the Pillowed Member is picritic in composition; the darker, amygdaloidal poor margins are basaltic and pillow basalts from MR [9158 3776] are basaltic andesite in composition. The 'sheeted dyke complex', the Mbizi Sheeted Dyke Formation, is comprised entirely of sub - alkalic basalts. Within the Harker variation diagrams of wt % K_20 and Na_2O verses wt % SiO_2 (Fig. 3.1 b and c), some samples from both formations plot as alkalic basalts. According to Wilson (1989), these basalts should be termed 'transitional basalts'.

The analysis of trace elements via variation and spider diagrams is useful in determining tectonic origin, i.e., at mid - ocean ridges, island - arc complexes or within plate (Pearce & Cann, 1973; Meschende, 1986; Pearce 1983). The trace elements Nb, Ce, Zr, Y, Sc, Cr and Ni are considered to be relatively immobile during hydrothermal alteration and metamorphism (Humphris & Thompson, 1977; Brekke *et al.*, 1984; Brouxel *et al.*, 1989). Since the Ophiolite Terrane has undergone regional, amphibolite facies metamorphism, only these immobile elements can be regarded as representing, or close to representing the original pre - metamorphic concentrations (Brekke *et al.*, 1984). Because only 7 immobile trace elements have been analysed (Nb, Ce, Zr, Y, Sc, Cr and Ni) the number of tectonic discrimination diagrams will be limited. Figure 3.1 d and e are discrimination diagrams plotting Ti/100, Zr, Y*3 (Pearce & Cann, 1973) and Nb*2, Zr/4, Y (Meschende, 1986) parts per million (ppm) per whole rock for the basaltic and basaltic andesite compositions only. In the first diagram (Fig 3.1 d), both formations plot within the field of modern day mid - ocean ridge basalts (N -

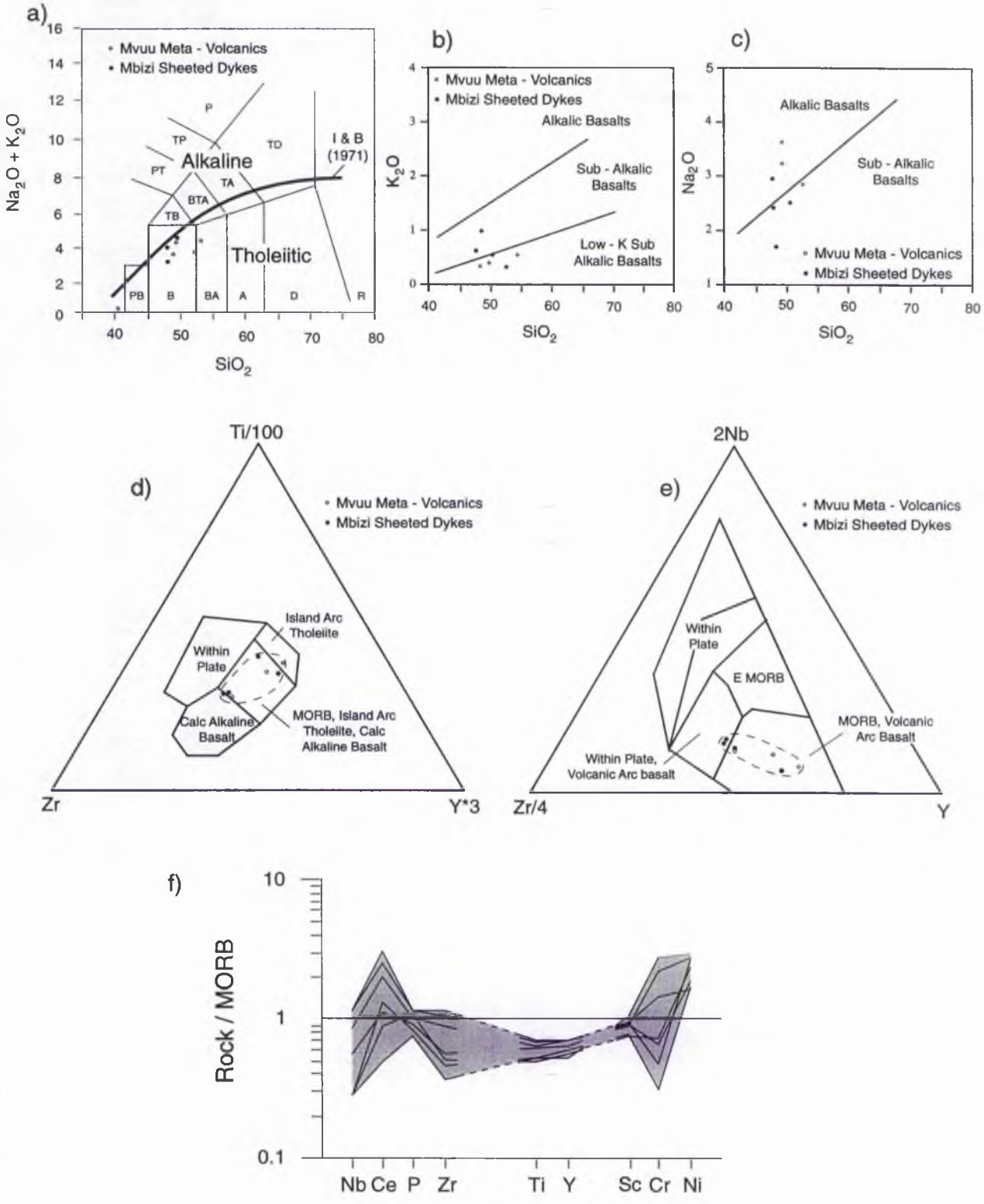

Fig. 3.1 Whole rock and trace element Harker, discrimination and MORB normalised spider plots for the Mvuu Meta - Volcanic and Mbizi Sheeted Dyke Formation meta - basalts. For discussion see text. (3.1.a) after Le Maitre, 1989 and Irvine & Bargar, 1971; b and c) after Middlemost, 1975; d) after Pearce & Cann, 1973; e) after Meschende, 1986; e) after Pearce, 1983).

MORB), one analysis of the Mvuu Meta - Mafic Volcanic Formation plots just outside this field. Within Fig. 3.1 e, all samples of the Mvuu Meta - Mafic Volcanic Formation plot within the N - MORB field while two samples of the Mbizi Sheeted Dyke Formation plot just outside. Both discrimination diagrams indicate that both the volcanic section (Mvuu Meta - Mafic Volcanic Formation) and the sheeted dyke section (Mbizi Sheeted Dyke Formation) contain trace element ratios similar to basalts from modern day mid - ocean ridges. Table 3.1 summarises the other major and trace element discrimination plots. Fig 3.1 f is a MORB normalised spider plot after Pearce (1983) showing all individual analyses from the Mvuu Meta - Mafic Volcanic and Mbizi Sheeted Dyke Formations. Figure 3.2 compares the MORB normalised spider trace for the Mvuu Meta - Mafic Volcanic and Mbizi Sheeted Dyke Formations (shaded area with individual analyses removed) with basalts produced within other tectonic environments. The Mvuu and Mbizi samples produce a flat trace from Zr to Sc which is relatively depleted compared to that of N - MORB. There is a marked negative Nb anomaly (1 - 5 ppm); positive Ce anomaly (5 - 25 ppm) and variable Cr contents (77 - 700 ppm). In comparison with other tectonic environments (Fig. 3.2) this trace is similar to that produced at destructive plate margins (ensialic arcs, ensimatic arcs and marginal basins) where the trace element characteristics have a significant input from the dehydrating, subducting, lithospheric slab (Wilson, 1989) and dissimilar to that of mid - ocean ridge basalts (MORB), continental flood basalts (CFB), ocean island basalts (OIB) and basalts from large igneous provinces (LIPs). The similarity with arc - type basalts is also illustrated in Fig. 3.3 a, a triangular discrimination plot of Y/15, La/10 verses Nb/8 (after Canbis & Lecolle, 1989) where the Mvuu Meta - Mafic Volcanic and Mbizi Sheeted Dyke Formations plot within the fields of marginal basins and various arc - derived basalts. Chondrite normalised trace element patterns (Fig. 3.3 b) are most similar to basalts from juvenile marginal basins (Brouxel

Mvuu Meta - Mafic Volcanic and Mbizi Sheeted Dyke Formations

Elements Plotted	Reference	Comments
Major Elements		
TiO2-MnO*10-P2O5	Mullen,1983	(6) IAT, (1) MORB, (1) CAB.
FeO-MgO-Al2O3	Pearce *et al.*, 1977	(3) WPB, (4) OI, (2) MORB
Function 1-Function 2	Pearce, 1976	(1) MORB, (7) outside all fields
Trace Elements		
Nb/Y-Ti/Y	Pearce, 1982	(4) MORB, (4) MORB and VAB
Zr-Ti	Pearce and Cann, 1973	(3) CAB, (3) MORB and IAT, (1) IAT, (1) outside all fields
Zr-Ti	Pearce, 1982	(4) MORB and VAB, (1) MORB and WP, (3) VAB
Zr-Zr/Y	Pearce and Norry, 1979	(2) MORB, (2) VAB, (4) outside all fields
Zr-Zr/Y	Pearce, 1983	(3) OA, (2) CA, (4) OA and CA

Table. 3.1 Summary of the major and trace element discrimination diagrams for the Mvuu Meta - Mafic Volcanic and Mbizi Sheeted Dyke Formations.

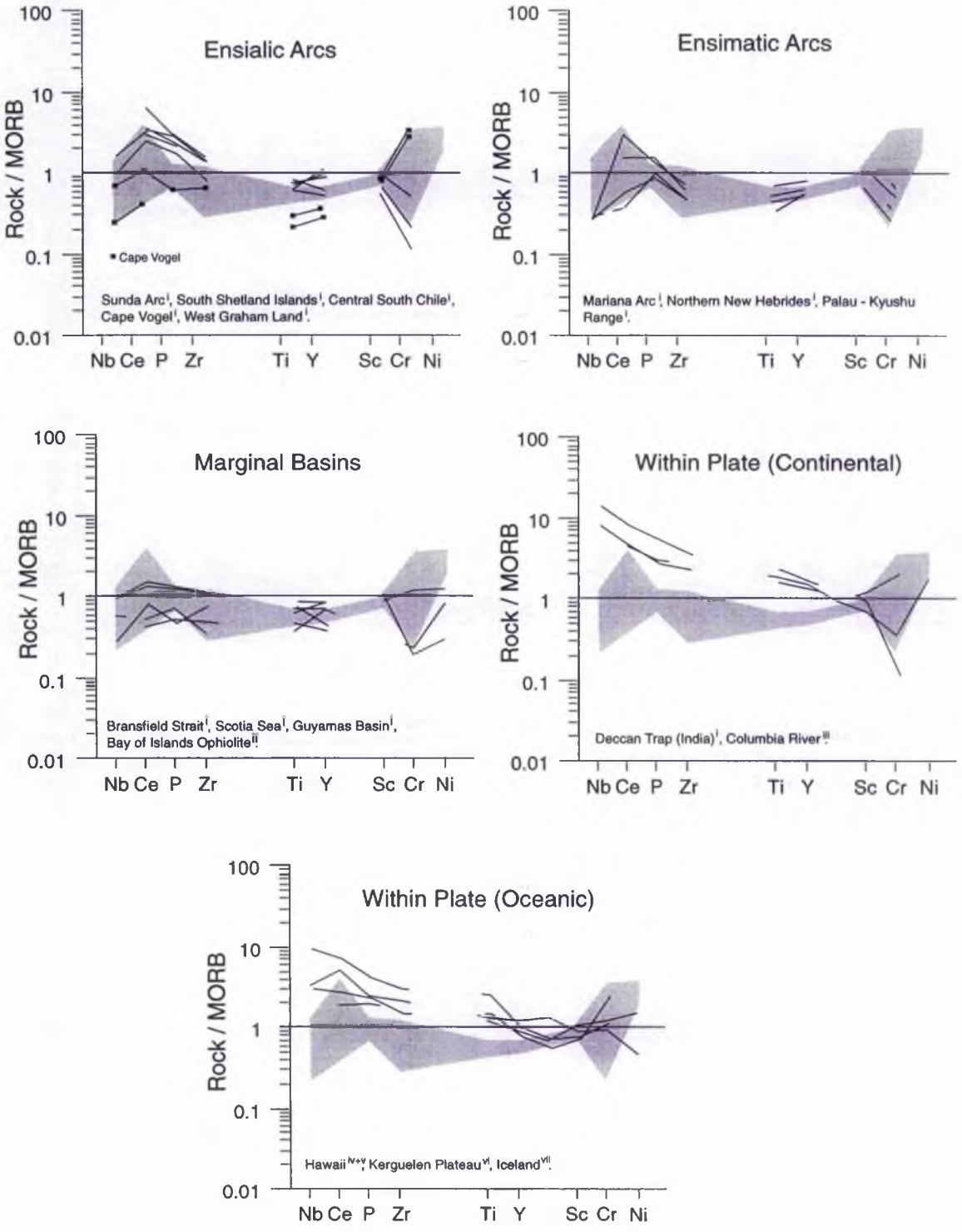

Fig. 3.2 MORB normalised spider plots (after Pearce, 1983) comparing the immobile trace elements of the Mvuu Meta - Volcanic and Mbizi Sheeted Dyke Formation meta - basalts (lightly shaded) with basalts from other tectonic environments. For discussion see text. Data sources for i) Brekke *et al.*, 1984; ii) Elthon, 1991; iii and iv) Basaltic Volcanism Study Project, 1981; v) West *et al.*, 1992; vi) Mahoney *et al.*, 1995; vii) Schilling *et al.*, 1983.

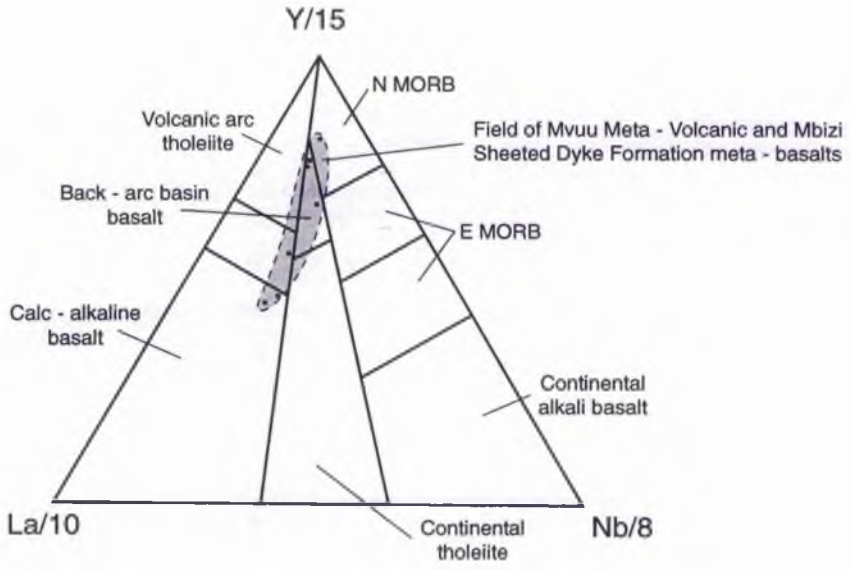

Fig 3.3 a. Triangular discrimination diagram (after Cabnis & Lecolle, 1989) for the Mvuu Meta - Volcanic and Mbizi Sheeted Dyke Formations. For discussion see text.

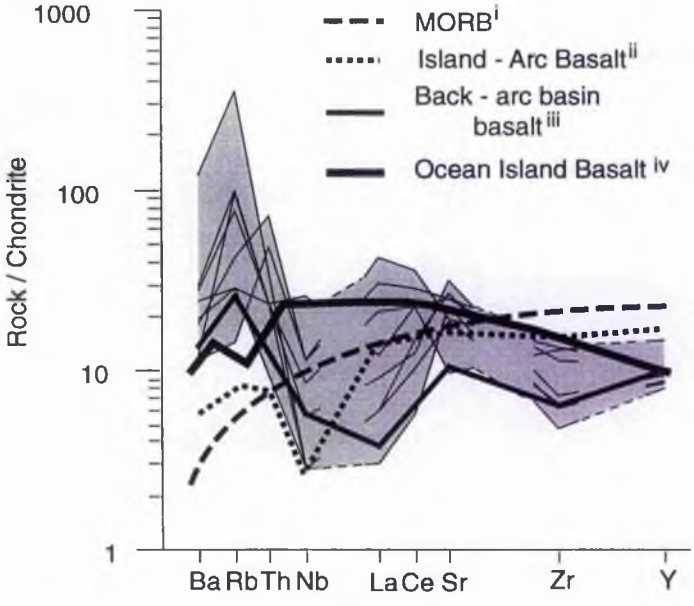

Fig. 3.3 b. Chondrite normalised trace element diagram (after Thompson, 1982) comparing the Mvuu Meta - Volcanic and Mbizi Sheeted Dyke meta - basalt Formations (lightly shaded) with those from other tectonic environments. Data source for i) Rollinson, 1993; ii) Gribble *et al.*, 1998; iii) Brouxel *et al.*, 1989; iv) Basaltic Volcanism Studies Project, 1981.

et al., 1989).

Niobium is commonly used in the literature to distinguish between ensimatic - arc basalts and those derived from ensilaic and marginal basin settings (Brekke *et al.*, 1984; Wilson, 1989; Brouxel *et al.*, 1989; Saunders and Tarney, 1979). Ensimatic arcs are characterised by very low Nb levels (0.7 - 1 ppm) (summarised in Brekke *et al.*, 1984 and Wilson, 1989), whereas ensialic arcs and marginal basins are characterised by more variable Nb concentrations (1 - 5 ppm) (summarised in Brekke *et al.*, 1984; Elthon, 1991). The higher Nb concentrations of between 1 and 5 ppm, for the Mvuu and Mbizi samples indicate that these meta - basalts did not originate within an ensimatic arc setting. The MORB normalised spider patterns (after Pearce, 1983) for ensialic arcs are generally enriched in the more compatible immobile trace elements i.e., Nb, Ce and Zr and depleted in the more incompatible immobile trace elements i.e., Sc, Cr and Ni, compared to MORB (Brekke *et al.*, 1984) thus producing a sloping, top left to bottom right trace element pattern (with the exception of Cape Vogel, which produces a flat trace), (Fig. 3.2). The neutral trace of the Mvuu Meta - Mafic Volcanic and Mbizi Sheeted Dyke Formations are therefore unlike that of ensialic arcs (with the exception of Cape Vogel). Although Cape Vogel also displays a neutral trace, the Mvuu and Mbizi samples display greater Ce, Ti and Y and lower Cr concentrations. The presence of a sheeted dyke complex, association with an ophiolitic type lithostratigraphy (i.e., oceanic crust), lack of sialic continental crust and voluminous tonalitic and calc - alkaline intrusions also suggest that the Maunde Ophiolite Group meta - basalts were not derived from an ensialic, destructive plate margin setting. The trace element characteristics of the Mvuu Meta - Mafic Volcanic and Mbizi Sheeted Dyke Formations are therefore most like those of basalts produced within modern day marginal basins.

3.2.2 Meta - Gabbros and Hornblendites.

It is interpreted from field relationships (section 2.2.6) that the hornblendites of the Ingwe Meta - Mafic Cumulate Formation are lithologically related to the meta - gabbros of the Twiza Meta - Gabbro Formation since samples [SJ 213Ha] (hornblendite) and [SJ 213 Hb] (meta - gabbro). They are interpreted to be in igneous contact (section 2.2.6 and Plate. 2.5 e). This genetic relationship will be tested by the comparison of the whole rock major and trace element geochemical characteristics.

The whole rock major and trace element analyses are given in Appendix C. The Harker variation diagram of total alkalis verses silica (Fig. 3.4 a) indicates that both formations are basaltic in composition with the exception of one analysis of the Ingwe Meta - Mafic Cumulate Formation [SJ 213 Hd] and the High Strain Member [SJ 215 B] of the Twiza Meta - Gabbro Formation which are picro - basalts. Figures 3.4 b and c are Harker variation diagrams (after Middlemost, 1975) of K_2O and Na_2O verses SiO_2 and indicate that all members are sub - alkalic. In Fig 3.4 d, which is a plot of TiO_2 verses SiO_2, it is evident that three samples, [SJ 213 Hd] (one analysis of the Ingwe Meta - Mafic Cumulate Formation), [SJ 215 B] and [SJ 215 F] (two analyses of the High Strain Member of the Twiza Meta - Gabbro Formation) plot with high TiO_2 values (2 - 5 wt%). The same three samples plot with high Fe_2O_3 values on an Fe_2O_3 verses SiO_2 plot (Fig. 3.4 e). These three samples are possibly related by significant Fe - Ti opaque mineral accumulation due to crystal settling. This is confirmed by thin section analyses (section 2.2.5, 2.2.6 and appendix B) where opaque minerals are modally important in samples [SJ 213 Hd], [SJ 215 B] and [SJ 215 F] and absent within all other Ingwe and Twiza Meta - Gabbro Formation thin sections.

The triangular discrimination plots of Ti/100, Zr, Y*3 (Pearce & Cann, 1973) and Nb*2, Zr/4, Y (Meschende, 1986) (Figures 3.3 f and g) cannot be used for the tectonic discrimination of mafic plutonics. However they are

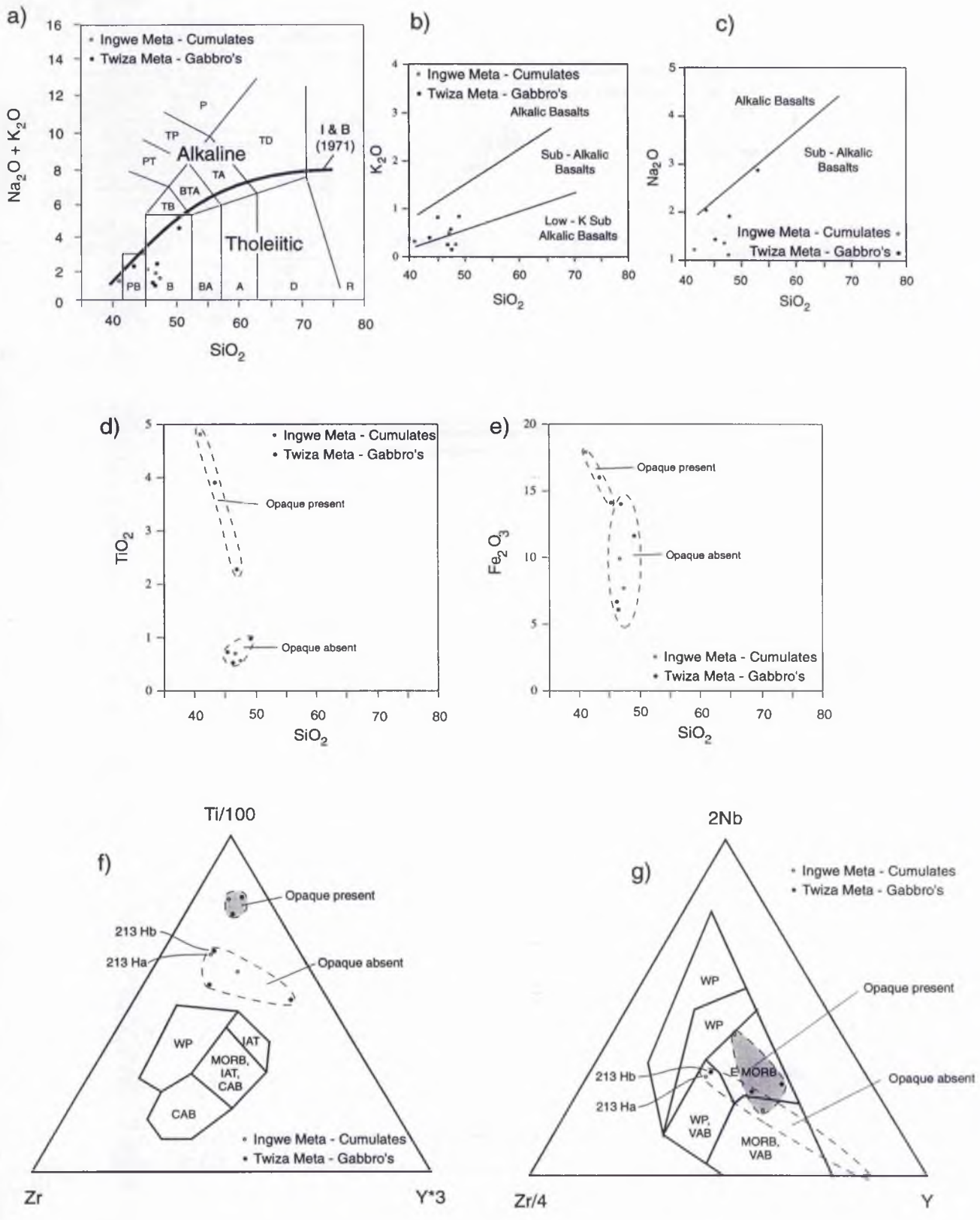

Fig. 3.4 Whole rock major and trace element Harker and triangular discrimination diagrams for the Ingwe Meta - Mafic Cumulate and Twiza Meta - Gabbro Formations. For discussion see text. (3.1.a) after Le Maitre, 1989 and Irvine & Baragar, 1971); b and c) after Middlemost, 1975; f) after Pearce & Cann, 1973; g) after Meschende, 1986).

useful in demonstrating the similarity in trace element geochemistry between samples [SJ 213 Hb] (meta - gabbro) and [SJ 213 Ha] (hornblendite), which plot in similar positions on both diagrams. Figure 3.5 a, is a MORB normalised spider diagram after Pearce (1983) of the low TiO_2 samples (which include [SJ 213 Ha] and [SJ 213 Hb]). Again both meta - gabbros and hornblendites plot with similar trends indicating a common parental source for both formations. Overlain for comparison are the traces of two meta - gabbros from the Bay of Islands Ophiolite, Newfoundland (Suen *et al.*, 1979), which is also interpreted as a remnant of marginal basin crust (Suen *et al.*, 1979; Elthon, 1991). It is evident that both the Maunde Ophiolite Group and Bay of Islands meta - gabbros display similar 'U' shaped trace element patterns.

Figure 3.5 b is a MORB normalised spider plot (after Pearce, 1983) of the high TiO_2 samples. It is clear that they plot unlike both the low TiO_2 samples and the marginal basin meta - basalts of the Mvuu and Mbizi Sheeted Dyke Formations (*c.f.* Fig. 3.1 f) indicating that the presence of opaque minerals within these samples has greatly altered the trace element geochemistry. The anomalous phosphorous peak of sample [SJ 215 B] suggests significant accumulation of apatite. This sample also contains the greatest proportion of opaque minerals and a low SiO_2 content (43.31 wt %) indicating its refractory and cumulate nature.

3.2.3 Plagiogranite.

Thin section analysis reveal that the plagiogranite sheets are comprised predominantly of quartz and albite. Normative recalculation of the whole rock major element data using CIPW norms (section 2.2.6 and Appendix B) confirm the thin section analysis. Using the nomneclature of the IUGS subcommission based on Le Maitre (1989) this lithology is classified as a tonalite or trondhjemite (Fig. 3.6 a). Figure 3.6 b is a triangular plot of

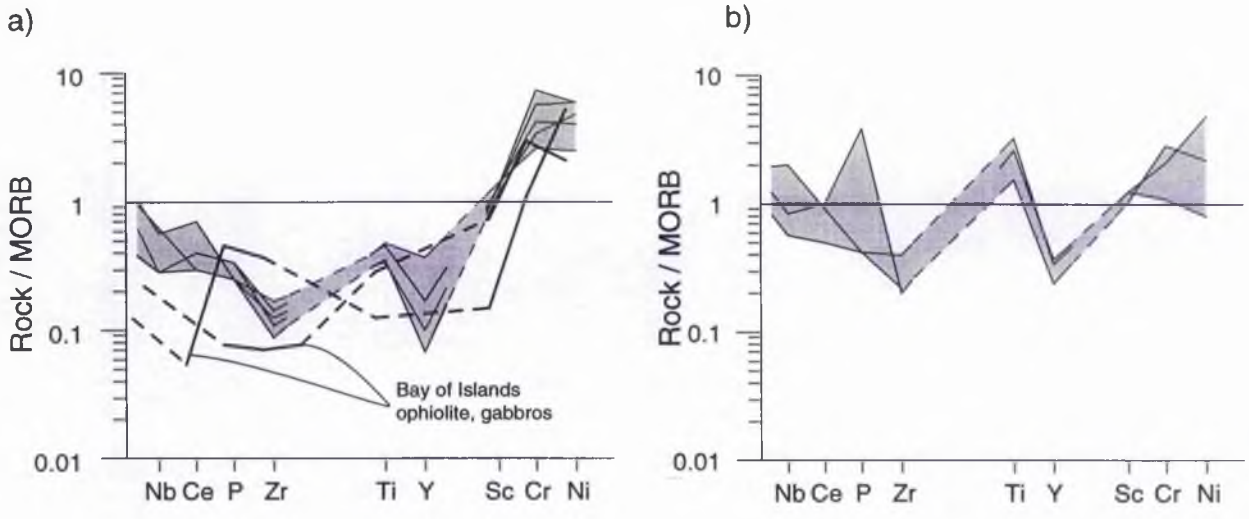

Fig. 3.5 MORB normalised spider plots (after Pearce, 1983) of the a) Opaque absent and b) opaque present Ingwe Meta - Mafic Cumulate and Twiza Meta - Gabbro Formations. In plot a) the opaque absent samples are compared with meta - gabbros from the Bay of Islands Ophiolite (Suen *et al.*, 1979). The dashed lines indicate that no analysis is availiable. For discussion see text.

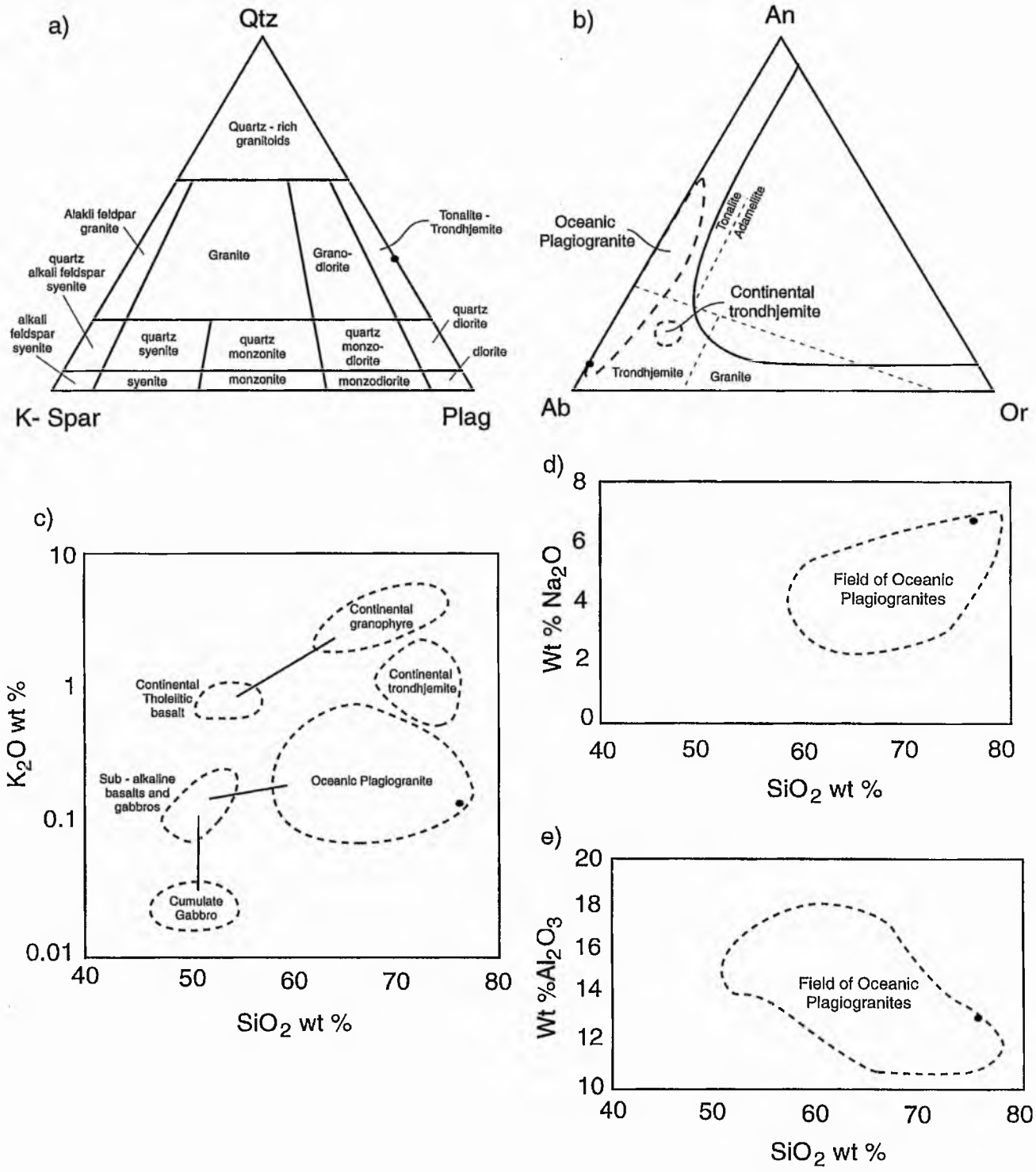

Fig. 3.6 Major element variation diagrams for the Plagiogranite Sheets of the Twiza Meta - Gabbro Formation. For discussion see text. (3.6.a) after Le Maitre, 1989; b) after O'Conner, 1965 and Coleman, 1977; c) Coleman, 1977 and Gerlach *et al.*, 1981; d and e) Gerlach *et al.*, 1981).

anorthite (An), albite (Ab) and orthoclase (Or) with the various rock types based on their feldspar ratios (O'Conner 1965), and the fields of oceanic plagiogranites and continental tholeiites superimposed (Coleman, 1977). According to the classification of O'Conner (1965), the presence of albite rather than anorthite indicates that is sample is a trondhjemite. The sample plots within the field of oceanic plagiogranites rather than that of continental trondhjemites (Figs. 3.6 c, d and e after Gerlach *et al.*, 1981).

3.2.4 Ultramafics.

The whole rock major and trace element data for the serpentinite assemblages of the Ngwena Ultramafic Formation are given in appendix C. Figure 3.7 is a variation diagram of wt % MgO verses wt % MgO / CaO after Meisel *et al.*, (1997). The figure shows the field for all known, unaltered mantle xenoliths and massive peridotites which fall on a line that intersects the position of primitive upper mantle (PUM), (McDonough & Sun, 1995). The Ngwena Ultramafic Formation lithologies plot outside this field towards lower MgO and MgO / CaO wt % values indicating that all Ngwena Ultramafic Formation samples show metasomatic alteration and removal of certain major elements (including MgO and CaO) due to serpentinisation (Meisel *et al.*, 1997). It is therefore likely that the trace elements have also been modified from their original concentrations. However, comparison with unaltered ultramafics from the Bay of Islands Ophiolite, reveal similar but not identical trace element ratio's when normalised to MORB (Fig. 3.8). Both display 'U' shaped trace element spider patterns with a negative Ce and Zr anomalies relative to phosphorous and similar Sc, Cr and Ni concentrations. In section 4.2.1 it is noted that during metamorphism and serpentinisation, Cr^{3+} within chromite grains has progressively been replaced with Fe^{3+}, with the mobilised Cr^{3+} being accommodated within serpentine. The similarity in the whole rock, Cr concentrations between the Ngwena Ultramafic Formation

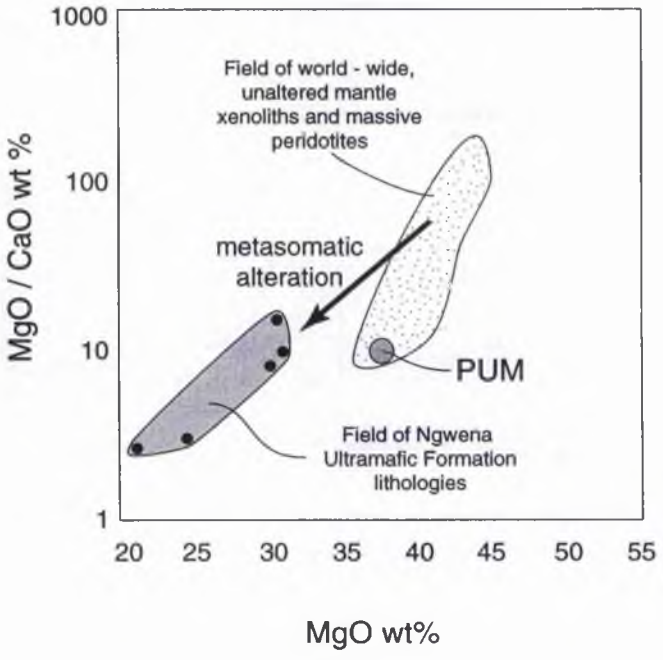

Fig. 3.7 Whole rock variation diagram illustrating the field for unaltered mantle xenoliths and massive peridoties (stippled); the Ngwena Ultramafic Formation lithologies (lightly shaded) indicate whole rock alteration due to metasomatism and serpentinisation. For discussion see text.
Data for for PUM (primative upper mantle), xenoliths and peridotites is from Meisel *et al.*, (1997).

lithologies and those from the Bay of Islands attests to the fact during metamorphism Cr may be mobile on the grain scale, but on the hand specimen and whole rock scale is relatively immobile.

3.2.5 Discussion.

Meta - Basalts.

From the various discrimination diagrams and Harker variation plots, both Maunde Ophiolite Group meta - basalt formations are interpreted to comprise mainly of tholeiitic to transitional basalts. Trace element discrimination diagrams (Fig. 3.1 d and e) indicate trace element ratios similar to that of MORB and / or arc - derived basalts. MORB normalised spider plots (after Pearce, 1983) indicate that the immobile trace elements are most similar to basalts formed within destructive plate margins i.e., where there is significant input from a dehydrating, subducting lithospheric slab. Further discrimination suggests formation within a marginal basin setting. However, apart from dissimilar Nb concentrations, it is difficult to distinguish between basalts formed within a juvenile marginal basin setting and those formed within an ensimatic arc. Gribble *et al.*, (1998) indicates that the immobile trace element concentrations (and spider traces) between ensimatic arc and juvenile marginal basin basalts are relatively similar. As the marginal basin matures from the rifting to spreading stage, adiabatic decompression melting of the mantle becomes predominant and the input from the subducting slab decreases. The trace element concentrations of the spreading centre marginal basin basalts become distinct from those produced within the associated arc.

It is interpreted therefore that the Mvuu Meta - Mafic Volcanic and Mbizi Sheeted Dyke Formation formed within a marginal basin setting similar to modern day back - arc basins such as the Scotia Basin, Mariana Trough and Lau Basin, rather than at a mid - ocean ridge analogous to the modern day Atlantic or Pacific Oceans. This is not surprising since the

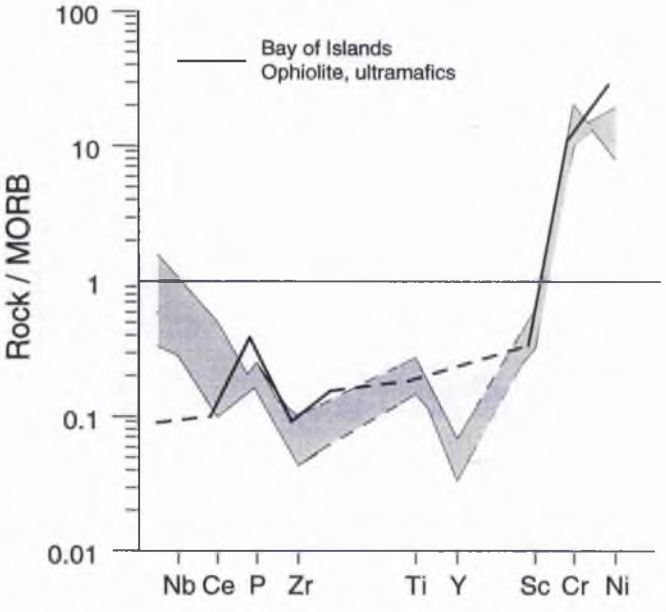

Fig. 3.8 MORB normalised spider plot (after Pearce, 1983) of the Ngwena Ultramafic Formation lithologies (lightly shaded). Overlain are trace element data for the Bay of Islands Ophiolite ultramafics (Suen *et al.*, 1979). Dashed lines indicate that no analysis is availiable. For discussion see text.

majority of Phanerozoic ophiolitic fragments are interpreted to have formed within a marginal basin setting rather than that of a mid - ocean ridge (Wilson, 1989; Saunders *et al.*, 1979; Taylor *et al.*, 1992; Smith, 1993).

Meta - Gabbros and Hornblendites.

The major and trace element geochemistry show that these formations contain two distinct geochemical signatures, one characterised by high TiO_2 and Fe_2O_3 values (indicating significant Fe - Ti opaque mineral contents) and the other by low TiO_2 and Fe_2O_3 values. The variability in concentration of opaque contents is not confined to individual formations. Two analyses of the High Strain Member of the Twiza Meta - Gabbro Formation and one analysis of the Ingwe Meta - Mafic Cumulate Formation contain opaques. Other members of these formations are opaque absent. The contrast in opaque oxide abundances might be due to accumulation by gravity settling.

The fine grained nature of the High Strain Member (section 2.2.6) and its similar outcrop appearance compared to the Mbizi Sheeted Dyke Formation might lead to the interpretation that they are equivalents. However, the dissimilarity in whole rock, trace and major element geochemistry indicates that this is not the case. The similarity in chemistry between the High Strain Member and the Ingwe and Twiza Meta - Gabbro Formation lead to the interpretation that they are geochemical (but not textural) equivalents. The fine grained nature of the High Strain Member (in comparison with the relatively coarse grained nature of both the Ingwe and Twiza Meta - Gabbro Formations) indicates that it is likely to have undergone intense grain size reduction and mylonitisation during a high strain deformation event (section 5.3). In fact, coarser grained and gabbroic textures are described from what might be described as low strain zones (section 2.2.6).

Figure 3.9 a and b are MORB normalised spider plots after Pearce, (1983). Figure 3.9 a, displays the immobile trace elements for both the meta - basaltic and meta - gabbroic formations of the Maunde Ophiolite Group while Fig. 3.9 b shows the immobile trace elements for meta - basalts and meta - gabbros from the Bay of Islands Ophiolite. It is evident that for both the Maunde Ophiolite Group and the Bay of Islands Ophiolite there is a similar trace element relationship between the meta - basalts and meta - gabbro complexes. The Bay of Islands Ophiolite gabbros are interpreted to represent plagioclase cumulates from which a basaltic melt has been extracted (Suen *et al.*, 1979). The similarity in trace element ratios between the meta - basalts and meta - gabbros of the Maunde Ophiolite Group and those from the Bay of Islands Ophiolite might also be interpreted in the same way. This is confirmed from Fig. 3.9 c, d and e which are major and trace element variation plots that illustrate the fractionation or removal of olivine and / or clinopyroxene. It is evident that in all plots, the Ingwe and Twiza Meta - Gabbro Formations are related to the Mvuu Meta - Mafic Volcanic and Mbizi Sheeted Dyke Formations via olivine and clinopyroxene fractionation.

Plagiogranite.

Major element analysis classifies this as an oceanic plagiogranite. It has been interpreted by many authors, including Coleman (1977) and Gerlach *et al.*, (1981), that the association of plagiogranites with high level, layered or massive gabbros and mafic cumulate rocks is evidence that a genetic link between them exists. This has been confirmed by Gerlach *et al.*, (1981) with the analysis of REE. However without the aid of REE and / or isotope analysis, direct geochemical evidence of a genetic link between both the plagiogranite sheets and the rest of the Ingwe and Twiza Meta - Gabbro Formations is not possible. However, the intimate nature of the plagiogranite with the massive and layered meta - gabbros and mafic cumulates of the

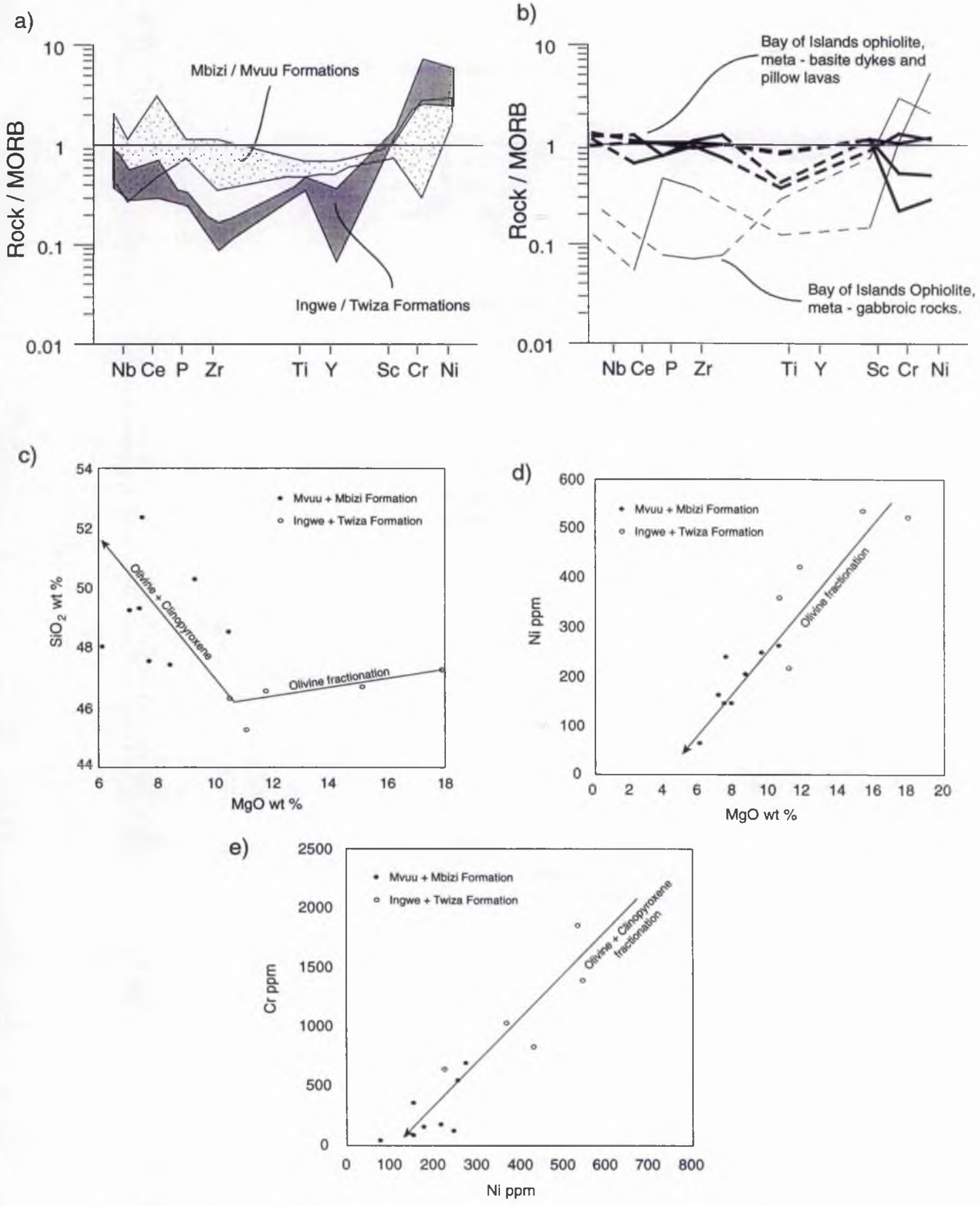

Fig. 3.9 a) MORB normalised spider plots (after Pearce, 1983) comparing the trace elements and relationships between the Ingwe Meta - Cumulate + Twiza Meta - Gabbro and Mvuu Meta - Volcanic + Mbizi Sheeted Dyke Formations. The Bay of Islands Ophiolite gabbros and basalts are given in b) as a comparison. Data for b) is from Suen *et al.*,1979). For discussion see text.
c, d and e) are whole rock major and trace element variation plots displaying the relationship (olivine and clinopyroxene fractionation) between the Ingwe Meta - Cumulate + Twiza Meta - Gabbro and Mvuu Meta - Volcanic + Mbizi Sheeted Dyke Formations. A comparison of wt % Mgo vs ppm Ni with other world wide tectonic environments is given in Fig. 3.19. Arrow indicates direction and trend of fractionation path. For discussion see text.

Twiza and Ingwe Meta - Mafic Cumulate Formations as fine networking veins, and variable thickness dykes is altogether suggestive of a genetic relationship. It is interpreted therefore that the plagiogranites are of similar origin to those within other ophiolite complexes.

Ultramafics.

In section 2.2.7, it was suggested that the ultramafic lithologies of the Ngwena Ultramafic Formation are of mantle origin and represent a tectonised section of an ophiolitic 'Ultramafic Complex'. Since the major element chemistry has been altered by metamorphism and serpentinisation it is impossible to make any direct comparisons; however, the immobile trace element geochemistry is similar to other unaltered ultramafics from the Bay of Islands Ophiolite. This must be treated with caution since it can be shown that on the grain scale the immobile elements such as Cr are mobile.

Summary.

From the whole rock major and trace element geochemistry it is evident that the Maunde Ophiolite Group formations share similar geochemical characteristics with the equivalent lithological counterparts in other ophiolite complexes. Analysis of meta - basalts with modern - day analogues indicate an origin within a marginal basin setting.

3.3 The Kaourera Island - Arc Group.

In the previous chapter (section 2.3) the Kaourera Island - Arc Group was interpreted as representing an extrusive volcanic complex. The variability of the lithostratigraphic units was tentatively interpreted as representing volcanism within an island - arc type environment. In this section the whole rock, major and trace element geochemistry of each formation will be analysed in order to test this hypothesis.

3.3.1 Overview of the Kaourera Island - Arc Group.

Figure 3.10 a, b and c are selected major element variation diagrams for all the Kaourera Island - Arc Group samples. The Harker variation TAS diagram (Fig. 3.10 a) indicates that the various lithostratigraphic units comprise a continuous range of rock compositions from 43 to 79 wt % SiO_2 (i.e., picro - basalt to rhyolite). The majority of samples (basalt to rhyolite) plot below the line that separates the tholeiitic from alkaline fields, indicating a tholeiitic fractionation trend. A similar tholeiitic fractionation trend is evident within the triangular plot of FeO (total), $Na_2O + K_2O$ and MgO (Fig. 3.9 b). However, some samples (mainly basalts and basaltic andesites) display a fractionation trend parallel to that of the Cascade Lava, calc - alkaline trend (Carmichael, 1964). It is possible that the major element chemistry of these samples has been altered by hydrothermal alteration and subsequent metamorphism. Figure 3.10 c is a plot of K_2O verses SiO_2 showing the major subdivisions of the island - arc volcanic rock suites. There is a poor grouping of data towards higher SiO_2 compositions. This may be due to the mobility of K_2O during hydrothermal alteration and metamorphism or be due to the presence of two fractionation suites, a low - K series and a calc - alkaline series, such is evident at the modern day South Sandwich Arc (Wilson, 1989).

3.3.2 Bere Amphibolite Formation.

This formation is characterised by amygdaloidal, extrusive volcanics (section 2.3.2) of picro - basaltic and basaltic compositions (Fig. 3.11 a). All samples plot within the tholeiitic field of Figs. 3.11 a and b. Within the triangular discrimination plot of 2Nb, Zr/4 verses Y, (Fig. 3.11 c) the data plots mainly within the MORB field with one analyses [SJ 285] plotting as a within plate or volcanic arc basalt. Within the Ti/100, Zr verses Y*3 triangular plot (Fig. 3.11 d), the same sample plots on the boundary between that of calc - alkali and MORB basalts. The remaining samples plot on the border of MORB and

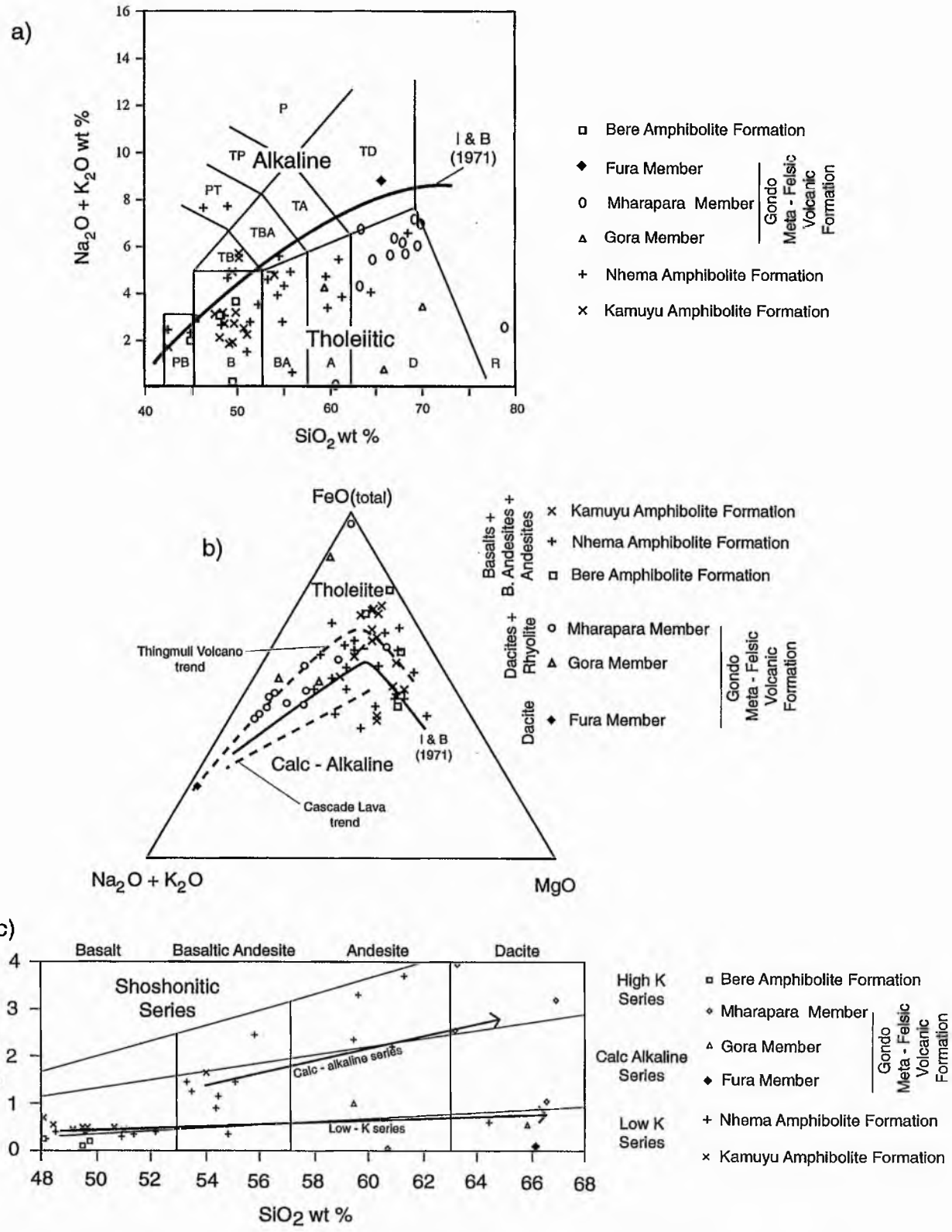

Fig 3.10 Whole rock major element variation diagrams for all Kaourera Island - Arc Group samples. For discussion see text. (3.10.a) after Le Maitre, 1989 and Irvine & Baragar, 1971. b) AFM diagram with the boundary between the calc - alkaline and tholeiitic fields after Irvine & Baragar, 1971. Also shown for comparison are trends for a typical tholeiitic (Thingmuli Volcano) and calc - alkaline (Cascades Lava) series from Carmichael, 1964. c) K_2O vs SiO_2 wt % plot with fields from Wilson, 1989.

island - arc tholeiites. One sample [SJ 498] is relatively rich in TiO_2 (*c.* 4.4wt%) and plots outside the field of all the discrimination fields. Within hand specimen both [SJ 285 and 498] are highly altered. Sample [SJ 285] contains abundant matrix and amygdaloidal epidote (appendix B) which is reflected in the high CaO (17.25 wt %) and low Na_2O (0.13 wt %) and K_2O (0.12 wt %) contents. Sample [SJ 498] is also highly altered with elevated TiO_2 (4.4wt%) and Fe_2O_3 (20.84 wt %) contents, suggesting increased opaque oxide concentrations compared to the other meta - basaltic members. Both these samples plot above the rest of the formation on the MORB normalised spider diagram (Fig. 3.11 e) indicating that the trace element geochemistry has also been altered during this metamorphic / alteration event. These two samples will therefore not be considered any further. Table 3.2 is a summary of the other major and trace element discrimination diagrams for the Bere Amphibolite Formation.

Figure 3.12 compares the MORB normalised, immobile trace element spider patterns for the Bere Amphibolite Formation (shaded area with individual analyses removed) with basalts produced within other tectonic environments. The Bere Amphibolite Formation trace element pattern is relatively flat from Zr to Sc with most trace elements (with the exception of Cr and Ni) being depleted compared to that of MORB. Again a destructive plate margin origin is evident. It might be interpreted from the range in Nb concentrations of between 2 to 3 ppm, compared to 0.7 - 1 ppm in ensimatic arcs, (summarised in Brekke *et al.*, 1984 and Wilson, 1989) that this formation did not originate within an ensimatic arc setting. However, the limit of detection for Nb in XRF analysis is 1 ppm ± 1 - 2 ppm (Calder, *pers comm.*). All samples of the Bere Amphibolite Formation *could* therefore, within error estimations, contain a negative Nb anomaly comparable to basalts within ensimatic island - arcs. The near, neutral trace of the Bere Amphibolite Formation is unlike the sloping trace produced by that of ensialic arcs, with

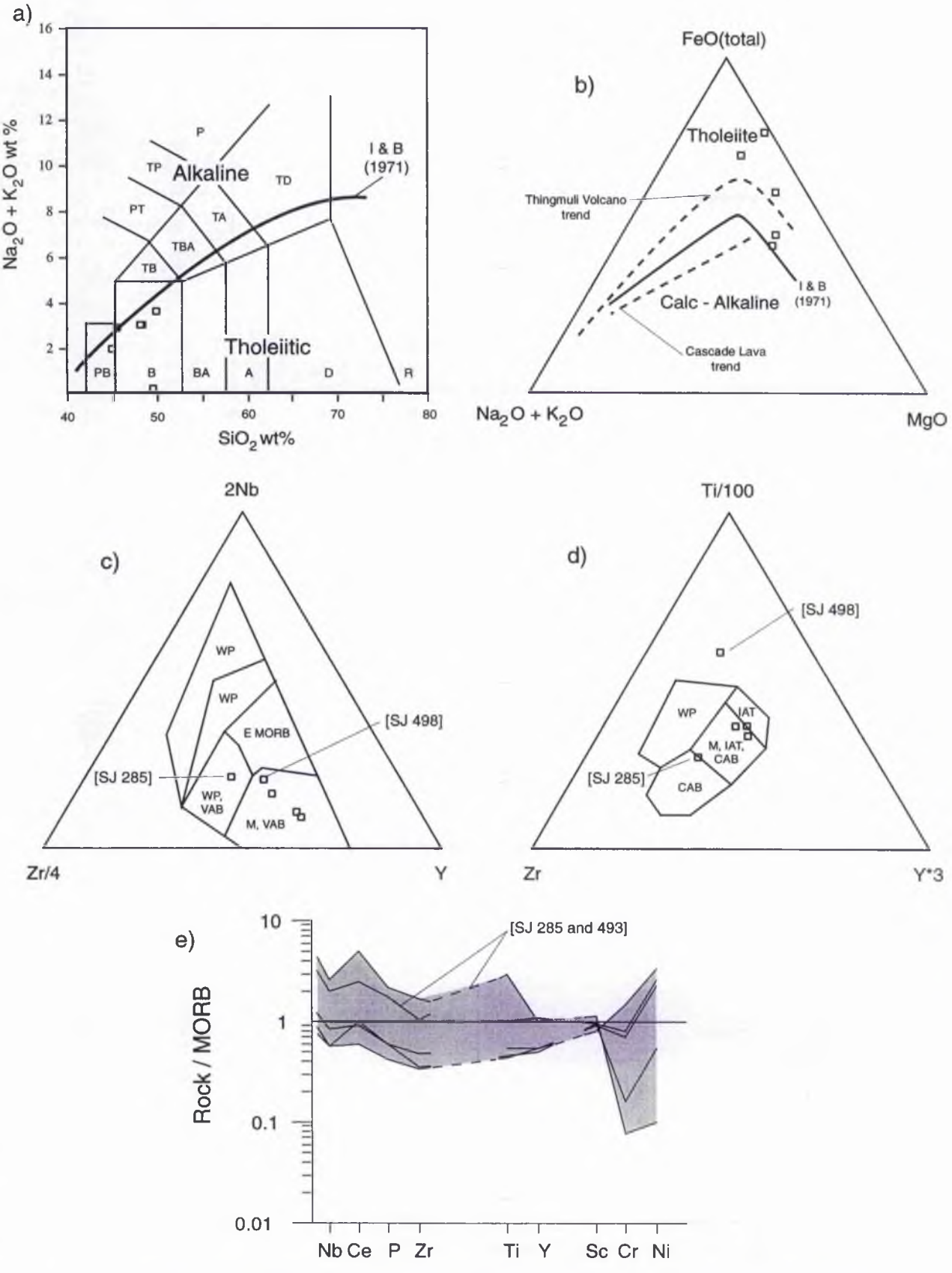

Fig. 3.11 Whole rock major and trace element Harker, discrimination and MORB normalised spider plots for the Bere Amphibolite Formation. For discussion see text. (3.11.a) after Le Maitre,1989 and Irvine & Baragar, 1971; b) after Irvine & Baragar, 1971 and Carmichael, 1964; c) after Meschende, 1986; d) after Pearce & Cann, 1973; e) after Pearce, 1983).

Bere Amphibolite Formation

Elements Plotted	Reference	Comments
Major Elements		
TiO2-MnO*10-P2O5	Mullen,1983	(1) MORB, (3) IAT, (1) Bon
FeO-MgO-Al2O3	Pearce *et al.*, 1977	(2) MORB, (2) OI, (1) SC
Function 1-Function 2	Pearce, 1976	(3) CAB, (2) WP
Trace Elements		
Nb/Y-Ti/Y	Pearce, 1982	(4) VAB and MORB, (1) outside all fields
Zr-Ti	Pearce and Cann, 1973	(1) CAB, (1) IAT, (3) outside all fields
Zr-Ti	Pearce, 1982	(3) VAB, (1) WP, (1) outside all fields
Zr-Zr/Y	Pearce and Norry, 1979	(3) VAB, (1) VAB and MORB, (1) WP
Zr-Zr/Y	Pearce, 1983	(3) OA, (1) CA, (1) OA and CA

Table. 3.2 Summary of the Major and Trace element discrimination diagrams for the Bere Amphibolite Formation.

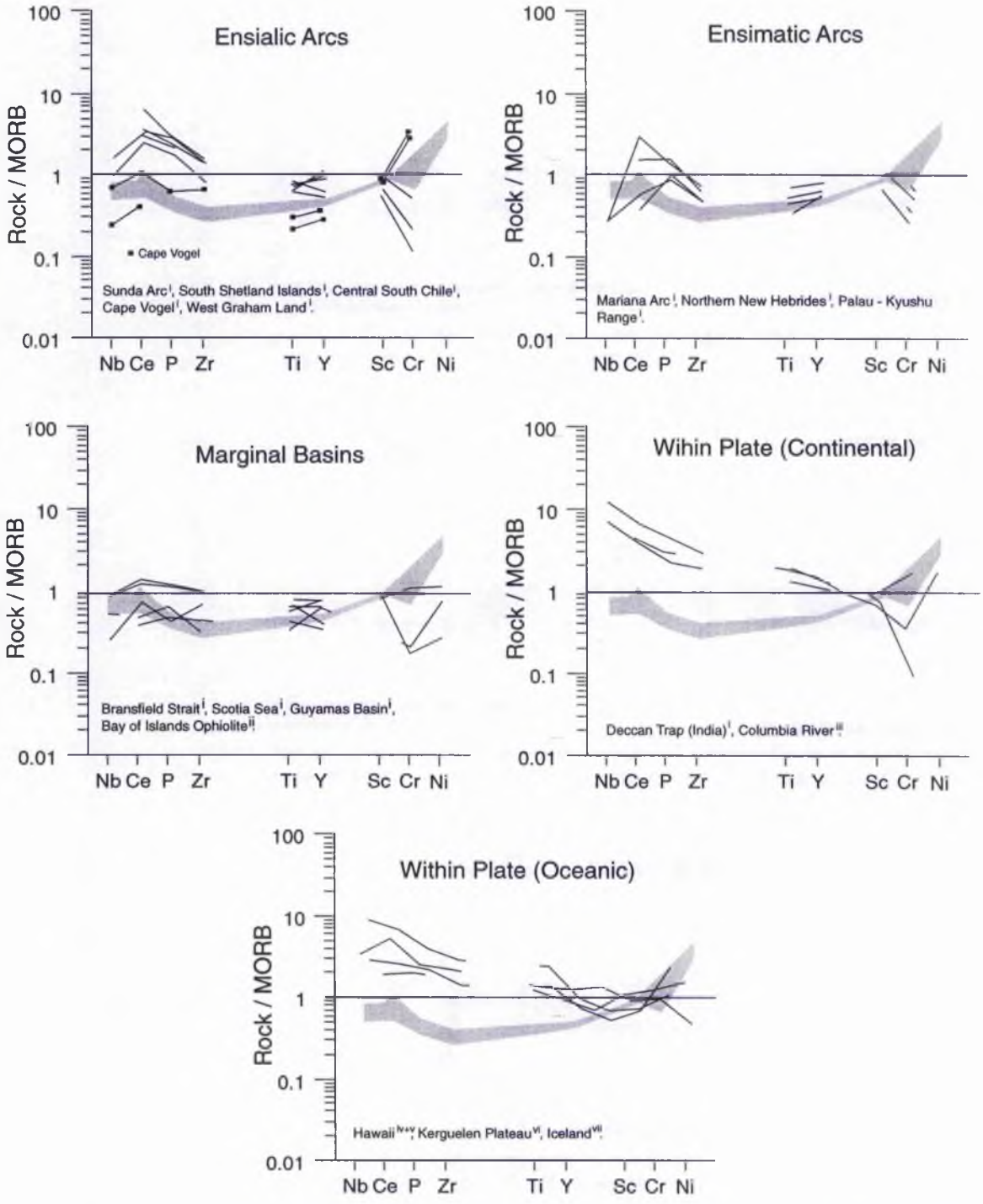

Fig. 3.12 MORB normalised spider plots (after Pearce, 1983) comparing the immobile trace elements of the Bere Amphibolite Formation (lightly shaded) with basalts from other tectonic environments. For discussion see text. Data sources for i) Brekke *et al.*, 1984; ii) Elthon, 1991; iii and iv) Basaltic Volcanism Study Project, 1981; v) West *et al.*, 1992; vi) Mahoney *et al.*, 1995; vii) Schilling *et al.*, 1983.

the exception of Cape Vogel which contains proportionally more Ti and Y and Less Cr than the Bere Amphibolite Formation. As discussed in section 3.2.5 it is difficult to discriminate between island - arc, low - K tholeiitic basalts and their counterparts from the associated, juvenile marginal basin since both trace element signatures contain a significant component from the dehydrating, subducting slab (Gribble *et al.*, 1998). This might be reflected in the similarity between the trace element patterns for the Bere Amphibolite Formation and that of the Mvuu Meta - Mafic Volcanic and Mbizi Sheeted Dyke Formations (*c.f.* Fig. 3.1 f and 3.2). It is also possible that the Bere Amphibolite Formation represents slices of marginal basin volcanics that have been imbricated into the island - arc complex either during obduction or subsequent deformation. The Bere Amphibolite Formation is a discrete, mappable unit which is visually distinct from the Mvuu Meta - Mafic Volcanic Formation. Considering the Bere Amphibolite Formations association with more silicic volcanics, lack of obvious tectonic contacts with the neighbouring formations and the discrete mappable nature of the formation, it is interpreted that the basalts are related to island - arc volcanism rather than that within a marginal basin. However, a more precise determination of the Nb concentration and / or REE analysis is needed to test this hypothesis.

3.3.3 Nhema Amphibolite Formation.

This formation is characterised by both biotite and hornblende - bearing meta - volcanics. Major element analyses indicates picro - basaltic to dacite compositions (Fig. 3.13 a). The majority of analyses (with the exception of 4 samples) display a tholeiitic fractionation trend. The four alkalic samples of Fig. 3.13 a, plot with a calc - alkaline trend in Fig 3. 13 b. Only basalt to andesite compositions have been plotted on the triangular discrimination plots of Fig. 3.12 c and d. In the 2Nb, Zr/4 verses Y diagram (Fig. 3.12 c) the

majority of the data is well constrained and plots in the field of volcanic arc basalts. In Fig. 3.12 d (Ti/100, Zr verses Y*3 triangular plot), the data is more variable and plots within the calc - alkaline basalt and MORB, island - arc tholeiite and calc - alkali fields. Table 3.3 is a summary of the other major and trace element discrimination diagrams. The MORB normalised spider plot (after Pearce, 1983) displays a moderately constrained data set. Figure 3.14 compares the MORB normalised, immobile trace elements of the Nhema Amphibolite Formation (shaded region with individual analyses removed) with basalts produced within other tectonic environments. It is evident that a similar trace is produced to the Mvuu Meta - Mafic Volcanic and Mbizi Sheeted Dyke Formations. However, the Nhema Amphibolite Formation displays a narrower, and lower range in Nb contents (1 - 3 ppm), a much reduced Ce peak and a narrower range in Zr contents.

The Nhema Amphibolite Formation produces a flat spider trace from Zr to Sc which is depleted in comparison to MORB. The low Nb contents (1 - 3 ppm) and depleted, flat traces, again suggest a destructive plate margin setting similar to either ensimatic - arcs or marginal basins (Brekke *et al.*, 1984; Wilson, 1989). With the margin of error for the Nb analysis being 1 to 2 ppm as discussed in section 3.3.2, discrimination between ensimatic island - arc and marginal basin settings is difficult without further analysis of REE or obtaining a more accurate Nb analysis.

3.3.4 Kamuyu Amphibolite Formation.

This formation is characterised by strongly deformed meta - basalts (section 2.3.7). The TAS diagram (Fig. 3.15 a) indicates that the majority of samples are tholeiitic basalts. The alkaline samples of Fig. 3.15 a, plot with a tholeiitic fractionation trend on Fig 3.15 b suggesting that the major elements may have been altered by hydrothermal and / or metamorphic alteration. Within the 2Nb, Zr/4 verses Y discrimination diagram (Fig. 3.15 c), the data is poorly

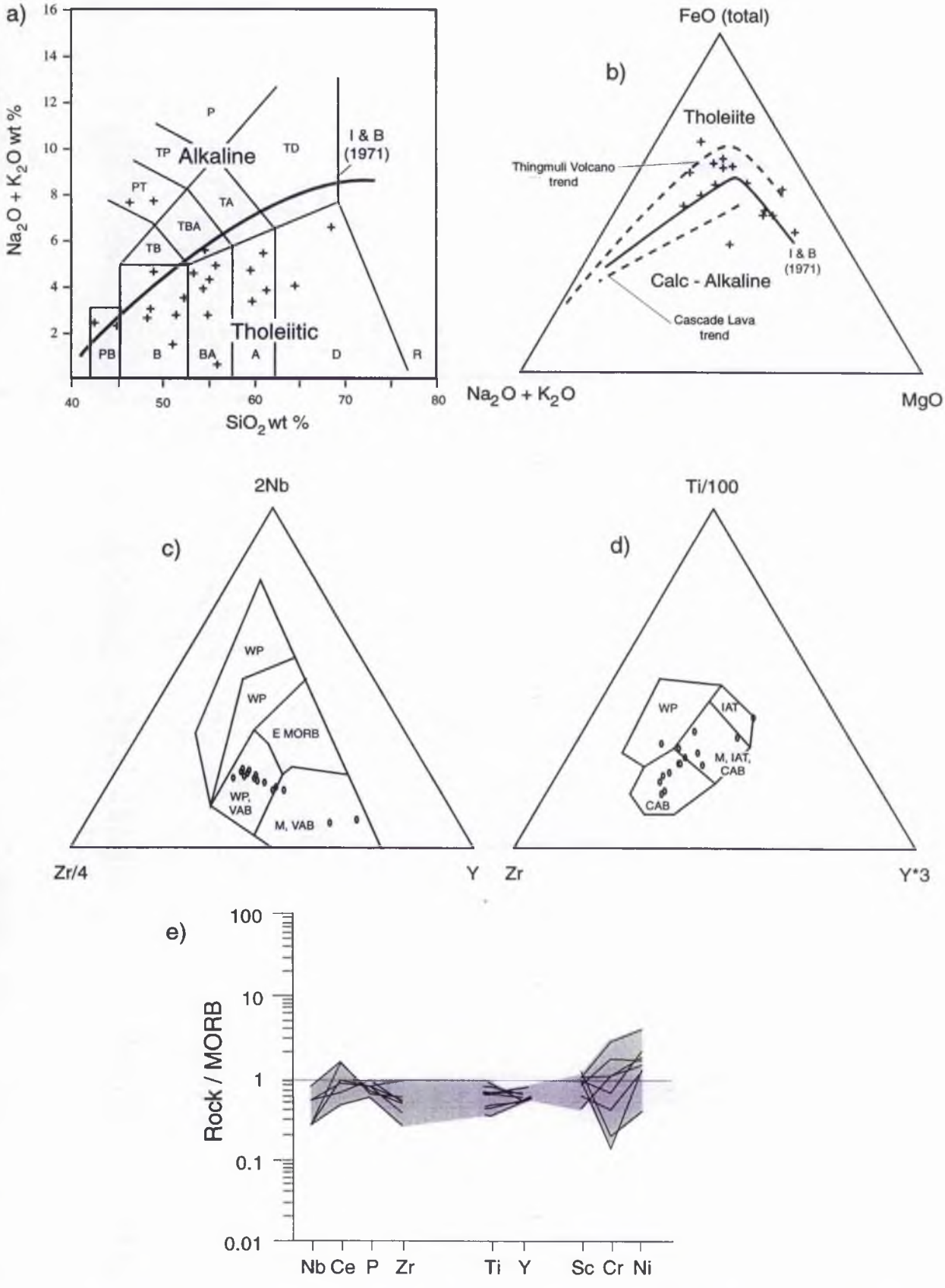

Fig. 3.13 Whole rock major and trace element Harker, discrimination and MORB normalised spider plots for the Nhema Amphibolite Formation. For discussion see text. 3.11.a) after Le Maitre, 1989 and Irvine & Baragar, 1971; b) after Ivine & Baragar, 1971 and Carmichael, 1964; c) after Meschende, 1986; d) after Pearce & Cann, 1973; e) after Pearce, 1983).

Nhema Amphibolite Formation

Elements Plotted	Reference	Comments
Major Elements		
TiO2-MnO*10-P2O5	Mullen,1983	(5) IAT, (5) MORB, (1) OIT, (1) Bon
FeO-MgO-Al2O3	Pearce *et al.*, 1977	(2) SC, (4) WP, (6) MORB
Function 1-Function 2	Pearce, 1976	(4) CAB and IAT, (8) outside all fields
Trace Elements		
Nb/Y-Ti/Y	Pearce, 1982	(4) WPT, (6) MORB, (2) VAB
Zr-Ti	Pearce and Cann, 1973	(5) IAT, (1) IAT and MORB, (3) CAB, (2) MORB
Zr-Ti	Pearce, 1982	(2) VAB, (2) VAB and MORB, (1) MORB, (6) WP
Zr-Zr/Y	Pearce and Norry, 1979	(7) WP, (2) MORB, (2) VAB, (1) outside all fields
Zr-Zr/Y	Pearce, 1983	(10) CA, (2) OA

Table. 3.3 Summary of the major and trace element discrimination diagrams for the Nhema Amphibolite Formation.

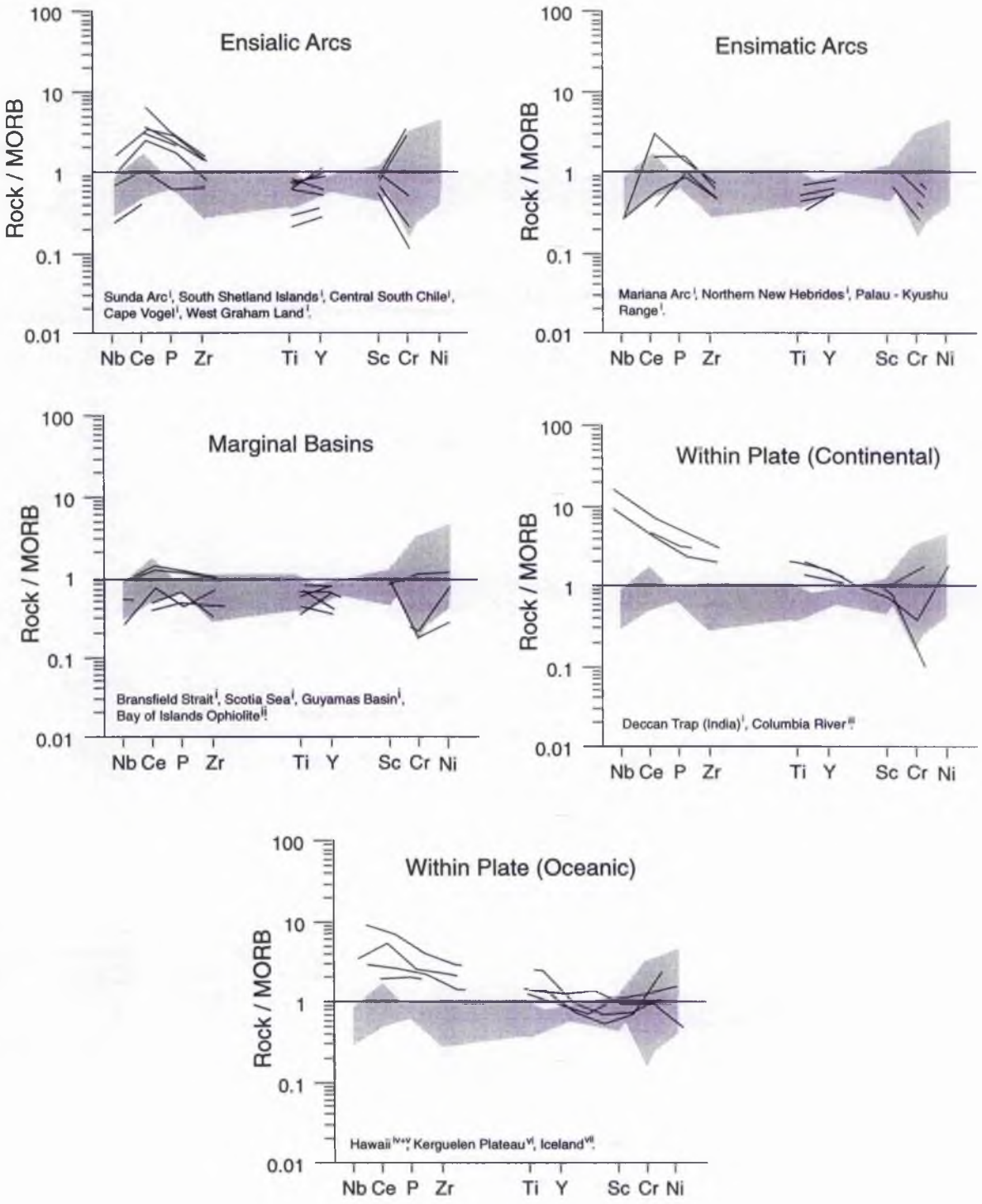

Fig. 3.14 MORB normalised spider plots (after Pearce, 1983) comparing the immobile trace elements of the Nhema Amphibolite Formation (lightly shaded) with basalts from other tectonic environments. For discussion see text. Data sources for i) Brekke *et al.*, 1984; ii) Elthon, 1991; iii and iv) Basaltic Volcanism Study Project, 1981; v) West *et al.*, 1992; vi) Mahoney *et al.*, 1995; vii) Schilling *et al.*, 1983.

constrained but is evenly distributed between the fields of MORB, volcanic arc, within plate and E type MORB, while in the Ti/100, Zr verses Y*3 triangular plot (Fig. 3.15 d), the data is again poorly constrained, plotting within the MORB, island - arc tholeiite, calc - alkali field; calc - alkali and within plate field. Table 3.4 is a summary of the other major and trace element discrimination diagrams. The MORB normalised spider plot (Fig. 3.15 e) of immobile trace elements displays a moderately well constrained data set which slopes gently from top left to bottom right, indicating increasing enrichment in the incompatible, immobile trace elements (Nb and Ce). The most characteristic feature of this trace element pattern is the elevated Nb contents of between 3 and 19 ppm. The lowest three samples [SJ 135, 156 and 165] display trace element patterns similar to those of the Mvuu and Mbizi Sheeted Dyke Formations (Fig. 3.15 f). These three samples also plot in similar positions within the triangular discrimination diagrams (*c.f.* Fig. 3.15 c, d and Fig. 3.1 d, e). The intense strain displayed by the Kamuyu Amphibolite Formation makes the visual distinction between possible island - arc and marginal basin derived meta - basalts difficult. It is therefore possible that samples [SJ 135, 156 and 165] are slices of marginal basin crust imbricated within the Kamuyu Amphibolite Formation.

Figure 3.16 compares the MORB normalised, immobile trace element patterns of the Kamuyu Amphibolite Formation (shaded region with samples [SJ 135, 156 and 165] removed from the data set) with basalts produced within other tectonic environments. The gently sloping trace, showing enrichment in the incompatible, immobile, trace elements and depletion in the more compatible, immobile, trace elements indicates that formation at a destructive or constructive plate margin is unlikely. The trace element pattern is most like those of basalts derived from within - plates. Figure 3.16 shows the trace element patterns for basalts formed both within oceanic plates (such as Hawaii, Iceland and Kerguelen) and within continental plates (such as the

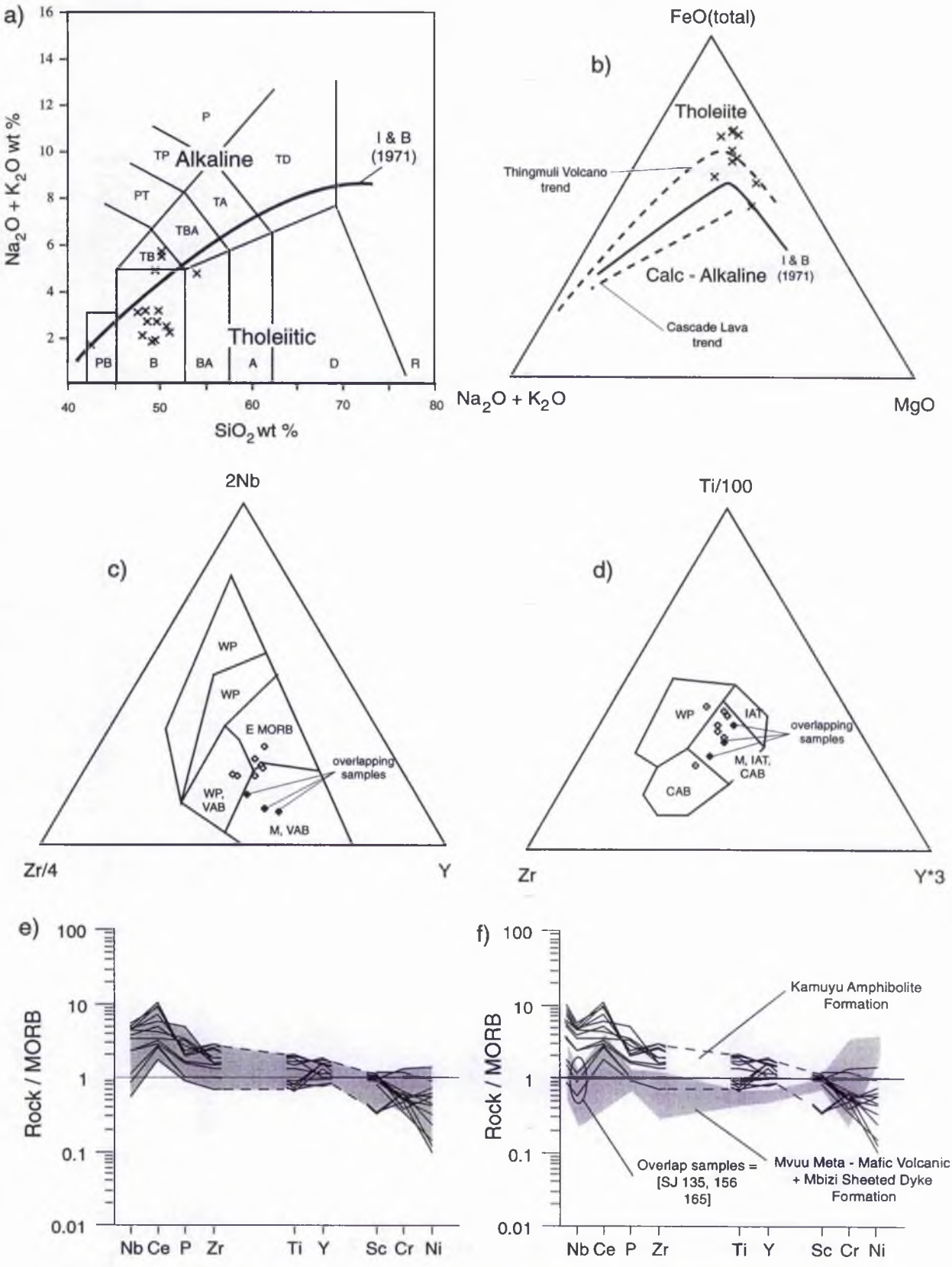

Fig. 3.15 Whole rock major and trace element Harker, discrimination and MORB normalised spider plots for the Kamuyu Amphibolite Formation. For discussion see text. 3.11.a) after Le Maitre, 1989 and Irvine & Baragar, 1971; b) after Irvine & Baragar, 1971 and Carmichael, 1964; c) after Meschende, 1986; d) after Pearce & Cann, 1973; e) after Pearce, 1983).

Kamuyu Amphibolite Formation

Elements Plotted	Reference	Comments
Major Elements		
TiO2-MnO*10-P2O5	Mullen,1983	(3) IAT, (4) MORB, (2) OIT, (1) OIA
FeO-MgO-Al2O3	Pearce *et al.*, 1977	(7) WP, (3) OI
Function 1-Function 2	Pearce, 1976	(3) MORB, (2) WP, (1) CAB and IAT, (4) outside all fields
Trace Elements		
Nb/Y-Ti/Y	Pearce, 1982	(4) MORB, (2) VAB and MORB, (2) WPT
Zr-Ti	Pearce and Cann, 1973	(2) MORB, (2) IAT and MORB, (1) IAT, (5) outside fields
Zr-Ti	Pearce, 1982	(7) WP, (3) MORB
Zr-Zr/Y	Pearce and Norry, 1979	(6) MORB, (2) MORB and VAB, (2) WP
Zr-Zr/Y	Pearce, 1983	(3) CA, (1) OA, (1) CA and OA, (5) outside all fields

Table. 3.4 Summary of the major and trace element discrimination diagrams for the Kamuyu Amphibolite Formation.

Deccan Traps and Columbia River flood basalts). The traces for both oceanic and continental within plate basalts are similar to that of the Kamuyu Amphibolite Formation, however, the Nb (3 - 9 ppm) and Ti (152 - 187 ppm) contents are relatively low for these meta - basalts to have formed within a continental plate. It is therefore interpreted that the Kamuyu Amphibolite Formation represents a sequence of within oceanic plate meta - basalts (imbricated with marginal basin crust). Thus there are three possible tectonic origins for this formation, namely, within plate hot spot, such as Hawaii; mid - ocean ridge hot spot, such as Ascension Island and Iceland and Large Igneous Province such as Kerguelen. Both Hawaii and Ascension Island are associated with alkalic fractionation trends and production of trachybasalts (Wilson, 1989). The lack of such alkalic basalts within the Kamuyu Amphibolite Formation suggests that this formation is not related to either within plate hot spot or mid - ocean ridge hot spot volcanism. However, Thingmuli Volcano in eastern Iceland displays a tholeiitic fractionation trend (Carmichael, 1964). Figure 3.17 is a trace element variation diagram of Zr/Nb verses Y/Nb (after Wilson, 1989) which discriminates between plume type (P - MORB) and normal (N - MORB) mid - ocean ridge basalts, the intermediate being transitional (T - MORB). Also plotted are the fields for Hawaii (within plate hot spot), Ascension (mid - ocean ridge hot spot), Kerguelen (large igneous province) and the Mid - Atlantic Ridge (N - MORB). It is evident that both the Kamuyu Amphibolite Formation and Kerguelen plot as T - MORB while Hawaii and Ascension plot clearly as P - MORB. The similarity in trace element abundances and the tholeiitic nature of the Kamuyu Amphibolite Formation meta - basalts compared with those from Kerguelen (Mahony *et al.*, 1995), suggest that this formation may be a remnant of a large igneous province. However this hypothesis cannot be confirmed without analysis of either :- REE and / or Sr, Nd and Pb isotopes.

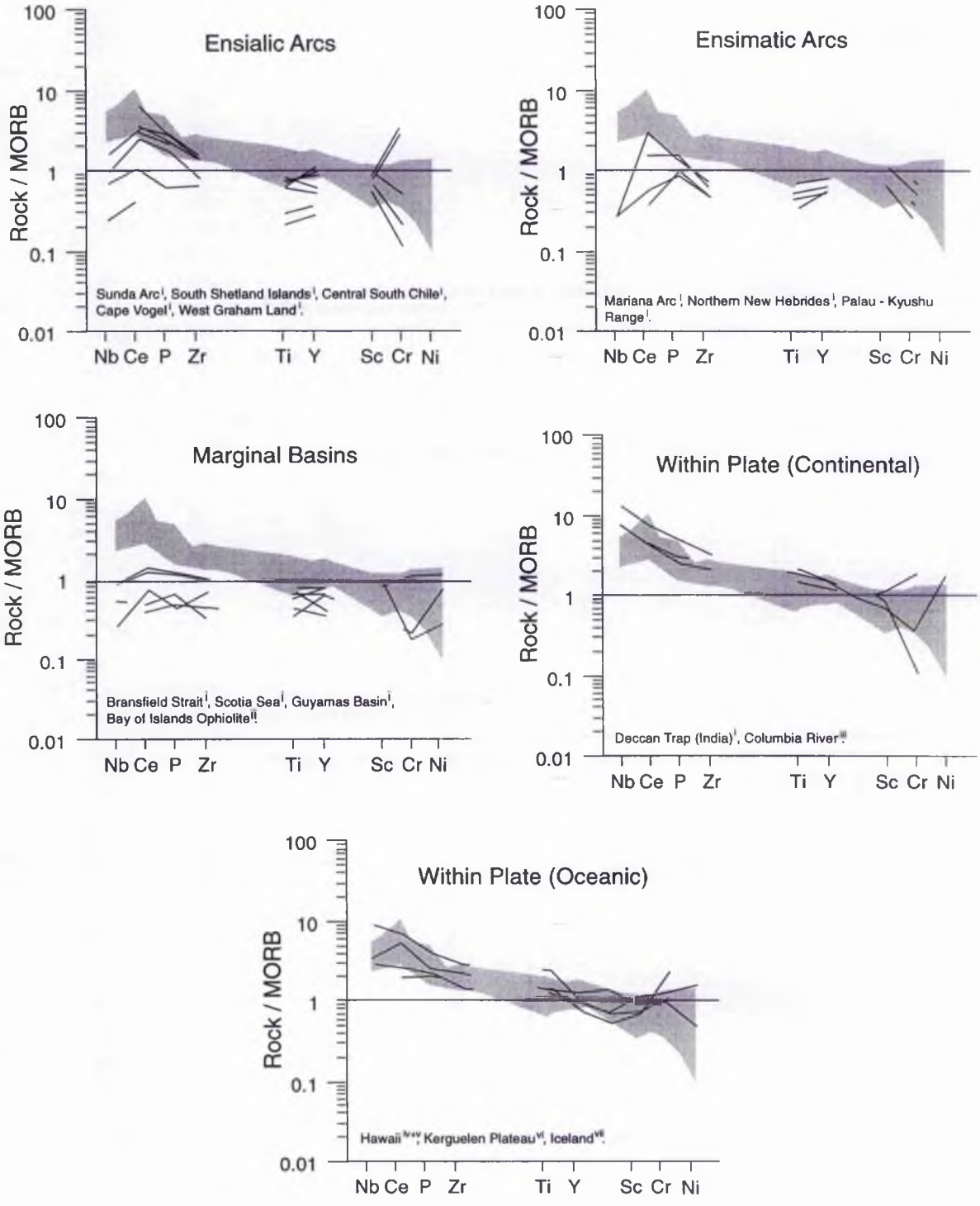

Fig. 3.16 MORB normalised spider plots (after Pearce, 1983) comparing the immobile trace elements of the Kamuyu Amphibolite Formation (lightly shaded) with basalts from other tectonic environments. For discussion see text. Data sources for i) Brekke *et al.*, 1984; ii) Elthon, 1991; iii and iv) Basaltic Volcanism Study Project, 1981; v) West *et al.*, 1992; vi) Mahoney *et al.*, 1995; vii) Schilling *et al.*, 1983.

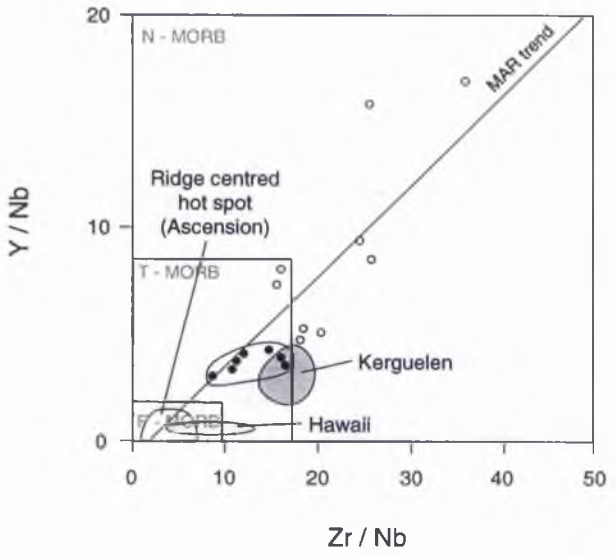

Fig. 3.17 Trace element variation diagram of Y / Nb verses Zr / Nb (after Wilson, 1989), discriminating between N (normal), T (transitional) and P (plume) type MORB. The Kamuyu Amphibolite Formation (solid circles) plots similar to Kerguelen while other Kaourera Island - Arc Group meta - basalts (open circles) plot similar to the Mid Atlantic Ridge (MAR) trend.

3.3.5 Gondo Meta - Felsic Volcanic Formation.

Mharapara and Gora Members.

These members are characterised by silica rich , fine grained, layered and sometimes pillowed volcanics (sections 2.3.3 and 2.3.4). Whole rock major element analyses indicates that the majority of samples are dacitic and tholeiitic, while one sample of the Mharapara Member [SJ 222BII] plots as a tholeiitic rhyolite (Fig. 3.18 a and b) and one sample of the Gora Member plots as a tholeiitic andesite (Fig. 3.18 c and d).

Fura Member.

The Fura Formation is represented by a single sample [SJ 220] which is described in section 2.3.5 as a banded, pale cream, plagioclase and quartz dominant meta - volcanic. The major element data indicates an alkaline, trachydacite composition (Fig. 3.18 e). The sample has a high $Na_2O + K_2O$ to a low FeO and MgO ratio (Fig. 3.18 f) and plots at the end of the Thingmuli Volcano tholeiitic fractionation trend.

3.3.6 Discussion.

The major element geochemistry indicates that the lithostratigraphic units of the Kaourera Island - Arc Group display a continuous range in predominantly tholeiitic rock compositions from 43 to 79 wt% SiO_2. Field structures such as pillow lavas (section 2.3.4 and Plate. 2.7 f) and micro - structures such as relict igneous phenocrysts (section 2.3.3, 2.3.4 and Plate 4.3 a and b) indicate that the group is of an extrusive, igneous origin. An island - arc system is one of the only tectonic environments capable of producing such a complex, extremely varied range of tholeiitic magma compositions (Wilson, 1989). However, Thingmuli Volcano in eastern Iceland also shows this varied tholeiitic fractionation suite. Figure 3.19 illustrates the modal proportion of mafic to silicic volcanics produced within a typical tholeiitic island - arc suite, Thingmuli Volcano and the Kaourera Island - Arc Group. There is a strong similarity between the Kaourera Island - Arc Group and that of a typical tholeiitic island - arc suite. It is also evident from the trace element data (section 3.3.2 - 3.3.3) that the Kaourera Island - Arc Group meta - basalts (Bere and Nhema Amphibolite Formations) are similar to those produced within island - arc systems and dissimilar to those produced at mid - ocean ridge hot spots.

Some Kaourera Island - Arc Group meta - basalts display elevated K_2O contents possibly indicating the presence of a separate calc - alkaline fractionation series. The similarity in immobile trace elements of the calc - alkaline meta - basalts, to the low - K tholeiitic meta - basalts suggest that this may be an artefact of hydrothermal and / or metamorphic alteration of the major elements within the former. However, since the majority of calc - alkaline samples are spatially located within the top thrust sheet (Fig. 3.20) of the Maunde Domain this might suggest that this fractionation suite is present. Further and more complete sampling of this region is needed to test this hypothesis.

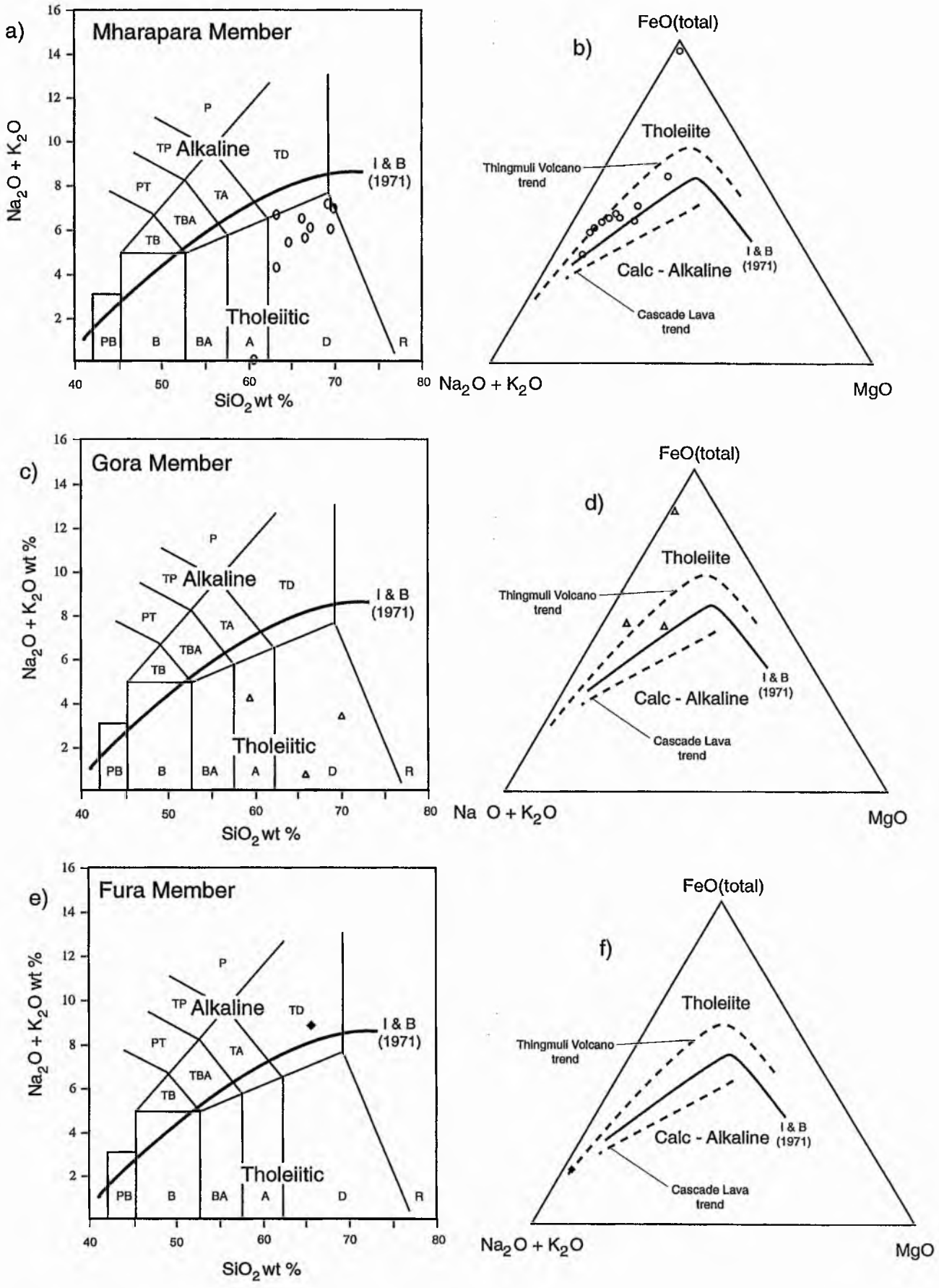

Fig. 3.18 Whole rock major element variation diagrams for the Gondo Meta - Felsic Volcanic Formation. For discussion see text. Total alkalis vs silica diagram is after Le Maitre, 1989 and Irvine & Baragar, 1971; FeO(tot), total alkalis vs MgO triplot is after Irvine & Baragar, 1971 and Carmichael, 1964.

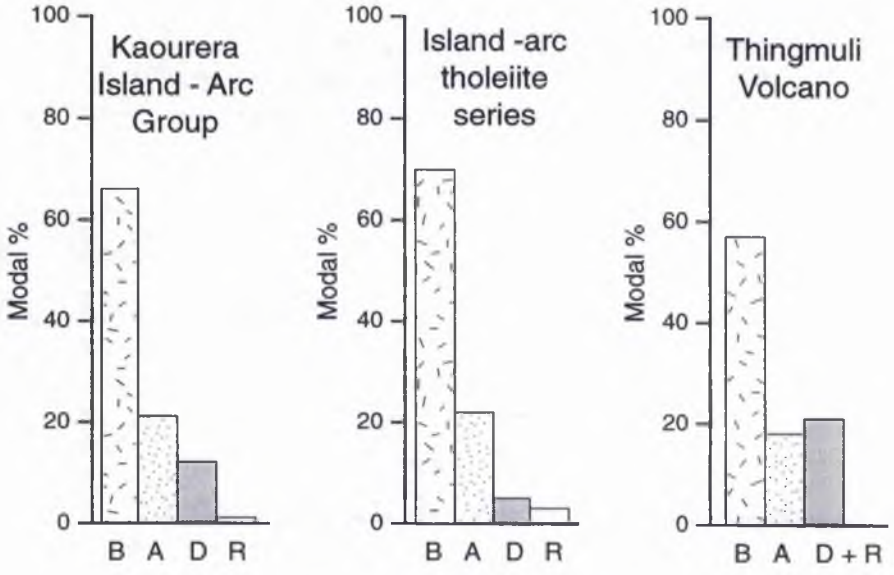

Fig. 3.19 Modal proportion of mafic to silicic volcanics produced within a typical island - arc suite (Wilson, 1989) and Thingmuli Volcano, Iceland (Carmichael, 1964) compared with the Kaourera Island - Arc Group.

Trace element analysis of the Bere and Nhema Amphibolite Formation meta - basalts indicates formation at a destructive plate margin while Kamuyu Amphibolite Formation meta - basalts indicate formation within an oceanic plate environment. Figure 3.21 shows major and trace element variation diagrams of Wt % MgO verses Ni ppm and Ce ppm verses La ppm for the Kaourera Island - Arc Group meta - basalt formations compared with the fields for other tectonic environments. It is evident that all formations (including the Kamuyu Amphibolite Formation) plot with a single trend in each diagram, suggesting derivation from a similar mantle source. In both plots it is evident that the mantle source of the Kaourera Island - Arc Group is unlike that of the present day South Shetland and West Coast of Graham Land, Antarctica, which is of an ensialic arc origin. Within the wt % MgO verses Ni ppm plot, further discrimination is made between the Kaourera Island - Arc Group and the basalts from Hawaii. Combined with the other trace element analysis (sections 3.3.2 - 3.3.4), it is interpreted that the Bere and Nhema Amphibolite Formation meta - basalts have trace element ratios similar to that of basalts formed within an ensimatic arc environment.

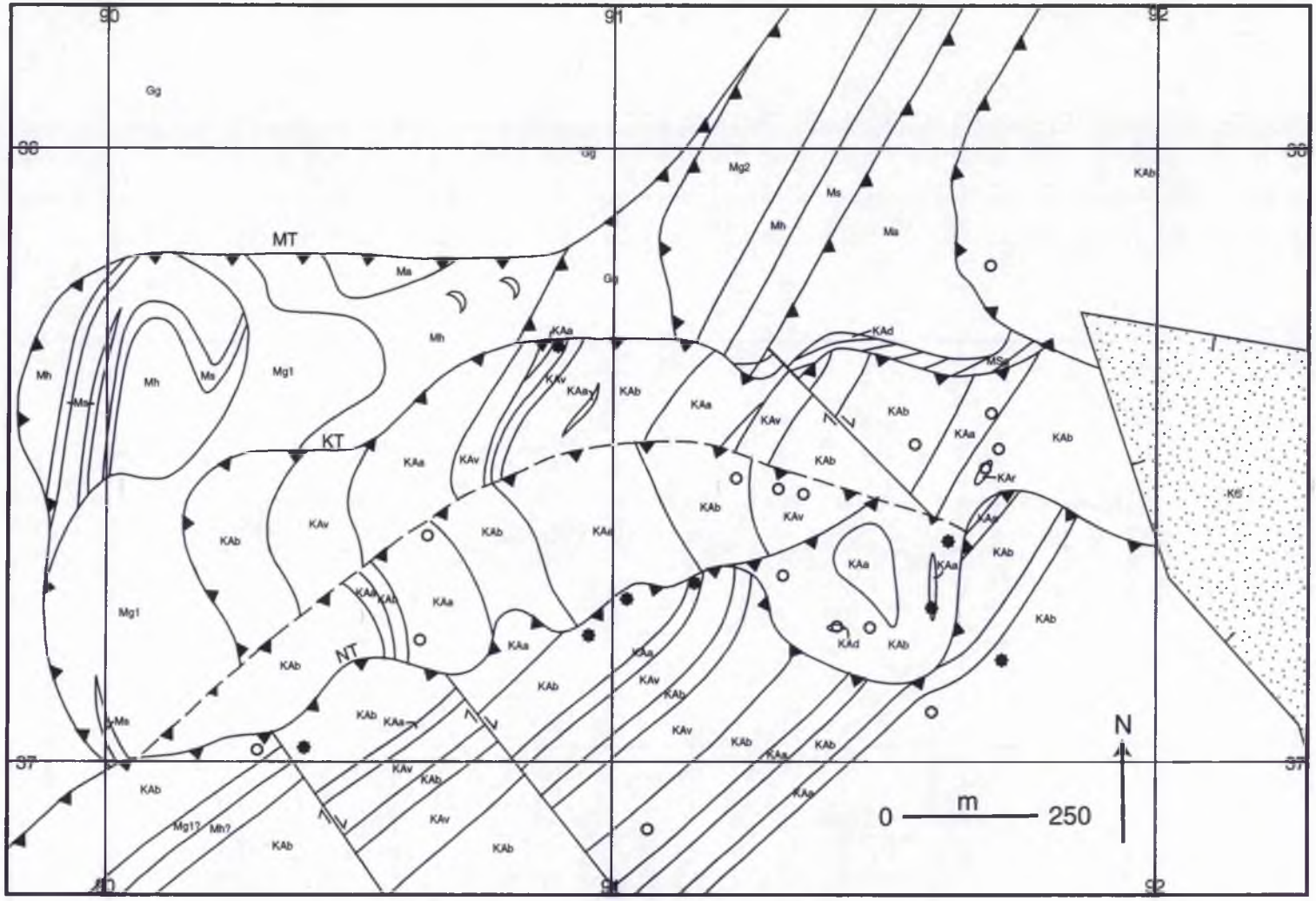

Fig. 3.20 Map of the Maunde region illustrating the distribution of tholeiitic and calc - alkaline volcanics within the Kaourera Island - Arc Group. Open circles represent tholeiitic analyses and closed stars indicate calc - alkaline analyses. For key to lithological and geological symbols refer to map insert 2.

However, the concentration of Nb within these meta - basalts are 1 to 2 ppm greater than that of basalts from modern ensimatic arcs and these meta - basalts might be better interpreted as being formed within a marginal basin setting. These elevated Nb concentrations might be an artefact of the XRF analysis which is at or near the limit of detection. The intimate association of the Nhema and Bere Amphibolite Formation meta - basalts with tholeiitic andesites, dacites and rhyolites and the relative proportion of these silica variable rocks, altogether suggest that these meta - basalts are the product of ensimatic island - arc volcanism rather than back - arc basin spreading.

The tholeiitic fractionation series is produced throughout the life of an island - arc system but is spatially related to the region nearest the trench (Wilson, 1989) of the subducting plate (Fig. 3.22), while the calc - alkaline series is both temporally and spatially related to the island - arc system (Fig. 3.22). As an island - arc system temporally develops, tholeiitic magmatism gives way to calc - alkaline magmatism and then eventually to high - K and shoshonitic magmatism (Wilson, 1989). Such an example is the modern day South Sandwich island - arc system which during the early stages of its development erupted predominantly tholeiitic volcanics but has since given way to calc - alkaline fractionation trends (Wilson 1989). The Kaourera Island - Arc Group is dominated by a tholeiitic fractionation series with a possible, minor calc - alkaline component. It is therefore possible that the 'Kaourera' island - arc system was temporally within its middle stages (see Fig 3.22).

The Kamuyu Amphibolite Formation is interpreted as representing volcanism at an intra - oceanic hot spot analogous to the present day Kerguelen plateau and might represent a marginal basin seamount.

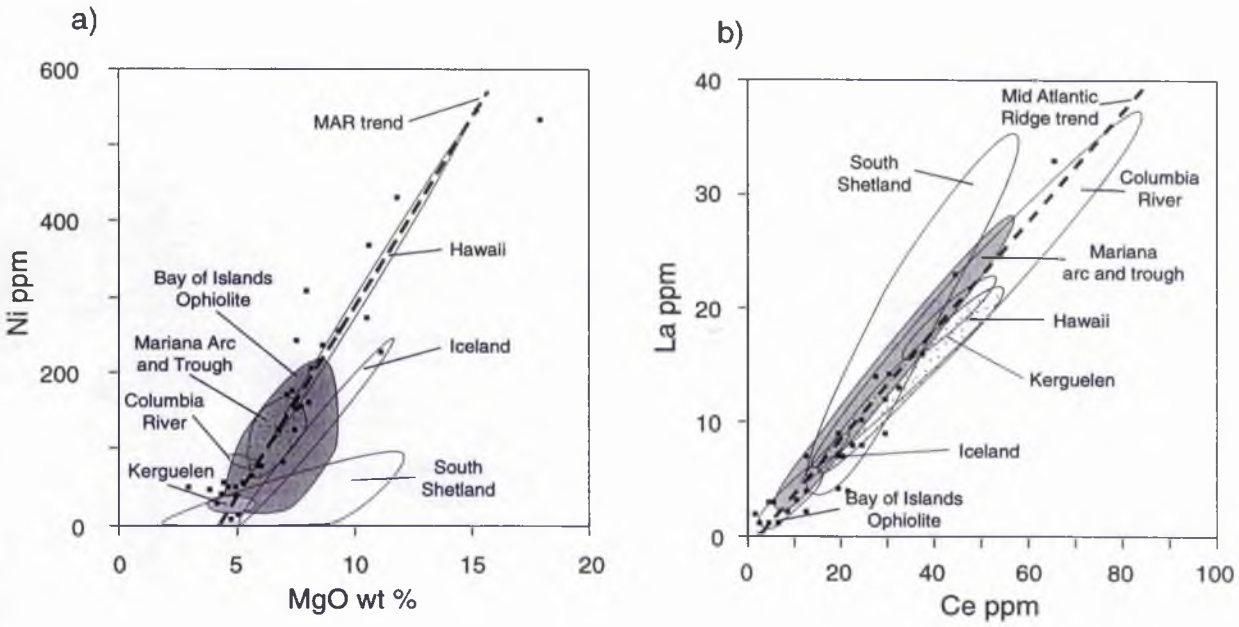

Fig. 3.21 Whole rock major and trace element variation diagrams for the Bere and Nhema Amphibolite Formations combined (Closed squares). Overlain are the fields of other world wide tectonic environments. Data for the various fields for both a and b) are from :- Suen *et al.*, 1979 and Elthon, 1991 (Bay Of Islands Ophiolite); Basaltic Volcanism Study Project, 1981 (Columbia River Plateau); Basaltic Volcanism Study Project, 1981 and West *et al.*, 1992 (Hawaii); Schilling *et al.*, 1983 and Furman *et al.*, 1995 (Iceland); Mahoney *et al.*, 1995 (Kerguelen); Wilson, 1989 (MAR - Mid Atlantic Ridge trend); Hawkins *et al.*, 1990 and Gribble *et al.*, 1998 (Mariana Arc and Trough); Saunders *et al.*, 1979 (South Shetland and West Coast of Graham Land).

3.4 The Kadunguri Whiteschists.

The aim of this section is to present the whole rock, major and trace element geochemistry of the petrologically important, talc and kyanite bearing whiteschists, in an attempt to identify their rather exceptional protolith.

3.4.1 *Major and Trace Element Analysis.*

The protoliths of the Foliated and Unfoliated Qtz Whiteschists, Gedrite Whiteschist and the Yoderite Whiteschist must be rather exceptional since they are comprised from only MgO, Fe_2O_3, Al_2O_3 and SiO_2 (Appendix C and Table 3.5) and thus belong to the simple $MF^{3+}ASH$ system (plus some minor Na and B). The presence of talc and kyanite within the same metamorphic assemblage was first described by Schreyer and Seifert (1969) and was subsequently termed a 'whiteschist' assemblage by Schreyer (1973). Geochemical analyses of whiteschist assemblages indicated that they are characterised by the simple $MF^{3+}ASH$ system. The major element data of the Kadunguri whiteschist assemblages compare well with that of the other known whiteschist occurrences from around the globe (Table 3.5). The positions of the major element analysis and coexisting phases of the various examples are plotted in Fig. 3.23 a. Schreyer (1977) indicates that "most of the components present within whiteschists can theoretically be represented by the assemblage Mg - chlorite plus quartz" since, "the projection points of major element analysis onto a modalised SiO_2 - MgO - Al_2O_3 triangular diagram are concentrated within a two phase field of chlorite solid solutions with quartz". The Kadunguri Whiteschists plot within or lie close to this two phase field, indicating that the protolith was also dominated by chlorite and quartz. The Yoderite Whiteschist plots closer to chlorite than the other Kadunguri samples, suggesting that its protolith was dominated predominantly by chlorite.

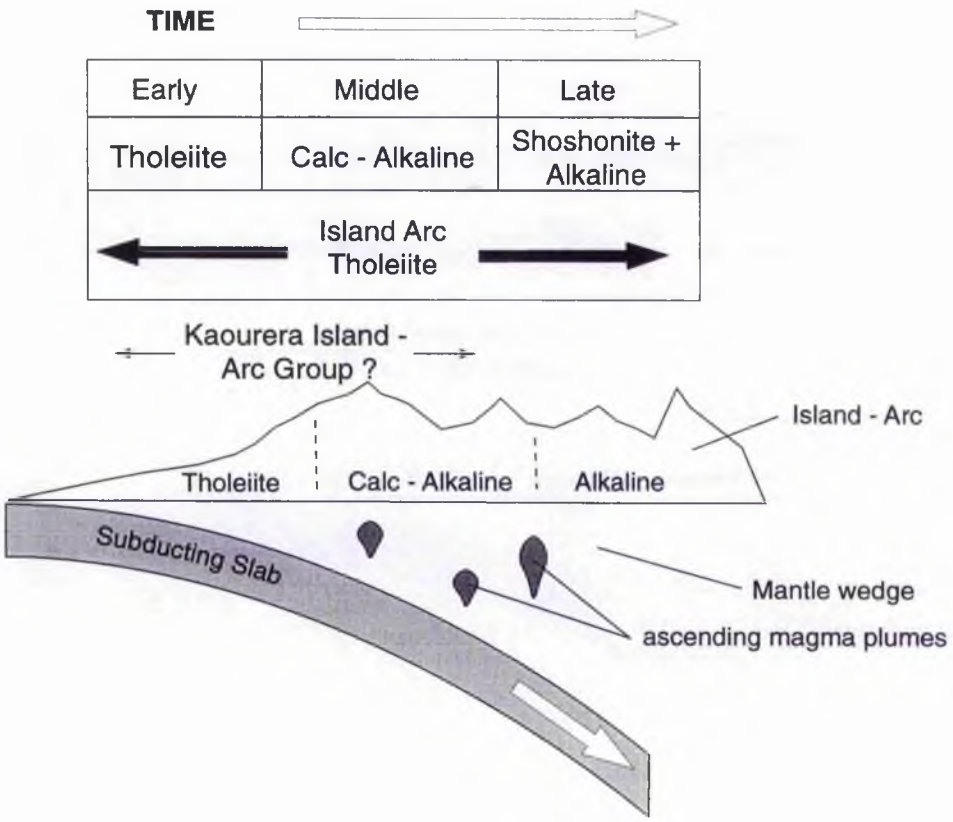

Fig. 3.22 Cartoon cross section of an Island - Arc system, illustrating both the temporal and spatial distribution of the main magmatic suites (tholeiite, calc - alkaline, alkaline and shoshonitic). Illustration after Wilson, 1989.

The trace element geochemistry is given in appendix C. As yet there is no published account of the trace element geochemistry of other whiteschists; thus a comparison cannot be made. Fig. 3.23 b is a MORB normalised spider diagram for the Kadunguri Whiteschist examples, excluding the Yoderite Whiteschist. These three examples, although containing a slightly different mineral assemblage produce similar traces, which are unlike that of MORB, but similar to that of island - arc basalts.

3.4.2 Discussion.

The restricted bulk rock, major element geochemistry of whiteschists ($MF^{3+}ASH$), including those of the Kadunguri Whiteschists, is unique within the rock record. There is no primary, unaltered sedimentary or igneous rock with a similar chemistry and therefore it is interpreted by many authors that this unique chemistry occurs by the metamorphism and alteration / metasomatism of various sedimentary or igneous sources. However, it is pointed out by Kulke & Schreyer (1973) that modern day evaporitic mudstones of the Sahara Atlas of north Africa do show similar, but not identical, bulk rock compositions. Since the major element chemistry of these Kadunguri rocks have been altered by metamorphism / metasomatism a direct comparison of major elements with possible protoliths is not possible. The trace elements must also be treated with such caution. Below is a list of interpretations of whiteschist protoliths :-

i) Mudstones associated with evaporite deposits which when metamorphosed produce talc, kyanite and scapolite (Kulke & Schreyer, 1973; Fockenberg & Schreyer, 1994).

ii) Interaction of hydrothermal fluids with dolomite and quartzite producing talc, kyanite and magnesite (Bodenlos, 1955).

iii) In - situ weathering and metamorphism of saponitic bentonites producing talc, quartz and kyanite (McKie, 1959).

	Chewore Hills			Mautia Hill	Zambia				Sar e Sang
Weight %	SJ 130	SJ 417	SJ 128	T	Z157	Z159	Z161	Z234	A42
SiO2	51.95	56.37	35.46	74.54	61.20	67.00	71.40	57.20	56.20
TiO2	1.15	1.38	0.27	0.27	1.14	1.51	1.22	1.18	0.30
Al2O3	15.50	16.07	23.80	8.13	13.40	13.10	10.70	16.20	16.00
B2O3	0.00	0.00	0.00	n.rep	0.01	0.01	0.02	0.13	0.34
Fe2O3	2.29	7.59	12.97	1.92	0.10	4.40	5.10	5.20	0.30
FeO	0.00	0.00	0.00	0.90	0.30	0.30	0.30	0.70	0.10
MnO	0.00	0.03	0.02	0.11	0.00	0.00	0.00	0.00	<0.01
MgO	18.99	16.24	20.35	12.33	20.00	11.50	9.60	11.40	22.90
CaO	0.11	0.02	0.18	trace	0.10	0.10	0.10	0.20	0.10
Na2O	0.10	0.40	0.33	0.14	0.30	0.20	0.10	5.30	0.60
K2O	0.02	0.01	0.00	0.03	0.10	0.10	0.10	0.70	0.20
P2O5	0.07	0.06	0.05	trace	0.02	0.27	0.00	0.04	<0.02
LOI	10.60	1.80	6.80	H2O 1.87	3.90	2.00	1.70	2.30	3.50
Total	100.78	99.95	100.23	100.24	100.57	100.49	100.34	100.55	100.54

Explanation : n.rep = not reported.

Table. 3.5 Representitive whole - rock major - element analysis of the Foliated Quartz Whiteschist (SJ 130)
Unfoliated Quartz Whiteschist (SJ 417) and Yoderite Whiteschist (SJ 128) compared to other whiteschist occurrences (data from Schreyer, 1977).

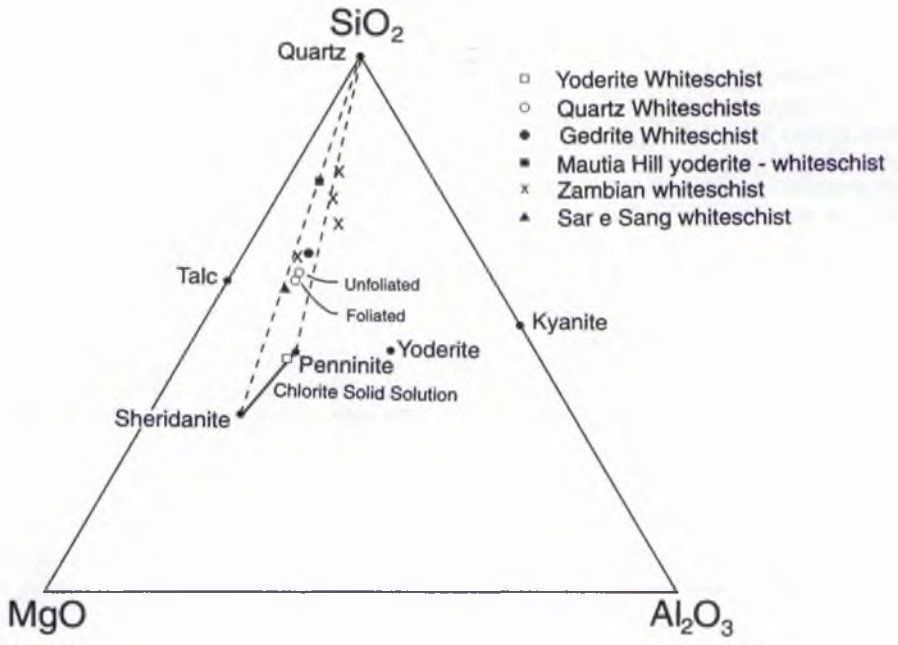

Fig. 3.23a Triangular compatibility diagram (in the presence of excess H_2O, FeO and Fe_2O_3) showing the positions of the co - existing phases and whole rock major element analyses for the Quartz, Yoderite and Gedrite Whiteschists and other world wide whiteschist occurrences. For discussion see text. Analyses for Mautia Hill, Zambia and Sar e Sang are from Schreyer, 1977.

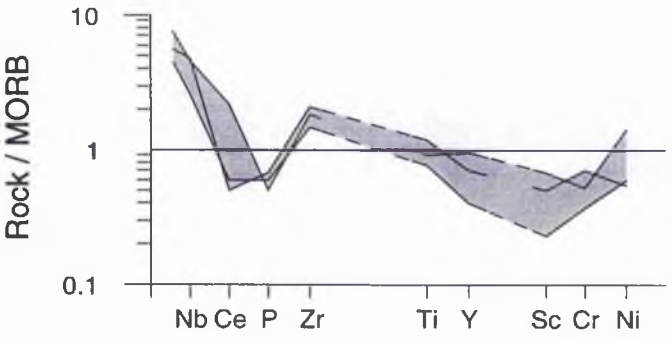

Fig. 3.23b MORB normalised spider plot (after Pearce, 1983) of the Quartz and Gedrite Whiteschists. For discussion see text.

iv) Metasomatism of peridotite and serpentinite producing talc and chlorite (Curtis & Brown, 1969).

v) Hydrothermal alteration of meta-basic volcanics producing talc and kyanite (Vrána & Barr, 1972; Vrána, 1975).

The large size of the Kadunguri Whiteschists (6 x 3 km) makes it one of the largest, single, continuous outcrops of talc + kyanite + quartz rock recorded anywhere in the world. This alone suggests that its precursor was homogeneous on a kilometre scale and this would therefore seem to exclude a localised evaporite or a bentonite origin. The lack of any recognisable sedimentary features and/or any magnesite/scapolite mineralisation also seems to indicate a non - sedimentary source. A large homogeneous body of the size and composition indicated is likely to have an igneous origin (i.e., basaltic or ultramafic). Since the Maunde Ophiolite and Kaourera Island - Arc Groups which lie directly to the north, are comprised of both mafic and ultramafic igneous assemblages it is not unreasonable to suggest that one of these lithotypes may have been altered to produce a chlorite + quartz - rich assemblage.

In comparison with the other rock types within the Ophiolite Terrane, i.e., meta - gabbros, serpentinites, meta - arc basalts and meta - dacites, the trace element geochemistry (Fig. 3.24) is *most* similar (but not identical) to that of the island - arc derived meta - basalts, *moderately* like the marginal basin meta - basalts and *unlike* that of the serpentinites, meta - gabbros and meta - dacites. However, the Kadunguri whiteschists do not display the characteristic negative Nb anomaly that is associated with island - arc and marginal basin volcanics.

Considering the highly altered nature of these rocks, it is unlikely that an identical comparison could be made with any other assemblage. The similarity of the trace element geochemistry of the whiteschists to the island -

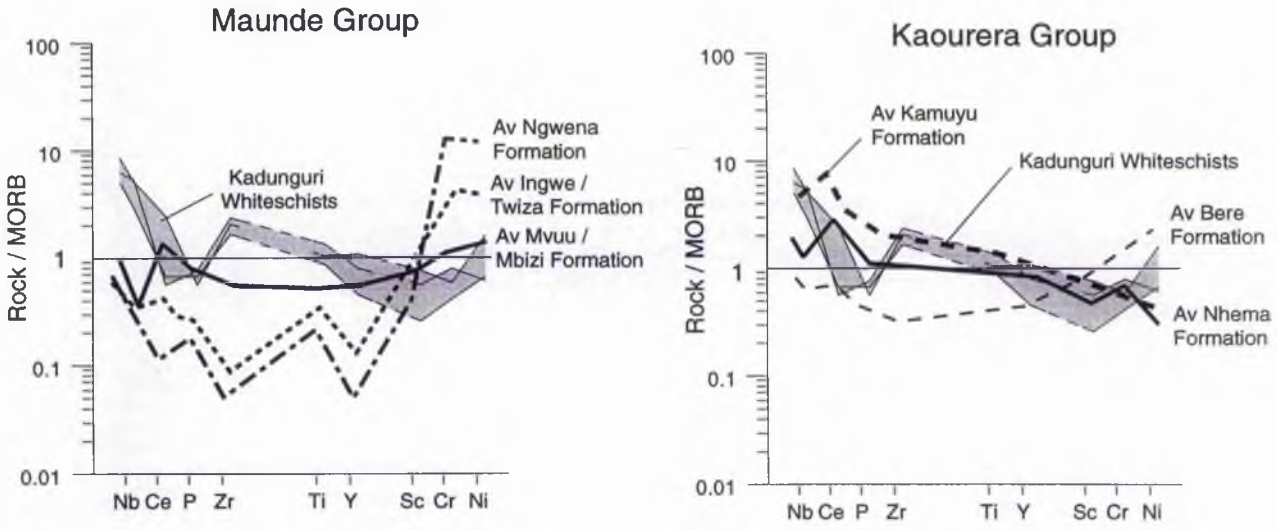

Fig. 3.24 MORB normalised spider plots (after Pearce, 1983) of the Kadunguri Whiteschists (lightly shaded). Overlain are the traces of the various Maunde Ophiolite and Kaourera Island - Arc Group formations. For discussion see text.

arc meta - basalts and the dissimilarity with all other formations suggest that this may be the protolith to the Kadunguri Whiteschists. If this is the case, then metasomatism and / or hydrothermal alteration must have removed the alkalis (CaO, Na_2O and K_2O) and Fe_2O_3 from these island - arc meta - basaltic rocks thus relatively increasing the SiO_2 and MgO contents. The Yoderite Whiteschist is possibly an extreme example of this metasomatism since it is most enriched in Al_2O_3, MgO and Fe_2O_3. However the proportion of SiO_2 within the Yoderite Whiteschist is significantly less than within the other members indicating that this was a site of SiO_2 removal during the metasomatic event.

A similar meta - basaltic origin is envisaged for the Zambian whiteschists (Vrána & Barr, 1972; Vrána, 1975), the closest of which crops out only 90 km to the north west of the Kadunguri Whiteschists.

3.5 Conclusions.

It is concluded that:-

1) The Maunde Ophiolite Group contains a suite of lithologies that are geochemically related and have affinities with Phanerozoic ophiolite suites. Meta - basalts display chemistries similar modern day basalts formed within a marginal basin setting.

2) The Kaourera Island - Arc Group contains a suite of silica and potassium variable lithologies, chemically analogous to Phanerozoic island - arc suites. The group is dominated by low - K fractionation trends with a minor calc - alkaline fractionation component indicating a moderately evolved arc system.

3) The whole rock geochemistry of the Kadunguri Whiteschists indicates that the lithologies have undergone extensive alteration by metasomatic processes prior or during metamorphism. Trace element analysis reveals a similarity to low - K tholeiitic basalts of the Kaourera Island - Arc Group.

Chapter Four

Metamorphism.

4.1 Introduction.

The aims of the chapter are :-

1) To document the compositions of the main metamorphic minerals within the different assemblages.

2) To present textural evidence for prograde metamorphism.

3) To utilise the chemical composition of specific mineral species to construct a PTt path for prograde metamorphism.

4) To compare and contrast the PTt paths of prograde metamorphism of the Ophiolite Terrane with that of the other Chewore terranes.

4.2 Mineral Chemistry.

The aim of this section is to briefly describe and classify the main metamorphic minerals present within the Ophiolite Terrane. Since the Kadunguri Whiteschists displays an unusual chemistry and unique mineral assemblages compared to the Kaourera Island - Arc and Maunde Ophiolite Groups, these phases will be considered separately.

4.2.1 *Maunde Ophiolite And Kaourera Island - Arc Groups.*

Amphiboles (refer to Appendix D for analysis).

Amphibole is the predominant mineral within the Maunde Ophiolite and Kaourera Island - Arc Groups where it is part of a meta - mafic mineral assemblage, i.e., tholeiitic, meta - basaltic, amphibolites; meta - gabbros; hornblendites and as part of the meta - ultramafic Ngwena Ultramafic Formation of the Maunde Ophiolite Group.

The amphiboles are classified using the nomneclature of Leake (1978) and calculated on a water free basis to 23 oxygens and 15 cations per formula unit (p.f.u). Within the Maunde Ophiolite and Kaourera Island - Arc Groups the amphiboles are calcic since $(Ca+Na)_B > 1.34$ and $Na_B < 0.67$ p.f.u. (Fig. 4.1 and Appendix D). Subdivision of all the amphiboles is on the basis of (Na+K) in the A site and content of Si and Mg / $(Mg+Fe^2)$ p.f.u. within the unit cell.

Within the Maunde Ophiolite and Kaourera Island - Arc Groups, amphiboles from four lithologically contrasting formations were analysed (Fig. 4.1). The Banded Member amphibolite assemblages of the Kamuyu Amphibolite Formation are characterised by ferroan - pargasite to ferroan - pargasitic hornblende while the Calc - Silicate Member contains ferro - tschermakite. The mafic - hornblendite assemblage of the Ingwe Meta - Mafic Cumulate Formation contains both porphyroblastic and matrix amphiboles. Porphyroblast cores and matrix amphiboles are comprised of edenite to edenitic hornblende while porphyroblast rims are comprised of actinolitic to magnesio - hornblende. The ultra - mafic assemblages of the Ngwena Ultramafic Formation contain tremolite.

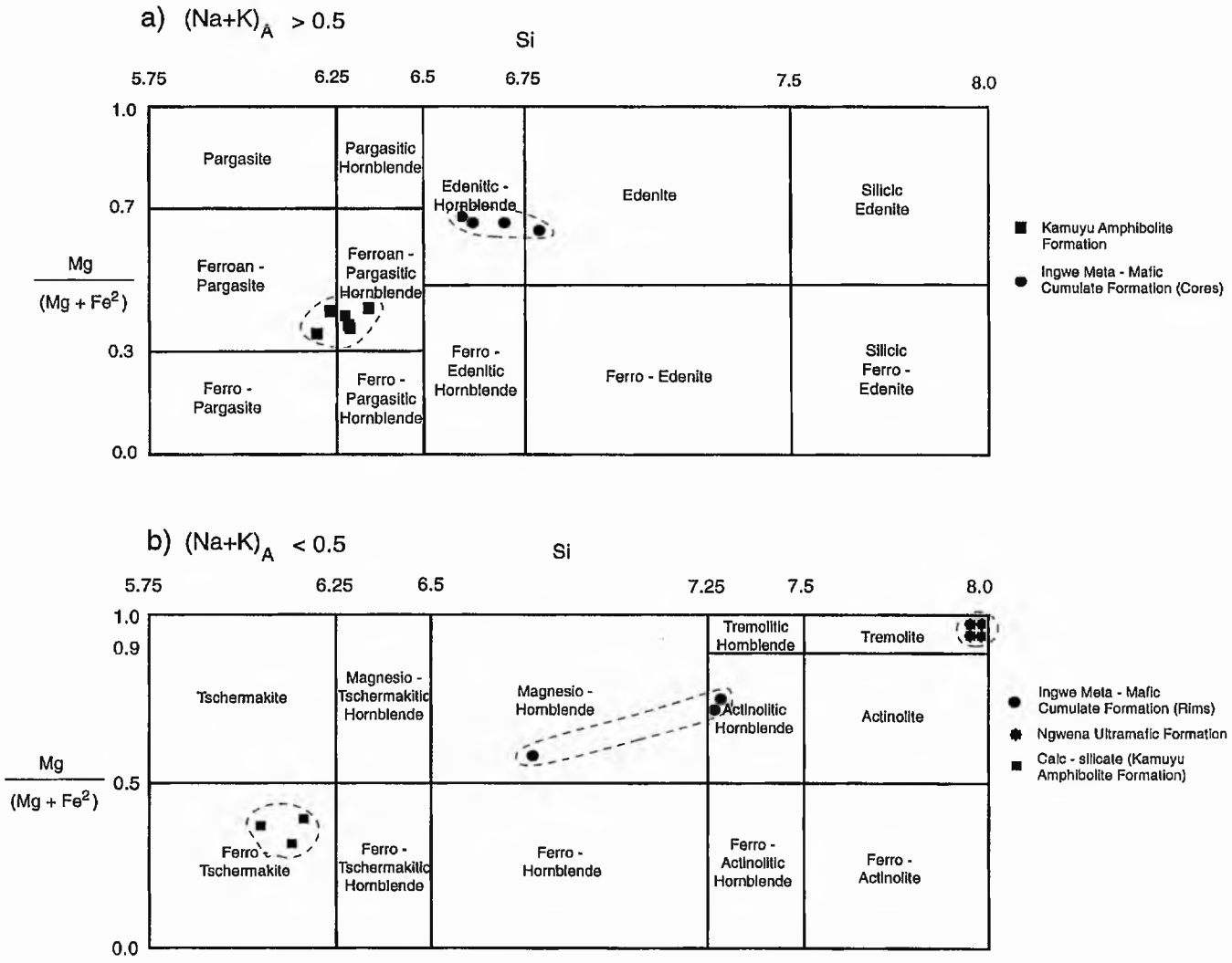

Fig. 4.1 Classification of the calcic amphiboles where (Ca + Na)B > 1.34 after Leake, (1978). Amphiboles for tholeiitic meta - basalts, meta - mafic cumulates, calc - silicate and serpentenite lithologies of the Maunde Ophiolite and Kaourera Island - Arc Groups are plotted.

Feldspar (refer to Appendix D for analyses).

Feldspar is the third most abundant mineral (after amphibole and quartz) within the Ophiolite Terrane. Feldspar also dominates the Gneissic Terrane but has not been analysed in this study. Figure 4.2 is a triangular plot displaying the chemical variation of feldspar within the different metamorphic assemblages. Plagioclase is the predominant feldspar with compositions ranging from An $_{25}$ to An $_{35}$ (oligoclase and andesine) and An $_{76}$ and An $_{87}$ (Bytownite). Within the tholeiitic amphibolite assemblages the plagioclase composition is well constrained to oligoclase compositions. Within the calc - alkaline, meta - basaltic assemblage (biotite, plagioclase ± hornblende) of sample [SJ 110], core and rims vary from oligoclase to andesine respectively, reflecting the progressive change of plagioclase compositions to more anorthitic values during prograde, barrovian type metamorphism (Harte and Graham, 1975; Yardley, 1989). Within the calc - silicate sample [SJ 134] both bytownite and orthoclase are present as fine intergrowths (Fig. 4.15 b).

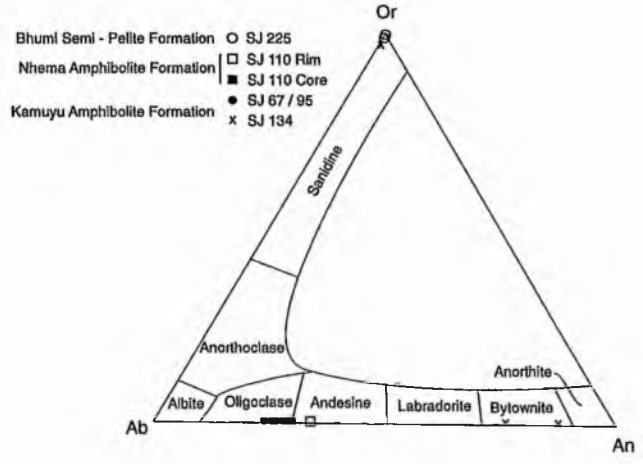

Fig. 4.2 Triangular plot of feldspar nomneclature. Plotted are feldspar compositions of the various Ophiolite Terrane lithologies.

Garnet. (refer to Appendix D for analyses.)

Garnet is a rare but important mineral within the Ophiolite Terrane. It occurs within tholeiitic and calc - alkaline meta - basaltic, calc - silicate and

pelitic assemblages, all of which are widely distributed throughout the Ophiolite Terrane.

Within all assemblages the garnet is of the pyralspite series and dominated by almandine (57.9 - 84.7 %), with subordinate grossular (3.4 - 28.0 %), pyrope (5.5 - 17.0 %) and spessartine (0.6 - 9.4 %). The predominance of almandine garnet is interpreted by Deer *et al.*, (1992) to indicate moderate *P* and *T*, Barrovian style metamorphism. Most garnets are chemically zoned (Fig. 4.3) with cores which are slightly depleted in almandine and pyrope and elevated in spessartine (except [SJ 370]) and rims which are elevated in almandine and pyrope and depleted in spessartine. The bell shaped profiles defined by the spessartine component indicates that the garnets are growth zoned and thus did not exceed temperatures to cause diffusion (Spear, 1993). The pelitic sample [SJ 370] displays flat profiles from core to rim and highly elevated almandine contents (up to 84.7 %). This sample may have *either* : exceeded temperatures which have allowed the mobilisation and diffusion of elements within the porphyroblast causing rehomogenisation, *or* since growth zoning arises due to changing *PT* conditions (Spear, 1993), these porphyroblasts may have grown within a static, stable *PT* environment. If growth within a static *PT* environment is envisaged then the large size of these porphyroblasts (upto 6mm diameter) suggests extremely rapid growth. Garnet with almandine contents greater than 84.7 % are extremely rare but have been reported from the Black Mountains in New Hampshire (Rumble, 1971) where they are part of a pelitic, Barrovian style, amphibolite facies metamorphic event.

Chlorite. (refer to Appendix D for analyses).

Chlorite is a minor phase occurring within pelitic, ultramafic and meta - cumulate lithologies. Chlorite is a primary matrix phase within pelitic

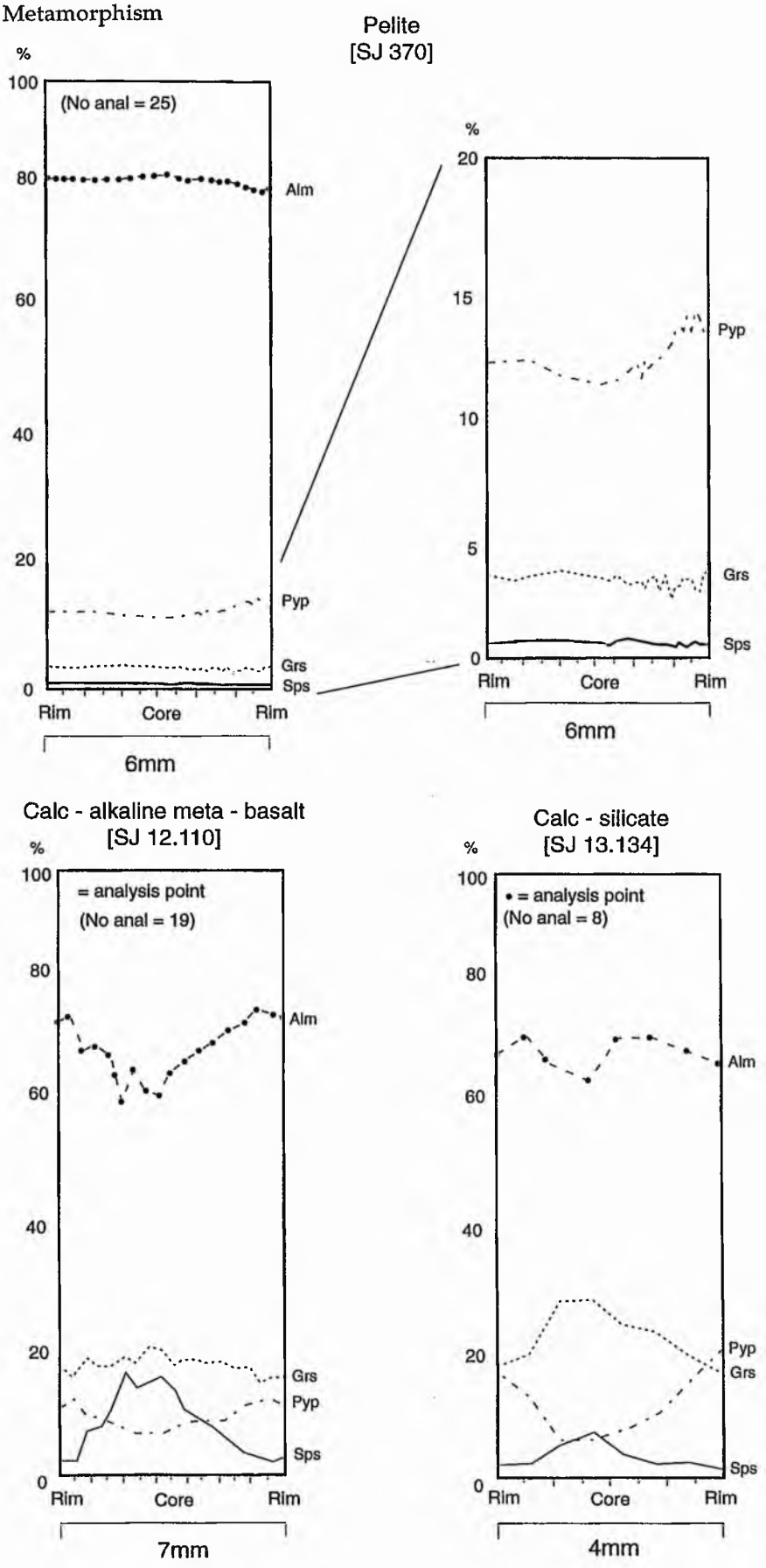

Fig. 4.3 Line traverse's through garnet porphyroblasts illustrating the spatial distribution of elements within the porphyroblast.

assemblages, whereas in the mafic - cumulate and ultramafic assemblages of the Maunde Ophiolite Group, it is associated with corroded garnet or amphibole porphyroblasts and as cross cutting lenses and bands (section 2.2.4).

All chlorites contain less than 4 % Fe_2O_3. Figure 4.4 plots $Fe^{2+} + Fe^{3+}$ (i.e., Fe $^{Tot\ 2+}$) against $Fe^{2+} + Fe^{3+}$ / $Fe^{2+} + Fe^{3+} + Mg$ and Si p.f.u. contents of the unit cell (after Hey, 1954). Penninite occurs as replacement veins within the ultramafic assemblages and ripidolite as the retrogressive matrix phase within the pelites and as inclusions and replacement textures within the meta - cumulate assemblages.

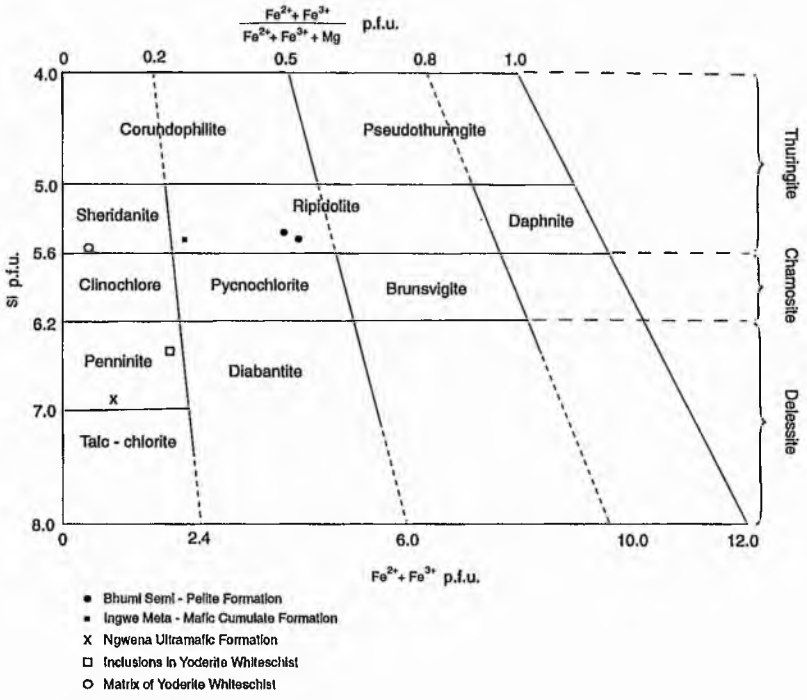

Fig. 4.4 Nomneclature of the ortho and oxidised chlorites (after Hey, 1954). Chlorite compositions from the various Ophiolite Terrane lithologies are plotted.

Biotite and Muscovite. (refer to Appendix D for analyses).

Biotite occurs as a major matrix phase in both the calc - alkaline meta - mafics and Kaourera Island - Arc Group pelites. Muscovite is a major pelitic phase and a minor calc - alkaline and meta - dacitic phase. Within the calc - alkaline samples there is very little difference between the

composition of biotite cores and rims - Ann $_{40}$, Ph $_{43}$ and Ann $_{39}$, Ph $_{42}$ respectively. Minor muscovites have compositions with a significant phengitic component - Mu $_{70}$, Pa $_{7}$ and Pgt $_{26}$. There is little variation in the composition between end members of both muscovite - Mu $_{67 - 70}$ and Pa $_{3 - 18}$ and biotite - Ann $_{39 - 48}$ and Ph $_{33 - 43}$ within the pelitic assemblages.

Serpentine. (refer to Appendix D for analyses).

Serpentine occurs only within the Ngwena Ultramafic Formation of the Maunde Ophiolite Group. The Al_2O_3 content is high *c.* 4 wt % (0.22 p.f.u) and is thus classified as an aluminous serpentine. The serpentine also contains significant proportions of Cr^{3+} i.e., upto 0.45 wt % (0.02 p.f.u). This might be due to the mobilisation of this element from chromite breaks down during amphibolite facies metamorphism (see *Opaques* section). The acicular nature of the mineral under transmitted light microscopy also suggests that the serpentine is an aluminous crysolite (Deer *et al.*, 1992).

Epidote. (refer to Appendix D for analyses).

Epidote is present as an accessory mineral within most assemblages of the Ophiolite Terrane. Epidote was analysed from the pelitic and calc - silicate assemblages. All iron was calculated as Fe^{3+} and the unit cell from 12.5 oxygens and 8 cations. The epidote composition ranges from Ps $_{18 - 22}$ (Ps = pistacite molecule) and Cz $_{78 - 82}$ (Cz = clinozoisite molecule). According to Deer *et al.*, (1992), an experimental immiscibility gap between Ps $_{13}$ to Ps $_{25}$ is present in epidotes which formed at low temperature. There is a continuous range in Fe^{3+} in higher temperature epidotes. This suggests that these samples formed during higher temperature metamorphism possibly equivalent to that of epidote amphibolite facies (> 500° C).

However, Deer *et al.*, (1992) also indicates that this immiscibility gap may not exist since the role of f_{O_2} has yet to be considered.

Opaques. (refer to Appendix D for analyses).

Opaque minerals occur as accessory phases in many of the Ophiolite Terrane lithologies. Pelitic and mafic assemblages the opaque minerals are represented by ilmenite with equal proportions of both Ti and Fe^{2+} with little or no Fe^{3+}. Fe - chromite forms the opaque phase within the ultramafic assemblages of the Ngwena Ultramafic Formation. The chromite grains are zoned such that chromite cores are richer in Cr^{3+} while the rims are concentrated in Fe^{3+}. In comparison with other ultramafic chromites (Deer *et al.*, 1962) the proportion (of both cores and rims) of Cr^{3+} is relatively low, Fe^{3+} / $^{2+}$ relatively high and the absence of Al and Mg enigmatic. Figure 4.5 shows the variation in both Cr^{3+} and Fe^{3+} p.f.u. between cores and rims of the chromite grains. It is evident that Fe^{3+} is substituting 'one for one' with Cr^{3+}, during metamorphism. This metamorphic effect has been investigated by Abazlov (1998) who indicates that with increasing metamorphic grade and predominantly during amphibolite facies metamorphism, Cr^{3+} is replaced with magnetite and or hematite (depending on the oxidation state) progressively from rim to core. The mobilised Cr^{3+} is accommodated within newly developing serpentine crystals as is evident within the Ngwena Ultramafic Formation serpentines. Most chromites contain very little Fe^{3+} and thus if all the substituted Fe^{3+} is removed from the unit cell (i.e., where the slope intercepts the x axis) and replaced with the corresponding Cr^{3+}, the unit cell therefore contains 16 p.f.u. of Cr^{3+}.

Combined with the remaining Fe^{2+}, this gives a formula of

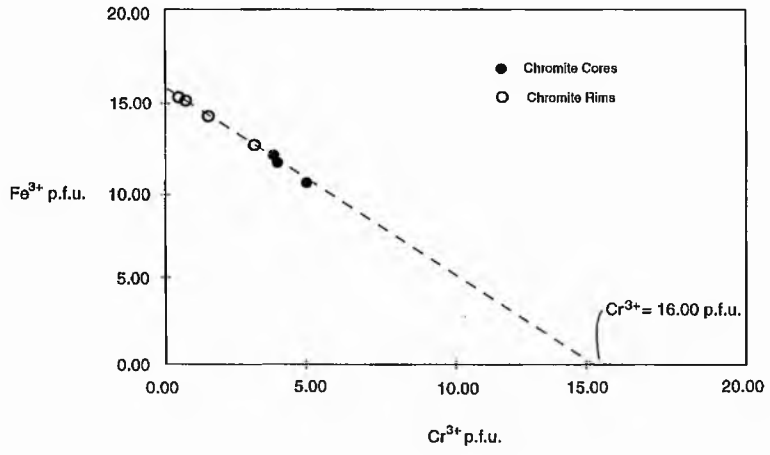

Fig. 4.5 Variation plot of Fe^{3+} verses Cr^{3+} p.f.u for chromite core and rim compositions. It is evident that Fe^{3+} is substituting for Cr^{3+} in the chromite structure.

$Fe_8Cr_{16}O_8$ or $FeCr_2O_4$ which is comparable to pure end member chromite. However, this pure end member is rare since Mg and Al substitute readily for Fe^{2+} and Cr^{3+} respectively. It is possible that Mg and Al have also been substituted by Fe^{2+} and Fe^{3+} respectively during the metamorphic event.

4.2.2 The Kadunguri Whiteschists.

In this section the chemistry of the minerals which are unique to this whiteschist dominant group will be discussed.

Yoderite. (refer to Appendix D for analyses).

Since this is the second natural occurrence of this mineral in nature (section 2.4.2) both its chemistry and mineralogical properties will be described in detail. A comparison will also be made with the other yoderite occurrence at Mautia Hill, Tanzania (McKie, 1958; McKie & Bradshaw, 1966; Mrurma & Basu, 1987).

In hand specimen the yoderite is pale green with a glassy lustre. In thin section the mineral is colourless, has high relief and one strong cleavage (010) with a maximum extinction angle of 29°. The α/β sections

display a birefringence of 0.002 (low first order grey) whereas the α/γ sections display a birefringence of 0.013 (upper first order red), similar to synthetic phases recorded by Higgins *et al.* (1982) and Fockenberg & Schreyer (1991) (Plate. 4.1 a, c and d). The mineral is monoclinic and positive with a $2V\gamma$ ~30° (see Fig. 4.6).

The usual occurrence of yoderite at Mautia Hill is predominantly a strong purple coloured variety (Plate. 4.1 b) but a rare, pale green variety also exists. Compared to Chewore yoderite, the optical properties of Mautia Hill green yoderite are very similar e.g., α/β sections, birefringence = 0.002; α/γ sections, birefringence = 0.021 (all ± 0.003) and $2V\gamma = 30°$. The strong purple colouration of the dominant yoderite variety is due to the presence of the manganese chromophore group (Mn^{2+} - O - Mn^{3+}) (Abu - Eid *et al.*, 1978). Despite its strong colouration, its mineralogical and optical properties are also very similar to the green variety: e.g., α/β sections, birefringence = 0.002, α/γ sections, birefringence = 0.026 (all ± 0.002), is monoclinic and positive with a $2V\gamma = 25°$.

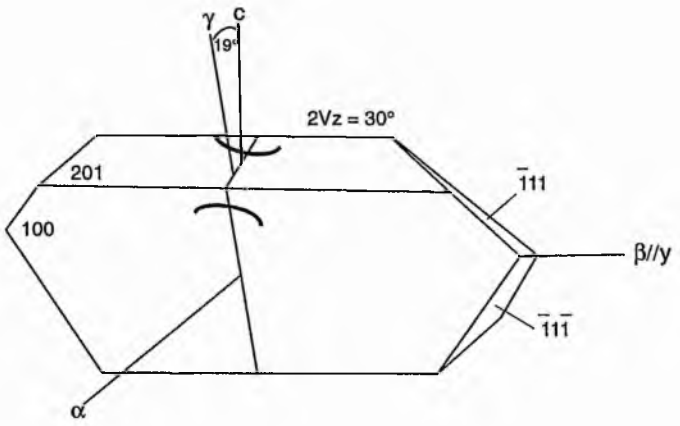

Fig. 4.6 Crystal morphology and orientation of indicatrix of green yoderite containing 0.3 p.f.u. Fe^{3+} (after Fockenberg & Schreyer, 1991).

The composition of yoderite is calculated on the basis of 19 oxygens and 12 cations (Yoder, 1952; Mckie, 1959). The chemical formula of the green Chewore yoderite is $Mg_2Al_{5.7}Fe_{0.3}Si_4O_{18}(OH)_2$ which contains a little less Fe than in the green yoderite reported by Higgins *et al.* (1982), $Mg_2Al_{5.6}Fe_{0.4}Si_4O_{18}(OH)_2$, or in purple yoderite $Mg_{1.98}Al_{5.63}Fe_{0.4}Mn_{0.09}Si_{3.92}O_{18.06}(OH)_{1.94}$ reported by McKie & Bradshaw (1966) for the Mautia Hill examples. The difference in molar proportion of Fe^{3+} and Al^{3+} suggests that minor substitution of Al^{3+} for Fe^{3+} occurs within the A (3) site of the crystal structure (Higgins *et al.*, 1982). Although the ideal formula can be written as $Mg_2(Al,Fe)_6Si_4O_{18}(OH)_2$, the amount of Fe^{3+} in the structure appears to lie within the range 0.2 - 0.4 p.f.u as calculated by Fockenberg & Schreyer (1991). Saturation of Fe^{3+} (up to 0.7 p.f.u.) in synthetic yoderite occurs when the mineral is in equilibrium with hematite (Fockenberg & Schreyer, 1991). In the Chewore Hills sample, only yoderite which is in direct contact with hematite (Plate. 4.1 d) displays rims slightly elevated in Fe^{3+}, up to but not beyond 0.4 p.f.u.

Talc. (refer to Appendix D for analyses).

Talc occurs within all the whiteschist lithologies. Its composition is near ideal ($Mg_3Si_4O_{10}(OH)_2$). Within the Gedrite Whiteschist substitution of Na and Al into the crystal structure (Al - 0.19 p.f.u. and Na - 0.02 p.f.u.) gives a formula of $Mg_{2.86}Al_{0.19}Na_{0.02}Si_{3.91}O_{10}(OH)_2$.

Kyanite. (refer to Appendix D for analyses).

Kyanite occurs within the majority of whiteschist lithologies. Although its colour varies in hand specimen from pale blue / colourless to pale green its composition remains constant. There is minor Fe^{3+} substitution for Al^{3+} in the unit cell giving a formula of $[Al_{1.98}Fe_{0.02}][SiO_5]$.

Chlorite. (refer to Appendix D for analyses).

Chlorite occurs only within the Yoderite Whiteschist as both a primary matrix phase (sheridanite) and as inclusions (penninite) within most other prograde metamorphic phases (Fig. 4.4).

Amphibole. (refer to Appendix D for analyses).

Within the Gedrite Whiteschist the amphiboles are classified as iron - magnesium - manganese amphiboles since $(Ca+Na)_B < 1.34$. Magnesio - gedrite dominates the assemblage with minor subordinate magnesio - anthophyllite (Fig. 4.7). Magnesio - gedrite has the formula - $Si_{6.7}Al_{2.3}Mg_{5.8}Fe_{0.2}Na_{0.3}$ and magnesio - anthophyllite has the formula - $Si_{7.3}Al_{0.7}Mg_7$.

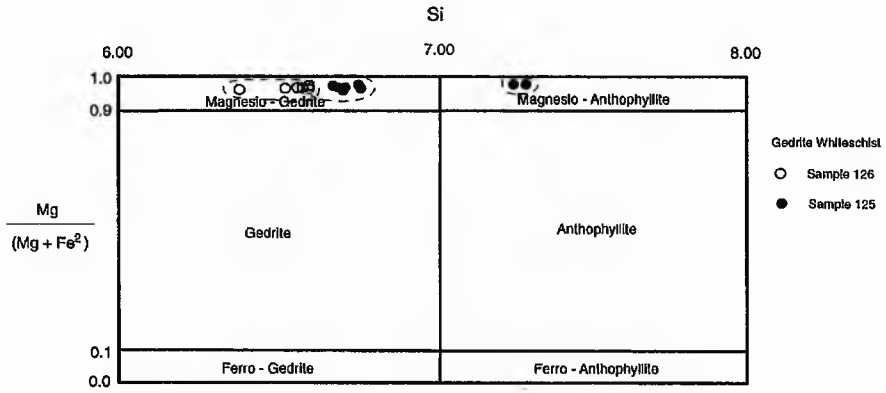

Fig. 4.7 Nomneclature of the iron - magnesium - manganese amphiboles where $(Ca + Na)_B<1.34$ (after Leake, 1978). Amphiboles from the Nyati Formation are plotted.

Dravite. (refer to Appendix D for analyses).

The sodium and magnesium bearing tourmaline (dravite) is present within most whiteschist lithologies. Boron has not been analysed but is interpreted from the standard dravite formula (Deer *et al.*, 1992) - $Mg_{2.43}Al_{6.05}B_3Fe_{0.42}Na_{0.68}Si_{5.95}O_{24.5}(OH)_4$, calculated on the basis of 24.5 oxygens and 15.5 cations.

Opaque Minerals. (refer to Appendix D for analyses).

Opaque minerals occur within every member of the Kadunguri Whiteschists. Hematite dominates the opaque phases indicating that the Fe is highly oxidised (Fe^{3+}). This is in contrast to the other groups, where Fe is predominantly unoxidised i.e., Fe^{2+} and thus occurs combined in ilmenite. The Yoderite Whiteschist contains hematite with fine needles of possibly exsolved rutile (Plate. 4.1 e).

4.3 Metamorphic Reactions and *PT*t paths.

The aim of this section is to describe the metamorphic assemblage of the various lithotypes and to determine peak metamorphic *PT* conditions of the Ophiolite Terrane.

4.3.1 *Maunde Ophiolite and Kaourera Island - Arc Groups.*

Tholeiitic Meta - Basalts.

Tholeiitic meta - basalts of both the Maunde Ophiolite (Mvuu Meta - Mafic Volcanic and Mbizi Sheeted Dyke Formations) and Kaourera Island - Arc Groups (Kamuyu, Nhema and Bere Amphibolite Formations) have a similar metamorphic assemblage :-

calcic amphibole + quartz + oligoclase ± epidote ± sphene ± Ti - rich opaques ± garnet ± chlorite (Appendix B).

The coexistence of epidote and amphibole within an equilibrium assemblage is characteristic of the epidote - amphibolite (i.e., lower amphibolite) facies (Spear, 1993) which is the higher pressure transition from the greenschist to amphibolite facies. Garnet porphyroblasts are rare within the Ophiolite Terrane meta - basalts; however, when present they

are associated with oligoclase and a notable lack of epidote suggesting that the peak metamorphic grade of these garnet - bearing samples is nearer that of the upper amphibolite rather than the lower amphibolite facies (Yardley, 1989).

The dominant textural features of these amphibolites include elongate to tabular amphiboles which are well aligned into a strong *SL* fabric which itself is occasionally crenulated by the bending and fracturing of amphibole blades (Plate. 5.2 b). Plagioclase and quartz occur as interstitial, granoblastic, lensoid aggregates and discontinuous layers (Plate. 4.2 a).

Garnet - bearing assemblages reveal significantly more about their metamorphic and structural past. Garnet porphyroblasts are relatively small (0.5 - 1 mm diameter), are randomly distributed, contain abundant inclusions of quartz and more rarely amphibole / biotite and plagioclase and are relatively sparse comprising no greater than 5 % of the total rock volume. Most porphyroblasts display corroded rims which are replaced by and mantled by plagioclase (Fig. 4.8). For a discussion on the timing of metamorphism in relation to associated deformation, i.e., the relation of internal and external garnet porphyroblast fabrics, see section 5.4). Analysis reveals almandine dominated porphyroblasts with bell shaped spessartine profiles (section 4.2.1) which are typical of prograde growth zoning in both greenschist and amphibolite facies rocks (Spear, 1993).

The various phases of the meta - basaltic amphiboles are plotted in Fig. 4.9 (for classification see section 4.2.1). All samples plot within or close to the intermediate pressure facies series of the Haast River and Dalradian Terranes, again indicating Barrovian type, greenschist to amphibolite facies metamorphism (Laird & Albee, 1981).

Temperature estimations for the peak of metamorphism of these meta - mafics are based on the Fe - Mg exchange reaction between garnet

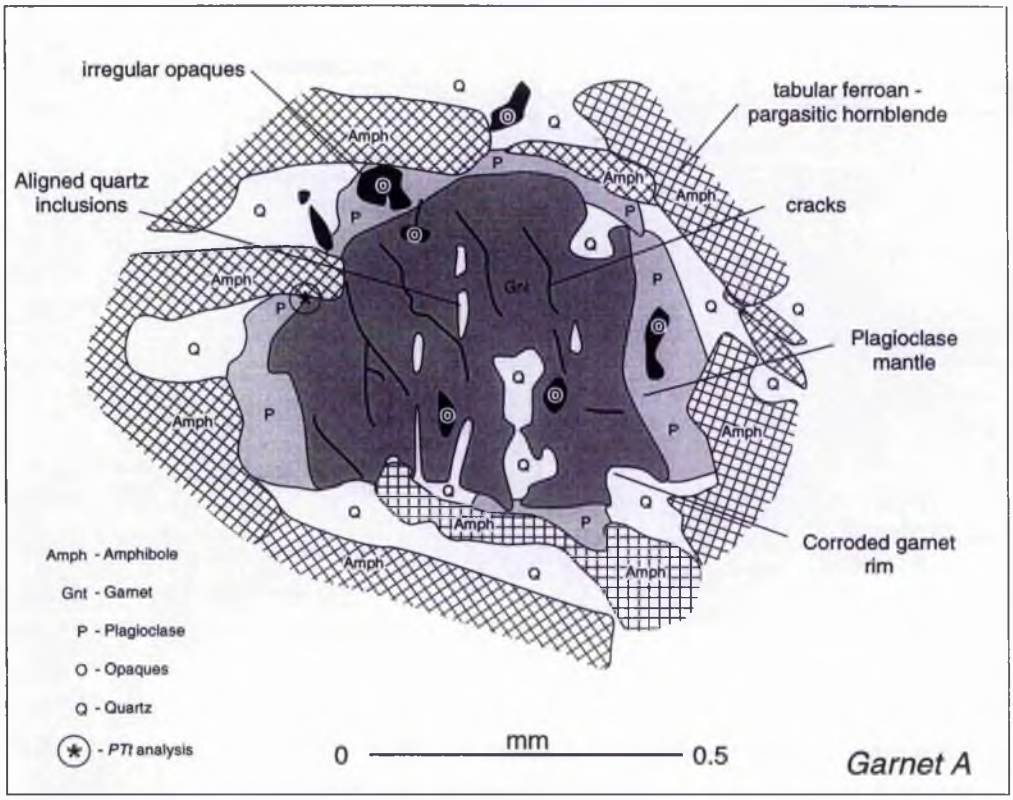

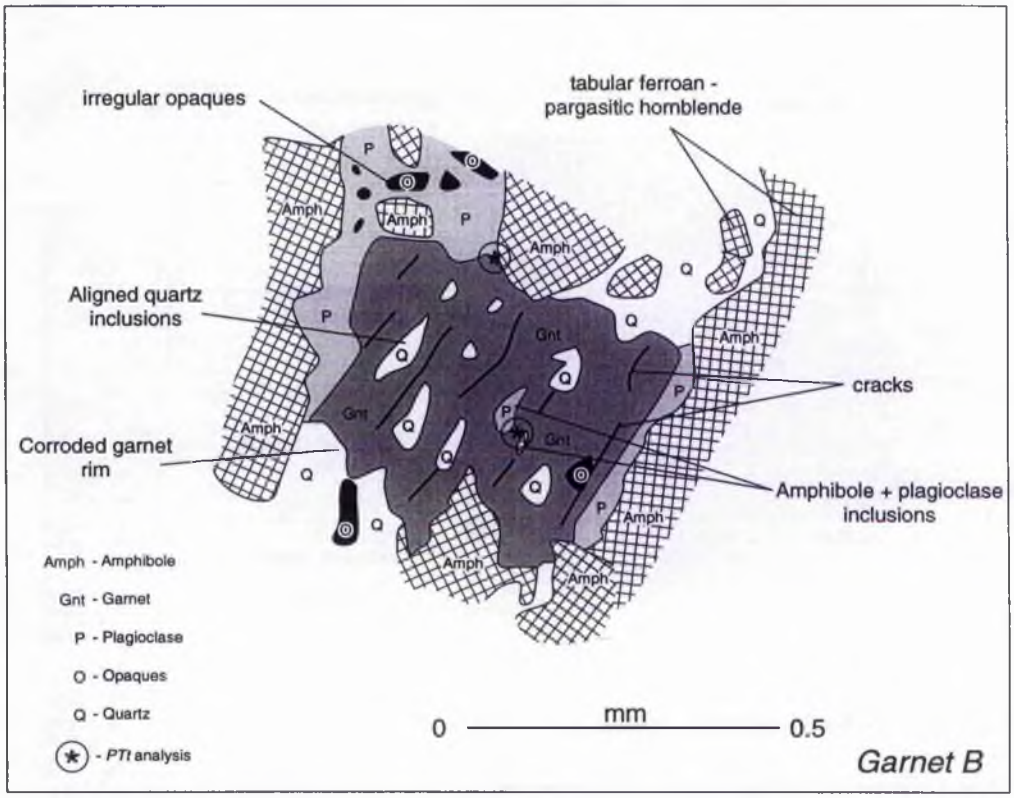

Fig. 4.8 Sketch of garnet porphyroblasts and associated matrix minerals in sample [SJ 8.67] illustrating the corroded nature of the porphyroblasts rims. Plagioclase and quartz are apparently replacing garnet. Note the positions analysed for PTt analysis. There is not PT analyses for the core of Garnet A since plagioclase and / or amphibole inclusions were not present.

and amphibole (reaction [1]) calibrated by Graham & Powell (1984).

[1] $Garnet^{Mg} + Amphibole^{Fe} = Garnet^{Fe} + Amphibole^{Mg}$

Pressure estimations are based on various net transfer reactions between garnet, amphibole, quartz and plagioclase (see below).

Since many net transfer reactions exist for garnet amphibolite assemblages (Thompson, 1982; Hodges & Crowley, 1985; Kohn & Spear, 1989, 1990) each of which produce slightly different results, the Fe and Mg tschermakite end member net transfer reactions [2] and [3] (Kohn & Spear, 1990) have been applied, since this is the most recent barometer.

[2] $Plagioclase^{Ca} + Amphibole^{Ca/Mg} = Garnet^{Ca} + Garnet^{Mg} + Amphibole^{Ca/Mg} + Quartz$

[3] $Plagioclase^{Ca} + Amphibole^{Ca/Fe} = Garnet^{Ca} + Garnet^{Fe} + Amphibole^{Ca/Fe} + Quartz$

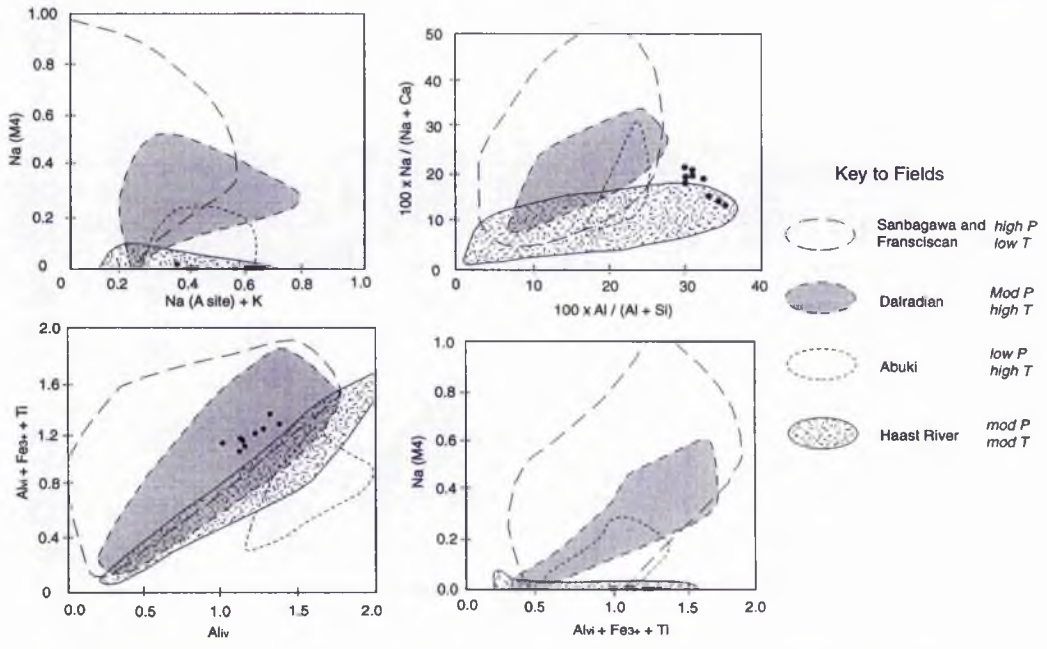

Fig. 4.9 Compositional plot for metamorphic amphiboles (after Laird & Albee, 1981). Amphiboles from the tholeiitic meta - basalts are plotted. Also shown are the fields for amphiboles from other tectonic regimes. For discussion see text.

Since most garnet porphyroblasts exhibit some degree of retrogression i.e., corrosion and replacement of rims with plagioclase, care was taken to ensure that only analyses were taken in regions of the porphyroblast which displayed little or no corrosion and where the rim was in direct contact with matrix amphibole. Few garnet porphyroblasts contain inclusions of plagioclase and / or amphibole, making it difficult to calculate *PT*'s associated with the earliest part of the metamorphic event. Where suitable inclusions were analysed, both core (inclusions) and rim *PT*'s are calculated. Figure 4.10 is a plot of the exchange reaction elements for the garnet and amphibole pairs (joined by a solid line). The consistency between data points for both meta - basalt samples [SJ 8.67 and 10.95] indicate that the samples are well equilibrated (Spear, 1993); and therefore display similar *PT* conditions between samples and between the cores and rims of each sample.

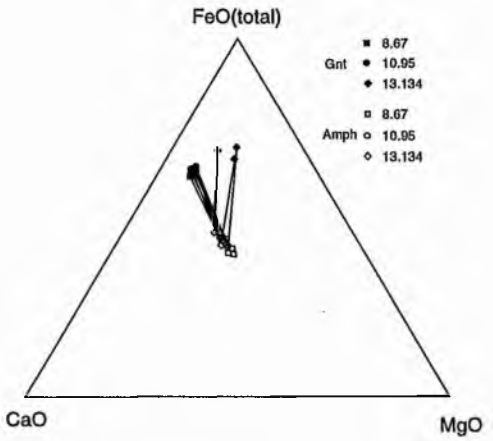

Fig. 4.10 Triangular plot of garnet and amphibole compositions from the tholeiitic meta - basalts and calc - silicates. For discussion see text.

All the calculations were processed using the unpublished computer program "Thermobarometry" by Kohn & Spear (version 2.0, 1996). Results are summarised in Fig. 4.11. Garnet cores yield *PT* values of 9.5 ± 0.5 kbar and 625°C ± 25°C while garnet rims yield *PT* values of between 6.75 - 10.5 ± 0.5 kbar and 650 - 700°C ± 25°C (error estimations from

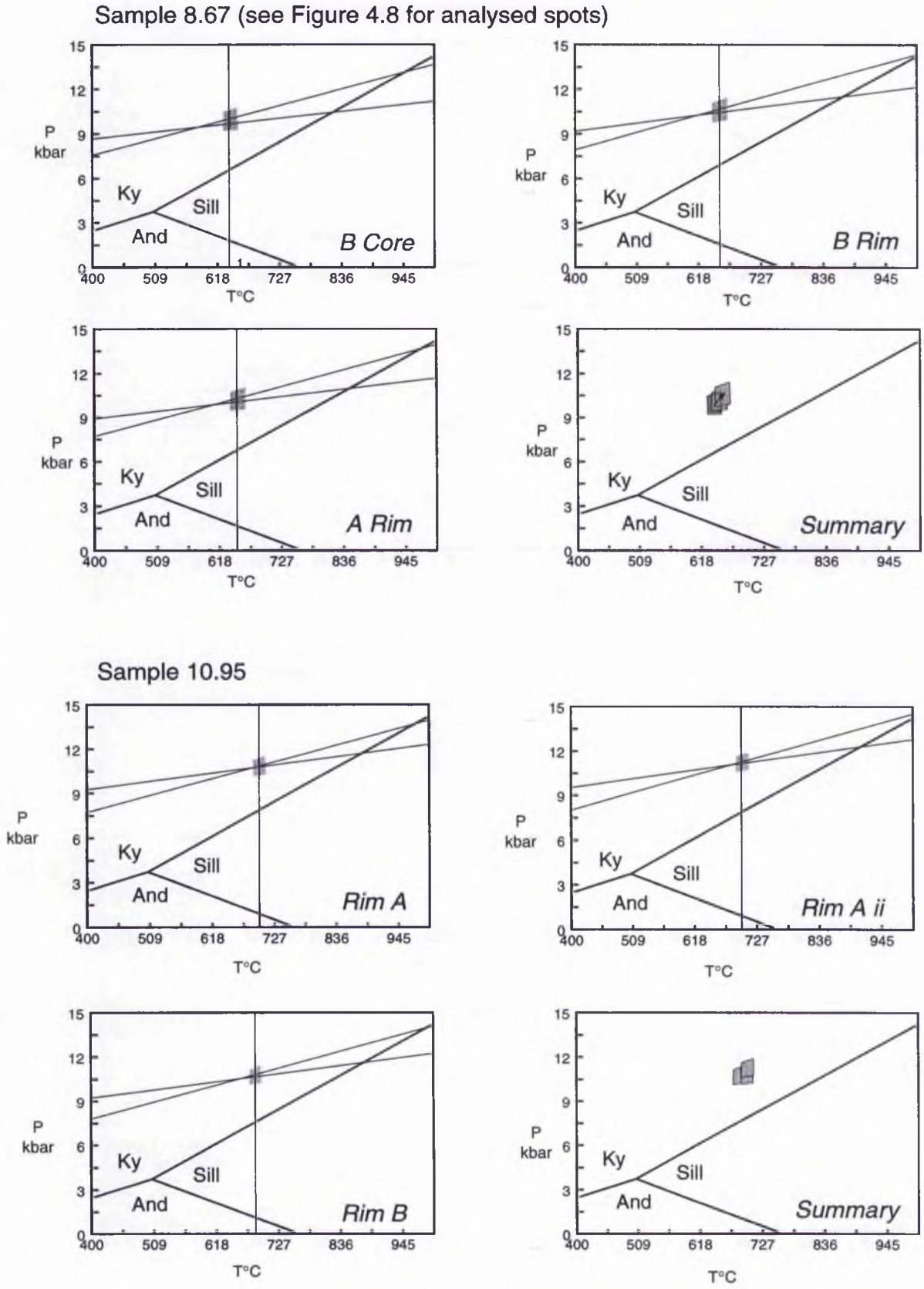

Fig. 4.11 Garnet - amphibole - plagioclase *PT* loci of tholeiitic meta - basalts of the Kamuyu Amphibolite Formation. LnKd lines plotted after Graham & Powell, (1984) and Kohn & Spear, (1990) Fe and Mg tschermakite end members. Summary diagrams illustrate the combined data for the sample showing PT of cores and rims where applicable (joined by an arrow). Where analyses for cores are not shown, garnet porphyroblasts lack the appropriate mineral inclusions.

Kohn & Spear, 1990). The lower temperature, lower pressure nature of the garnet cores compared to the garnet rims, indicate that metamorphism proceeded from lower to higher *P* and *T*.

These *PT* estimates are consistant with those of the upper amphibolite facies with the almandine - oligoclase - amphibole assemblage lacking chlorite and epidote. The disappearance of epidote and chlorite from the assemblage and the appearance of garnet suggets a garnet forming reaction involving epidote and chlorite as reactants. However, a complete balanced reaction is difficult to write since there are so many net transfer reactions which also involve plagioclase and amphibole. The stability and growth of garnet porphyroblasts are also dependent on the whole rock chemistry of the sample e.g., garnet is only stable in meta - basalts which are significantly Fe and Mn - rich (Spear, 1993).

Calc - alkaline Meta - Basalts

Calc - alkaline meta - basalt lithologies of the Nhema Amphibolite Formation comprise the metamorphic assemblage :-

biotite + plagioclase + quartz ± amphibole ± muscovite ± garnet ± epidote ± alkali feldspar (Appendix B).

The mafic portion of the metamorphic assemblage is dominated by biotite rather than amphibole (Plate. 4.2 b, c and d). This reflects the whole rock major element chemistry of the calc - alkaline lithologies which are relatively enriched in K_2O (c. 7 wt %) and depleted in Na_2O (c. 1 wt %) and CaO (c. 2 wt %) compared to that of a typical tholeiitic meta - basalt from the Mvuu Meta - Mafic Volcanic Formation which is dominated by calcic - sodic amphibole, e.g., K_2O (c. <0.5 wt %) Na_2O (c. 4 wt %) CaO (c. 10 wt%).

Only two calc - alkaline meta - basalt lithologies contain garnet. The porphyroblasts are relatively large (upto 8 mm diameter), euhedral to

subhedral and display variably corroded rims (Plate. 4.2 b and d). All porphyroblasts contain abundant quartz, opaque ± plag ± biotite inclusions, most of which define internal fabrics which are discordant to the external fabric (see section 5.3 and Plate. 4.2 d). Garnet compositions are dominated by almandine while analysis core to rim reveal bell shaped spessartine profiles (Fig. 4.3) indicating growth zoning concordant with amphibolite facies metamorphism (Spear, 1993). In comparison with the tholeiitic meta - basalt garnet porphyroblasts, the calc - alkaline garnets are relatively depleted in CaO which is again related to the whole major element chemistry of this lithology.

PT estimates were calculated using the Mg - Fe, garnet - biotite exchange thermometer (Ferry & Spear, 1978) and the Fe and Mg, R2 net transfer reactions between garnet, biotite and plagioclase (Hoish, 1990). Care was taken to analyse regions which displayed the least garnet rim corrosion and where garnet porphyroblast rims were in direct contact with matrix biotite. Figure 4.12 is an FeO, Al_2O_3, MgO composition plot of corresponding garnet - biotite pairs.

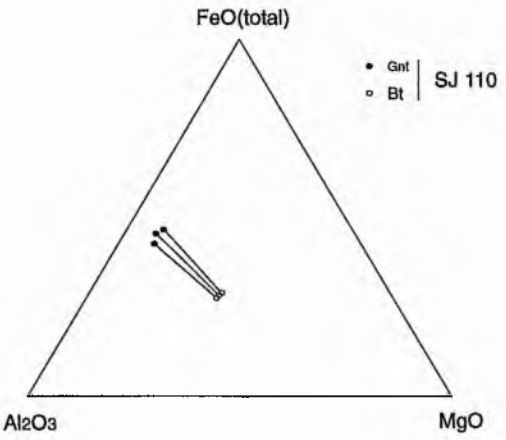

Fig. 4.12 Triangular plot of garnet and biotite compositions from the calc - alkaline meta - basalts. For discussion see text.

There is a small spread in garnet compositions suggesting either formation at different *PT*'s or that one garnet porphyroblast is poorly equilibrated

(Spear, 1993). The garnet core yields a *PT* of 8 kbar ± 0.5 kbar and 525°C ± 25°C while the rims yield *PT*'s of between 8.5 and 12 kbar ± 0.5 kbar and 625 to 630°C ± 25°C (see Fig 4.13) which lie at the lower *PT* end of those calculated for the garnet - bearing, tholeiitic, meta - basalt mineral assemblages. The higher pressure *PT* estimate for the rim of garnet B in sample [SJ 110] and the difference in garnet composition illustrated in Fig. 4.12 altogether suggest that this porphyroblast is not well equilibrated.

Meta - Dacites.

Meta - dacitic assemblages of the Kaourera Island - Arc Group comprise :-

plagioclase + amphibole + epidote + K - feldspar (Appendix B).

Plagioclase and quartz dominate the mineral assemblage as a less than 0.1 mm, granoblastic matrix with rare, upto 1.5 mm long, euhedral and sometimes resorbed, randomly oriented, simple twinned plagioclase crystals (Plate. 4.3 a and b). It is possible that these are original, volcanic phenocrysts, however, an alternative hypothesis is that they are porphyroblasts related to the M_1 metamorphic event. These crystals are aligned sub - parallel to the tectonic foliation and contain randomly oriented epidote inclusions. Amphibole occurs as large (upto 6 mm long), euhedral, tabular and lozenge shaped porphyroblasts which aggregate into elongate lenses of upto 15 mm long. Epidote is present as inclusions within all phases and as less than 0.1 mm diameter, anhedral porphyroblasts. The presence of both amphibole and epidote indicate lower amphibolite facies grade metamorphism.

Sample 12.110

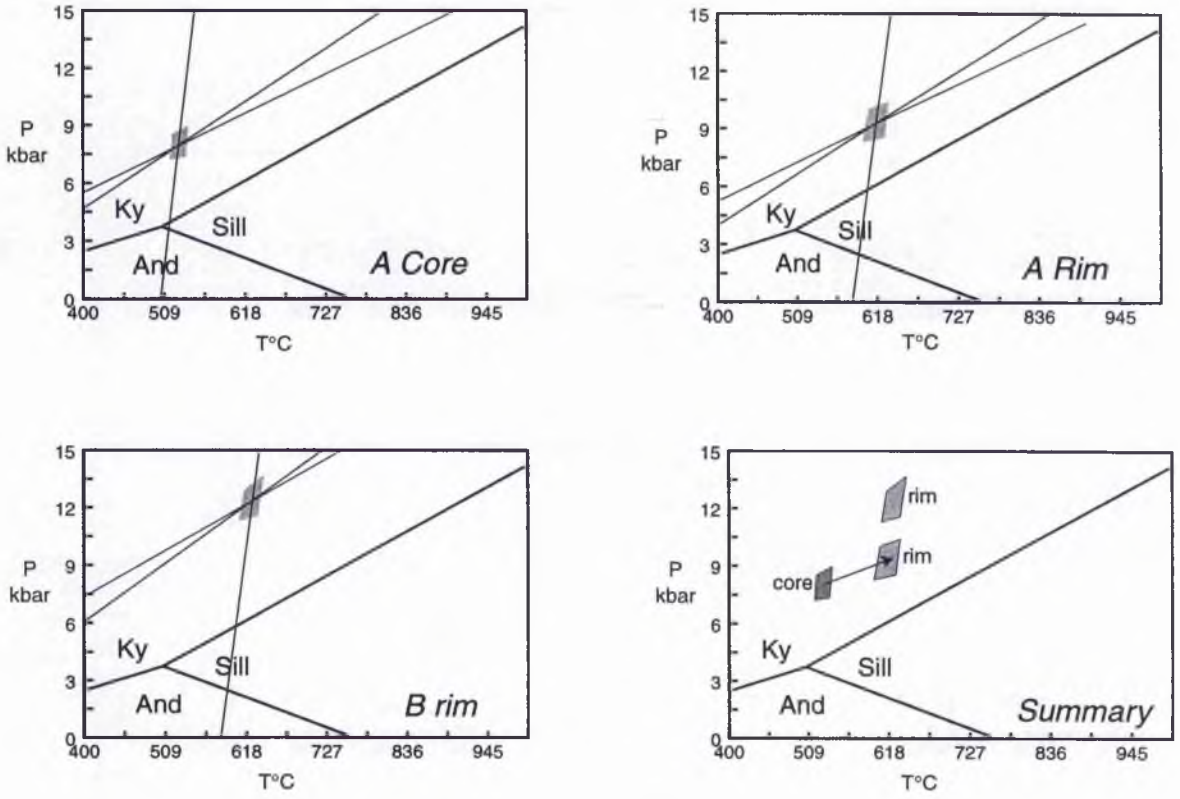

Fig. 4.13 Garnet - biotite - plagioclase *PT* loci of calc - alkaline meta - basalts from the Nhema Amphibolite Formation. LnKd lines plotted after Ferry & Spear, (1978) and Hoisch, (1990). The summary diagram combines *PT* analyses for the sample. Appropriate core and rims are joined by an arrow indicating the path of prograde metamorphism. Garnet B does not contain the appropriate mineral inclusions (plagioclase and biotite) to allow estimation of core *PT*'s.

Calc - Silicates

Sample [SJ 13.134] is the only calc - silicate lithology to be mapped within the Maunde Ophiolite or Kaourera Island - Arc Groups. The metamorphic assemblage comprises:-

plagioclase + quartz + amphibole + epidote + garnet + orthoclase + opaques (Appendix B).

Plagioclase and quartz dominate the specimen as a less than 0.1 mm, granoblastic matrix containing abundant, very fine grained epidote. Amphibole porphyroblasts are upto 9 mm long and aggregate into discontinuous layers of upto 30 mm in length (Plate. 4.3 c). Garnet and plagioclase porphyroblasts are preferentially located within these more mafic layers. Garnet porphyroblasts are euhedral, upto 3 mm in diameter, display variably corroded rims (replaced by very fine grained quartz, plagioclase and epidote) and contain minor, randomly oriented and distributed epidote and quartz inclusions (Fig. 4.14 a). Bytownite, plagioclase porphyroblasts display possible exsolution textures with K-feldspar (Fig. 4.14 b). The K - feldspar 'exsolution' occurs as dendritic and irregular shaped patches predominantly originating from the porphyroblast margin. The sodic composition of the host plagioclase (An_{75-86}) indicates that this cannot be an exsolution or intergrowth texture since within the quartz - plagioclase - orthoclase system, only exsolution and / or intergrowth textures between orthoclase - albite, orthoclase - quartz or albite - quartz are possible (Tuttle & Bowen, 1958; Shelley, 1983). However, considering the CaO and Na_2O content of the whole rock (18.91 wt %) and (0.22 wt %) respectively, only anorthite dominated plagioclase can develop. The minor concentrations of K_2O (0.41 wt %) within the whole rock seem to have been partitioned into orthoclase feldspar only. Since orthoclase and bytownite are immiscible (Tuttle & Bowen, 1958) the two intergrow

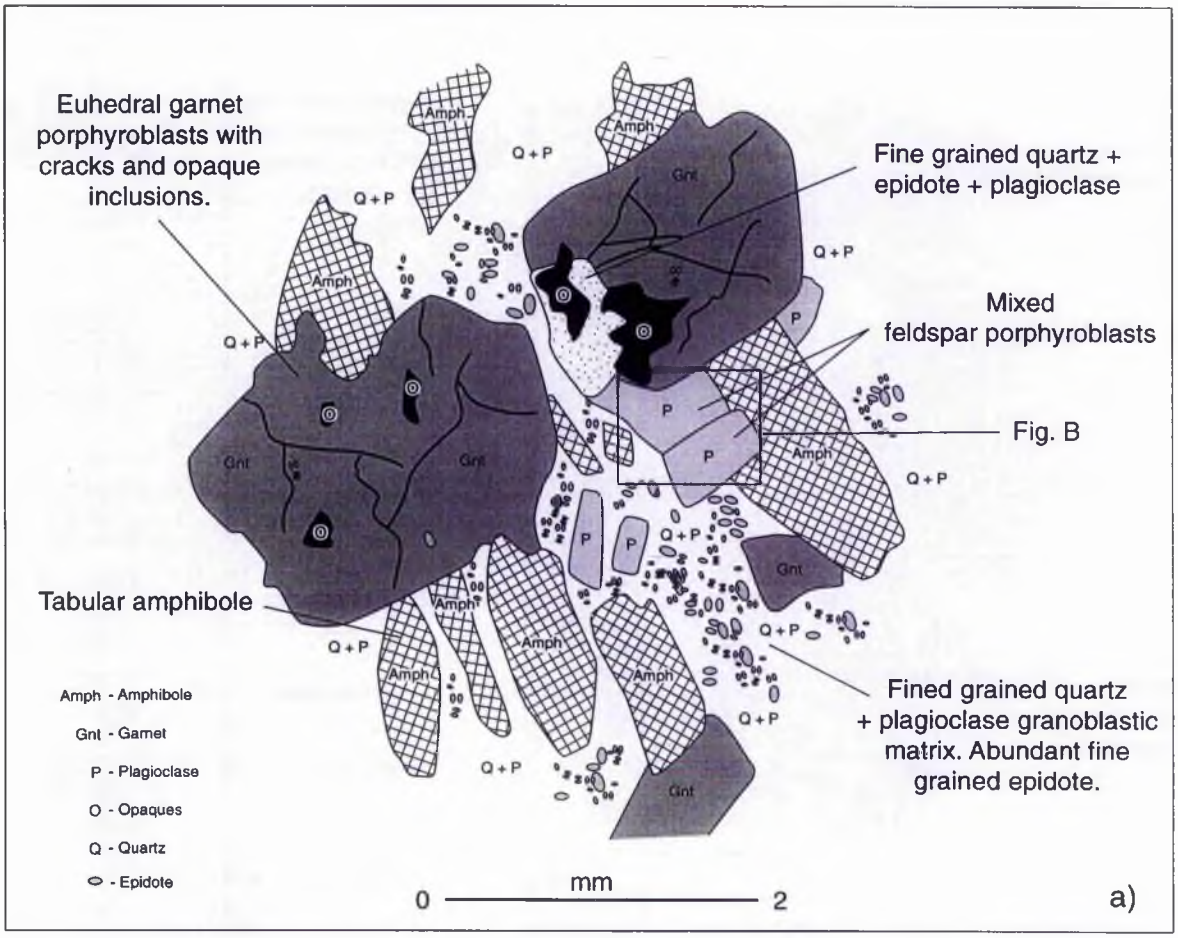

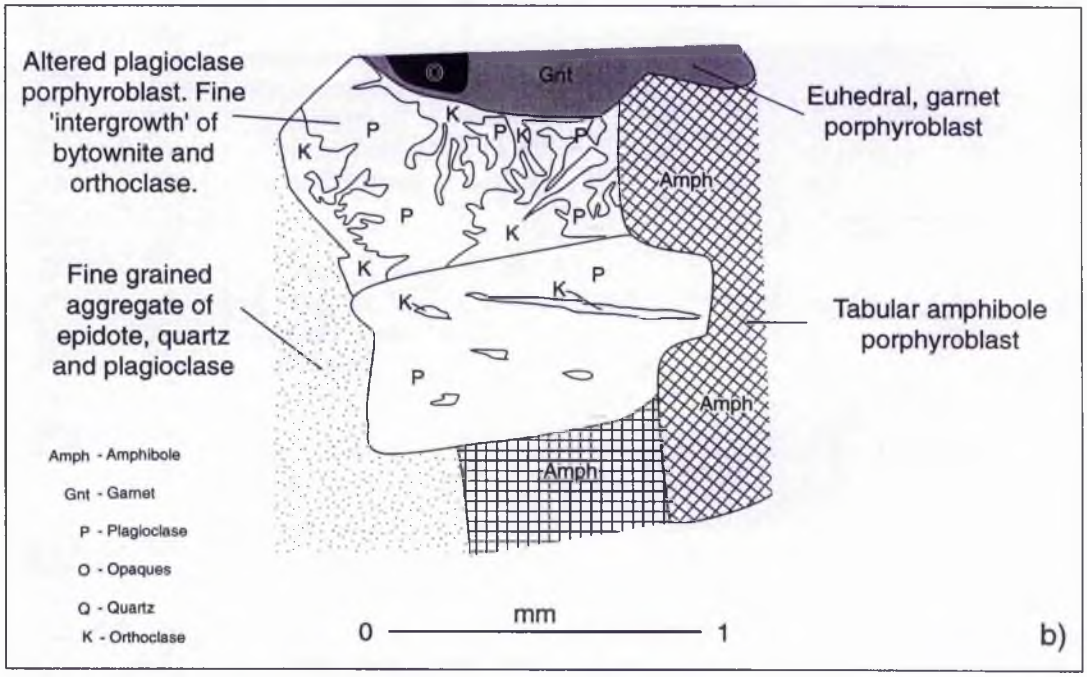

Fig. 4.14 Sketch of a) porphyroblastic texture of the garnet - bearing, calc - silicate sample [SJ 134]. b) is an enlargement of the area shown in a) to illustrate the 'intergrowth' texture between bytownite and orthoclase feldspar.

with each other produce the evident mixing textures.

Garnet porphyroblasts are dominated by almandine while core to rim analysis again reveal bell shaped profiles for the spessartine component (Fig. 4.3). Figure 4.10 displays the ratio of the phase components FeO, CaO and MgO of the garnet and amphibole pairs. There is a significant spread of data points for the garnet analyses indicating that this sample is poorly equilibrated. The unequilibrated nature of the garnet porphyroblasts and the calcic and mixed nature of the plagioclase mineral phase makes accurate *PT* estimations impossible and thus will not be considered for this assemblage.

Pelites.

Pelitic lithologies are rare within both the Maunde Ophiolite and Kaourera Island - Arc Groups; however, they are represented by the Nzou Meta - Greywacke and Bhumi Semi - Pelite Formation respectively (section 2.2.1 and 2.3.6). The pelitic Nzou Meta - Greywacke Formation is comprised of :-

biotite + calcite + plagioclase + quartz + muscovite + epidote + opaques (Appendix B and Plate. 4.3 d)

The lack of garnet and aluminium silicates suggests that this is a low grade, greenschist facies, biotite zone assemblage. This is somewhat surprising since this lithology is in contact with lower amphibolite grade meta - basalts. The semi - pelitic Bhumi Semi - Pelite Formation is comprised of :-

quartz + garnet + chlorite + muscovite + tourmaline (Appendix B)

No aluminium silicates or plagioclase are present. The Bhumi Semi - Pelite Formation is dominated by quartz, muscovite and chlorite. Both

phyllosilicates are elongate, parallel and wrap around garnet porphyroblasts and quartz lenses (Plate. 4.4 a and b). Chlorite also occurs as radiating masses and filling cracks within garnet porphyroblasts. The presence of both chlorite and garnet within the same assemblage and the radiating nature of some chlorite crystals indicate that it is a retrogressive phase. The parallel nature of most chlorite laths within the matrix and its association with muscovite suggest that chlorite is replacing biotite via reaction [4].

[4] biotite + phengite poor muscovite + quartz + water = phengite + chlorite

Garnet porphyroblasts are euhedral, upto 10 mm diameter, predominantly inclusion free and where cracked are filled by randomly oriented retrogressive chlorite blades. Microprobe analysis reveals that the porphyroblasts are almandine - rich and display flat profiles for all components (Fig. 4.3) suggesting that they have undergone homogenisation (Spear, 1993). The lack of plagioclase makes pressure estimations for this sample impossible, however, temperature estimations are based on the garnet - chlorite exchange thermometer calibrated by Dickenson & Hewitt, (1986) and modified in Laird, (1988); Hodges & Spear, (1982); Ganguly & Saxena, (1984) and Bermann, (1990) are summarised in Table 4.1.

Since chlorite is interpreted as a retrogressive phase these temperature calculations estimate only minimum temperatures and not those of peak metamorphism. Calculations were processed using the unpublished computer program "Thermobarometry" (Kohn & Spear, 1996). Garnet rim temperatures range from 495 to 555 °C ± 25°C depending on which calibration and estimate of pressure is used. However, if the garnet porphyroblasts have been homogenised at peak metamorphic temperatures, then these temperature estimations are inapplicable.

Serpentinites

The ultramafic assemblages of the Ngwena Ultramafic Formation are comprised of :-

tremolite + serpentine + chromite ± chlorite ± calcite ± talc (Appendix B)

In section 3.2.4 and Fig. 3.7, it was demonstrated that these serpentinite bearing ultramafic lithologies of the Ngwena Ultramafic Formation have undergone major element and possibly trace element chemical alteration during serpentinisation and / or metasomatism. It is therefore likely that the metamorphic mineral assemblage now seen is a result of this alteration. However, some important relict textures remain which merit further discussion.

P (kbar)	T°C			
	(1)	(2)	(3)	(4)
1	510	525	495	523
2	513	528	498	527
3	516	531	502	530
4	519	534	404	534
5	522	537	507	537
6	525	540	510	541
7	528	543	513	544
8	531	546	516	548
9	534	548	519	551
10	537	551	522	555

Table 4.1 Summary of garnet - chlorite temperatures for the Bhumi Semi - Pelite Formation meta - pelites. Temperature calibrations are based on (1) Dickenson & Hewitt, 1986 and modified in Laird, 1988; (2) Hodges & Spear, 1982; (3) Ganguly & Saxena, 1984 and (4) Bermann, 1990.

The Tremolite Member and the Layered Tremolite Member are dominated by a fine grained tremolitic matrix. Individual tremolite crystals are euhedral to subhedral, tabular, are on average 0.5 - 1 mm in length and are aligned to define a tectonic fabric. Randomly dispersed within matrix are anhedral to sphericular, 1 to 2mm diameter tremolite porphyroblasts and irregular, 1 - 2 mm diameter chromite grains. The cores of the tremolite porphyroblasts contain abundant, very fine grained chromite inclusions which display no preferred orientation and are generally confined to the central portion of each porphyroblast, the margins of which are generally irregular but sometimes sharply bounded (Fig. 4.15). Within the Layered Tremolite Member, the tremolite porphyroblasts and irregular shaped chromite grains aggregate within upto 10 cm long, 1 - 5 mm thick, disrupted layers (Plate. 2.4 f). Tremolite with chromite inclusions might be produced from the breakdown of diopside in reaction [5] :-

[5] Chromium diopside + CO_2 + H_2O = Tremolite + Calcite + Quartz + Chromite.

It is possible therefore that the tremolite porphyroblasts pseudomorph relict Cr - diopside phenocrysts. Elongate chlorite lenses upto 10 mm long, are sub - parallel to and occasionally cross - cut the fabric defined by the fine grained tremolitic matrix (Fig. 4.15).

The Serpentinite Member is dominated by fine grained (less than 0.1 mm), randomly oriented serpentine with subordinate tremolite and talc blades. Rare, 1 - 2 mm diameter, tremolite porphyroblasts and irregular chromite grains are randomly spaced throughout the matrix (Plate. 4.4 c and d). Deer *et al.*, (1992) indicate that serpentine is produced by the breakdown of olivine from reaction [6] :-

[6] 3 forsterite + quartz + 4 H_2O = 2 serpentine

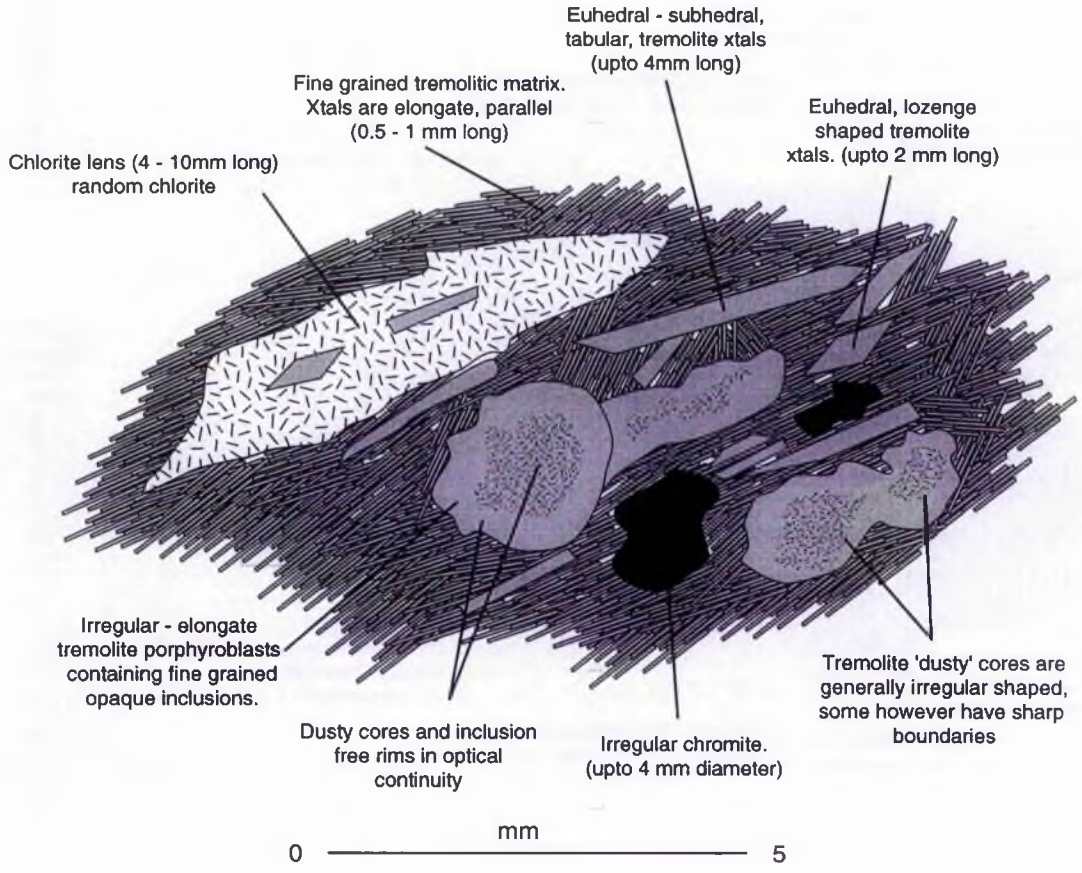

Fig. 4.15 Sketch of the main textural features of the Tremolite Member from thin section [SJ 213 A]. Note the tremolite porphyroblasts with cores rich in chromite inclusions.

while talc is produced by the breakdown of clinopyroxene from reaction [7] and [8] :-

[7] 5 enstatite + H_2O = talc + forsterite

[8] 3 enstatite + quartz + H_2O = talc

The dominance of serpentine in this member suggests that the original mineralogy was dominated by olivine, while the presence of lesser amounts of tremolite and talc within the matrix indicate that diopside and orthopyroxene were present but possibly in subordinate proportions. However, the since all these ultramafic lithologies have undergone chemical changes it is difficult to interpret the original mineralogy of the protolith.

The podiform rock is texturally the most revealing rock. It is comprised of a fine grained, randomly oriented serpentine dominant matrix with upto 4 cm long, 2 cm wide lenses of tremolite and serpentine. The 'pods' are evenly spaced and distributed and do not form trains or layers. However it is possible that they may have once formed continuous or semi continuous layers which have since been disrupted by deformation (Plate. 2.5 a). The pods are comprised of serpentine aggregates which pseudomorph relict, euhedral, upto 3 mm long, olivine crystals and tremolite porphyroblasts which pseudomorph relict, euhedral, diopside crystals (Plate. 2.5 b). The contacts between all relict igneous crystals are near 120°. The rims of the relict diopside crystals are mantled in fine grained acicular tremolite and talc which is in optical continuity with the tremolite porphyroblast. Tremolite porphyroblast cores again contain fine grained inclusions of chromite. The relict olivine crystals contain randomly oriented trains of chromite which fill possible fractures within the original olivine crystal. The near 120° interfacial angles between relict

crystals and relict euhedral crystal forms altogether suggest that these pods represent relict olivine and diopside cumulates layers which have subsequently been boudinaged during deformation.

The association of serpentine + talc + tremolite + calcite within all members is interpreted by Evans (in Robinson *et al.*, 1981) to represent metamorphosed peridotite in the greenschist to lower amphibolite facies. Spear (1993) also indicates that crysolite has an upper stability limit of between 500 to 600°C between 0 and 15 kbar respectively also indicating greenschist to lower amphibolite facies metamorphism.

Summary.

The majority of metamorphic assemblages within the Maunde Ophiolite and Kaourera Island - Arc Groups are comprised of amphibole + plagioclase + epidote without garnet. There are no relict higher *PT* minerals or inclusions within porphyroblasts indicating that metamorphism peaked within the lower amphibolite facies. Garnet bearing lithologies are rare and located only within the Kaourera Island - Arc Group. Figure 4.16 is a summary diagram illustrating the combined

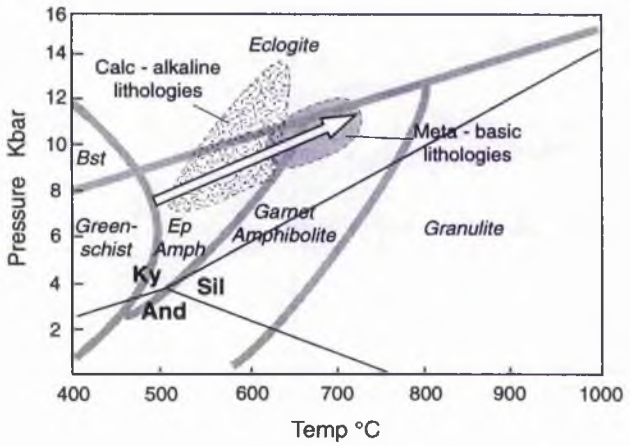

Fig. 4.16 Diagram summarising the *PT* conditions for the garnet bearing assemblages of the Ophiolite Terrane. Abbreviations :- Bst = blueschist; Ep Amph = epidote amphibolite (lower amphibolite); Ky = kyanite; Sil = Sillimanite; And = andalusite.

peak metamorphic *PT* estimations for garnet bearing tholeiitic and calc alkaline meta - basalts for the Ophiolite Terrane. The summary figure is a compilation of Figs. 4.11 and 4.13.

4.3.2 Kadunguri Whiteschists.

The Kadunguri Whiteschists are chemically rather exceptional since all the mineral assemblages can be represented by only five major phase components MgO, Fe_2O_3, Al_2O_3, SiO_2, and H_2O ($MF^{3+}ASH$) and three minor phase components namely, FeO, Na_2O and B_2O_3. Metamorphic reactions within this MFASH group have been studied experimentally by various authors (Yoder, 1952; Schreyer & Yoder, 1968; Schreyer & Seifert, 1969a and b, Schreyer, 1977, 1988; Massonne, 1989; Fockenberg & Schreyer, 1991, 1994). There are no direct exchange thermometers or net transfer reactions between mineral phases within this group and thus estimations of *PT* conditions are based on the recognition of key metamorphic reactions compared to experimental results.

The Kadunguri Whiteschists are comprised of 3 main mineral assemblages, the quartz - bearing Foliated and Unfoliated Quartz Whiteschists; the Gedrite - bearing, Gedrite Whiteschist and the Yoderite Whiteschist which contains the second natural occurrence of the mineral yoderite.

The three main mineral assemblages contain eight components (MgO, Fe_2O_3, FeO, Al_2O_3, SiO_2, H_2O, Na_2O and B_2O_3), which form a variety of phases :-

talc, kyanite, chlorite, yoderite, dravite, hematite, quartz, gedrite and anthophyllite.

The Fe_2O_3 component is present almost entirely as pure hematite which is present in abundance within all three assemblages. Chlorite and gedrite

are the only phases to contain minor proportions of Fe^{2+} (see section 4.2.2 and Appendix D) while dravite (which is also present within all assemblages) is the only phase to contain significant amounts of Na_2O and B_2O_3. Therefore the mineralogical variation between within three assemblages is due to the combination of the three components MgO, Al_2O_3 and SiO_2. This mineralogical variation can be represented on a triangular diagram (Fig. 4.17). As previously discussed in section 3.4.1 and represented in Fig. 4.17, most of the components within the three assemblages and other whiteschist occurrences, can be theoretically be represented by the assemblage Mg - chlorite plus quartz (Schreyer, 1977).

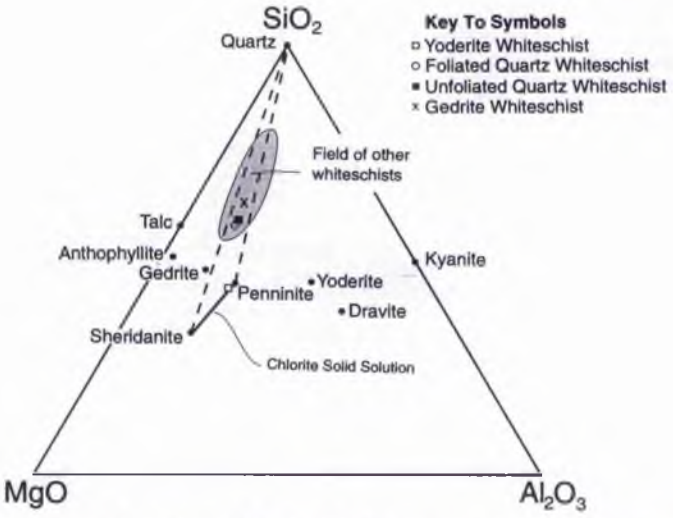

Fig.4.17 Modalised triangular plot of the MFASH system showing the compositions of the main mineral phases and the whole rock major element compositions of the Kadunguri Whiteschists formations and the field for other world - wide whiteschists (from Schreyer, 1977).

Foliated and Unfoliated Quartz Whiteschists.

This assemblage contains the least number of mineral phases :-

quartz + kyanite + talc + hematite + dravite (Appendix B and Plate. 4.5 a).

If, according to Schreyer, (1977) the protolith is presumed to have been once comprised predominantly of quartz and chlorite then with

increasing *PT*, chlorite and quartz would become unstable to form talc and kyanite via reaction [9] (Massonne, 1989).

[9] quartz + chlorite = talc + kyanite + H_2O

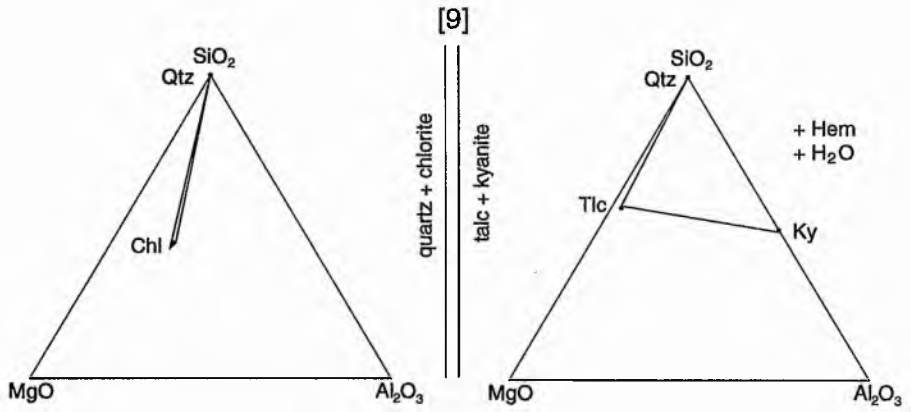

According to the Korzhinskii Phase Rule (Korzhinskii, 1959) assuming that the degrees of freedom are *P* and *T*, then the number of solid phases in the mineral assemblage (P_S) equals the number of inert components (C_i), which in this case equals five. Therefore three of the phase components are mobile, namely H_2O, Na_2O and B_2O_3. Since dravite is the only solid phase to contain Na_2O and B_2O_3 it is therefore likely that dravite formed at this time, possibly due to reaction [10].

[10] 3 chlorite + 4 quartz + 1.4 Na + B* = 1 dravite + 3 talc + 1.5 hematite + H_2O

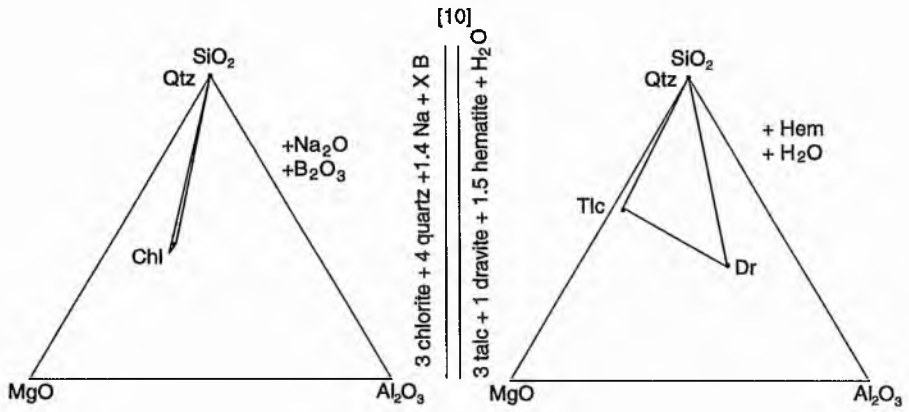

The chlorite is presumed to be Mg - chlorite and the dravite stoichiometry is taken from Appendix D (* in reaction [10] indicates that since B_2O_3 in dravite was not analysed, the quantity of boron to be added to the left hand side of the equation is unknown). This leads to the combined general reaction [11].

[11] chlorite + quartz + Na + B + O_2 = talc + kyanite + hematite + dravite + H_2O.

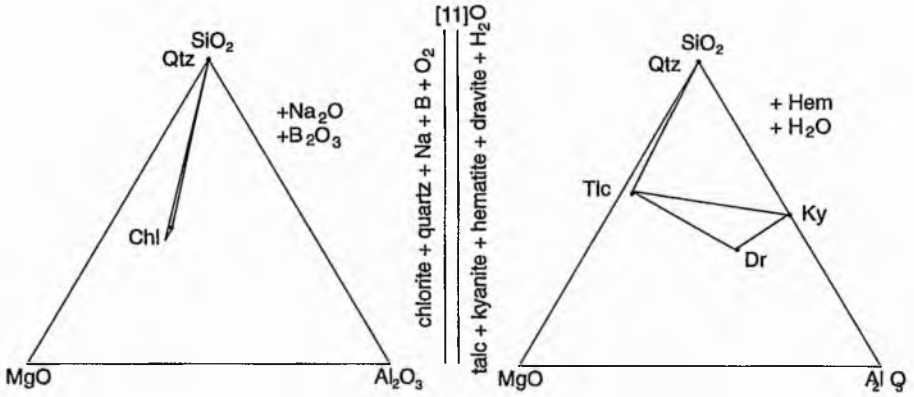

The production of hematite and the change of oxidation state of the iron from Fe^{2+} to Fe^{3+} indicates that this is a redox reaction and input of O_2 on the reactant side is needed to balance this equation. A high oxygen fugacity is therefore a prerequisite for this reaction to proceed. It is unclear whether all of the hematite within this assemblage has been produced via reaction [11] or whether the pre - metamorphic assemblage contained igneous iron oxides which were oxidised to hematite.

The experimental upper thermal stability limit of reaction [9], calibrated by Massonne (1989) is shown in Fig. 4.18. The addition of the minor phase components Na_2O and B_2O_3 are likely to shift this limit to lower temperatures (Grew *et al.*, 1998). The effects of a variable oxygen fugacity and fluid pressure also have unknown effects.

Gedrite Whiteschist.

This assemblage contains the following solid phases

gedrite + quartz + dravite + hematite + kyanite ± talc ± anthophyllite (Appendix B).

Again if the protolith is assumed to be dominated by quartz and Mg - chlorite then reactions [9], [10] and [11] also apply. Gedrite is the dominant mineral phase within this assemblage. It occurs as radially arranged

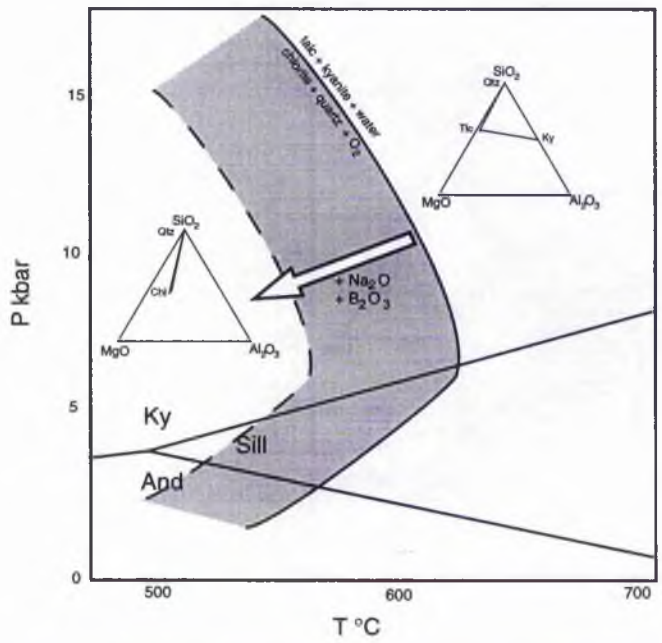

Fig. 4.18 Petrogenetic grid for the MFASH system showing the upper stability limit for chlorite + quartz - reaction curve [9] and the effect of adding additional components i.e., Na and B. Also shown are SMA diagrams illustrating the change in mineral assemblages.

acicular crystals upto 30 mm long and as euhedral basal sections (Plate. 4.5 b). Occasionally gedrites are retrogressed and replaced by talc (Plate. 4.5 c). The proportion of anthophyllite in the assemblage is small (<0.5%) but is also an important solid phase. The petrogenesis of gedrite within the MASH system has been experimentally studied by Tilley (1939) and Schreyer & Seifert (1969a and b) who indicate that with increasing *T*,

kyanite and talc become unstable to form gedrite and quartz via reaction [12] :-

[12] talc + kyanite = gedrite + quartz + water.

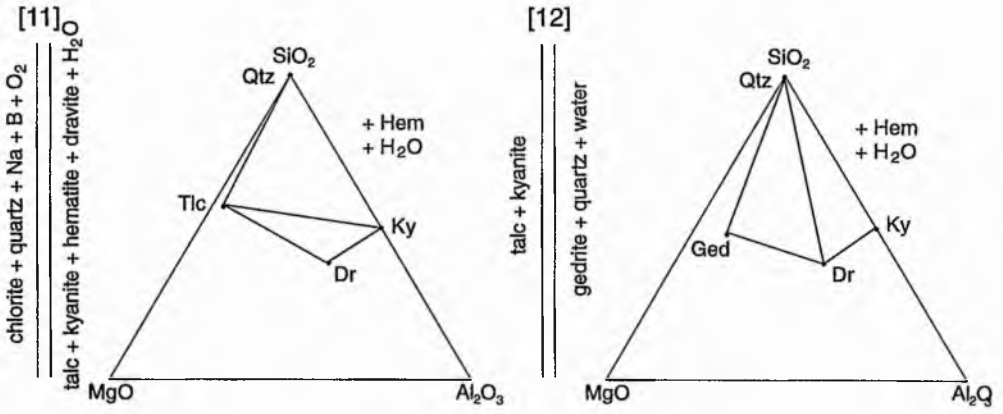

The petrogenesis of anthophyllite in MASH or MFASH assemblages has yet to be studied; however, a possible reaction is [13]

[13] 15 talc + 4 chlorite = 6 anthophyllite + 10 gedrite + 44 quartz + water.

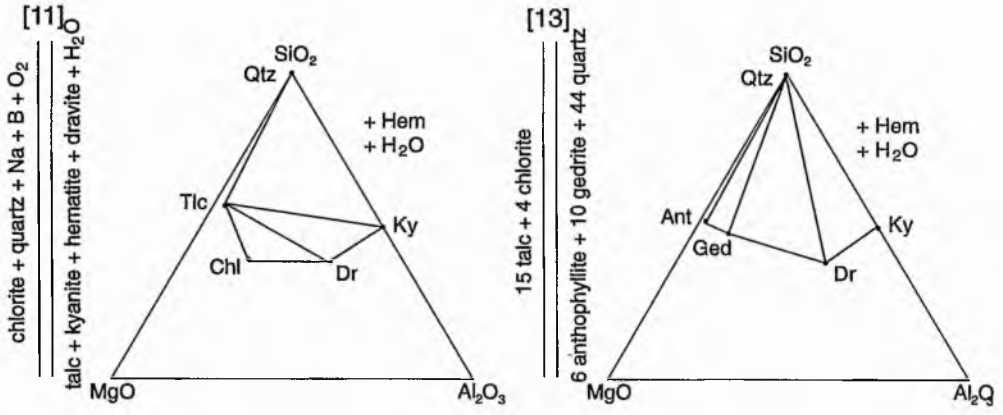

The upper thermal stability limit for reaction [12] is shown in Fig. 4.19 which indicates minimum temperatures of around 900°C. As reaction [13] has not been experimentally studied its stability is unknown.

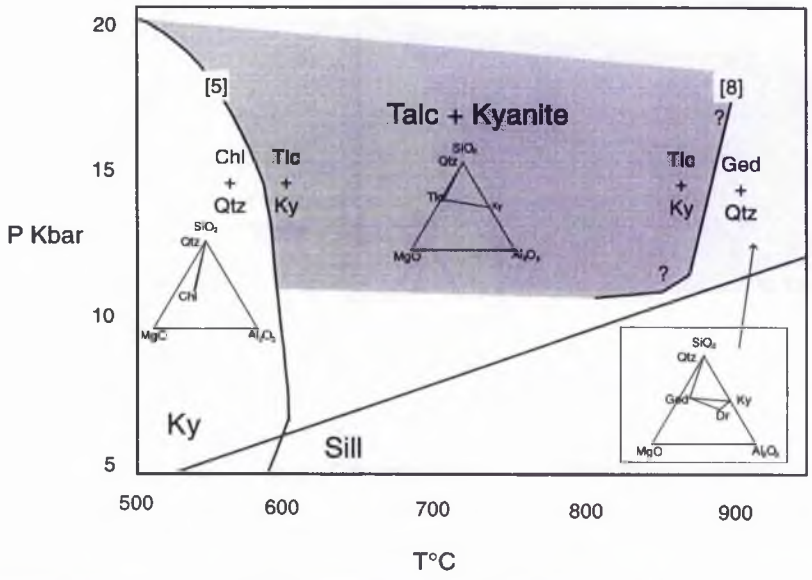

Fig.4.19 Petrogenetic grid for the MFASH system showing the upper and lower stability of talc + kyanite. Also shown are SMA diagrams illustrating the change in mineral assemblages.

On the completion of reaction [11], the assemblage of the Gedrite and Quartz Whiteschists will contain similar solid mineral phases, namely :-

talc + kyanite + quartz + dravite + hematite.

The Unfoliated Quartz Whiteschist and Gedrite Whiteschist assemblages are interpreted to be in stratigraphic contact, the boundary between the two being gradational over some 5 - 20 m. Microprobe analysis of both talc and gedrite reveal the presence of minor Na_2O in the crystal structure (upto 0.7 wt % in talc and 1.7 - 2.0 wt% in gedrite). Natural gedrites normally contain a small proportion of Na but the talc structure does not allow any substitution for alkalis (Deer *et al.*, 1992). It is possible that the Na within the talc is accommodated as interlayer ions (Deer *et al.*, 1992). Introduction of Na into the gedrite crystal structure lowers its thermal stability (Grew *et al.*, 1998) as does the inclusion of Na as interlayer ions within the talc structure. Analysis of talc within the Quartz Whiteschists reveal no Na. Both assemblages possibly underwent metamorphism at similar

temperatures, but the presence of Na within the solid phases of the Gedrite Whiteschist have permitted reaction [12] to proceed at lower temperatures. Production of gedrite is therefore a function of Na availability.

When applying the Korzhinskii Phase Rule to this assemblage, assuming that anthophyllite and talc are part of the stable assemblage, then the number of solid phases equals seven and thus there is only one mobile phase, namely H_2O. This indicates that both Na_2O and B_2O_3 were inert components at this time and that Na must have been a component in one of the solid reactant phases within reaction [12] i.e., talc or kyanite. However, if the talc is considered to be retrogressive, since it replaces gedrite (Plate. 4.5 c) and the anthophyllite the product of a later reaction [13], then $P_S = 5$, therefore Na_2O, B_2O_3 and H_2O were mobile during reaction [12] and none of the solid reaction phases therefore need to contain Na. If Na^{2+} was dissolved in the fluid phase at this time then gedrite was formed as a direct result of Na metasomatism via reaction [14].

[14] talc + kyanite + Na = gedrite + quartz + H_2O

The absence of gedrite within the Quartz Whiteschists suggest that metasomatism at this stage was a localised occurrence, restricted to those assemblages which now contain gedrite. Prolonged Na metasomatism might have increased the whole rock Na_2O wt % content of the assemblage. However, since the proportion of Na in gedrite is small the effect is negligible.

It is concluded that this assemblage was :-

1) originally dominated by quartz and chlorite

2) underwent reaction [11] to produce talc + kyanite + dravite + hematite ± chlorite

3) prolonged Na metasomatism lowered the stability of reaction [14] to produce gedrite + quartz + dravite + hematite + kyanite

4) syn or post - (3), reaction [13] produced anthophyllite + gedrite + quartz + dravite + hematite + kyanite

Yoderite Whiteschist.

The Yoderite Whiteschist consists of a randomly oriented assemblage of :-

chlorite + kyanite + dravite + hematite + yoderite + talc (Appendix B and Plate. 2.9).

All mineral phases are interpreted to be in textural equilibrium (Plate. 4.1 a, c and d and Plate. 4.6 a, b and c). It is important to note that there is no quartz in the rock. This assemblage is so far unique within nature since the yoderite - bearing assemblage at Mautia Hill is dominated by quartz and consists of :-

quartz + yoderite + talc + kyanite

The Yoderite Whiteschist lies within the two phase field of quartz and chlorite on an SiO_2, Al_2O_3, MgO triplot (Fig. 4.17). Note that this member plots below a tie line that would join talc - kyanite, whereas the other two assemblages (Quartz Whiteschists and Gedrite Whiteschist) plot above it. This indicates that during prograde metamorphism of the Yoderite Whiteschist, quartz and chlorite will become mutually exclusive.

With an increase it *P* and *T*, quartz and chlorite, become unstable to form talc and kyanite. Chlorite inclusions within the cores of kyanite and

hematite crystals (which may represent the composition of the original chlorite within the quartz - chlorite protolith), have a formula of $Mg_3Al_{2.5}Fe_1Si_{3.2}O_{10}(OH)_8$ (penninite, see Fig. 4.17). Reaction [9] can therefore be balanced in respect to this assemblage :-

[15] 100 $Mg_3Al_{2.5}Fe_1Si_{3.2}O_{10}(OH)_8$ + 205 SiO_2 + 32.5 O_2 = 100 $Mg_3Si_4O_{10}(OH)_2$
Penninite Quartz Oxygen Talc

+ 125 Al_2SiO_5 + 50 Fe_2O_3 + 300 H_2O
Kyanite Hematite Water

and reaction [10] therefore becomes :-

[16] 24 $Mg_3Al_{2.5}Fe_1Si_{3.2}O_{10}(OH)_8$ + 45.6 SiO_2 + Na + B + 42 O_2 =
Penninite Quartz Sodium Boron Oxygen

15.6 $Mg_3Si_4O_{10}(OH)_2$ +10 $Mg_{2.5}Al_6Fe_{0.5}Si_6O_{24.5}(OH)_2$ + 9.5 Fe_2O_3 + 106 H_2O
Talc Dravite Hematite Water

which leads to the combined reaction [17]

[17] 124 Penninite + 250.6 Quartz + Sodium + Boron + 75.4 Oxygen =
115.6 Talc + 125 Kyanite + 10 Dravite + 59.5 Hematite + 406 Water

Again note that the above reactions are redox ones and are therefore dependent on a high fO_2. The chlorite which comprises the coarse - grained matrix is actually Fe - poor, Mg - rich, sheridanite ($Mg_{4.5}Al_{2.5}Fe_{0.05}Si_{2.8}O_{10}(OH)_8$). The chlorites probably form a solid solution series as shown in Fig. 4.17. Since the whole rock analyses of the Yoderite Member plots close to the chlorite field, it is likely that the protolith was once comprised predominantly of chlorite. As illustrated in reaction [17], two moles of quartz are reacted for every mole of chlorite and will therefore become exhausted by reaction [17] before chlorite (since chlorite

predominates quartz in this assemblage). If the fO_2 remains high then sheridanite might be produced via reaction [18]:-

[18] $500\ Mg_3Al_{2.5}Fe_1Si_{3.2}O_{10}(OH)_8 + 173.5\ O_2 =$
Penninite Oxygen

$230\ Mg_{4.5}Al_{2.5}Fe_{0.05}Si_{2.8}O_{10}(OH)_8 + 155\ Mg_3Si_4O_{10}(OH)_2 + 338\ Al_2SiO_5$
Sheridanite Talc Kyanite

$+ 244\ Fe_2O_3 + 925\ H_2O$
Hematite Water

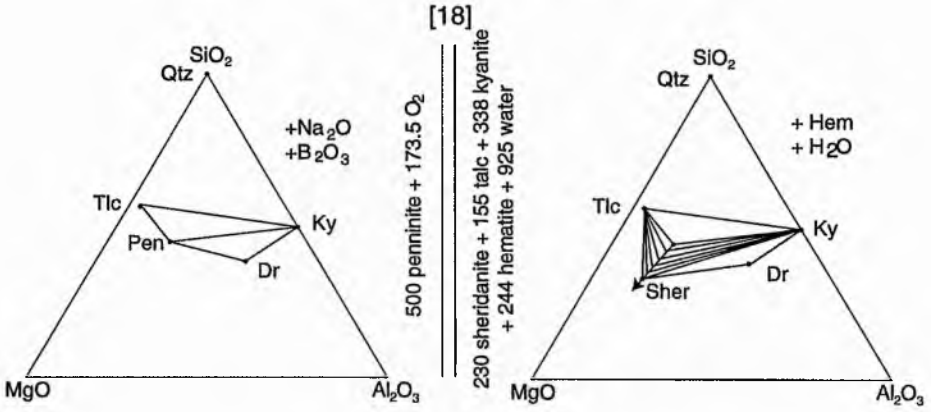

Dravite can no longer form since its production is dependent on the presence of quartz. Since penninite and sheridanite are related by solid solution it is likely that all intermediate compositions are produced at some point. All of these intermediate compositions possibly react with O_2 in a reaction similar to that of reaction [18] ultimately resulting as end member sheridanite. Note how dravite lies outside the chlorite - talc - kyanite field and thus cannot be produced during reaction [18].

Experimental work by Fockenberg & Schreyer (1994) indicates a variety of possible yoderite - forming reactions in the MgO - Fe_2O_3 - Al_2O_3 - SiO_2 - H_2O (MFASH) system. The *P* - *T* stability field of yoderite and possible yoderite forming reactions (after Fig. 11 in Fockenberg & Schreyer, 1994) are illustrated in Fig. 4.20. The molecular proportions of the whole rock major element compositions of the Yoderite Whiteschist and the

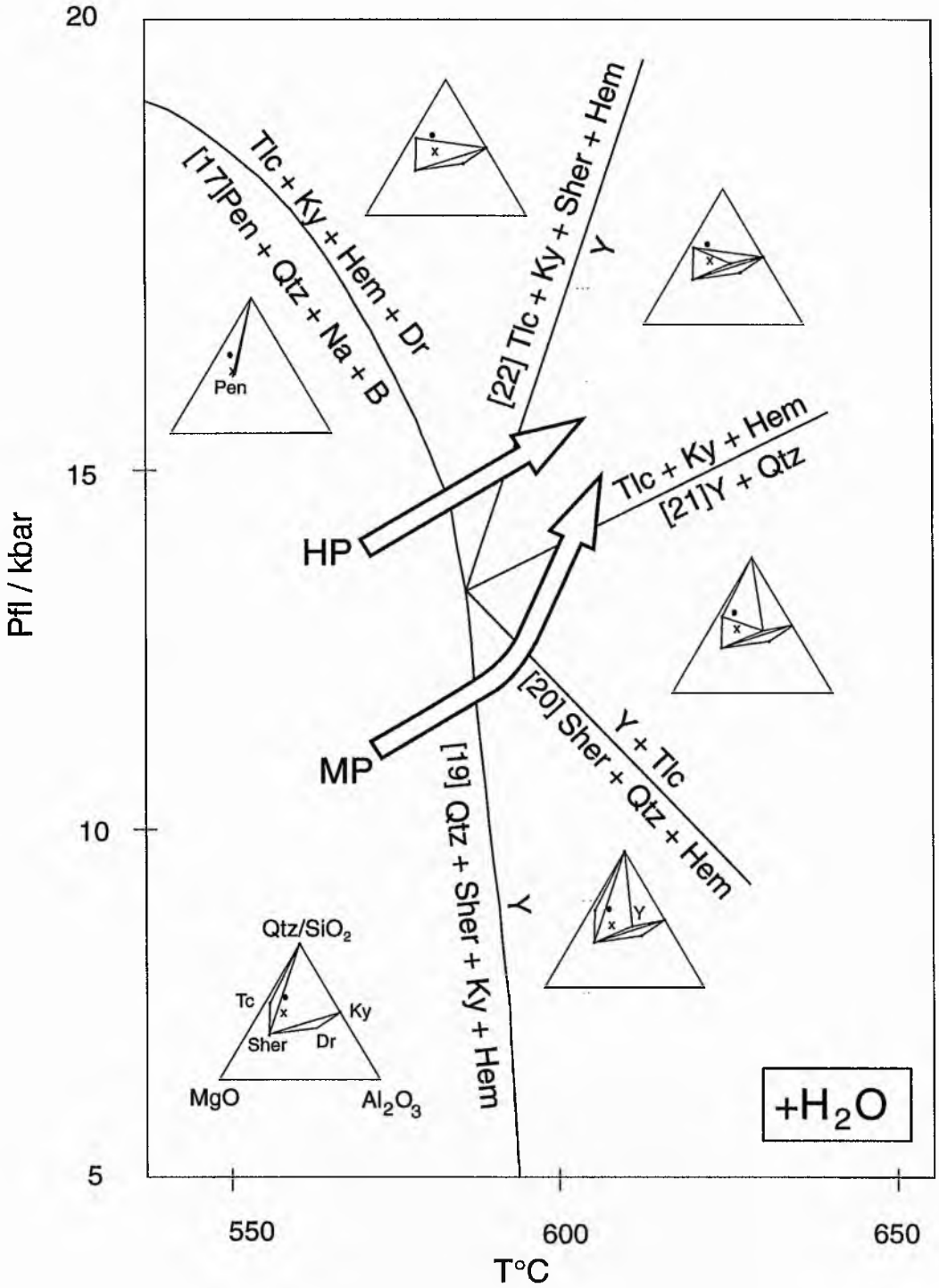

Fig. 4.20 Petrogenetic grid for the MFASH system showing the the lower *PT* stability of yoderite (from Fockenberg & Schreyer, 1994). Also shown are SiO2, MgO Al2O3 diagrams illustrating the various mineral assemblages. Two possible PTt paths are shown (HP - high pressure and MP - moderate pressure), both of which end in the same yoderite without quartz field. Mineral abbreviations as in the text. On the triangular plots the closed circle represents the Quartz and Gedrite Whiteschists; the cross represents the Yoderite Whiteschist. For discussion see text.

other two main assemblages of the Kadunguri Whiteschists (now illustrated as a single assemblage) are indicated in this diagram. Two possible *P* - *T* paths are possible (medium and higher pressure), both of which will end in the identical yoderite without quartz field. If metamorphism proceeded via the medium pressure path, yoderite would initially be produced in *all* of the Kadunguri Whiteschists rocks as a result of reaction [19]. Further progressive metamorphism is via reaction [20] and [21]:-

[19] 2.22 $Mg_{4.5}Al_{2.5}Fe_{0.05}Si_{2.8}O_{10}(OH)_8$ + 11.47 Al_2SiO_5 + 2 SiO_2 + 0.7 Fe_2O_3
Sheridanite Kyanite Quartz Hematite

= 5 $Mg_2Al_{5.7}Fe_{0.3}Si_4O_{18}(OH)_2$ + 3.9 H_2O
Yoderite Water

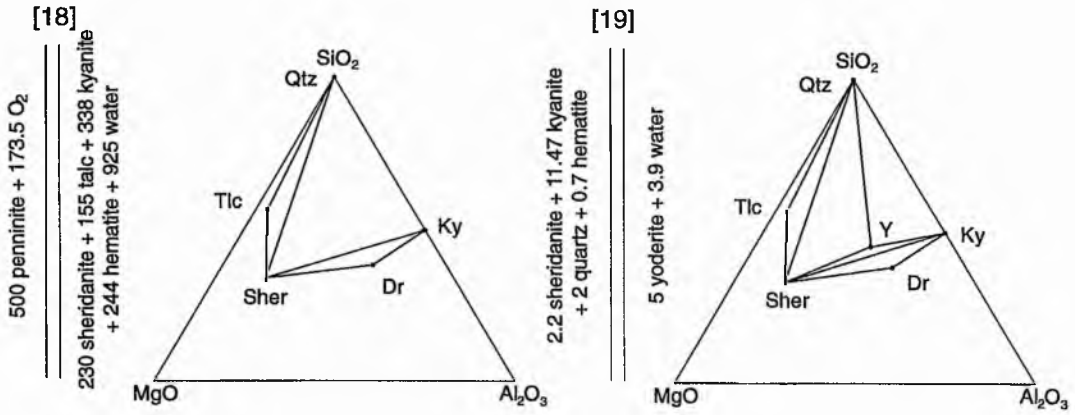

[20] 33.1 $Mg_{4.5}Al_{2.5}Fe_{0.05}Si_{2.8}O_{10}(OH)_8$ + 124 SiO_2 + 1.3 Fe_2O_3 =
Sheridanite Quartz Hematite

40 $Mg_3Si_4O_{10}(OH)_2$ + 14.5 $Mg_2Al_{5.7}Fe_{0.3}Si_4O_{18}(OH)_2$ + 78 H_2O
Talc Yoderite Water

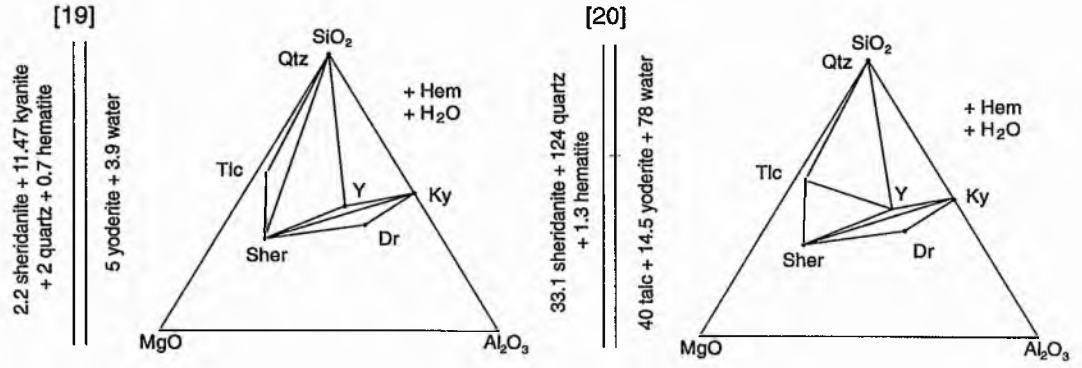

[21] $15\ Mg_2Al_{5.7}Fe_{0.3}Si_4O_{18}(OH)_2 + 22.8\ SiO_2 =$
Yoderite Quartz

$10\ Mg_3Si_4O_{10}(OH)_2 + 42.8\ Al_2SiO_5 + 2.3\ Fe_2O_3 + 5\ H_2O$
Talc Kyanite Hematite Water

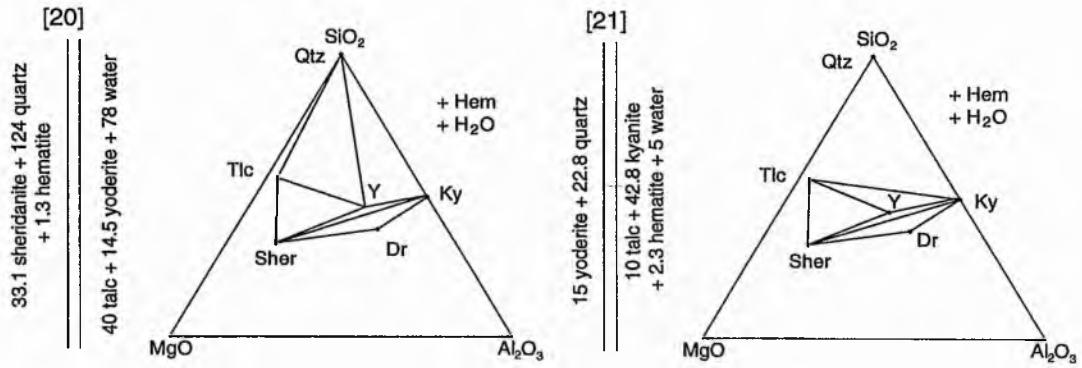

Thus reactions [19] and [20] produce yoderite in silica-rich whiteschists. Reaction [21] produces talc + chlorite + kyanite + yoderite in Mg - rich compositions (i.e. the Yoderite Member) and talc + kyanite + quartz *without* chlorite or yoderite in the Si - rich whiteschists.

If metamorphism proceeded via the higher pressure path then these whiteschists would evolve via reaction [17] so that chlorite and quartz become mutually exclusive. Yoderite will be produced in chlorite + talc + kyanite assemblages *without* quartz through reaction [22].

[22] $54.2\ Mg_3Si_4O_{10}(OH)_2 + 120\ Mg_{4.5}Al_{2.5}Fe_{0.05}Si_{2.8}O_{10}(OH)_8 + 848\ Al_2SiO_5$
Talc Sheridanite Kyanite

$$+ 50\ Fe_2O_3 = 350\ Mg_2Al_{5.7}Fe_{0.3}Si_4O_{18}(OH)_2 + 183.4\ H_2O$$
Hematite Yoderite Water

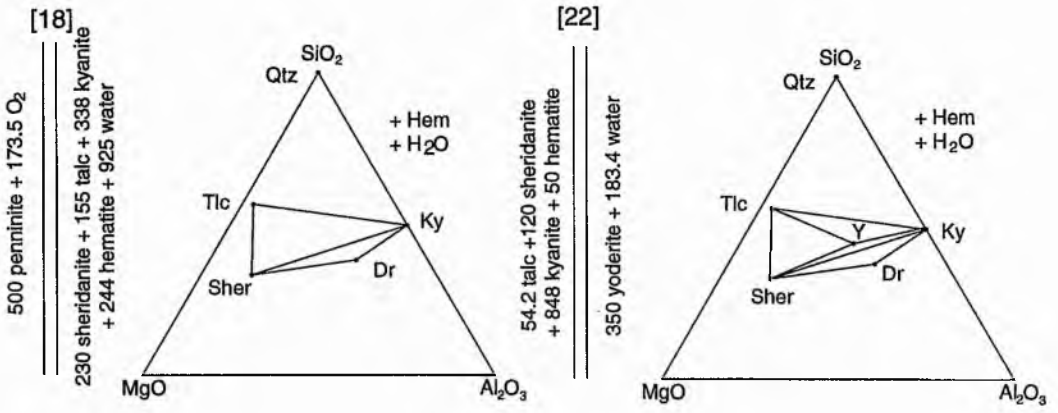

Thus the Quartz Whiteschists which surround the Yoderite Whiteschist will never have contained yoderite (in contrast to the medium pressure path).

The higher pressure path of metamorphism for the Yoderite Whiteschist and thus the Kadunguri Whiteschists is supported by textural evidence, i.e. there is a notable lack of relict quartz inclusions within yoderite crystals in the Yoderite Whiteschist and an absence of relict yoderite crystals or inclusions within the surrounding Quartz Whiteschist assemblages. There is no textural evidence for reactions [19], [20] or [21] which might have been expected to leave behind some relict inclusions.

Experimental stability conditions for a quartz - free yoderite assemblage in the MFASH system where aH_2O and fO_2 are high, are at a minimum pressure of 13 kbar at 590°C and a maximum pressure of 21 kbar at 650°C (Fig. 4.20 and 4.21), (if staurolite is not involved, see details in Fig. 11 in Fockenberg & Schreyer, 1994). Note however that Fe_2O_3 is present in excess and so many of the reactions become redox ones. The stabilities of the reactions will be dependent on the fugacity of O_2. Since chlorite has mainly Fe^{2+}, the fO_2 - T relations for the yoderite - forming reactions become complex. The P - T stability can be affected by the partitioning of

Fe^{2+} and Fe^{3+} among the phases (e.g., chlorite and yoderite). Hence the *P* - *T* estimate for the Yoderite Whiteschist and surrounding whiteschist assemblages may be somewhat lower than indicated. However, since chlorite has only 0.05 p.f.u. Fe^{2+} and yoderite has 0.3 p.f.u Fe^{3+} this effect may not be significant.

Minor chlorite and kyanite, but not quartz, occurs within fractures in yoderite crystals. If quartz were present then it may be interpreted that this assemblage represents a retrogressive metamorphic event via the reverse of reaction [19] or [20], (see Fig. 4.20 and 4.21). However, detailed microprobe analyses of mineral phases within these fractures reveal that this chlorite has a composition identical to the matrix phase (Appendix D). The lack of quartz and the primary nature of the mineral phases suggest that this is not indicative of a retrogressive event.

Minor Lithologies and the Role of Fluids.

The Talc - Phlogopite Whiteschist is comprised of

quartz + talc + kyanite + chlorite + dravite + hematite ± white mica (Appendix B).

The white mica is identified as phlogopite ($KMg_3(Si_3Al)O_{10}(OH)_2$) by XRF analyses. Although the proportion of phlogopite is small (<1%) it indicates that this assemblage contains another minor component, namely K_2O and is thus represented within the KFMASH system. The phlogopite laths are randomly oriented and are in stable equilibrium with all the solid phases. It is possible that either

1) K_2O was present as a pre - metamorphic / metasomatic phase component, or

2) that K_2O was introduced to this assemblage within the fluid phase during metamorphism / metasomatism.

The KFASH, KMASH and KFMASH system assemblages are outlined by Spear & Cheney (1989) and Spear (1993). The presence of dravite in this assemblage suggests that a reaction similar to reaction [11] occurred even though K_2O is present. Muscovite may have been stable at this time (Spear, 1993). Spear & Cheney (1989) also indicate that Mg - chlorite becomes unstable to produce talc and kyanite. With a further increase in *P* and *T* both muscovite and talc become unstable to produce phlogopite and kyanite via reaction [23].

[23] muscovite + talc = phlogopite + kyanite

The upper thermal stability for reaction [23] is 650°C at pressures exceeding 9 kbar (Fig. 4.21). Again the addition of the Na_2O and B_2O_3 component in the form of dravite may lower the stability of this reaction to lower temperatures (Grew *et al.*, 1998).

The Quartz - Hematite Sheets are comprised of very fine grained (0.25 mm) granoblastic quartz and hematite with minor, randomly oriented, less than 0.25 mm long kyanite laths and minor talc blades (Plate. 4.6 d and e). At all localities the granoblastic matrix is cut by parallel bands (Plate. 2.8 f) or an anastamosing network (Plate. 2.10 a) of coarse grained (upto 5cm long) quartz + hematite + kyanite bands which are parallel / sub - parallel to the margins of the body. The unit is interpreted to be a discrete body (section 2.4.2) which parallels a zone of variable strain between the higher strained Foliated Quartz Whiteschists and the lower strained Unfoliated Quartz Whiteschists (section 2.4.2 and Fig. 2.4). It is unclear whether this member represents an original quartz + iron oxide banded iron formation or is related to hydrothermal or metasomatic replacement

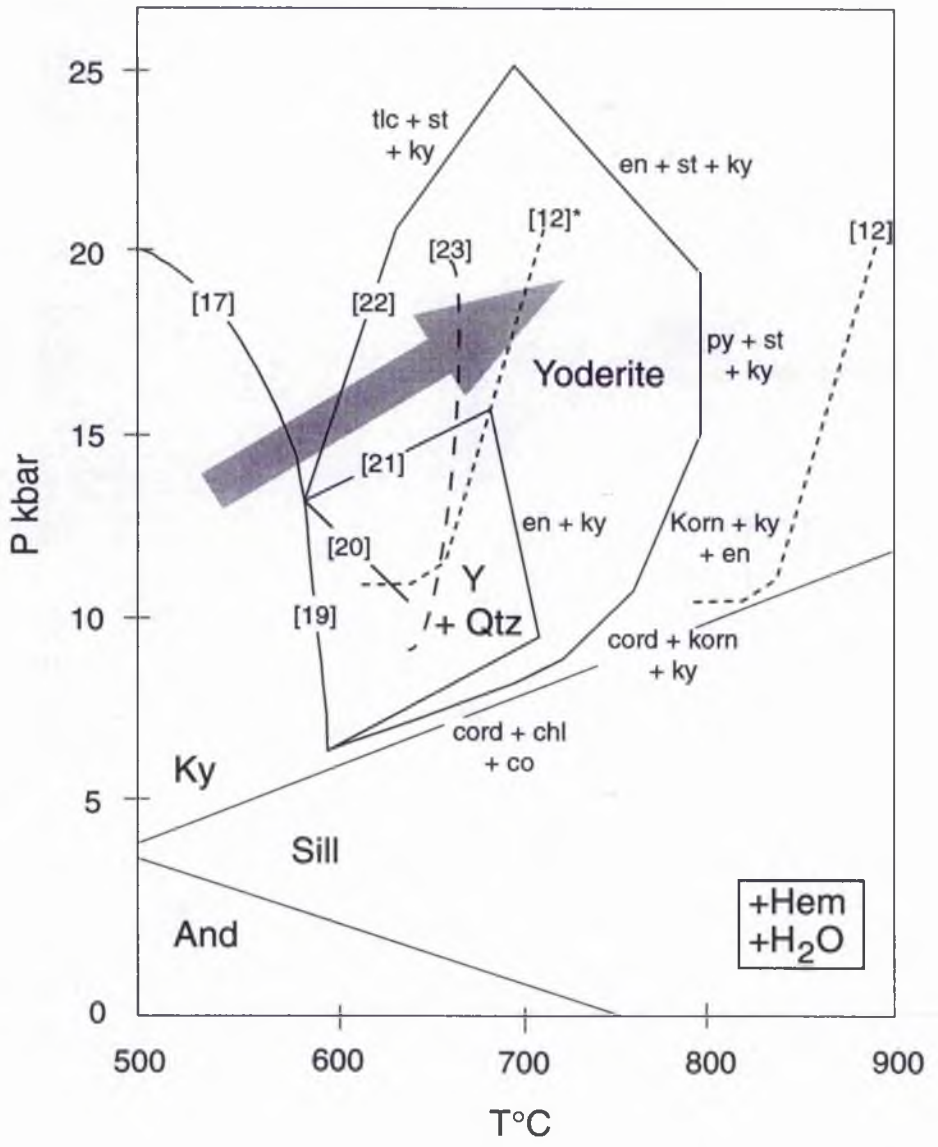

Fig. 4.21 Petrogenetic grid for the MFASH system showing the full *PT* stability of yoderite (from Fockenberg & Schreyer, 1994). Overlain are the reaction curves for reaction [23] in the KMFASH system and reaction [12] in the MFASH system. Note that with the addition of Na and B to reaction [12], the stability drops to lower temperatures, possibly [12*]. The shaded arrow is the estimated *PTt* path for the Kadunguri Whiteschists. Mineral abbreviations are as in the text.

of the country rocks during deformation and metamorphism. The coarse grained and high pressure nature of the mineral assemblage within the banding suggest that these mineral phases are related to metasomatic activity during metamorphism. It is therefore possible that the main body is also related to such metasomatic replacement. Similar, fine grained quartz and hematite bands are evident within the Gedrite Whiteschist. At MR [9652 3439] the radial gedrite structure is cross - cut by thin (1 to 30 cm thick), parallel, fine grained, granoblastic quartz + hematite bands akin to the fine grained matrix of the Unfoliated Quartz Whiteschist (Plate. 2.10 d). This suggests that metasomatic replacement within the Gedrite Whiteschist was either syn - or post - gedrite formation (reaction [12]). This confirms previous observations which indicate that during gedrite formation, Na_2O and other phase components were dissolved in a mobile fluid phase. However, the fluid phase at this time was locally restricted to present day, gedrite bearing lithologies. If the Quartz - Hematite Sheets are also interpreted to be of metasomatic origin then due to the absence of gedrite in the other talc and kyanite bearing lithologies, metasomatism must have occurred during the lower *PT* part of the *PTt* path i.e., to the left hand side of reaction [12*] in Fig. 4.21, while localised metasomatism continued within gedrite bearing - lithologies to the right hand side of reaction [12*].

Reactions [13] to [23] are dehydration reactions. In reaction [13] each mole of reactant releases 0.8 moles of water. It is probably no coincidence therefore that metasomatism plays an important role in the petrogenesis of this group.

Summary

Figure 4.21 displays the full *PT* stability of the mineral yoderite, with the other experientially derived reaction curves for the reactions [9] to [23]

overlain. If yoderite formed via reaction [22] then the *PT* path for this group must have passed between 590°C at 13 kbar and 640°C at 21.5 kbar. The reaction curve for the production of gedrite (reaction [12]) lies outside the field of yoderite, on the high temperature side. Since no yoderite 'out' reactions (refer to Fockenberg & Schreyer, 1994) are evident it is likely that the presence of Na within the gedrite crystal structure has lowered its thermal stability to lower temperatures, possibly to within the stability field of yoderite. The reaction curve for the production of phlogopite within the Talc - Phlogopite Whiteschist is also intersected at these *PT*'s.

It is concluded that the Kadunguri Whiteschists were metamorphosed at a minimum of 590°C at 13 kbar indicating a depth of burial of at least 50 km. The maximum geothermal requirement for this *PT* is 10°C per km^{-1} which is typical of subduction zone metamorphism (Yardley, 1989).

4.3.3 Discussion.

Metamorphism within the Maunde Ophiolite and Kaourera Island - Arc Groups is represented by one main phase of Barrovian type metamorphism which peaked in the amphibolite facies at 650 - 700°C at 10 kbar. On the southern margin, the Kadunguri Whiteschists are characterised by whiteschist lithologies which are interpreted to have peaked at a minimum of *c.* 650 - 700°C at 13 kbar which are equivalent *PT'sI* to the eclogite facies illustrated by Yardley (1989), and might be interpreted as subduction zone - type metamorphism. This marked contrast in metamorphic facies suggests that the boundary between the two is in fact a major bounding thrust. It is possible that both metamorphic terranes were metamorphosed contemporaneously but under different *PT* conditions as allocthonous terranes, or were metamorphosed at different

times and different *PT*'s and were ultimately juxtaposed (For discussion see section 5.4).

A geothermobarometric study of the Chewore Inliers has recently been undertaken by Goscombe *et al.*, (1998). This study has identified two major metamorphic terranes, one of moderate *PT*, amphibolite facies (Zambezi and Quartzite Terranes) which includes the Ophiolite Terrane of this study and a high - *T*, low - *P* granulite facies terrane (Granulite Terrane) which lies to the north of the Quartzite Terrane (Fig. 4.22). The Granulite Terrane is interpreted to have undergone two metamorphic episodes, the first (M_1), high - *T*, low - *P* granulite facies, peaked at around 738°C at 4.4 kbar, while the second (M_2) overprinting metamorphism (Ophiolite Terrane metamorphic event) peaked in the amphibolite facies. It was suggested that the preservation of high - *T* mineral inclusions and aligned fabrics within peak metamorphic garnets in the Zambezi and Quartzite Terranes, record the early high - *T*, low - *P* (M_1) metamorphic event. A lack of such inclusions within the Ophiolite Terrane assemblages suggest that this terrane did not undergo this M_1 metamorphic event. The boundary between the Ophiolite and Zambezi Terrane is thus another major bounding thrust which corresponds to the most southerly extent of M_1 metamorphism in the Zambezi and Granulite Terranes (Fig. 4.22).

Peak metamorphic *PT* conditions for M_2 metamorphism within the Zambezi and Quartzite Terranes (i.e., the first metamorphism (M_1 within the Ophiolite Terrane) is 590 - 717°C at 7.9 - 8.6 kbar, while garnet core and rim *PT* loci suggest near isothermal decompression through the peak of metamorphism (Goscombe *et al.*, 1998) (Fig. 4.23). Garnet *PT* loci of the Ophiolite Terrane indicate prograde metamorphism from lower to higher *P* and *T* along a straight geotherm (Fig. 4.23). The *PT* path for M_2 metamorphism of the Granulite Terrane is similar to that proposed for M_1 metamorphism within the Ophiolite Terrane. It is possible that the

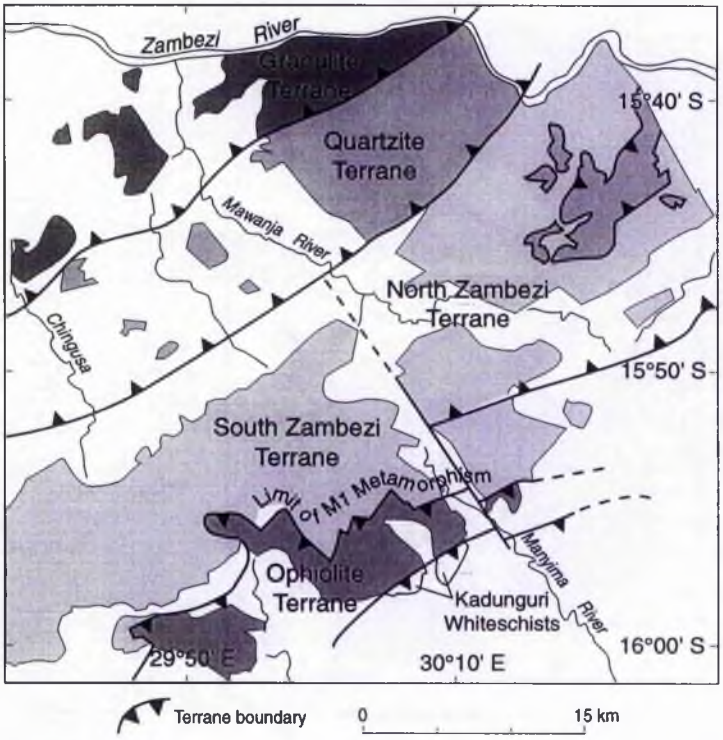

Fig. 4.22 Sketch map of the Chewore Inliers (adapted from Goscombe *et al.*, 1994) showing the terrane divisions and location of major terrane boundaries. Note the limit of M1 metamorphism (adapted from Goscombe *et al.*, 1998).

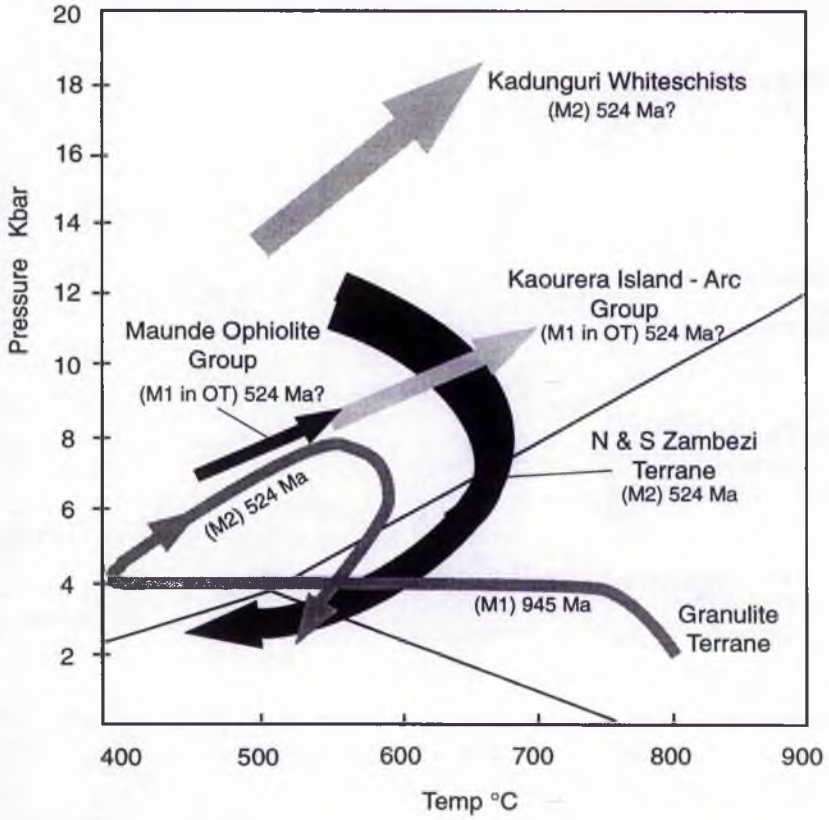

Fig. 4.23 Pressure - temperature grid showing the calculated *PTt* paths from garnet - bearing assemblages for the different terranes of the Chewore Inliers illustrated in Fig. 4.22. Analyses from this study are combined with those of Goscombe *et al.*, (1998). Note that both M1 and M2 (M1 within the Ophiolite Terrane - OT) metamorphic cycles of Goscombe *et al.*, 1998) are illustrated. For discussion see text.

Ophiolite Terrane and other sections of the Chewore Inliers were metamorphosed at different *PT*'s during their juxtaposition (section 5.4).

Metamorphic zircons within the Granulite Terrane have been dated with a SHRIMP by Goscombe *et al.*, (1997). M_1 metamorphism within this terrane is dated at 943 ± 34 Ma while zircon overgrowths, which are interpreted to represent the overprinting M_2 metamorphism (M_1 within the Ophiolite Terrane), are dated at 524 ± 16 Ma. Rb - Sr mineral cooling ages of 480 ± 12 Ma from the Zambezi and Quartzite Terrane and 407 Ma and 588 Ma from the Granulite Terrane are given to corroborate the age of this M_2 metamorphism (M_1 within the Ophiolite Terrane) (Goscombe *et al.*, 1997).

4.3.4 Conclusions.

It is concluded that :-

1) The Chewore Inliers consist of a mosaic of metamorphic terranes ranging from amphibolite; low - *P*, high *T* granulite and high - *P*, moderate - *T* eclogite facies.

2) The Maunde Ophiolite and Kaourera Island - Arc Groups of the Ophiolite Terrane underwent a single period of Barrovian type, regional metamorphism.

3) The Maunde Ophiolite Group peaked within the lower amphibolite facies.

4) The Kaourera Island - Arc Group mostly peaked in the lower amphibolite facies; some sections peaked in the upper amphibolite facies.

5) The Kadunguri Whiteschists underwent an unknown period of metamorphism peaking at a minimum of 650 - 700°C at 13 kbar equivalent to the eclogite facies. The maximum geotherm of 10°C / km^{-1} indicates a subduction zone / collisional suture zone type environment.

Plate. 4.1

a) Photomicrograph of pale green, yoderite (Y) from the Yoderite Whiteschist. Note the very pale green to colourless, high relief and fractured texture. A single cleavage is evident running bottom left to top right of the yoderite crystal which is in contact with kyanite (Ky) and surrounded by chlorite (Chl). Scale bar is 3 mm in length.

b) Photomicrograph of purple yoderite (Y) from Mautia Hill, Tanzania. Note how it mantles kyanite (Ky) and is surrounded by talc (Tlc) and quartz (Q). Scale bar is 2 mm in length.

c) Plane and cross polarised (PPL and XPL) photomicrograph of anhedral, Chewore yoderite (Y) from the Yoderite. The lone crystal is set in an interlocking, coarse grained, randomly oriented, equilibrium matrix of chlorite (Chl) and kyanite (Ky) without quartz. Scale bar is 0.25 mm in length.

d) PPL and XPL photomicrograph of Chewore Yoderite (Y) in contact with hematite (H). The yoderite rims are relatively enriched in Fe^{3+}. For discussion see text. Scale bar is 1 mm in length.

e) Backscattered electron image of hematite crystals (H) within the Yoderite Whiteschist. Note the needles of rutile (R). For discussion see text. Scale bar is 100 μm in length.

a)

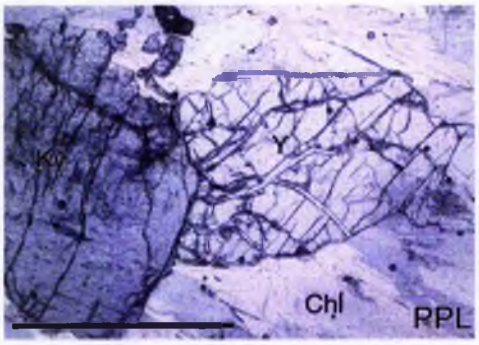
Ky
Y
Chl
PPL

b)

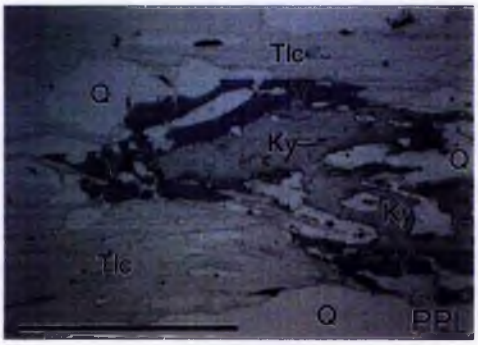
Tlc
Q
Ky
Q
Ky
Tlc
Q
PPL

c)

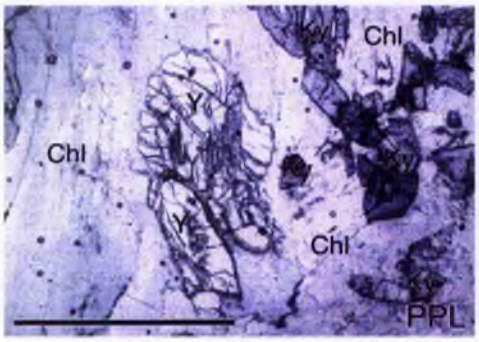
Ky
Chl
Y
Chl
Y
Chl
Ky
PPL

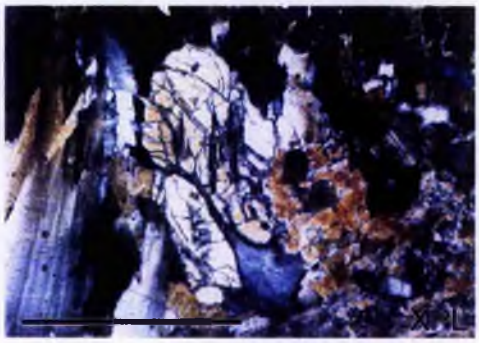
XPL

d)

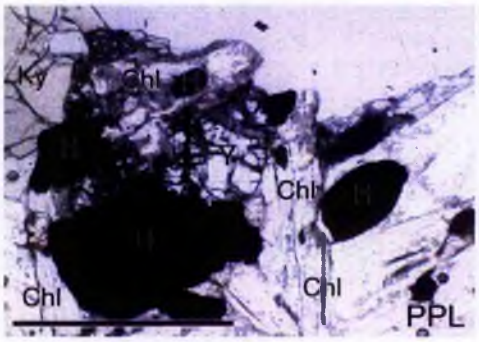
Ky
Chl
Chl
Chl
Chl
PPL

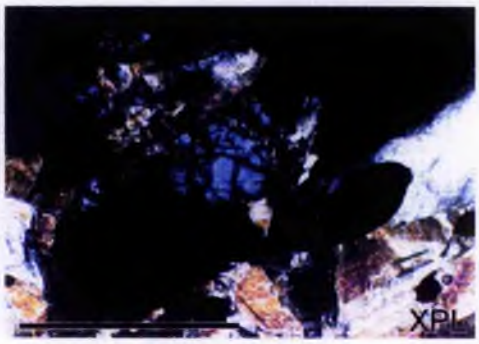
XPL

e)

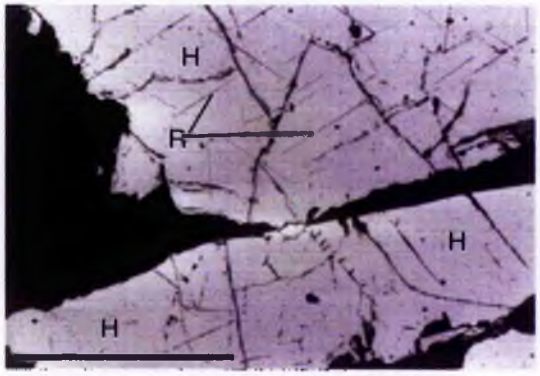
H
R
H
H

Plate. 4.2

a) PPL and XPL photomicrograph of a typical garnet - free tholeiitic meta - basalt from the Maunde Ophiolite or Kaourera Island - Arc Groups. Note the aligned, tabular amphiboles (A) and lenses of granoblastic quartz (Q) and plagioclase (P). The plagioclase illustrated in the photograph displays minor alteration to epidote. Scale bar is 2 mm in length.

b) Photograph of thin section [SJ 12.110] which is a garnet - bearing, calc - alkaline meta - basalt from the Nhema Amphibolite Formation of the Kaourera Island - Arc Group. The photo illustrates large garnet porphyroblasts (G), with aligned mineral inclusions (alignment direction shown by thick lines with arrows within garnet porphyroblasts) which are at an angle to the matrix fabric defined by aligned biotite laths. Scale bar is 12 mm in length.

c) PPL and XPL view of the biotite (Bt) dominated matrix of the calc - alkaline meta - basalts. Note the lensoid, granoblastic aggregations of plagioclase (P), quartz (Q) and epidote (e). Scale bar is 2 mm in length.

d) PPL views of garnet porphyroblasts and surrounding matrix within specimen [SJ 12.110]. Note how the aligned mineral inclusions within the garnet porphyroblasts (G) are at an angle to the biotite matrix and how chlorite (C) embays into the porphyroblast. Scale bar is 2.5 mm in length.

a)

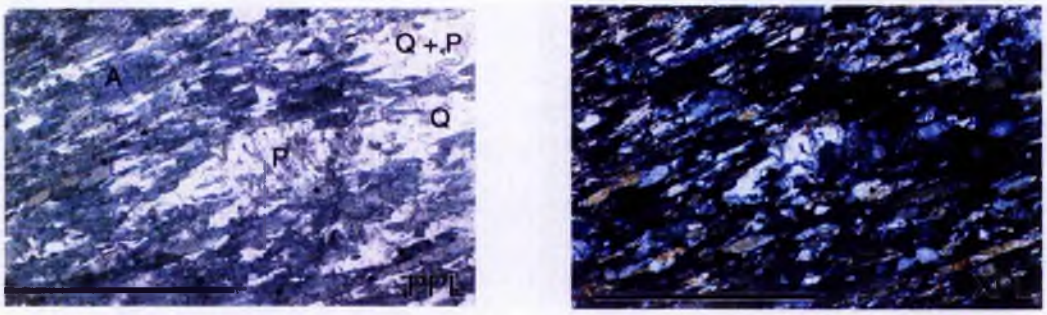

b)

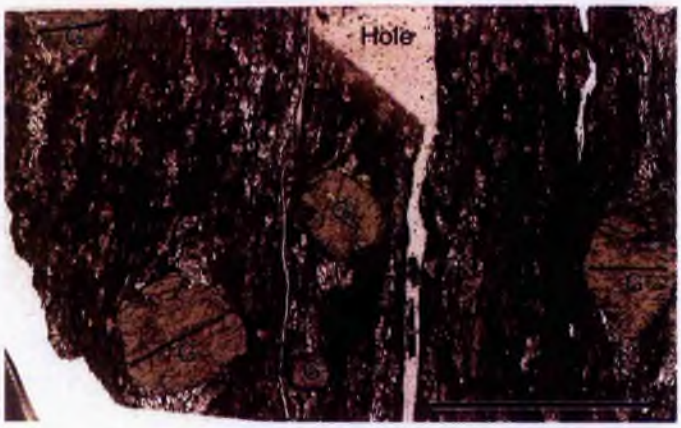

c)

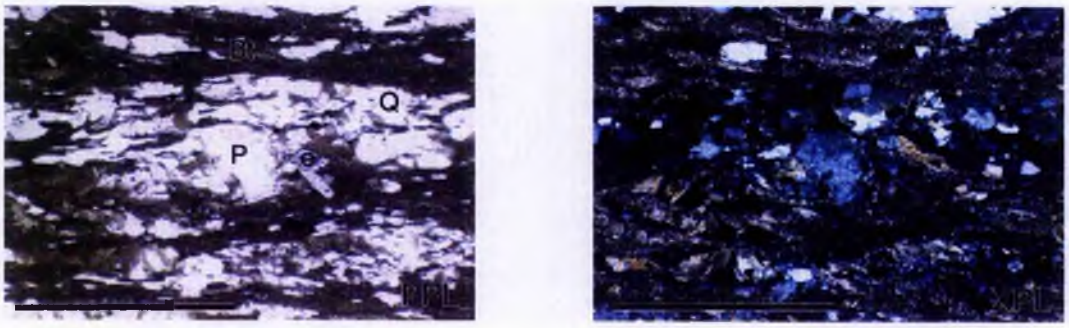

d)

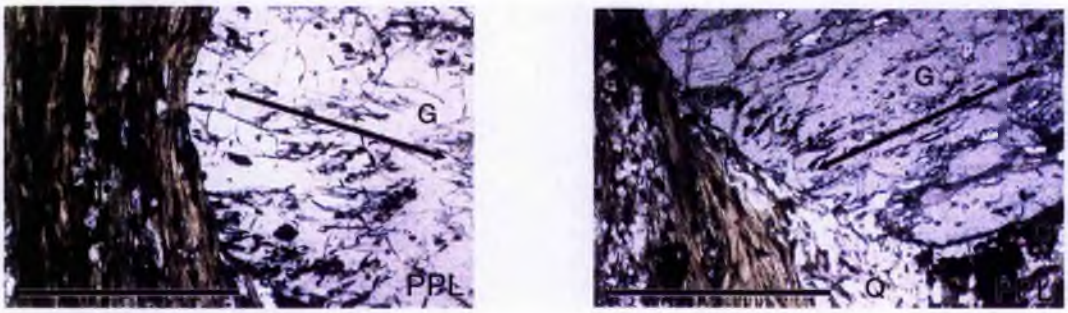

Plate. 4.3

a) and b) PPL and XPL view of possible relict, igneous, plagioclase phenocrysts (P) within the meta - dacitic samples of the Gora and Mharapara Members of the Gondo Meta - Felsic Volcanic Formation within the Kaourera Island - Arc Group. Note the parallel alignment of the long axis of the phenocryst with the external fabric defined by the alignment of fine grained, tabular biotite (Bt) set within a fine grained, granoblastic matrix of quartz (Q), plagioclase (P) and epidote (e). Also note the abundant epidote inclusions within the plagioclase phenocrysts. Scale bar is 1 mm in length.

c) Photograph of thin section [SJ 134] which is a calc - silicate rock. Note the garnet porphyroblasts (G) and large amphibole porphyroblats (A) which aggregate into discontinuous mafic layers. The matric is comprised of very fine grained epidote and plagioclase. Scale bar is 12 mm in length.

d) PPL and XPL view of a typical sample of the pelitic Nzou Meta - Greywacke Formation. Note the fine grained quartz and plagioclase matrix with aligned tabular biotite blades and coarse grained muscovite (Mu). Scale bar is 2 mm in length.

a)

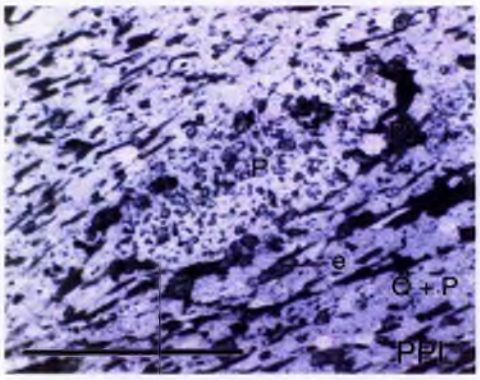

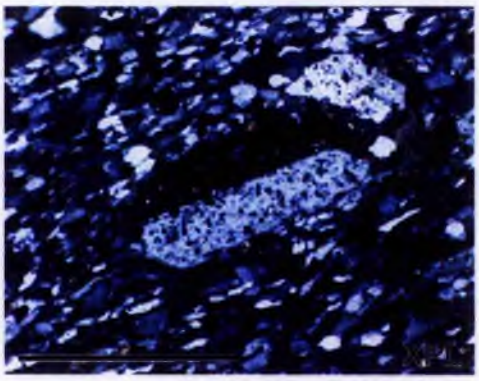

b)

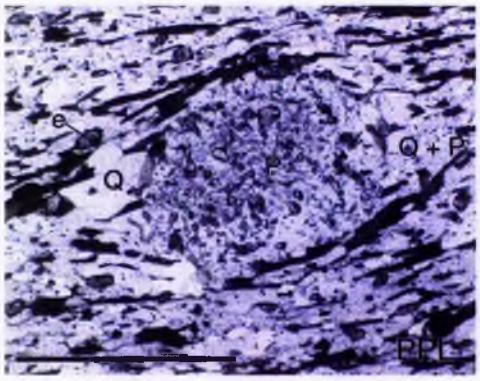

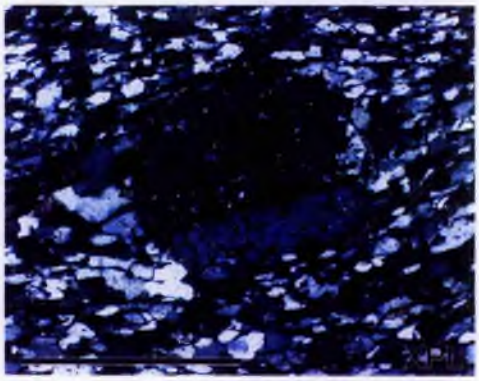

c)

d)

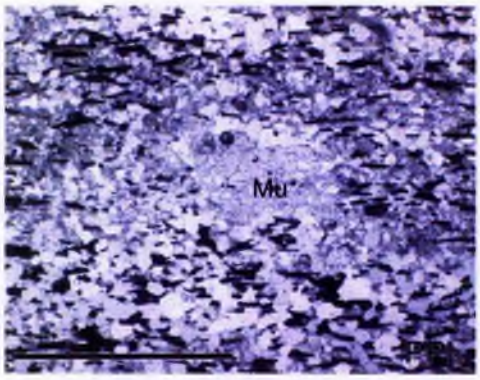

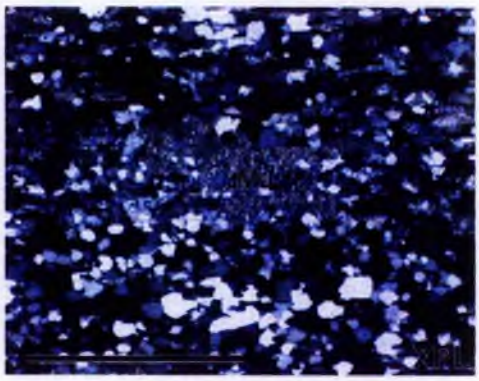

Plate. 4.4

a) Photograph of thin section [SJ 470] which is a semi - pelitic lithology from the Bhumi Semi - Peilte Formation of the Kaourera Island - Arc Group. Note the large garnet porphyroblasts (G) which are set in a coarse grained matrix of chlorite, quartz (Q), muscovite, epidote and tourmaline. Scale bar is 12 mm in length.

b) PPL view of the outlined area in Plate. 4.4 a. Note how the fabric defined by the aligned chlorite (Ch) blades, wrap around the garnet porphyroblast (G). Also note the presence of tourmaline (T), opaques (O) and quartz (Q). Scale bar is 2 mm in length.

c) PPL and XPL view of the Tremolite Member of the Ngwena Ultramafic Formation. Note the chromite crystals (Cm) within the fine grained, randomly oriented serpentine (S) dominant matrix. Scale bar is 2 mm in length.

d) PPL and XPL view of the porphyroblastic portion of the Tremolite and Layered Tremolite Members of the Ngwena Ultramafic Formation. Note the irregular chromite crystals (Cr) and the anhedral to subhedral tremolite porphyroblasts (Tr) which contain cores of fine grained chromite. Dotted line indicates the outline of the porphyroblasts. The tremolite rims are in optical continuity with the inclusion rich cores. Scale bar is 2 mm in length.

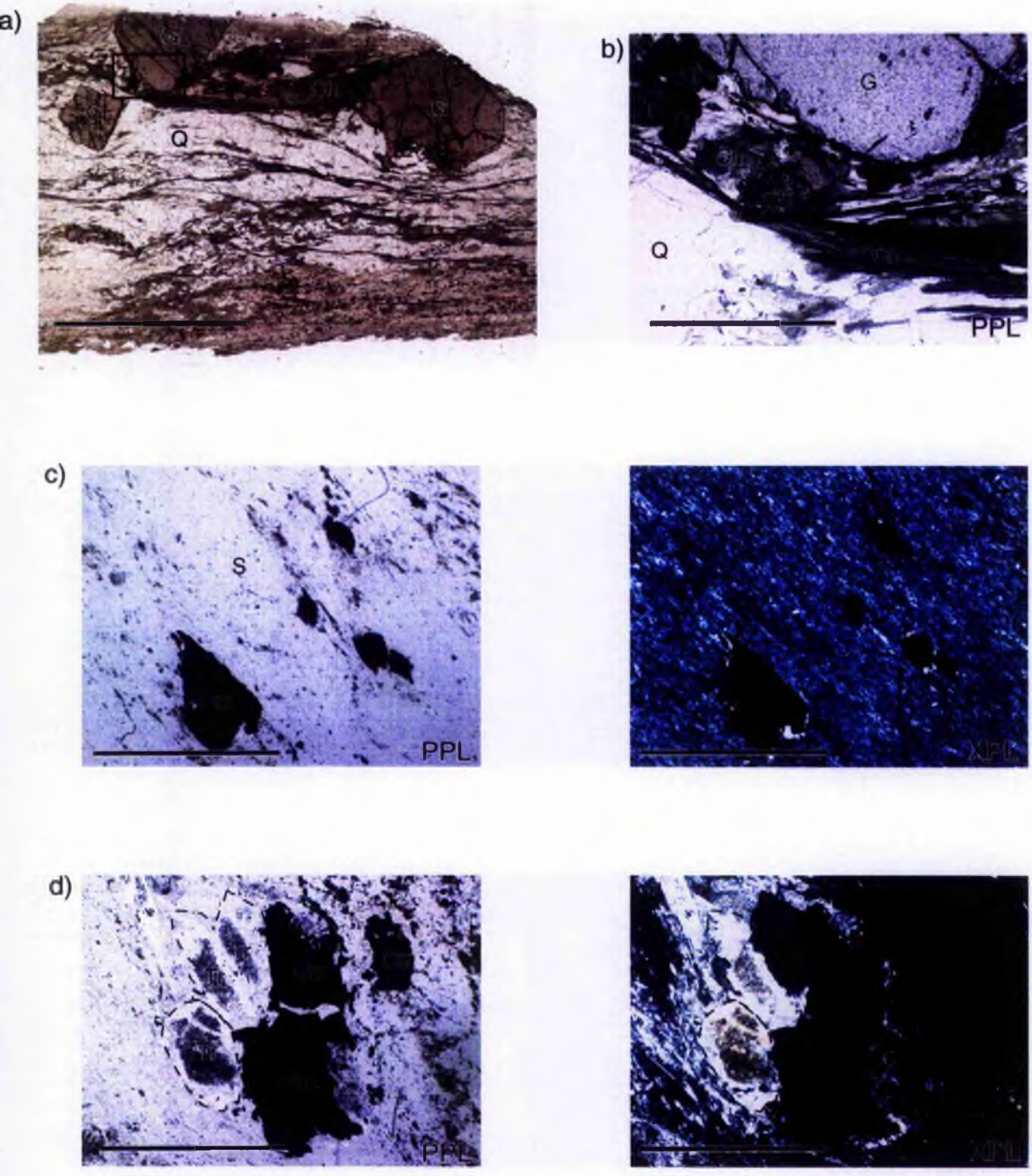
a)
Q
b)
G
Q
PPL
c)
S
PPL
d)
PPL

Plate. 4.5

a) PPL view of the Foliated Quartz Whiteschist. Note the presence of quartz (Q) in this assemblage. The matrix is comprised of aligned talc laths (Tlc) and kyanite crystals (Ky) which wrap around lenses of coarse grained quartz and porphyroblasts of dravite (not shown within this plate). Scale bar is 2 mm in length.

b) PPL and XPL view of the Gedrite Whiteschist. Note the acicular, radially arranged gedrite crystals (G) and interstitial quartz (Q) and kyanite (Ky). Scale bar is 2 mm in length.

c) PPL and XPL view of the Gedrite Whiteschist, showing the replacement of gedrite (G) with talc (Tlc). The field of view displays a single gedrite crystal in the centre and a quartz crystal in the top left of the picture. Gedrite has been replaced by talc indicating a retrogressive reaction i.e., the reverse of reaction [14]. For discussion see text. Scale bar is 0.25 mm in length.

a)

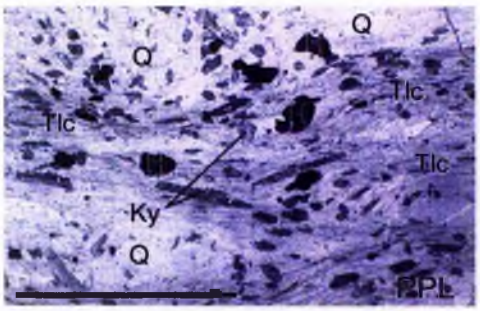
Q
Q
Tlc
Tlc
Tlc
Ky
Q
PPL

b)

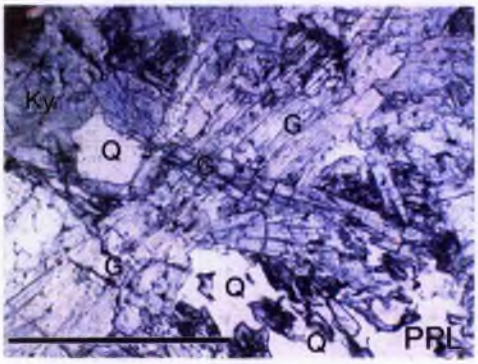
Ky
Q
G
G
Q
Q
PRL

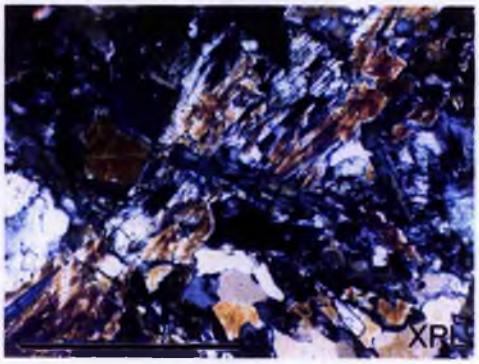
XRL

c)

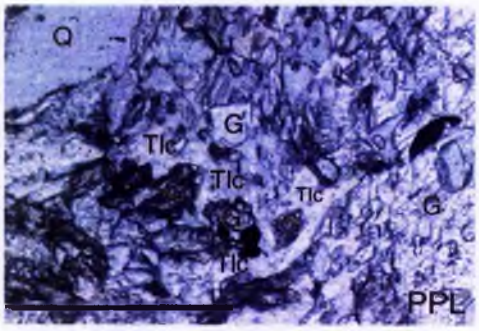
Q
G
Tlc
Tlc
Tlc
G
Tlc
PPL

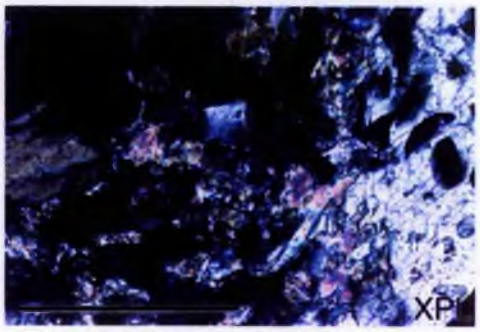
XPL

Plate. 4.6

a) PPL and XPL view of the Yoderite Whiteschist. Note the coarse grained dravite (Dr), hematite (H) and randomly oriented chlorite (Chl) which are in textural equilibrium. Scale bar is 4 mm in length.

b) PPL and XPL view of the Yoderite Whiteschist. Yoderite (Y) is shown in contact with, but not replacing kyanite (Ky), which are set in an equilibrium textured matrix of chlorite (Chl) and talc (Tlc). Scale bar is 2 mm in length.

c) XPL view of the Yoderite Whiteschist matrix which is comprised of chlorite (Chl) and talc (Tlc). The sharp and straight contacts between the talc and chlorite blades suggest that they are in equilibrium. Scale bar is 4 mm in length.

d) PPL view of the Quartz - Hematite Bands. Note the granoblastic matrix of quartz and hematite, with fine grained, interstitial, randomly oriented kyanite (Ky) and talc (Tlc) blades. Scale bar is 4 mm in length.

e) PPL view of a coarse hematite (Hem) and kyanite (Ky) band within the Quartz - Hematite Bands. Note how the coarse grained band has a relatively sharp contact with the granoblastic quartz and hematite matrix. Scale bar is 4 mm in length.

a)

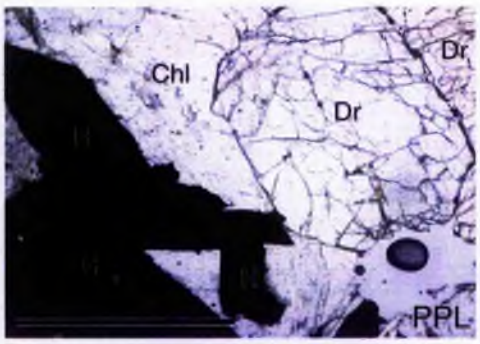
Chl
Dr
Dr
PPL

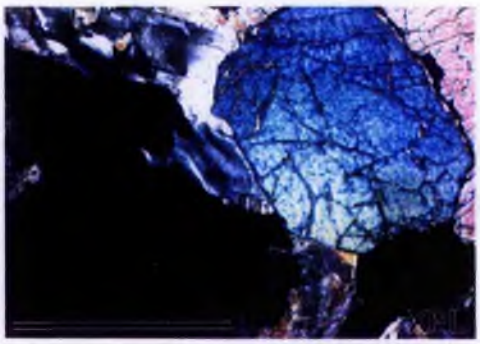

b)

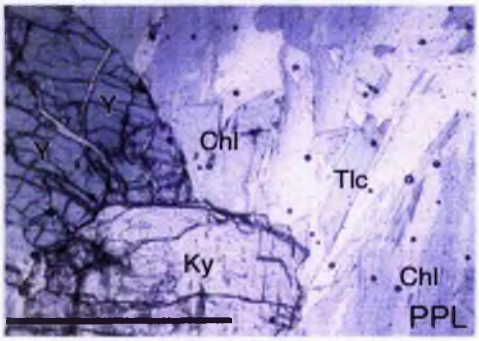
Y
Y
Chl
Tlc
Ky
Chl
PPL

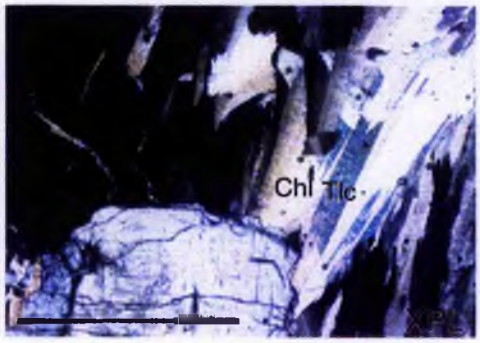
Chl
Tlc

c)

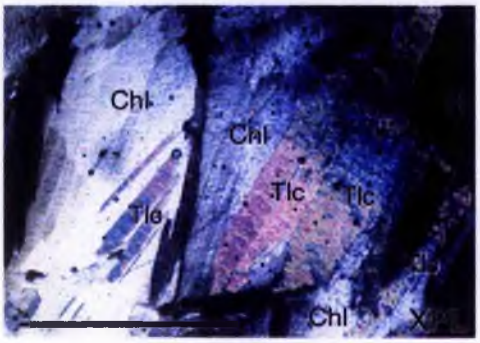
Chl
Chl
Tlc
Tlc
Tlc
Chl

d)

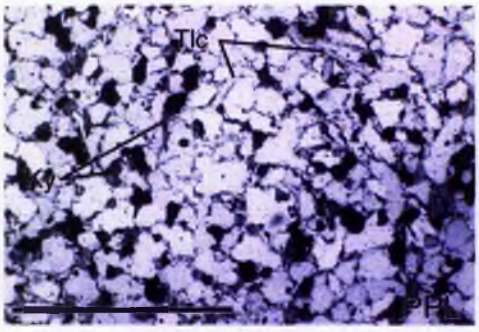
Tlc
Ky

e)

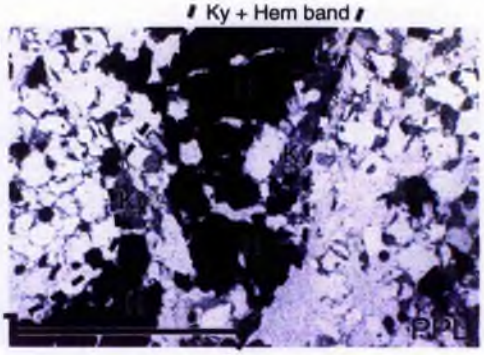
Ky + Hem band

Chapter Five

Structure.

5.1 Introduction.

The aims of this chapter are :-

1) To construct a structural framework for the Ophiolite Terrane.

2) Determine the relative timing of deformation to metamorphism.

3) To correlate this framework with the juxtaposed terranes.

5.2 Maps and Cross Sections.

The back pocket of this thesis contains 3 locality / sample maps and 3 geological maps each of which shows at least one cross section. Map 1 a / b is a 1 : 25 000 scale map produced during the first field season as a reconnaissance survey of the Ophiolite Terrane. The detailed 1 : 5000 scale maps were produced during the second field season to illustrate the structural and lithological details of the ophiolite, island - arc and whiteschist lithologies. Cross sections are based on a combination of structures identified in the field, distribution of lithotypes, orientation of structures, interpreted style of structural development and the thin skinned thrust tectonic model (Ramsay and Huber, 1987).

5.3 Structural Development of the Ophiolite Terrane.

The aim of this section is to describe the main structural features, the orientation and the distribution of these structures within the Ophiolite Terrane. There are 5 structural domains, namely, the Chitumbi, Kanhungwa, Kamuyu, Maunde and Kadunguri domains (Fig. 5.1) which have been defined in terms of orientations of original and tectonic features. The structural sequence of events are the same within each structural domain but the orientation of the structures between domains is variable. This section will define a sequence of events for the Ophiolite Terrane as a whole but discuss the orientation of tectonic structures in terms of domains.

5.3.1 *The Maunde Ophiolite and Kaourera Island - Arc Groups.*

Original Structures (S_0)

Original igneous and sedimentary structures are poorly preserved within the Ophiolite Terrane. High shear strain, non - coaxial deformation and amphibolite facies metamorphism have obliterated most primary structures. However, such structures are preserved within the lower strain, Maunde Ophiolite Group lithologies. The volcanic meta - basalts (Mvuu Meta - Mafic Volcanic Formation) display relict pillow lavas with deformed epidote, plagioclase and quartz filled amygdales (Plate. 2.2, b, c and Plate. 2.3). The sheeted dykes (Mbizi Sheeted Dyke Formation) display deformed amygdales (Plate. 2.2 e), dyke margin contacts (Plate. 2.4 a) and recrystallised chilled margins (Plate. 2.4 b). The meta - gabbros display gabbroic textures (Plate. 2.5 e), igneous layering (Plate. 2.6 a and b) and igneous contacts with hornblendite meta - mafic cumulates (Plate. 2.5 e). Within the Gondo Meta - Felsic Volcanic Formation of the Kaourera Island - Arc Group at MR [9143 3714], relict meta - dacitic pillow structures are also preserved (Plate. 2.7 f).

All S_0 structures are variably overprinted by later deformation fabrics. Pillow lavas and amygdales become elongate with the long axis parallel to lineation and flattened into the planes of the foliation while elongate bodies and tabular bodies such as the parallel sheeted dykes and plagiogranite dykes are rotated into parallelism with these fabrics.

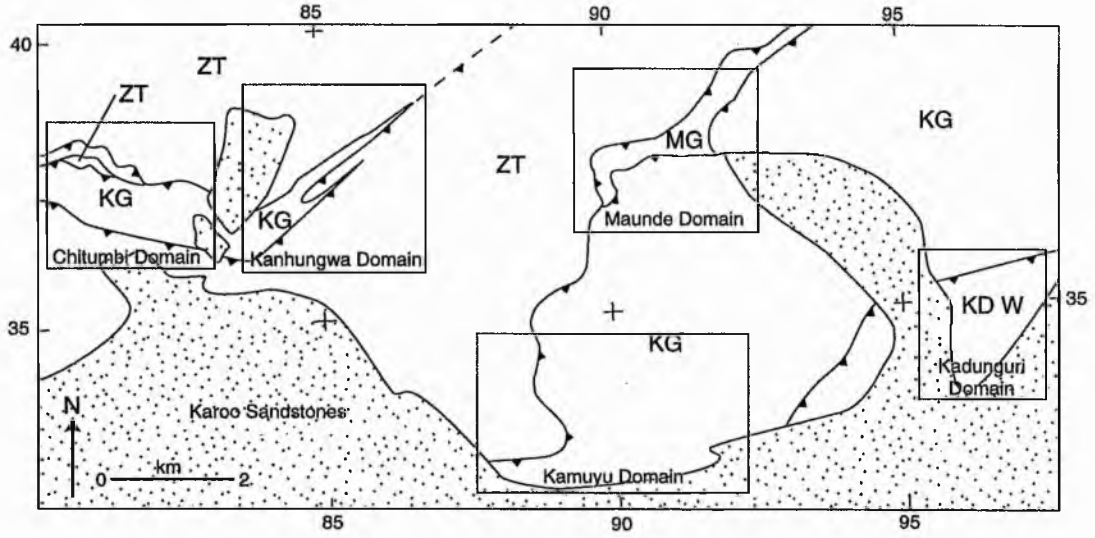

Fig. 5.1 Map of the Southern Chewore Hills illustrating the location of the 5 structural domains of the Ophiolite Terrane. ZT = Zambezi Terrane; KG = Kaourera Island - Arc Group; MG = Maunde Ophiolite Group; KD W = Kadunguri Whiteschists. Filled wedges indicate terrane boundaries i.e., thrusts.

D_1 Deformation (Schistose Gneissic Layering S_1)

The earliest tectonic structure evident in the Ophiolite Terrane is a millimetre scale gneissic layering based on the segregation of quartz and feldspar into discontinuous leucocratic layers. These are best developed within mafic mineral rich lithologies such as the tholeiitic and calc - alkaline meta - basalts of the Nhema and Kamuyu Amphibolite Formations. The layering is poorly developed within the Maunde Ophiolite Group meta - basalts, semi - pelitic assemblages and entirely absent within all other lithologies of the Maunde Ophiolite and Kaourera Island - Arc Groups.

The leucocratic layers are comprised of granoblastic quartz + plagioclase + epidote with minor, idioblastic hornblende (or biotite, within the calc - alkaline meta - basalts) and opaque grains. The melanocratic layers are comprised of idioblastic hornblende (or biotite) + sphene ± opaques, granoblastic quartz ± plagioclase ± epidote (Plate 4.2 a and c). Leucocratic bands are generally 1 - 2 mm thick and occasionally reach a maximum thickness of 5 mm. They are laterally discontinuous (< 50 cm) although the thicker layers can become more laterally persistent (> 5 m). Leucocratic layering comprises 15 - 20 % of the amphibolite assemblages (Plate. 5.1 a).

Within the semi - pelitic lithologies only a poor schistose layering is developed. Leucocratic layers are comprised of granoblastic quartz. The melanocratic layers are laterally non - persistent (< 5 cm) and are composed of chlorite and muscovite laths, rare garnet porphyroblasts, minor tourmaline and epidote (Plate 4.4 a and b). This layering may represent an original S_0 sedimentary structure. However, any possible sedimentary structures such as graded bedding or cross bedding have been destroyed by subsequent deformation and metamorphism.

D_2 Deformation (S_2, L_2 and F_2)

A second penetrative tectonic fabric (both foliation and lineation) is variably developed within all Ophiolite Terrane lithologies. Where the proportion of tabular and bladed minerals, namely, amphiboles and phyllosilicates are high, D_2 fabrics are strongly developed. All lithologies except the more quartzo - feldspathic lithologies such as the meta - dacitic Gondo Meta - Felsic Volcanic Formation display a strong S / L fabric (Plate. 5.1 b).

The planar S_2 foliation is defined by the alignment of bladed and tabular minerals i.e., amphiboles within the tholeiitic meta - basalts and ultramafic lithologies; biotite within the calc - alkaline meta - basalts, pelites and quartzo - feldspathic lithologies and chlorite and muscovite within the

semi - pelites. The L_2 lineation is only developed within the more mafic mineral - rich lithologies where it is defined by the alignment of the long axes of bladed hornblende or biotite and plagioclase laths and quartz and plagioclase aggregates. A poorly developed linear fabric within the semi - pelitic lithologies is defined by quartz and plagioclase aggregates.

The presence of a coeval foliation and extension lineation (S / L tectonites) indicate that the D_2 deformation event was characterised by flattening strains with a component of non - coaxial shearing with extension parallel to L_2 (Goscombe *et al.*, 1994, 1998; van der Pluijm & Marshak, 1997). The S_2 foliation is axial planar to F_2 intrafolial folds which are defined from the folding of the S_1 gneissic layering and are thus best developed (or recognised) in lithologies which display a strong S_1. Wavelengths and amplitudes of all F_2 folds are small i.e., 1 - 30 cm and 15 - 30 cm respectively (Plate. 5.1 c and Fig. 5.2). The L_2 lineation is parallel to the F_2 fold hinges suggesting that non - coaxial shearing, rather than buckle folding is the dominant deformation mechanism (Goscombe *et al.*, 1994, 1998; van der Pluijm & Marshak, 1997). The S_2 foliation is parallel to the S_1 layering in the limbs of the folds but cross cuts the layering in the fold closures. Due to continued layer parallel shearing, the fold profiles progressively thin and eventually the fold limbs and hinge zones become sheared out producing rootless folds. F_2 hinge zones therefore become rare, giving the impression that the S_1 layering and S_2 foliation are always parallel even though the two are temporally distinct.

Figure 5.3 (a) are equal area stereonets illustrating the orientation of the S_2 foliation and L_2 lineation for the Chitumbi, Kanhungwa, Kamuyu and Maunde domains. Overall, the S_2 foliation displays variable orientations while the L_2 lineation is moderately constrained. Within the Chitumbi domain the S_2 foliation cluster in a well defined group with a mean strike and dip of

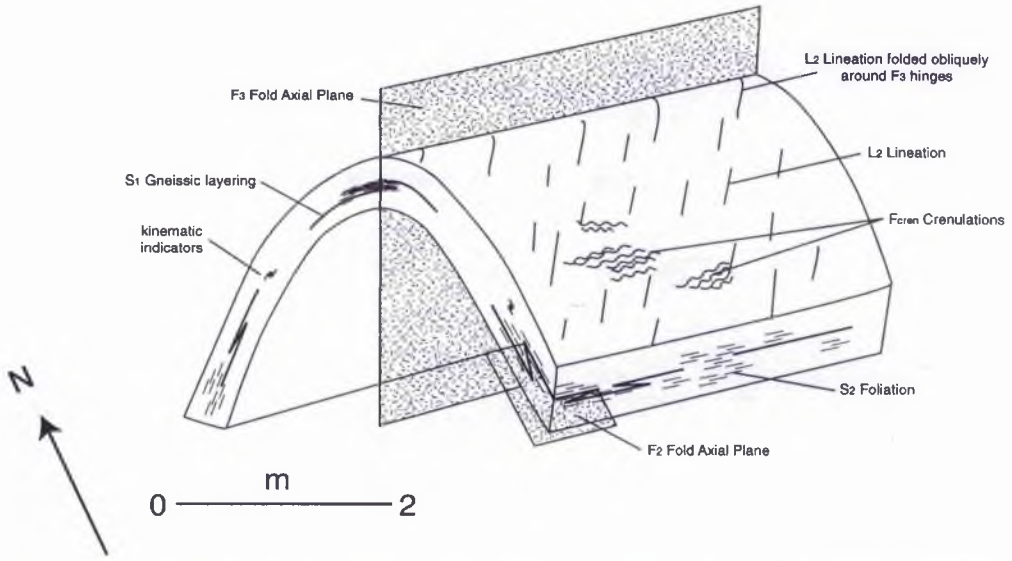

Fig. 5.2 Cartoon sketch of the various fold profiles and their relation within the Ophiolite Terrane.

094 / 45° SW. L_2 lineations also cluster within a well defined group with a mean trend and plunge of 20 to 195°. The L_2 lineation is down dip of the S_2 foliation. Within the Kanhungwa domain the poles to S_1 layering and S_2 foliation plot as a scattered group with mean strike and dip of 050 /60° SE and L_2 plot with a mean trend and plunge of 20 to 191°. It is evident that the trend and plunge of the L_2 lineation remains constant between these two juxtaposed domains indicating that the trend of the tectonic transport direction was essentially the same within both areas. However, the orientation of the $S_{1\text{-}2}$ fabric is rotated with respect to the L_2 lineation which is down dip within the Chitumbi domain and oblique within the Kanhungwa domain. The shear plane i.e., the footwall to the ductile thrusts within the Chitumbi domain were essentially orthogonal to the tectonic transport direction (i.e., frontal ramps), but are more oblique (oblique ramp) within the Kanhungwa domain. This might be interpreted to represent either one thrust system with both frontal and oblique ramp geometries or two thrust systems with differing footwall orientations (Fig 5.4). Such S_2 - L_2 relationships are also evident within the

a) S_1 / S_2 / L_2 Fabrics

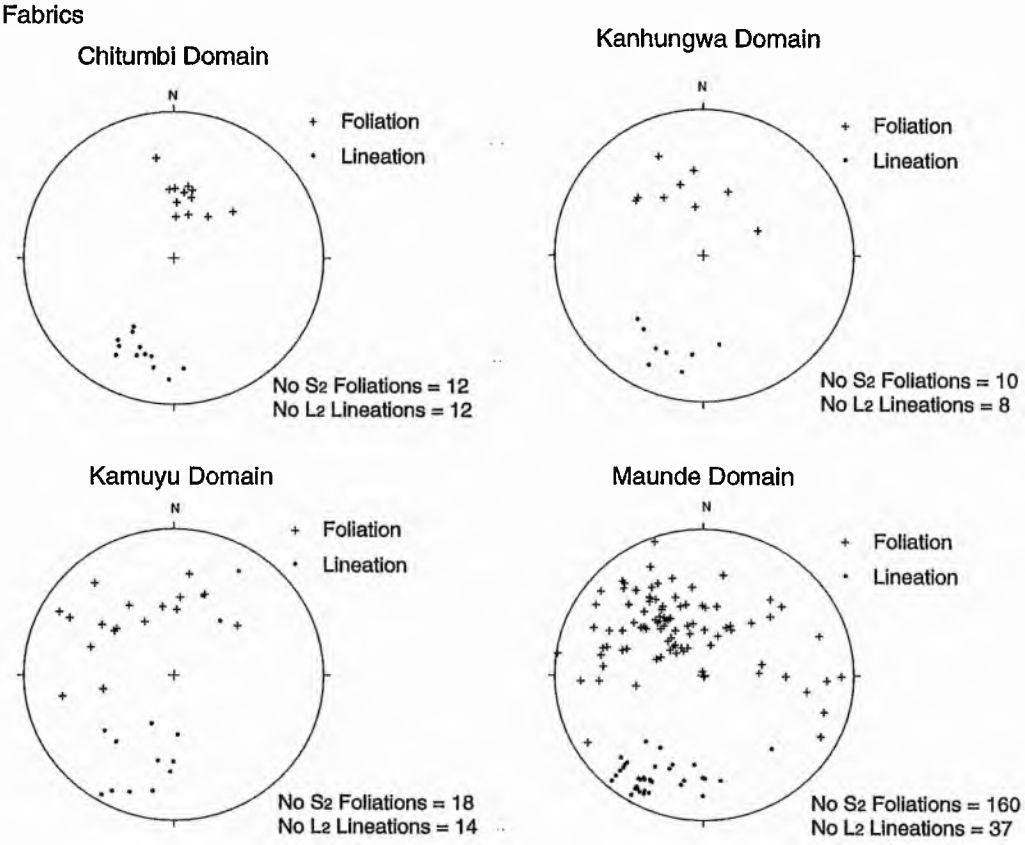

b) F_2 Fold Orientations

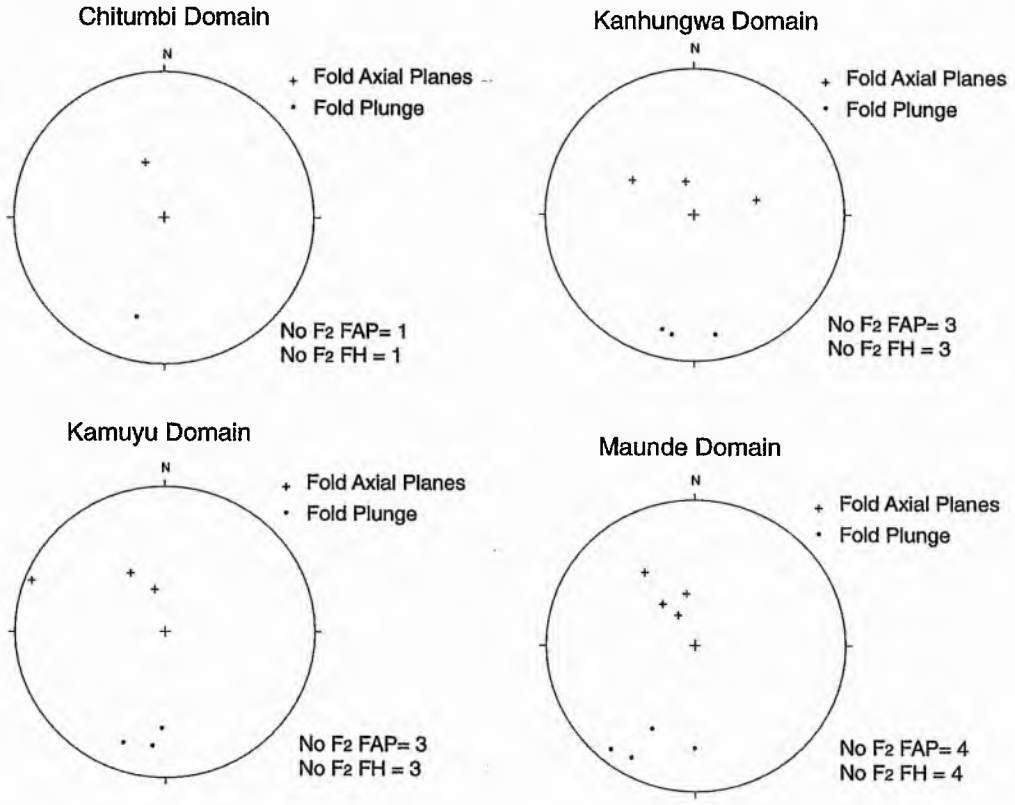

Fig. 5.3 Equal area stereonets illustrating the orientation of fabrics and folds associated with D_1 and D_2 deformation.

Kamuyu and Maunde domains. Within the Maunde domain contrasting lithotypes has allowed the recognition of several, structurally and lithologically distinct thrust sheets (Fig. 5.5) or sub - domains. Sub - domains I, VII, VIII and IX display a relatively tight grouping of S_2 and L_2 orientations. The other domains however, display poor S_2 orientations indicating that the spread in data is due to variable footwall orientations during ductile thrusting such is evident on the larger scale within the Kamuyu and Kanhungwa domains. Due to poor outcrop within these sub - domains, the recognition of such discrete ductile thrust planes has gone unrecognised.

Since F_2 folds are intrafolial, the orientation of the fold axial plane is parallel to the S_2 foliation and F2 fold hinges are parallel to the L_2 lineation (Fig 5.3 b).

D_3 Deformation (F_3 Open Folds)

A later period of outcrop scale folding (F_3) is recognised by the re - folding of the S_1 layering, S_2 foliation and L_2 lineations. The L_2 lineation is obliquely folded around the hinge of these folds (Fig. 5.2). F_3 folds are rare, but well developed within the Kamuyu domain where they display upright, open fold profiles with metre scale wavelengths and amplitudes (Plate. 5.1 d and Fig. 5.2). At MR [8875 3275] F_3 folds display tight fold profiles with centimetre scale dimensions (Plate. 5.1 e). There are no new, i.e., axial planar fabrics associated with these folds. F_3 fold orientations are variable (Fig. 5.6) but in general the axial planes strike east to west with a variable south - southeasterly dip and F_3 fold hinges plunge gently toward the east and south - east. The open style nature of the fold profiles, lack of a newly developed axial planar cleavage and poor constraint in orientation of F_3 folds suggests that D_3 is associated with much lower, inhomogenous strain. Such folds are produced by buckle mechanisms rather than non - coaxial shearing. The roughly W - E to NW - SE oriented fold hinges and axial planes indicate that

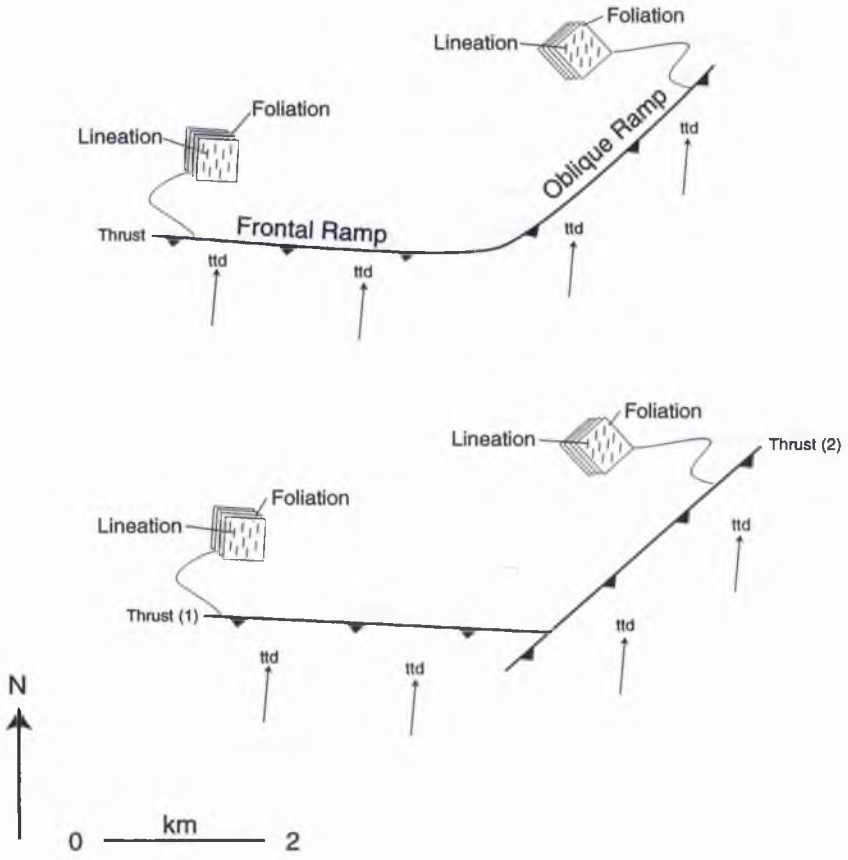

Fig. 5.4 Sketch map view of the possible structural relationships within the Chitumbi and Kanhungwa Domains with relation to D2 deformation. ttd = tectonic transport direction (based on sigma - type augens). For discussion see text.

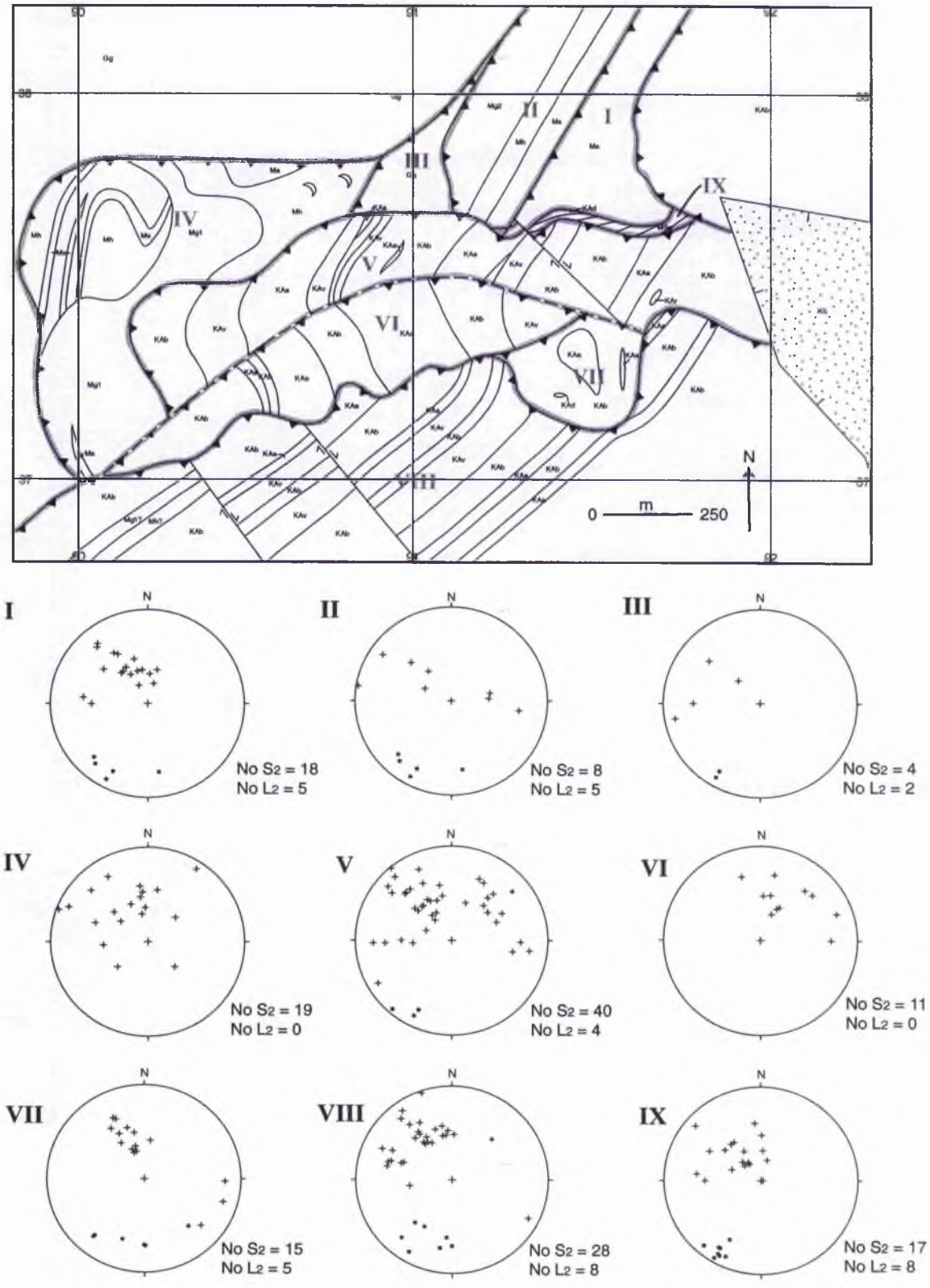

Fig. 5.5 Equal area stereonets illustrating the orientation of S2 and L2 fabrics within the Maunde Domain. The area is subdivided into 10 sub - domains outlined in the above map. Key to stereonet symbols are :- + S_2 foliation and · L_2 lineation. Data taken from map insert 2. For key to lithological and structural symbols refer to map insert 2.

D_3 is characterised by N - S to NE - SW shortening directions.

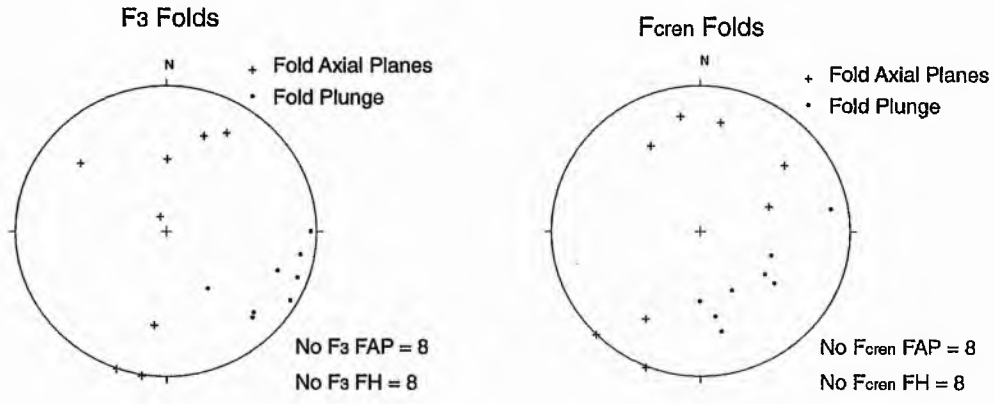

Fig. 5.6 Equal area stereonets illustrating the orientation of F_3 and F_{cren} folds within the Ophiolite Terrane

D_4 Deformation (F_{cren} Crenulations)

Centimetre scale crenulations (F_{cren}) are variably developed within the Kamuyu domain. The crenulations comprise a series of 1 - 2 cm wavelength, 1 cm amplitude, chevron folds (Plate. 5.2 a) which mechanically re - orientate amphibole blades around sharp hinges. There is no new growth of minerals or re - orientation of existing minerals into a crenulation cleavage (Plate. 5.2 b). At MR [9015 3335] there are two sets of intersecting crenulations which display a conjugate kink band arrangement. Similar to the F_3 folds, F_{cren} folds are variably oriented (Fig. 5.6 and 5.2), with fold axial planes trending between NE - SW and NW - SE, and fold hinges plunge moderately toward the east and south - east. Since both F_3 and F_{cren} folds have not been observed within the same outcrop, it is unclear as to the relationship between the two fold styles.

5.3.2 Kadunguri Domain

The earliest structure evident within the Kadunguri domain is a coarse grained, random fabric (S_1) comprised of high pressure, moderate temperature mineral assemblages (section 4.3.2) such as radially arranged

acicular gedrite crystals within the Gedrite Whiteschist (Plate. 4.5 b) and randomly oriented talc and kyanite laths within the Unfoliated Quartz Whiteschist.

A penetrative tectonic fabric (both foliation and lineation) is developed within the Foliated Quartz Whiteschist, which occurs within a zone, 50 to 500m wide bordering the thrust which separates the Kadunguri Whiteschists from the Kaourera Island - Arc Group. The S_2 foliation is defined by the alignment of talc blades and small (1mm) tabular kyanite crystals (Plate. 4.5 a). The L_2 lineation is variably developed in all talc schists within this zone. It is defined by the alignment of the long axes of the small, tabular, kyanite crystals and minor aggregations of quartz. The S_2 typically strikes 045 / 50 - 60° SE and the L_2 plunges 10 to 180° (Fig. 5.7). No F_2 folds have been identified.

At least two periods of crenulation have been identified within the zone that borders the main boundary thrust i.e., within the Foliated Quartz Whiteschist. Both are characterised by 1 - 2 cm wavelength, 0.5 cm amplitude, chevron folds (Plate. 5.2 c). The first crenulation episode, re - orientates talc crystals into a variably developed axial planar crenulation cleavage. In some areas i.e., MR [9675 3505], the crenulation cleavage is so well developed that it is almost impossible to distinguish it from the earlier S_2 foliation.

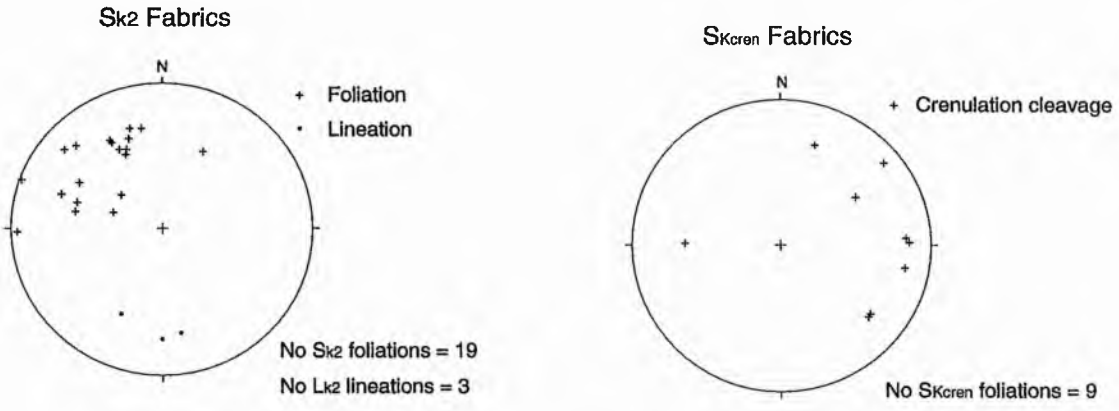

Fig. 5.7 Equal area stereonets illustrating the orientation of deformation fabrics within the Kadunguri domain of the Ophiolite Terrane.

Where this first axial planar cleavage is well developed, it is possible to distinguish a further crenulation event since it is itself crenulated. This second crenulation event predominantly bends and breaks talc crystals around the sharp hinges, although there is a poorly developed, weak, axial planar cleavage. Orientation of both crenulation events are poorly constrained (Fig. 5.7).

5.4 Juxtaposition of lithologies and the timing of metamorphism.

5.4.1 *Juxtaposition of Lithologies.*

From section 5.3 it is evident that the D_2 event represents ductile shearing with transport of material parallel to the L_2 lineation. The Ophiolite Terrane is comprised of many smaller structural sub - domains each of which display differently oriented shear planes. The sense of shear i.e., the tectonic transport direction associated with D_2 will be discussed in a separate section (see below).

Four major thrusts are identified in the Ophiolite Terrane (refer to map inserts 1, 2 and 3). The Maunde Thrust (MT) separates the Ophiolite Terrane, ophiolite - type lithologies from the Zambezi Terrane granitic gneisses; the Kaourera Thrust (KT) separates island - arc type lithologies of the Kaourera Island - Arc Group from the ophiolite lithologies of the Maunde Ophiolite Group; the Nhema Thrust (NT) which is a low angle thrust within the Maunde Domain, separates predominantly calc - alkaline from low K - tholeiite island - arc lithologies of the Kaourera Island - Arc Group and the Kadunguri Thrust (KdT) which separates the Kadunguri Whiteschist lithologies from the Kaourera Island - Arc Group lithologies. All other thrusts are interpreted to be smaller scale imbricate thrusts.

At MR [9130 3765] a major northeast - southwest striking, southeasterly dipping, ductile thrust plane (Kaourera Thrust) is exposed. The thrust separates the ophiolitic lithologies of the Maunde Ophiolite Group to the north and the island - arc type lithologies of the Kaourera Island - Arc Group to the south. The thrust is exposed along the Maunde River in a section cut orthogonal to the transport direction. The zone of intense shear is 30 cm thick and exposed along strike for ~30 m. The footwall is imbricated upto 50 m below the main high strain zone. Plate. 5.3 illustrates the anatomy of this high strain zone which is accommodated within the calc - alkaline meta - dacitic Gondo Meta - Felsic Volcanic Formation. The meta - dacites within the hangingwall contain a S - fabric defined by the alignment of biotite and muscovite flakes. The lack of exposure in the profile section makes it difficult to determine the presence and trend of an associated linear fabric. The foliation is sub - parallel to the shear plane within this section of the outcrop but is parallel to the regional shear plane which displays many minor corrugations. The basal 30 cm of the hangingwall is brecciated, displaying grain size reduction of the meta - dacite by brittle processes i.e., fracturing and milling of clasts. Individual clasts dimensions range from the sub - millimetre scale upto 15 cm diameter. All clasts are angular, irregular shaped and contained within a matrix comprised of very fine grained, randomly oriented phyllosilicates and milled quartz, epidote and plagioclase grains. All clasts over c. 1 cm diameter contain a strong S - fabric, defined by aligned phyllosilicates which have been disrupted and rotated due to brecciation. Over a distance of less than 2 cm, the zone of brecciation grades into a planar zone of intense ductile fabrics. Again since the profile plane section is unexposed it is difficult to determine the trend of the linear fabric. The S - fabric is defined by the alignment of very fine grained phyllosilicates which are parallel to the margins of both the footwall and hangingwall. The orientation of this fabric is therefore interpreted to represent the orientation of

the shear plane. The top 20 cm of the footwall meta - dacites are also brecciated, with clasts ranging from the sub - mm scale upto 4 - 5 cm diameter. The clasts are angular and irregular shaped and separated by a fine grained randomly oriented matrix of phyllosilicates and finely milled quartz, epidote and plagioclase (Plate. 5.2 d). The cm scale clasts contain a strong S - fabric which is parallel within all clasts and parallel to the S - fabric within the high strain zone and non - brecciated footwall meta - dacites (Plate. 5.3). This indicates that brecciation of the footwall occurred either :- prior to the ductile deformation or occurred post the ductile deformation without the re - orientation of clasts. The top *c.* 50 m of the footwall is imbricated on the metre to decimetre scale, comprising predominantly of Kaourera Island - Arc Group island - arc type lithologies, however, towards the base of the imbrication zone, Mvuu Meta - Mafic Volcanic Formation meta - basalts become more frequent.

The parallelism of the S_2 fabric within the hangingwall meta - dacites and the S - fabric within the high strain zone indicate that ductile deformation within the zone is coeval with the regional D_2 deformation. This tectonic event is characterised by elevated shear strains with intense deformation partitioned into narrow, discrete zones which are responsible for the juxtaposition of the Maunde and Kaourera Island - Arc Groups. Brecciation is interpreted to be post D_2 since brecciated clasts contain the S_2 fabric. However, it is unclear as to the relative age and tectonic nature of the brecciation. It might be interpreted to represent the transition of the thrust sheet into the brittle zone during the latter stages of D_2 deformation or due to reactivation during Karoo times which is characterised by brittle, extensional faulting.

The Kadunguri Whiteschists are also interpreted to have been juxtaposed during D_2 since S_1 random fabrics are overprinted by an intense S / L fabric which is parallel to the regional D_2 fabric in the Ophiolite Terrane.

At many localities the juxtaposition of Ophiolite Terrane lithologies and Zambezi Terrane granitic gneisses are marked by discrete zones of intense mylonitisation. The associated ultramyolinitic and mylonitic planar and linear fabrics are parallel to the Ophiolite Terrane S_2 - L_2 fabrics indicating that juxtaposition of terranes is also related to the D_2 event. At MR [9111 3771] mylonitised Twiza Meta - Gabbro Formation meta - gabbros (Plate 2.6 d) of the Maunde Ophiolite Group are separated by a gap in outcrop of *c.* 5 m from ultramylonitised augen gneisses (Plate. 2.11 b). The meta - gabbros display an intense S / L fabric and fine grained textures. The Augen Gneisses are comprised of fine grained (< 0.1 mm) quartz, microcline, plagioclase, biotite and muscovite. Quartz, microcline and plagioclase form ribbon aggregations parallel to the L - fabric defined by elongate biotite and muscovite. There are no microcline augens present. Outcrops which occur progressively away from the contact display a gradual coarsening in grain size and abundance in microcline augens, until at MR [9075 3775] i.e., 350 m west of the contact, the augen gneisses display textural characteristics typical of the Augen Gneiss. A similar relationship is evident at MR [8125 3785] where an ultramylonitised augen granite lens (horse) (Fig. 5.1) is enveloped by Kamuyu Amphibolite Formation meta - basalts. The margins of the granitic horse are ultramylonitised while the central portion displays augen structures. The S - L fabrics associated with the ultramylonitised portion of the granitic gneiss are parallel to S_2 - L_2 fabrics within the encompassing Kamuyu Amphibolite Formation. It is interpreted therefore that ductile shearing during D_2 deformation is the concequence of the juxtaposition of the Ophiolite and Zambezi Terranes.

5.4.2 *Transport Direction during D_2 within the Ophiolite Terrane*

Planar and linear fabrics associated with D_2 deformation are interpreted to represent a period of ductile shearing with transport parallel to the trend of

the lineation. The uniformity in orientation of the L_2 lineation within the Ophiolite Terrane indicates that the transport direction was either toward the N - NE or S - SW. Since the L_2 lineation is down - dip to slightly oblique to the S_2 foliation, transport directed toward the N - NE would be associated with a compressional, ductile thrust - type kinematics while S - SW directed transport would be associated with extensional - type tectonics. Interpretation of small scale kinematic indicators as described by Simpson & Schmid, (1983) and Passchier & Simpson, (1986) have been used to determine the transport direction associated with D_2.

Kinematic indicators in the Ophiolite Terrane are rare; however, where primary S_0 structures such as amygdales or peak - M_2 porphyroblasts such as garnet or amphibole are present, kinematic indicators are more common. Macroscopic indicators include δ type structures formed by the deformation and recrystallisation of relict amygdales or quartz - plagioclase lenses. Occasionally F_2 shear folds are exposed in the profile section so that the fold vergence can be interpreted. Macroscopic kinematic indicators from the ophiolite assemblages of the Maunde Ophiolite Group such as F_2 fold profiles (Plate. 5.4 a) clearly display a top to the north sense of vergence while asymmetric δ - type structures also display predominantly top to the north (Plate. 5.4 b, and c) but occasionally top to the south geometries (Plate. 5.4 d and Fig. 5.8). The origin of these top to the south or 'reversed' indicators is unclear since they are located within less than 100 m of 'normal' top to the north geometries (Fig. 5.8) without any obvious tectonic discontinuities between the two. It might be suggested that they represent a later period of deformation. However, the similarity in orientation of recrystallisation tails and the lack of re - oriented top to the north indicators suggest that they are related to the same temporal event. It is possible that these opposing shear sense indicators developed within a deformation period (D_2) characterised by heterogeneous simple shear. If, during a regional top to the north sense of

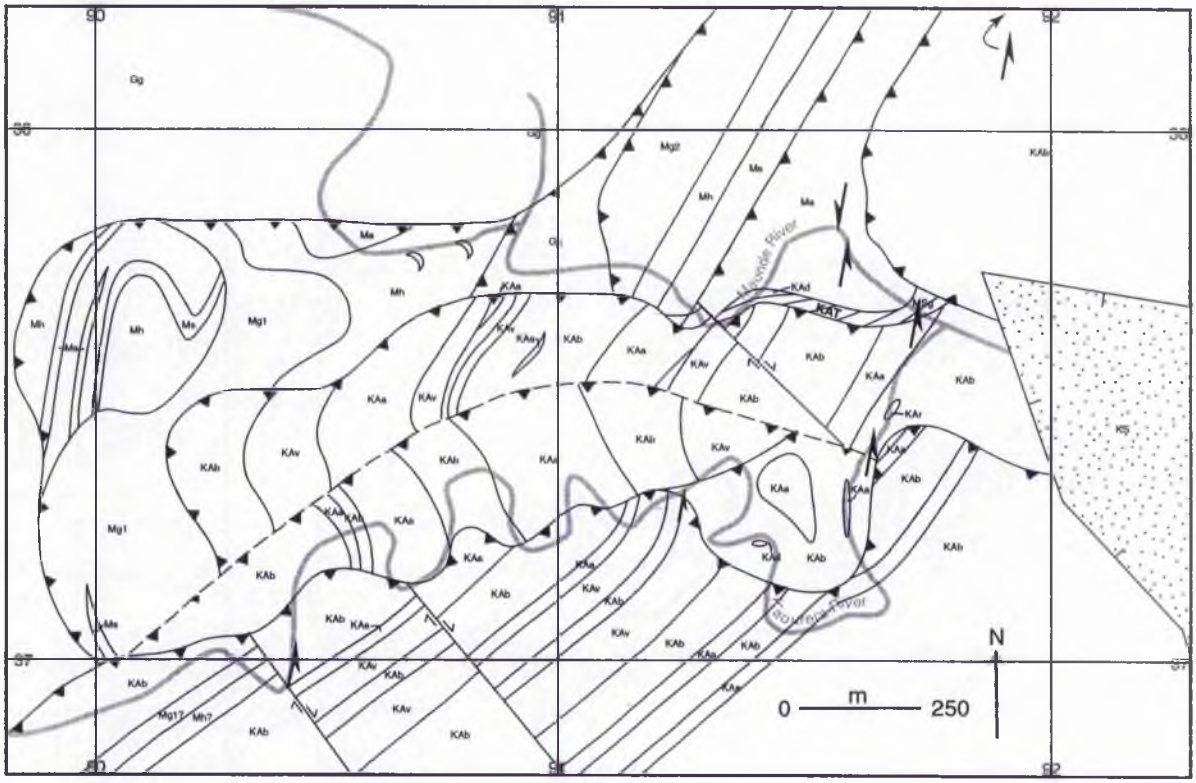

Fig. 5.8 Map of the Maunde Domain showing the location and shear sense of kinematic indicators. Arrows point to the direction of tectonic transport.

shear deformation, lower sections of the ductile thrust pile were transported relatively faster compared to the upper sections, local reversals in the sense of shear would result (Alsop *pers. comm.*) (Fig. 5.9). Overall, the majority of shear sense indicators reflect the regional kinematics i.e., top to the north, but in localised sections the sense of shear might be reversed.

Microstructural indicators such as σ and δ type porphyroblasts have only revealed top to the north geometries (Plate. 5.5 a, b and c).

The majority of macroscopic and microscopic kinematic indicators predominantly display a top to the north sense of shear indicating that D_2 deformation and shearing involved a northerly tectonic transport direction i.e., up - dip representing ductile thrusting rather than extensional tectonics.

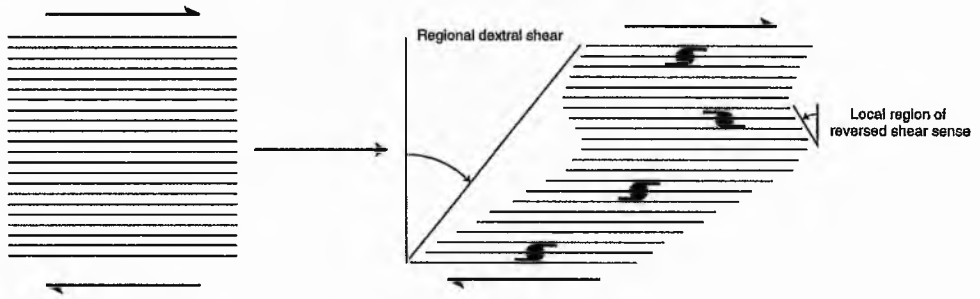

Fig. 5.9 Cartoon sketch illustrating the heterogeneous dextral shearing of a pack of cards. Note how the overall dextral strain is reflected by the majority of the σ type kinematic indicators. However, sinistral (i.e., reversed) kinematic indicators are produced due to localised heterogeneous strain (Alsop *pers comm*).

5.4.3 D_3 and D_4 Deformation within the Ophiolite Terrane

As indicated in section 5.2, the relationship between F_3 and F_{cren} folds is difficult to interpret. Both folding events are characterised predominantly by upright axial planes and open to moderate fold profiles, suggesting that they may be temporally related. The roughly E - W to NW - SE orientation of F_3 fold hinges and axial planes indicate that D_3 was characterised by N - S to NE - SW shortening directions. The orientation in shortening direction is similar to that during the D_2 event. The orthogonal nature of F_3 structures is due to a

change in folding mechanisms from non - coaxial shearing during D_2 to buckle folding during D_3. A similar but slightly less constrained shortening direction is also interpreted for the F_{cren} folds. The upright, symmetrical nature of both F_3 and F_{cren} fold profiles is interpreted to represent crustal shortening with a vertical extension direction.

5.4.4 *Timing of Deformation and Metamorphism*

M_2 metamorphism (M_1 within the Ophiolite Terrane) peaked within the amphibolite facies with the growth of amphiboles ± biotite and rare garnet porphyroblasts within the meta - basaltic lithologies. Elongate and tabular, peak metamorphic amphibole and biotite blades are aligned to form the S_2 foliation and L_2 lineation. Rare garnet and amphibole porphyroblasts display rotation and recrystallisation with σ type tails aligned parallel to the L_2 lineation. These textures altogether indicate that peak metamorphism pre - dated the main D_2 deformation. It is therefore possible that the S_1 gneissic layering which is interpreted by Goscombe *et al.*, (1994, 1998) to represent migmatitic layering represents the prograde and / or peak metamorphic portion of the M_2 cycle (M_1 within the Ophiolite Terrane). The lack of F_3 and F_{cren} axial planar cleavages, the breaking and mechanical re - orientation of amphibole blades around the hinges of these folds without the production of retrogressive minerals and similar compressional regime to D_2 also suggest that D_3 and D_4 occurred post -, peak - M_2 metamorphism (M_1 within the Ophiolite Terrane) and represent the waning stages of a single, progressive deformation event.

5.5 Correlation of the Ophiolite Terrane with the surrounding terranes.

Goscombe *et al.*, (1994) present a tectono - metamorphic history for the Quartzite, Zambezi and Granulite Terranes of the Chewore Inliers which is

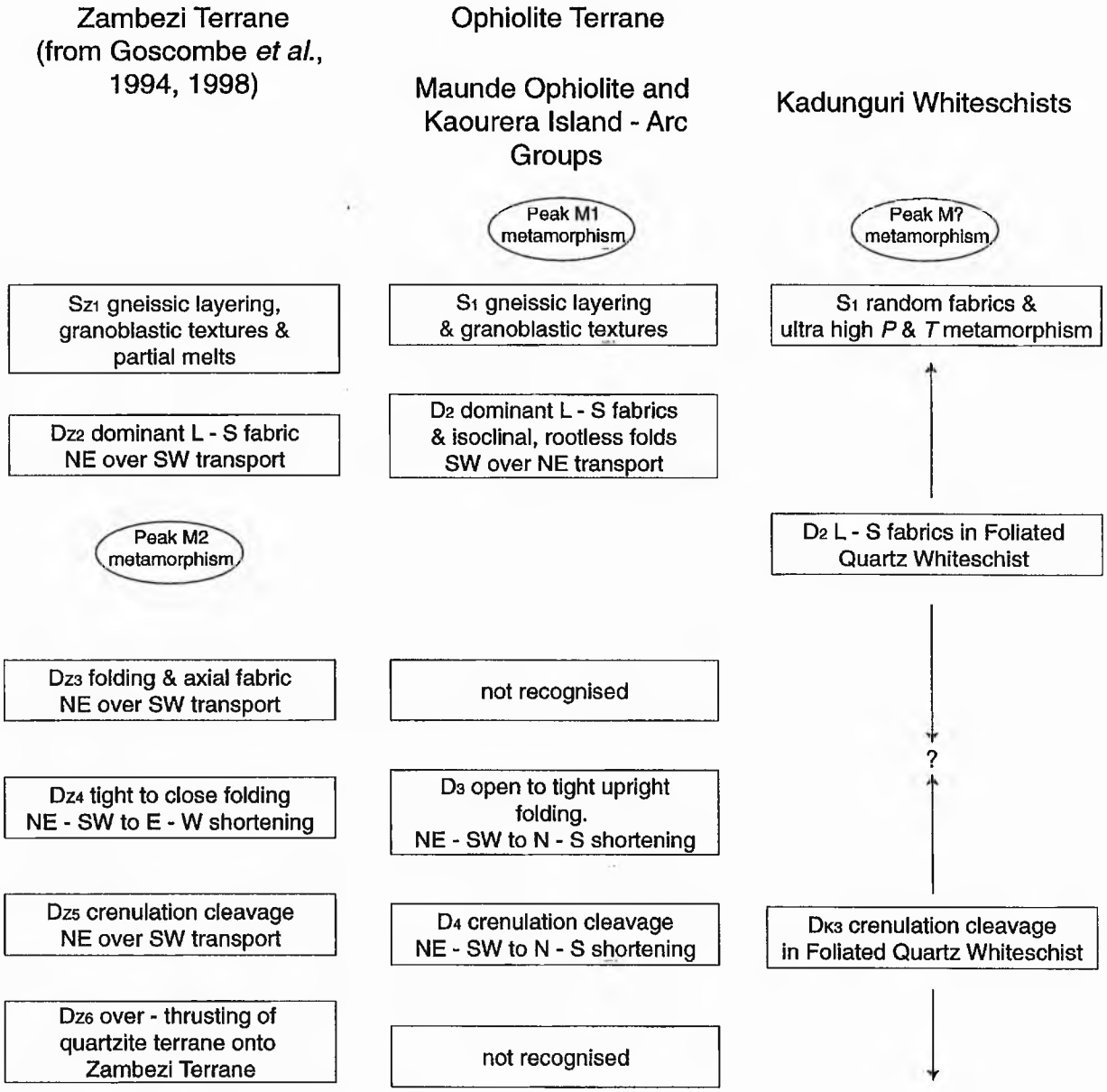

Fig. 5.10 The structural evolution of the Ophiolite Terrane during the M2 tectono - metamorphic cycle compared with the Juxtaposed Zambezi Terrane (after Goscombe *et al.*, 1998).

revised in Goscombe *et al.*, (1998) and presented in Fig. 5.10. The authors identify 6 periods of deformation within the Quartzite and Zambezi Terranes, of which two (D_{Z3} and D_{Z6}) were not recognised within the Ophiolite Terrane of this study.

D_{Z3} is interpreted to be coaxial with D_{Z2} (D_2 of this study) and represents ductile fold repetition parallel to F_2 folds. These F_{Z3} folds are identified by the isoclinal folding of the S_2 and L_2 fabric and are associated with a weak axial planar fabric. D_{Z2} and D_{Z3} deformation is interpreted by Goscombe *et al.*, (1998) to represent a single, prolonged non - coaxial shear dominated deformation event. In this study all post - F_2 folds i.e., folds which refold the S_2 foliation and L_2 lineation, display open fold profiles with vertical fold axial planes and roughly east to west trending, gently plunging fold hinges which correspond with the F_{Z4} folds of Goscombe *et al.*, (1994, 1998). F_{Z3} folds are interpreted by Goscombe *et al.*, (op. cit.) to account for reversals in shear sense. Unfolding of D_{Z3} effects indicates transport during D_{Z3} (and thus D_{Z2}) was NE over SW i.e., a SW directed tectonic transport direction. However, Fig. 5.11 illustrates how re - folding of σ and δ type kinematic indicators about a similar fold axis, during a progressive, high shear strain deformation event, cannot result in this apparent reversal of shear sense.

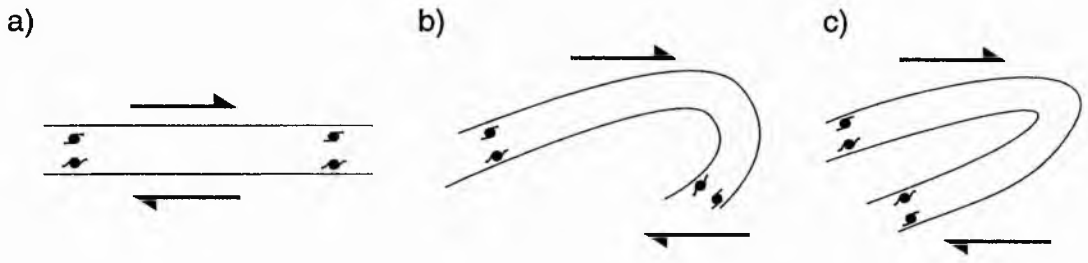

Fig. 5.11 Sketch illustrating how kinematic indicators cannot display reversals in shear sense when refolded about a similar axis i.e., from D_{Z2} to D_{Z3} after Goscombe *et al.*, (1998).

If tectonic transport was toward the SW, i.e., down - dip as interpreted by Goscombe *et al.*, (1998) then this progressive, high strain D_2 event would be

related to extensional tectonics and could not therefore result in crustal shortening and over - thickening by fold repetition seen in this study. The associated clockwise, moderate *P* and *T*, Barrovian style M_2 metamorphic cycle (M_1 within the Ophiolite Terrane) (section 4.3.1 and 4.3.3) is also incompatible with extensional type tectonics which is normally associated with an anticlockwise, high *T* and low to moderate *P* metamorphic path (Sandiford & Powell, 1986; Appel *et al.*, 1997; Gibson & Ireland, 1995). Since the majority of kinematic indicators in the Ophiolite Terrane indicate a NE directed transport direction, reversals are interpreted to represent heterogeneous strain during D_2 and thus a NE sense of transport is interpreted within this study.

D_{Z6} is represented in the Chewore Inliers as a narrow, steep, northerly dipping mylonite zone bordering the Granulite and Quartzite Terranes and is interpreted to represent a steep thrust contact related to the juxtaposition of the two terranes subsequent to all ductile fold events (Goscombe *et al.*, 1994, 1998). Transport directions during D_{Z6} are interpreted to be SW directed and resulted in the steepening in orientation of structures in the Quartzite Terrane.

5.6 Discussion

The tectono - metamorphic evolution of the Ophiolite Terrane is represented by one crustal thickening cycle. M_1 metamorphism within the Ophiolite Terrane (Fig. 5.10) resulted in a penetrative gneissic layering (S_1) and the growth of amphibole and garnet porphyroblasts. M_1 metamorphism (within the Ophiolite Terrane) peaked prior to the main phase of ductile deformation (D_2). D_2 deformation is associated with non - coaxial, high shear strains, production of a penetrative S / L fabric and localised, small scale intrafolial folds. Continued shearing along the S_2 planes resulted in the attenuation of

fold limbs and hinges to produce rootless folds. The majority of kinematic indicators associated with D_2 indicate that tectonic transport was toward the N to NE (i.e., N - S to NE - SW shortening), with SW verging indicators being interpreted as the result of heterogeneous strain during D_2. Goscombe *et al.*, (1994, 1998) identify a later, concordant deformation event (D_{Z3}) which re - folds the S_2 and L_2 fabric and kinematic indicators about an identical strain ellipsoid to D_{Z2}. The tectonic transport direction after the unfolding of their F_{Z3} folds are interpreted by them to be SW directed. However, D_{Z3} has not been identified in this study.

The parallelism of the regional D_2 fabrics with the ultra high strain deformation fabrics (both S and L) at the margins of both terranes indicate that juxtaposition of terranes was during D_2. Goscombe *et al.*, (1998) also suggest that juxtaposition was during D_2 since regional scale F_{Z3} folds, re - orientate the terrane boundaries.

D_3 and D_4 structures (within the Ophiolite Terrane) are interpreted to represent the waning stages of D_2 deformation since they are characterised by similar shortening directions, lower shear strains i.e., buckle rather than shear folds and an increased variation in fold orientations indicating inhomogenous strain. Goscombe *et al.*, (1994, 1998) indicate a later stage of deformation (D_{Z6}) associated with the backthrusting and juxtaposition of the Granulite Terrane with the Quartzite, Zambezi and Ophiolite Terranes. D_{Z6} has not been recognised in the Ophiolite Terrane in this study.

The Kadunguri Whiteschists are characterised by random fabrics associated with a high *P*, moderate *T* metamorphic assemblage unlike that of M_1 or M_2 within the Zambezi and Granulite Terranes and M_1 within the Ophiolite Terrane (section 4.3.2). It is unclear whether the Kadunguri Whiteschists were metamorphosed during M_1 or M_2 at different *PT*'s or metamorphosed during a completely different metamorphic cycle. It is possible therefore that the Kadunguri Whiteschists represent an allocthonous

terrane which is separate from the Ophiolite Terrane. However, it is interpreted from geochemical analysis (section 3.4) that the Kadunguri Whiteschist protoliths were most similar to metasomatised island - arc meta - basalts thus suggesting that two groups are part of the same terrane. D_2 deformation is represented as a zone of high strain (both S and L fabrics) along the boundary of the Kaourera Island - Arc Group and the Kadunguri Whiteschists. Since this fabric is parallel to the S_2 - L_2 fabric within the rest of the Ophiolite Terrane and parallel to the boundary of the two groups, it is interpreted that juxtaposition occurred during this event. Post D_2, crenulations are also present within this zone and are also interpreted to represent the waning stages of D_2.

5.7 Conclusions

It is concluded that :-

1) Tectonic evolution of the Chewore Inliers is characterised by a single period of crustal thickening, with a N - S, NE - SW shortening direction.

2) M_2 metamorphism peaked prior to the main period of ductile, non - coaxial, high strain deformation.

3) Kinematic shear sense indicators indicate that the main phase of ductile deformation is characterised by top to the N to NE directed shearing.

4) Juxtaposition of groups within the Ophiolite Terrane and terranes within the Chewore Inliers occurred during the high strain D_2 event.

5) Deformation associated with the waning stages of the crustal thickening event are characterised by variably oriented small scale, open folds and crenulations.

5.8 Cross Sections.

Cross section A to D (map 1b)

This section illustrates the structure of the Chitumbi Domain in the west of the region. Note that the cross section 'dog legs' to include important imbrications. It is evident that the Zambezi and Ophiolite Terranes are not mutually exclusive within this domain i.e., there are slices of granite gneiss within amphibolites and *vice versa*.

Cross Section E to F (map 2a)

This section illustrates the Maunde, Kaourera and Nhema Thrusts. The structure of the section is based on the thin skinned tectonic model with minor imbricate faults occurring between the major thrusts; however, the orientation of structures within some segments do not quite reflect the thin skinned model. This may be due to the higher grade of metamorphism (upper amphibolite facies) that accompanied the main phase of ductile deformation (section 5.3) compared with the brittle thin skinned tectonic model. From field relations it is evident that the Nhema Thrust is slightly later in the succession since it cross - cuts the Maunde and Kaourera Thrusts.

Cross Section G to H (map 2b)

This section illustrates the lithostratigraphic distribution of the Maunde Ophiolite Group, its relation to the Zambezi Terrane gneisses and the overlying Kaourera Island - Arc Group. The Maunde Thrust is bounded on either side by ultramyolinite (High Strain Member of the Twiza Meta -

Gabbro Formation within the Maunde Ophiolite Group and the Ultramyolinite Member within the Kanhungwa Gneisses. A small scale strike slip fault related to the emplacement of the Kaourera Island - Arc Group onto the Maunde Ophiolite Group does not affect the Nhema Thrust, indicating that the latter thrust is relatively younger than the others.

Cross Section I to J (map 3b)

This section illustrates the structure of the Kadunguri Whiteschists. The Kadunguri Thrust separates the Kaourera Island - Arc Group from the Kadunguri Whiteschists and imparts a tectonic foliation on the Tsoko Formation and the Foliated Member of the Shamwari Formation. All lithologies are interpreted to be in stratigraphic contact.

Plate. 5.1

a) Looking northwest. The AK 47 rifle is 1 metre long. At MR [8195 3680] a strong S_1 gneissic layering is developed within Kamuyu Amphibolite Formation meta - basalts. Individual leucocratic layers are upto 5 mm thick and > 1 m long. The leucocratic layering comprises *c.* 20 % of the outcrop.

b) Looking southwest. Width of view is 3 metres. At MR [9165 3762] a strong S_2 / L_2 fabric is developed within the Nzou Meta - Greywacke Formation pelites.

c) Looking north. Width of view is 1 metre. At MR [9040 3305] F_2 isoclinal folds are present within Kamuyu Amphibolite Formation meta - basalts. The view is parallel to the L_2 lineation. F_2 folds re - fold the S_1 gneissic layering and contain the axial planar S_2 foliation as illustrated in the sketch diagram. F_2 hinges are parallel to the lineation.

d) Looking east. Width of view is 2.5 metres. At MR [8838 3254] an F_3 open fold is evident within the Kamuyu Amphibolite Formation meta - basalts. The F_3 axial plane is upright and trends east - west while the F_3 hinge is horizontal. The fold is defined by the re - folding of the S_1 layering and S_2 / L_2 fabrics. No axial planar cleavages are developed within these folds.

e) Looking east. Compass clinometer is 10 cm in length. At MR [8875 3275] slightly inclined, tight F_3 folds are evident. They display a similar orientation to the F_3 open folds illustrated in Plate. 5.1 d.

a)

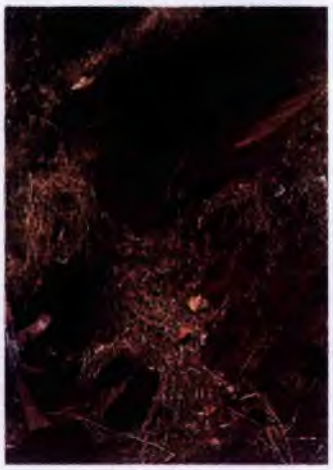

b)

c)

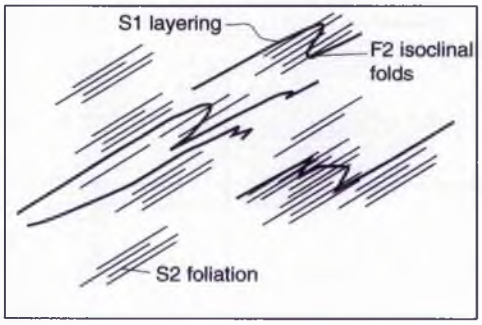

d)

e)

Plate. 5.2

a) Looking southeast. Compass clinometer is 20 cm in length. At MR [8970 3352] F_{cren} crenulation kink bands are evident within Kamuyu Amphbiolite Formation meta - basalts. F_{cren} axial planes are upright and trend roughly southeast - northwest with horizontal hinges.

b) PPL view of a crenulated Kamuyu Amphibolite Formation meta - basalt. Scale bar is 2 mm long. Note how amphibole blades are mechanically rotated around F_{cren} hinges and the lack of growth of new amphibole blades.

c) Looking east. Pencil is 6 cm in length. At MR [9676 3492] F_{cren} crenulations are evident within the Foliated Quartz Whiteschist.

d) XPL view of brecciated meta - dacite of the Gondo Meta - Felsic Volcanic Formation. Scale bar is 1 mm in length. Note how grain size reduction is restricted to narrow zones.

a)

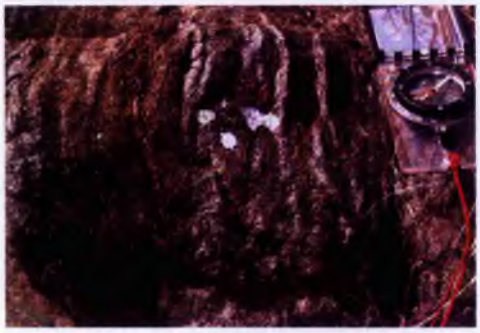

b)

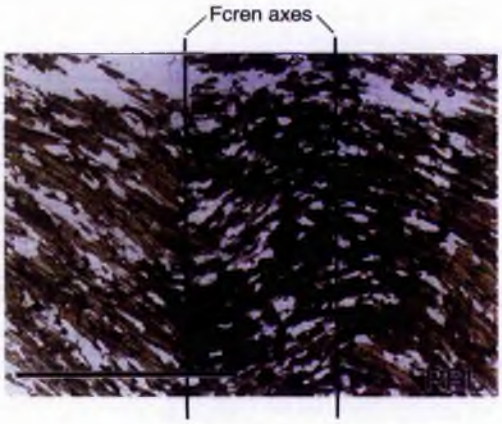

c)

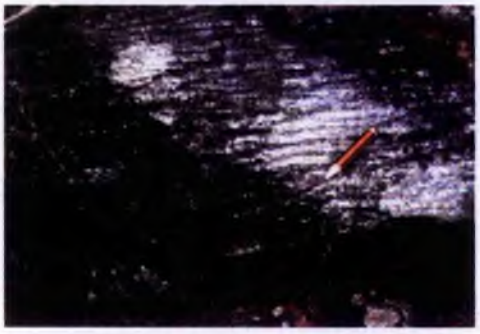

d)

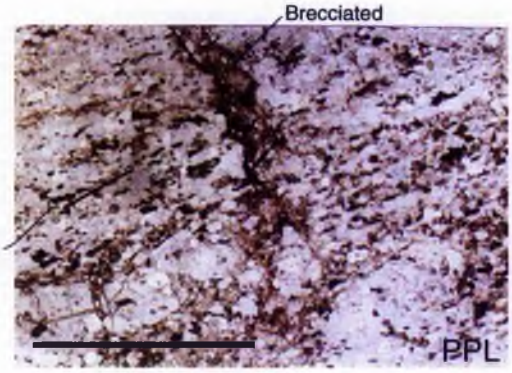

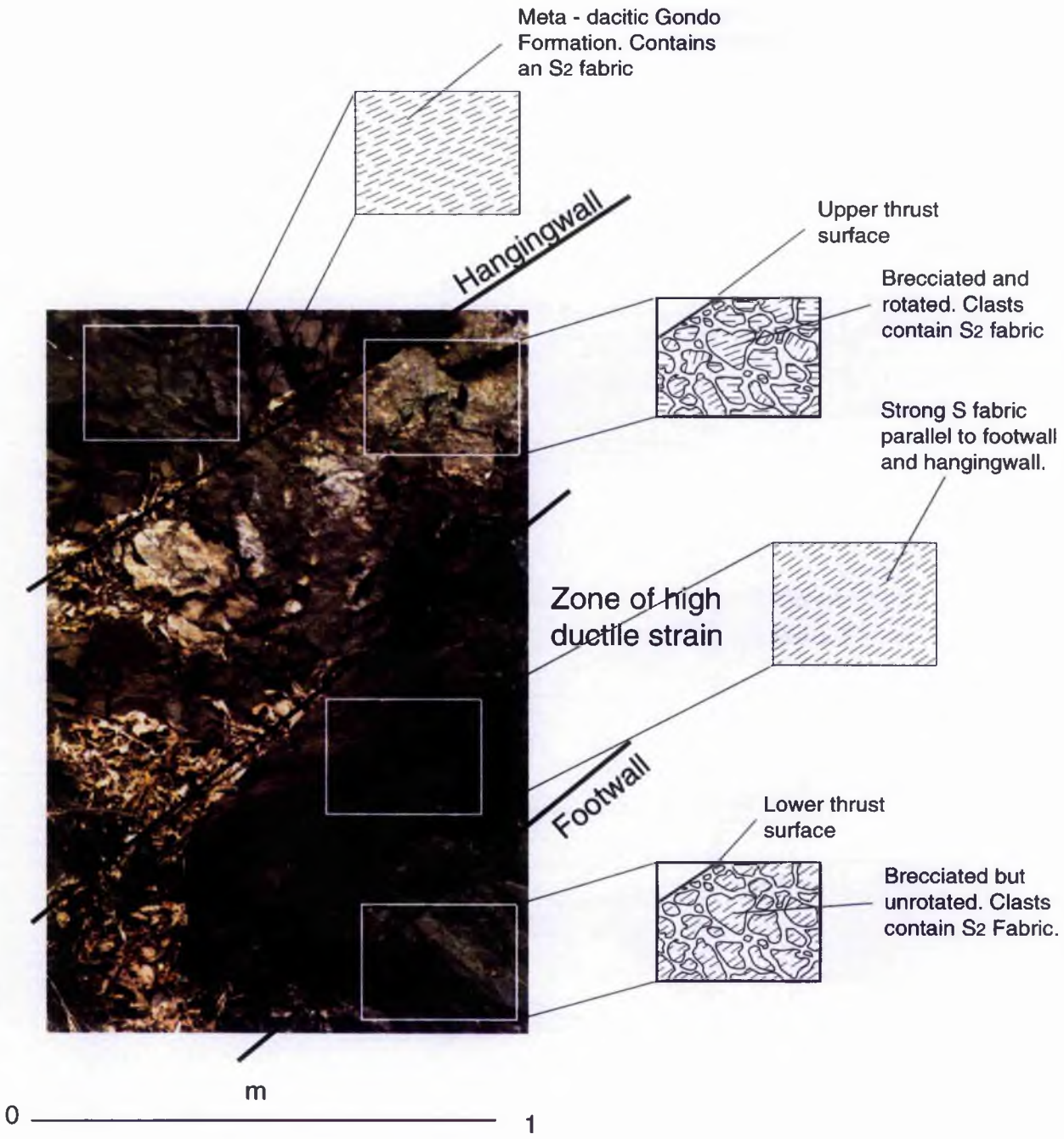

Plate. 5.3 Looking south. Width of photo shown is 1 m. At MR [9130 3765] a major northeast to southwest striking ductile thrust plane is exposed within the meta - dacitic Gondo Formation of the Kaourera Group. The view is parallel to the transport direction of the ductile thrust, however it is unclear as to whether the hangingwall has moved out of or into the page (i.e., towards the north or south).

Plate. 5.4

a) Looking west. Hammer is 50 cm in length. View is orthogonal to the L_2 lineation and in the plane of the S_2 foliation. At MR [9158 3778] a north verging, intrafolial, F_2 fold hinge is evident within the Mvuu Meta - Mafic Volcanic Formation meta - basalts.

b) Looking west. Pencil is 5 cm in length. View is orthogonal to the L_2 lineation and in the plane of the S_2 foliation. At MR [9168 3764] a north verging σ type kinematic indicator is evident within the Nzou Meta - Greywacke Formation pelites. The indicator is a recrystallised quartz lens.

c) Looking west. Width of view is 7 cm. View is orthogonal to the lineation and in the plane of the S_2 foliation. At MR [9032 3692] a north verging, σ type kinematic indicator is evident within the Nhema Amphibolite Formation meta - basalts. The indicator is a recrystallised epidote - filled amygdale.

d) Looking northwest. Width of view is 5 cm. View is orthogonal to the lineation and in the plane of the S_2 foliation. At MR [9152 3777] a south verging, σ type kinematic indicator is evident within the Mbizi Sheeted Dyke Formation meta - basalts. The indicator is a recrystallised epidote - filled amygdale.

a)

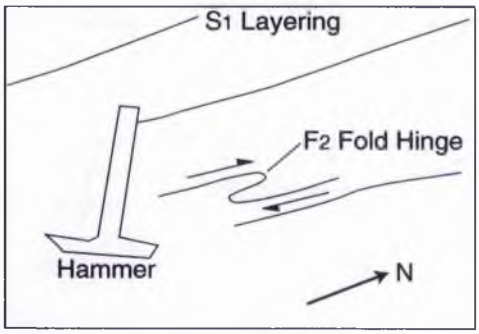
S1 Layering
F2 Fold Hinge
Hammer
N

b)

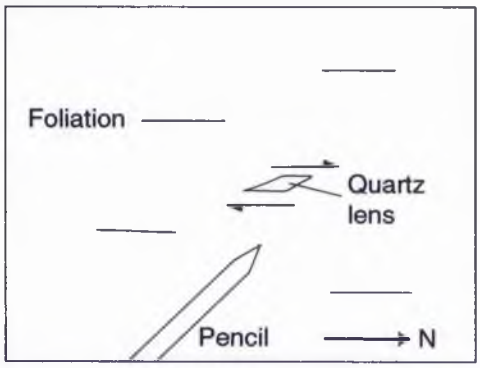
Foliation
Quartz lens
Pencil
N

c)

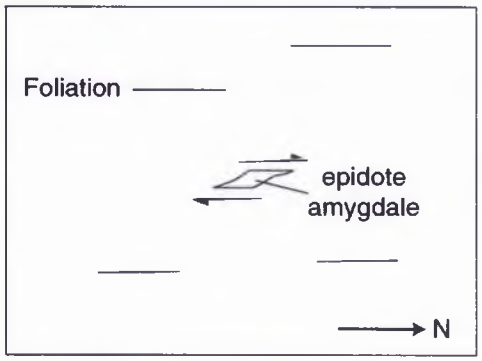
Foliation
epidote amygdale
N

d)

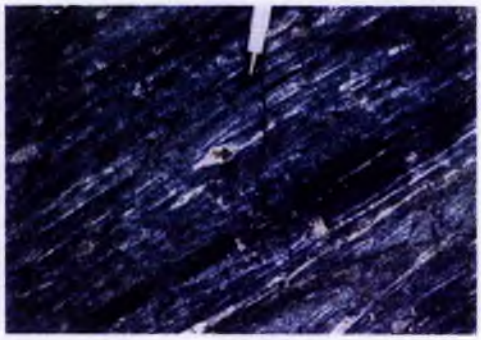

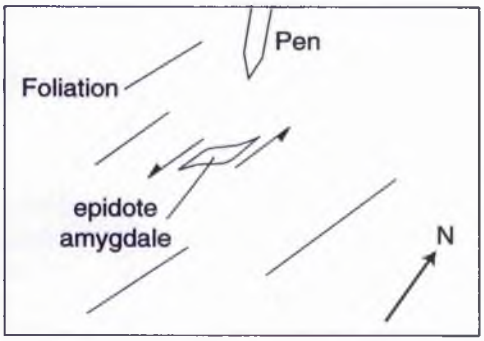
Pen
Foliation
epidote amygdale
N

Plate. 5.5

a) Photograph and sketch of the Granular Member of the Nhema Amphibolite Formation (thin section [SJ 287]). The scale bar is 1.5 cm in length. The photo and sketch illustrates σ - type kinematic indicators with a dextral sense of shear. Amphibole porphyroblasts are recrystallised into fine grained tails.

b) Photograph and sketch of the Coarse Member of the Bhumi Semi - Pelite Formation (thin section [SJ 370]). Scale bar is 1.5 cm in length. The photo and sketch illustrate δ - type kinematic indicators. Garnet porphyroblasts with pressure shadow tails and parallel inclusion-trails displays a dextral sense of rotation.

c) Photograph and sketch of the Coarse Member of the Bhumi Semi -Pelite Formation (thin section [SJ 370]). Scale bar is 1.5 cm in length. The photo and sketch illustrate 3 types of kinematic indicator. At the top of the plate a large tabular garnet porphyroblast is fractured and pulled apart. The space between fragments is larger at the top than the bottom suggesting a dextral sense of rotation. In the centre a small garnet porphyroblast is fractured into many smaller 'granules' which trail away from the top part of the porphyroblast with a dextral sense of shear. At the bottom a δ - type garnet porphyroblast with pressure shadow tails and parallel inclusion trails, displays a dextral sense of rotation.

a)

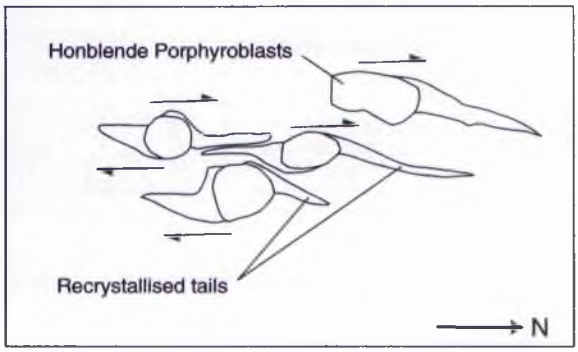
Honblende Porphyroblasts
Recrystallised tails
N

b)

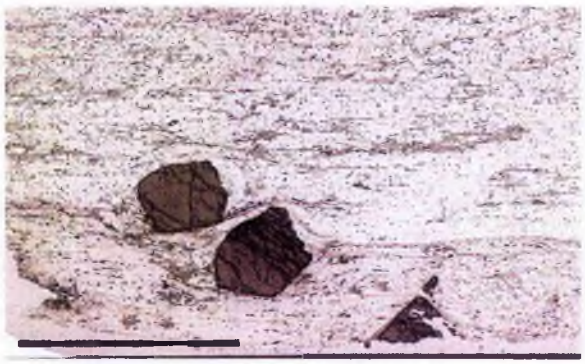

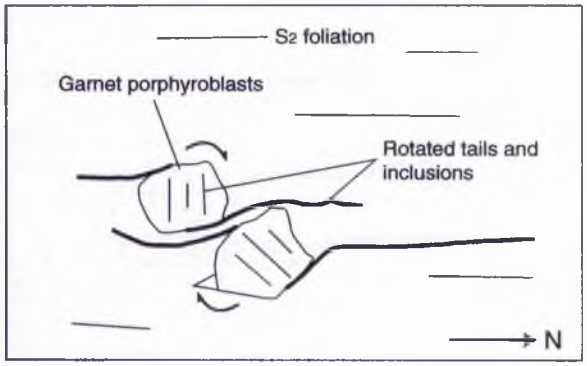
S2 foliation
Garnet porphyroblasts
Rotated tails and inclusions
N

c)

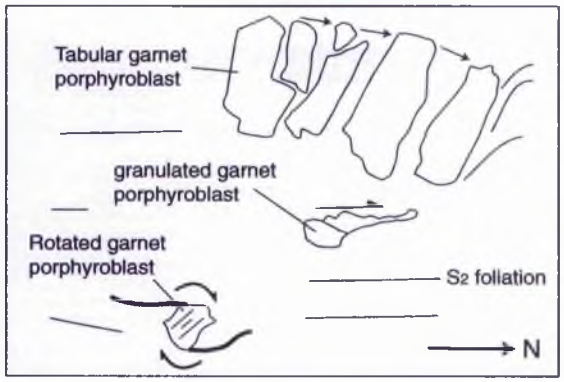
Tabular garnet porphyroblast
granulated garnet porphyroblast
Rotated garnet porphyroblast
S2 foliation
N

Chapter Six

Radiometric Age Determinations.

6.1 Introduction.

The aim of this chapter is to present a new U / Pb SHRIMP age determination for magmatic zircons within the Maunde Ophiolite Group.

6.2 U / Pb SHRIMP Age Of The Maunde Group.

In an attempt to date the protolith of the Ophiolite Terrane, zircons from a 30 cm thick plagiogranite sheet within the Twiza Formation of the Maunde Ophiolite Group were separated and the isotopes of Zr, Pb, U and Th were kindly analysed by I.S. Williams at The Australian National University with a Super High Resolution Ion Microprobe (SHRIMP).

The plagiogranite sheet is located at MR [9105 3770]. It is intrusive into mylonitised meta - gabbros of the Twiza Meta - gabbro Formation and is parallel to the S_2 foliation (Plate. 6.1, 6.2). The margins of the sheet are variably mylonitised while the central portion is equigranular and unmylonitised. Other plagiogranite sheets within the formation are parallel to sub - parallel with the S_2 foliation, are unmylonitised and are occasionally boudinaged. Whole rock major element geochemistry indicates that they are chemically similar to plagiogranites within other Phanerozoic ophiolite complexes and unlike those of continental, orogenic origin (section 3.2.3 and Fig. 3.6). Since ophiolitic plagiogranites are interpreted to be co - genetic with magmatism within the rest of the ophiolite complex (Coleman, 1977; Gerlach *et al.*, 1981), magmatic zircon age dates of this lithology can be taken as representative for the rest of the suite.

Four kilograms of plagiogranite [SJ 106.1], taken from the central, unmylonitised portion of the sheet were coarsely crushed, washed and underwent heavy mineral separation, (kindly provided by the University of Zimbabwe). The zircons were extracted from this heavy mineral separate by hand picking and were examined under electron backscattered imaging. Thirty four of these were selected and sent to Dr. I. S. Williams at the Australian National University for SHRIMP analysis.

The zircons were mostly euhedral, relatively large (>200μm diameter), prismatic grains with simple pyramid terminations which contained significant internal fracturing and inclusions. Under cathodoluminescence imaging, the zircons are internally zoned with concentric euhedral zoning parallel to the external faces of the grain (see Plate. 6.3) or simple sector zoning. There was no evidence for major discontinuities that might indicate the presence of an inherited core. It is interpreted that the zircons have grown relatively quickly during a single igneous event from a magma that contained no older zircon. They have subsequently been closely fractured, then corroded, and secondary minerals grown along the fracture planes (Williams *pers comm.*, 1996).

The SHRIMP analyses were made using a procedure described in detail by Williams & Claesson (1987). In brief, 10 analyses of 7 grains were monitored for the isotopes :- ^{204}Pb, ^{206}Pb, ^{207}Pb, ^{208}Pb, ^{238}U, ^{248}ThO and ^{254}UO (Table. 6.1, 6.2 and 6.3).

Grain spot	Pb/ppm	U/ppm	Th/ppm	Th/U
1.1	9	38	15	0.40
2.1	24	87	58	0.66
2.2	30	116	71	0.61
3.1	3	12	4	0.32
3.2	9	35	16	0.45
4.1	20	77	41	0.53
5.1	29	109	69	0.63
6.1	13	52	24	0.46
6.2	4	18	4	0.25
7.1	26	101	54	0.54

Table 6.1. Isotope content of the seven zircon grains.

Grain Spot	204Pb/206Pb	±204/206	%206	208Pb/206Pb	±208/206	208Pb/232Th	±208/232	206Pb/238U	±206/238	207Pb/235U	±207/235	207Pb/206Pb	±207/206
1.1	0.00012	0.00019	0.19	0.1199	0.0071	0.0717	0.0049	0.2367	0.0074	2.993	0.151	0.0917	0.0033
2.1	0.00016	0.00008	0.25	0.1896	0.0038	0.0713	0.0020	0.2492	0.0045	2.980	0.085	0.0868	0.0017
2.2	0.00008	0.00007	0.13	0.1817	0.0029	0.0717	0.0018	0.2396	0.0041	2.895	0.071	0.0876	0.0014
3.1	0.00104	0.00058	1.66	0.0666	0.0212	0.0497	0.0160	0.2363	0.0089	2.482	0.335	0.0762	0.0095
3.2	0.00029	0.00017	0.47	0.1297	0.0069	0.0698	0.0041	0.2401	0.0056	2.906	0.133	0.0878	0.0032
4.1	0.00007	0.00008	0.11	0.1588	0.0036	0.0726	0.0022	0.2440	0.0043	2.863	0.083	0.0851	0.0018
5.1	0.00008	0.00005	0.13	0.1828	0.0026	0.0699	0.0015	0.2412	0.0037	2.887	0.62	0.0868	0.0012
6.1	0.00039	0.00014	0.62	0.1249	0.0064	0.0641	0.0041	0.2373	0.0080	2.759	0.146	0.0843	0.0031
6.2	0.00050	0.00052	0.80	0.0731	0.0191	0.0693	0.0183	0.2404	0.0076	3.011	0.304	0.0909	0.0084
7.1	0.00010	0.00008	0.15	0.1540	0.0037	0.0680	0.0020	0.2376	0.0037	2.878	0.072	0.0878	0.0016

Grain Spot	Age 208/232	± age 208/232	Age 206/238	± age 206/238	Age 207/235	± age 207/235	Age 207/206	± age 207/206
1.1	1399.4	93.5	1369.7	38.9	1405.9	39.1	1461.2	69.4
2.1	1391.5	38.5	1434.2	23.3	1402.6	21.9	1354.9	38.8
2.2	1399.7	33.2	1384.7	21.2	1380.5	18.6	1374.1	30.3
3.1	981.1	310.3	1367.6	46.5	1266.7	102.8	1099.4	273.1
3.2	1364.2	78.5	1387.2	29.3	1383.6	35.3	1377.9	72.1
4.1	1417.0	40.9	1407.3	22.2	1372.2	22.0	1371.9	41.3
5.1	1364.9	29.0	1393.0	19.3	1378.6	16.5	1356.3	26.1
6.1	1255.4	78.6	1372.4	42.0	1344.4	40.1	1300.2	72.5
6.2	1355.1	349.6	1388.6	39.8	1410.4	80.2	1443.4	186.5
7.1	1329.2	38.1	1374.1	19.4	1376.2	19.1	1379.3	34.5

Table 6.2. Age data for $^{208}Pb/^{232}Th$, $^{206}Pb/^{238}U$, $^{207}Pb/^{235}U$, $^{207}Pb/^{206}Pb$.

Grain Spot	204Pb/206Pb	±204/206	%206	206Pb/238U	±206/238	207Pb/235U	±207/235	207Pb/206Pb	±207/206
1.1	0.00012	0.00019	0.19	0.2364	0.0074	2.951	0.122	0.0905	0.0021
2.1	0.00016	0.00008	0.25	0.2492	0.0045	2.980	0.085	0.0868	0.0017
2.2	0.00008	0.00007	0.13	0.2394	0.0041	2.861	0.071	0.0867	0.0014
3.1	0.00104	0.00058	1.66	0.2393	0.0087	2.877	0.170	0.0872	0.0037
3.2	0.00029	0.00017	0.47	0.2403	0.0056	2.939	0.111	0.0887	0.0024
4.1	0.00007	0.00008	0.11	0.2438	0.0043	2.846	0.079	0.0847	0.0017
5.1	0.00008	0.00005	0.13	0.2412	0.0037	2.887	0.062	0.0868	0.0012
6.1	0.00039	0.00014	0.62	0.2386	0.0081	2.937	0.149	0.0893	0.0030
6.2	0.00050	0.00052	0.80	0.2406	0.0074	3.038	0.149	0.0916	0.0032
7.1	0.00010	0.00008	0.15	0.2376	0.0037	2.878	0.072	0.0878	0.0016

Grain Spot	Age 206/238	± age 206/238	Age 207/235	± age 207/235	Age 207/206	± age 207/206
1.1	1368.1	38.7	1395.2	31.9	1436.8	45.4
2.1	1434.2	23.3	1402.6	21.9	1354.9	38.8
2.2	1383.4	21.2	1371.7	18.8	1353.7	31.1
3.1	1383.1	45.5	1376.0	45.4	1365.0	83.0
3.2	1388.5	29.2	1392.1	29.1	1397.6	52.7
4.1	1406.7	22.1	1367.8	21.2	1307.6	38.7
5.1	1393.0	19.3	1378.6	16.5	1356.3	26.1
6.1	1379.4	42.2	1391.4	39.1	1409.9	65.8
6.2	1389.7	38.5	1417.2	38.1	1458.8	67.1
7.1	1374.1	19.4	1376.2	19.1	1379.3	34.5

Table 6.3. Age data for $^{206}Pb/^{238}U$, $^{207}Pb/^{235}U$ and $^{207}Pb/^{206}Pb$.

The U and Th contents were low to very low (>116 ppm and >71 ppm respectively) which is consistent with igneous zircons. The low concentrations of ^{204}Pb in the sample (<4 ppm) indicate that the sample has not been contaminated by common Pb, that no Pb has been introduced into the crystal structure of the zircon by irradiation damage and thus a precise age could be calculated. The consistency between the various ratios (Table 6.1, 6.2 and 6.3) $^{206}Pb/^{238}U$, $^{207}Pb/^{235}U$, $^{207}Pb/^{206}Pb$, indicate that there is no significant dispersion in the analyses between grains or cores and rims of each grain. However, one grain (grain 6) (Plate. 6.3), displayed a structural discontinuity between the centre and the edge, which might have been interpreted as being an overgrowth. The consistency between the measured isotopic ratios of the central part and possible overgrowth indicate that if there is an age difference it is significantly smaller than the measurements could resolve.

The mean $^{206}Pb/^{238}U$ age (1393 ± 22 Ma (σ)) of all grains is indistinguishable from the mean $^{207}Pb/^{235}U$ age (1382 ± 7 Ma (σ)) indicating that the mean analyses is concordant within analytical uncertainty and thus the age of the plagiogranite sheet could be calculated using either $^{207}Pb/^{206}Pb$ or $^{206}Pb/^{238}U$ ratios. After applying corrections for analytical errors and uncertainties the age is calculated as 1367± 29 Ma and 1393 ± 22 Ma respectively. Since the latter displays the smaller uncertainty in age 1393 ± 22 Ma (Fig. 6.1) is the best estimate of the protolith age of the plagiogranite sample [SJ 106.1], with 95% confidence limits. The protolith age of the Maunde Ophiolite Group is also therefore interpreted to be 1393 ± 22 Ma.

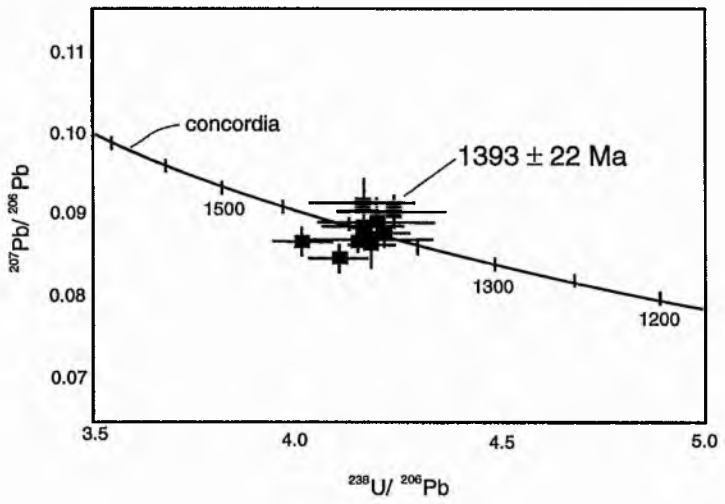

Fig. 6.1 U/Pb age dating concordia diagram with all analyses for SJ 106.1 plotted. The average intercept age is 1393 ± 22 Ma.

6.3 Discussion

The protolith age of this plagiogranite sample predates two periods of deformation, namely the Irumide Orogeny (equivalent to the Grenvillian Orogeny at around 1000 Ma Kampunzu, 1997) and the Pan - African Orogeny (between 500 - 800 Ma Kamona, 1997; Hanson *et al.*, 1994). Metamorphism associated with the latter orogeny peaked within the amphibolite facies. It might be expected that these zircons would have recorded these events in terms of overgrowths, but as already discussed this is not the case. All the zircon grains are heavily fractured possibly due to mylonitisation during D_2 (section 5.2). Williams (*pers comm.* 1996) indicates that zircon growth is not necessarily dependent on *P* or *T* but on the availability of zirconium and a medium to transport it since authogenic zircon can grow in sediments at low temperatures. Primary, unmantled zircons are also known from amphibolite facies, mylonite zones in Alaska (Williams *pers comm.* 1996). Grain 6 from sample [SJ 106.1] does contain an overgrowth (Plate. 6.3) however, the age

difference between the core and rim is undetectably small and therefore unrelated to any of these two major tectono - metamorphic cycles.

6.4 Conclusions

It is concluded that :-

1) The SHRIMP age of magmatic zircons from a plagiogranite sheet within the Twiza Formation is 1393 ± 22 Ma.

2) The field relations and geochemistry of the plagiogranite sheets are consistent with them being formed co - genetically with the ophiolite complex. The date of these sheets therefore dates the ophiolite suite at 1393 ± 22 Ma.

3) This is apparently the oldest dated ophiolite (*senso stricto*) in Africa (Oliver *et al.*, 1998).

Plate. 6.1 Looking north. Width of view is 2.5 metres. MR [9105 3770]. Plagiogranite dyke within the High Strain Member of the Twiza Formation (sample SJ 106) from which zircon grains were extracted and SHRIMP dated at 1393 ± 22 Ma. The dyke is 1m thick and parallel to the foliation.

Plate. 6.2 Looking north. Pencil is 8 cm in length. MR [9105 3770]. Close up view of the margin of the plagiogranite dyke, sample [SJ 106] (right hand side of plate). Note how the margins are mylonitised. The central portion however is unmylonitised.

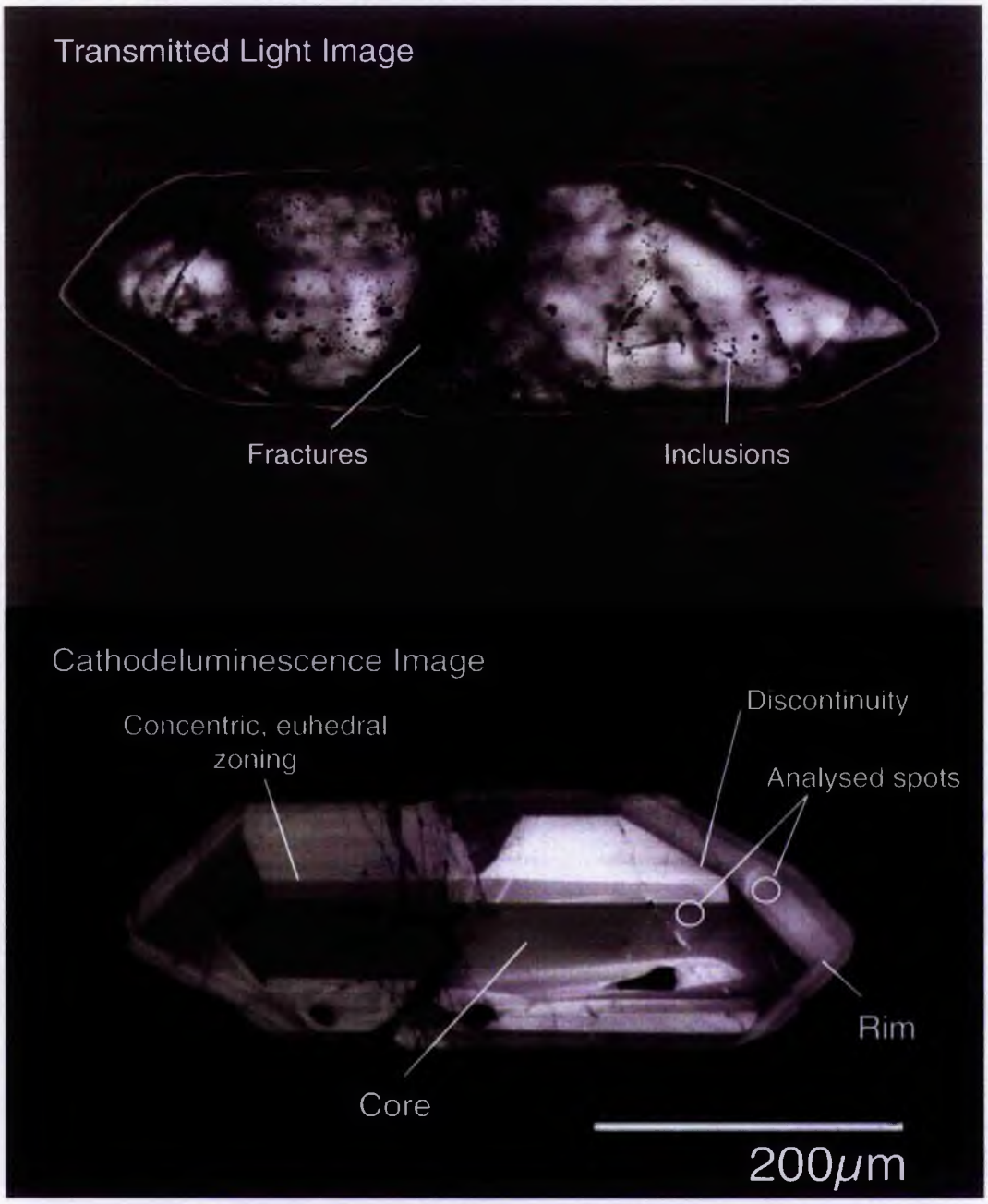

Plate. 6.3. Transmitted light and cathodeluminescence image of a magmatic zircon grain (grain 6) extracted from a plagiogranite dyke, sample [SJ 106] from the Twiza Formation of the Maunde Group. Note the euhedral grain shape characteristic of magmatic zircons. Also notice the apparent core and rim. SHRIMP analysis reveals a near concordant age for both the core and rim of 1393 ± 22 Ma.

Chapter Seven

Discussion, Synthesis and Conclusions.

7.1 Introduction.

The aim of this chapter is :-

1) To summarise the lithostratigraphy, geochemistry, metamorphism, structure and geochronology of the Ophiolite Terrane .

2) To demonstrate that the Maunde Ophiolite Group represents a tectonically excised ophiolite complex and the Kaourera Island - Arc Group represents an island - arc complex.

3) To illustrate the geodynamic evolution of the Ophiolite Terrane and the Chewore Inliers.

4) To provide a regional synthesis.

7.2 Geological Setting of The Ophiolite Terrane.

7.2.1 *The Maunde Ophiolite Group.*

The recognition of an ophiolite, as described by the Geological Society of America (GSA), Penrose conference (Anon, 1972) requires the identification of four major units:-

(1) a mafic, massive and pillowed, sediment free lava sequence,
(2) a mafic sheeted dyke section,

(3) gabbros and mafic and ultramafic cumulate rocks and
(4) tectonised peridotite,

all of which should be in an allocthonous setting. There should also be evidence that the units are inter - related, e.g. transitional zones such as sheeted dykes with mafic pillow screens or gabbroic dykes within the mantle sequence. Bickle *et al.*, (1994) points out that the majority of the Earth's ophiolite fragments are Phanerozoic in age, with very few being recognised from the Mid- Proterozoic to Archean period. It is possible that such ophiolitic fragments exist, but have gone unrecognised since they have been deformed and tectonised. Bickle *et al.*, (1994) also indicates that since each ophiolitic component can be formed in a variety of tectonic regimes in addition to mid - ocean ridges, at least three of the above four components must be present to invoke an origin analogous to Phanerozoic ophiolites.

The Maunde Ophiolite Group contains many distinct lithological units each of which share similar lithological and structural characteristics to those within Phanerozoic ophiolite complexes (section 2.2), namely :-

(1) Mvuu Meta - Mafic Volcanic Formation = mafic lava sequence,
(2) Mbizi Sheeted Dyke Formation = mafic sheeted dyke section,
(3) Ingwe Meta - Mafic Cumulate and Twiza Meta - Gabbro Formations = gabbro and mafic and ultramafic cumulates,
(4) Ngwena Ultramafic Formation = tectonised peridotite.

More than three of the ophiolitic components can be recognised within the Maunde Ophiolite Group, thus according to the analogies of Bickle *et al.*, (1994) the Maunde Ophiolite Group can be interpreted to represent an ophiolite complex; however, according to the proceedings of the GSA Penrose Conference on ophiolites (Anon, 1972), these components must be proven to

be inter - related. Since the Maunde Ophiolite Group has been extensively tectonically excised and the outcrop is relatively limited in extent, no transitional zones (sheeted mafic dykes with pillow screens etc.) between formations (i.e. ophiolitic components) have been identified. Tectonic excision and extensive ductile shearing have also thinned each unit and thus the component thicknesses are not comparable with those within Phanerozoic examples (section 2.2). However, the formations do occur in a predictable sequence. The top mafic section occurs in the correct top to bottom sequence (i.e. sediments, extrusive volcanics and pillow lavas and then sheeted dykes) lying in a southeasterly dipping, east to west striking section. The plutonic and ultramafic components also occur in the correct sequence (i.e. gabbro, mafic cumulates and tectonised peridotite) but inverted, lying also in a southeasterly dipping, east to west striking section so that the mafic sheeted dykes are juxtaposed against tectonised peridotite (Fig. 2.1). From the whole rock major and trace element analyses (section 3.2) it is evident that all the formations share either similar geochemical signatures to each other or more loosely to other Phanerozoic ophiolites. It is clear that not only are all ophiolitic components present, but these components occur in a predictable and geochemically inter - related sequence comparable to Phanerozoic ophiolites.

The trace element geochemistry of the ophiolite meta - basalts (section 3.2.5) are similar to those within back - arc marginal basins, rather than those of mid - ocean ridges. This is not altogether surprising since most Phanerozoic ophiolites are also segments of back - arc marginal basins. Since they are situated within a tectonically active region it is more likely that these type of fragments will become obducted (Windley, 1995). Minor sediments associated with the Maunde Ophiolite Group, namely the Nzou meta - Greywacke Formation are unlike those of typical mid - ocean ridges (i.e. cherts, pelagic muds and manganiferous sediments), since they contain abundant biotite,

calcite and plagioclase. These immature sediments indicate a deposition close to a terrestrial source and are thus consistent with deposition within a marginal basin rather than that of a mid - ocean ridge.

7.2.2 *The Kaourera Island - Arc Group.*

Within sections 2.3.8, 3.3.7 and 4.3.2, the Kaourera Island - Arc Group was interpreted as a relict, tectonically excised and metamorphosed island - arc complex. In the light of the previous discussion (section 7.2.1) this is not altogether surprising, since modern day marginal basins are located behind island arc systems (Karig, 1971). The closure of a marginal basin and obduction of an ophiolitic fragment is invariably followed by the accretion of the associated island arc complex, as is evident in many modern day and ancient counterparts, such as the present day South Chile Margin (Windley, 1995) and the 2.725 Ga Superior Province (Percival *et al.*, 1994).

The Kaourera Island - Arc Group comprises a low - K tholeiite and a calc - alkaline fractionation series: the former comprised of basalt to dacite and the latter, basaltic - andesite to rhyolite. The two fractionation series are spatially related within the Maunde domain (Fig. 3.20), so that the calc - alkaline series overlies the low - K series. The presence of both the low - K and calc - alkaline fractionation suites suggest that the island arc was temporally within its middle stages (Wilson, 1989). The lack of plutonic intrusions into any part of the Kaourera Island - Arc Group suggests that only the upper crustal sections of the magmatic arc are represented. Trace element analyses and the lack of silaic continental crustal material indicates that the arc - complex was ensimatic (intra - oceanic) and was initiated by simple ocean - ocean type collision and subduction.

The whole rock major and trace element geochemistry of the Kamuyu Amphibolite Formation is comparable to modern day large igneous provinces such as Kerguelen. The Kamuyu Amphibolite Formation might represent a

relict seamount which became dissected and interleaved with marginal basin crust during its attempted subduction.

7.2.3 Kadunguri Whiteschists

The Kadunguri Whiteschists are exceptional within the rock record due to their bulk geochemistry which is restricted to the MFASH system and its ultra high pressure mineral assemblage (known as whiteschist), which includes the second known natural occurrence of yoderite. Trace element analysis suggests a similarity with low - K, tholeiitic meta - basalts of the Kaourera Island - Arc Group. However major element analysis indicates that if this is the case then the meta - basalt protoliths have undergone extensive metasomatism. The radial arrangement of the peak, high *P* metamorphic mineralogy indicates that metamorphism and metasomatism occurred prior to the main phase of ductile deformation (D_2). However, it is unclear as to which metamorphic cycle the high *P* mineralogy is related to i.e., M_1, M_2 or a completely different event. Overprinting ductile fabrics indicate that juxtaposition with the Ophiolite Terrane was during the main D_2 deformation.

7.3 An Archean Greenstone Belt?

The Zimbabwe Craton is predominantly comprised of Archean Granite - Greenstone terranes. Since the Chewore Inliers are situated less than some 70 kms to the north of the nearest greenstone terrane (Makonde Greenstone belt), it could be suggested that the Maunde Ophiolite and Kaourera Island - Arc Groups represent a segment of such a terrane, and that the 1.4 Ga U/Pb zircon age of a 'plagiogranite sheet represents the age of tonalitic / trondhjemitic intrusions during the earliest Irumide deformation event.

In the light of modern analytical techniques and re - investigation of field structures, many authors (Windley, 1995; Kusky and Kidd, 1992; Dirks

and Jelsma, 1998) have interpreted that Archean Granite Greenstone terranes represent primitive oceanic crust and / or island arc successions. However, some authors such as Bickle *et al.*, (1994) do not believe that this is the case for some, most, or all greenstone terranes. Most greenstone belts can be sub - divided into 2 main groups, a lower volcanic group and an upper sedimentary group. The basal parts of the lower group are dominated by ultramafic rocks and are noted for the occurrence of komatiites, while the upper sections comprise submarine tholeiitic or calc - alkaline, mafic to felsic volcanics. The sediments associated with the volcanic complex are noted for the occurrence of banded - iron formations. The lithological make up of the upper sedimentary group is predominantly defined by the type of greenstone belt; however, most are comprised of terruginous clastic deposits such as conglomerates, greywackes and quartzites (Windley, 1995).

Lithostratigraphy.

The Zimbabwean greenstone belts have traditionally been subdivided into three age groups (Sebakwian ~ *c.* 3.75 - 3.8 Ga (Dodson *et al.*, 1988); Belingwe ~ *c.* 2.9 Ga (Moorbath *et al.*, 1987) and Bulawayan ~ *c.* 2.7 Ga (Wilson, 1981)), with the top section of the Bulawayan Belt representing the sedimentary group of other greenstone belts. Figure 7.1 illustrates the lithostratigraphy of the three groups.

It is apparent that there are some similarities between the Maunde Ophiolite and Kaourera Island - Arc Groups and the 'Zimbabwean' type greenstone belts, namely :- both have serpentinised ultramafics, mafic pillow lavas, mafic to felsic volcanics and quartz - mica schists. But, there are also major differences between the two, such as :- komatiites and banded iron formations.

Komatiitic lavas were prevalent within the Archean but have few Phanerozoic or Proterozoic analogues. The komatiitc lava suite are

characterised by a range of high MgO contents, from ~ 18 wt% (basaltic komatiite) to ~ 33 wt% MgO (peridotitic komatiite) and is interpreted to represent the outpourings from a hotter Archean mantle (i.e., 200 - 300°C hotter) than the present day (Windley, 1995). The quenching of the hot lavas lead to spinifex textures. It is evident that within some greenstone belts, komatiites can comprise upto 10 % of the volcanic section (Middlemost, 1985). The lack of any high MgO lavas within either the Maunde Ophiolite or Kaourera Island - Arc Groups (max. = 11.54 wt% MgO) and the lack of relict spinifex textured lavas indicates that komatiite suite lavas are not present.

Bulawayan Belt 2.6 Ga	Conglomerates, greywackes, quartz - mica schist.
	Komatiites, tuffs, agglomerates, calc - alkaline andesites.
Belingwe Belt 2.9 Ga	Basal conglomerate,mafic pillow lavas, andesites, dacites and calc - alkaline tholeiites.
	Unconformity
Sebakwian Belt 3.75 - 3.8 Ga	Serpentinised Ultramafics, various mafic schists,arenaceous and carbonaceous sediments, Banded Iron Formations.

Fig. 7.1. The lithostratigraphy of the 'Zimbabwean' type greenstone belts, compiled from Windley, (1995).

Volcanic sections of greenstone belts are associated with chemically precipitated sediments including banded iron formations (Windley, 1995) which are characterised by a quartz - magnetite facies. These formations can be of variable thickness, usually only a few metres, but can reach upto 50 m thick in some belts (Windley, 1995). Only one such banded quartz - Fe oxide specimen has been found within the Maunde Ophiolite or Kaourera Island -

Arc Groups (MR [8525 3745] sample [SJ 162]). The specimen was not in - situ and measured 30 cm by 25 cm.

A characteristic sedimentary facies are found within most sections of the greenstone belts. Arenaceous and carbonaceous sediments occur at the base of the Sebakwian Belt; basal conglomerates, alternating sandstones, iron - stones, shale and siltstones occur at the base of the Belingwe Belt while limestones become predominant within the upper sections of the Belingwe Belt (Hunter *et al.*, 1998) and conglomerates, greywackes and quartz - mica schists occur within the upper sections of the Bulawayan Belt (Fig. 7.1). No such sedimentary associations are evident within the Ophiolite Terrane.

From the lithostratigraphy alone, it is concluded that due to the lack of komatiites, banded iron formations and a typical greenstone sedimentary facies, the Ophiolite Terrane does not represent a typical Archean Greenstone Belt.

Structure.

The various greenstone belts of the world, especially those in Zimbabwe are characterised by long (upto 150 km long), curvilinear outcrops and are associated with voluminous, diapiric, granitic intrusions. Recent re - investigation of field structures (Kusky and Kidd, 1992; Dirks & Jelsma,1998) indicates the role of thrust and fold type tectonics; however, most invariably display complex, interfering fold patterns in - between granitic plutons. Although the Ophiolite Terrane is characterised by thrust and fold type tectonics, there is a lack of such complex fold structures.

It might be interpreted that the Kanhungwa Gneisses represent the post intrusive granitic counterpart of greenstone belts. However, the Kanhungwa Gneisses do not show any evidence for diapirism or ballooning as is evident within some granite terrane plutons, such as the Chinamora Batholith in northern Zimbabwe (Dirks *et al.*, 1998). Neither does this group

indicate any evidence for intrusion into the volcanic Maunde Ophiolite and Kaourera Island - Arc Groups. Since no radiometric age determinations exist for the gneisses they could in fact be significantly older or younger than both the Maunde Ophiolite and Kaourera Island - Arc Groups.

The recognition of a Phanerozoic type, spreading centre, 'plumbing system' within the Ophiolite Terrane, the lack of voluminous, intrusive granitic plutons and simple fold and thrust type tectonics without large or minor scale interference fold patterns, indicates that the internal and deformational evolution of the Ophiolite Terrane is unlike that of the Archean Granite - Greenstone Terranes.

Age of the Ophiolite Terrane.

The identification of Early Proterozoic 'ophiolites' such as the 1.96 Ga Jormua Ophiolite in Finland (Kontinen, 1987) suggests that modern day oceanic type crustal processes were operating at this time and that greenstone belt processes (interpreted as either primitive oceanic crust / island arc crust / oceanic island crust or as ensialic volcanogenic basins) did not last much beyond the Archean (Windley, 1995). The 1393 ± 22 Ma U / Pb SHRIMP age for the magmatic zircon within the plagiogranite dyke [SJ 106] of the Maunde Ophiolite Group indicates that the Ophiolite Terrane developed well within the period where Phanerozoic type crustal processes were operating.

Conclusions.

In conclusion, the lithostratigraphy, structure and age of the Ophiolite Terrane is most similar to that of Phanerozoic ophiolites rather than Archean Greenstone Belts. The Ophiolite Terrane is interpreted as a segment of marginal basin crust, overlain by a predominantly low - K tholeiitic and a calc - alkaline island arc complex, interleaved with a relict seamount.

7.4 Geodynamic evolution of Chewore Inliers and surrounding terranes.

7.4.1 *Geodynamic Evolution of the Ophiolite Terrane.*

The U / Pb SHRIMP magmatic zircon age of 1393 ± 22 Ma is interpreted to represent the minimum age of opening / initiation of the marginal basin. Furlong *et al.*, (1982) indicates that in Phanerozoic examples, back arc spreading and the initiation of mantle convection only occurs when the subducting lithospheric plate is > 80 Ma old such that it is consequently cold and dense. If simple ocean - ocean type subduction is inferred for the Ophiolite Terrane, then this suggests that oceanic type lithosphere was being produced within a constructive margin for at least some > 80 Ma prior to the > 1393 Ma (i.e. > 1470 Ma) back arc spreading (Fig. 7.2). The presence of calc - alkaline volcanics is interpreted by Wilson (1994) and Baker (1973) to indicate that an island arc system was temporally within its middle stages. The time scale for the evolution from tholeiitic to calc - alkaline volcanism is unknown since age constraints for Phanerozoic examples are poorly understood. Most Phanerozoic ophiolites of marginal basin origin are interpreted to have been obducted within 20 Ma of their production at the constructive ridge (Windley, 1995). If the same is assumed for this study, then the obduction of the Maunde Ophiolite Group occurred at *c.* 1370 ± 22 Ma. It is unclear whether obduction was associated with the accretion of the island arc system (Kaourera Island - Arc Group) or whether accretion occurred at a later date.

From sections 4.3 and 5.2 it is interpreted that the Ophiolite Terrane has undergone at least one period of amphibolite facies metamorphism (M_1) and associated deformation which is correlated by Goscombe *et al.*, (1998) with M_2 metamorphism in the Zambezi and Granulite Terranes in the north. Goscombe *et al.*, (1997) dates this amphibolite facies, M_2 metamorphism at 524 ± 16 Ma. Since the Ophiolite Terrane does not show any evidence of a previous metamorphic or deformational event it is interpreted that after the

Mid - ocean ridge initiation (>1470 Ma)
+ Island Arc Initiation (>1393 Ma)

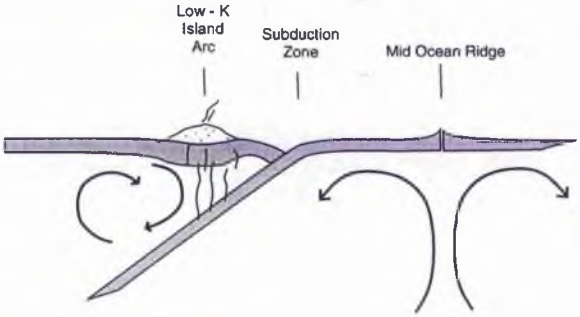

1393±22 Ma: Marginal Basin Formation

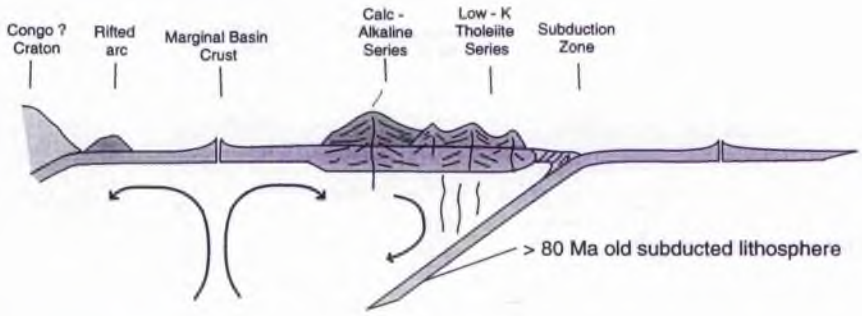

<1393±22 Ma: Evolution of Arc

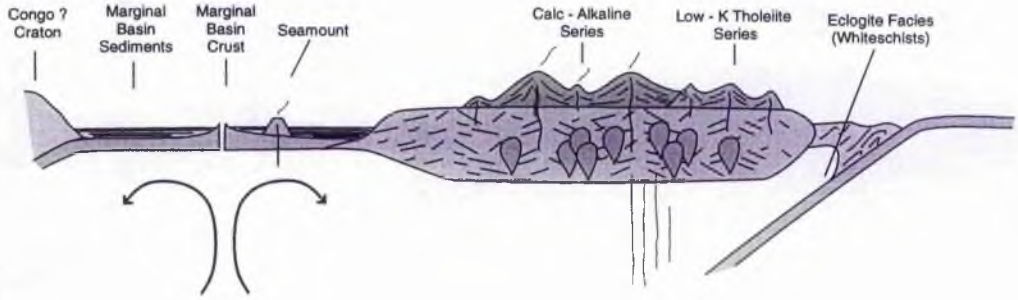

Obduction of Marginal Basin Crust (*c.* 1370 Ma ?)
Accretion of Island Arc (< 1370 Ma)

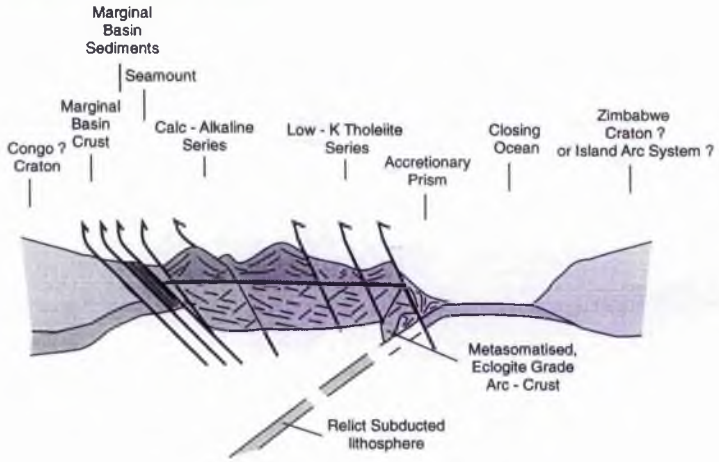

Fig. 7.2 Cartoon sections illustrating the evolution of the Ophiolite Terrane. For discussion refer to text.

accretion of the arc complex, the Maunde Ophiolite and Kaourera Island - Arc Groups have remained tectonically inactive until this amphibolite facies event (sometime between 1370 and 524 Ma). It is possible however, that a previous period of metamorphism and deformation has been completely overprinted by the 524 Ma, M_2 metamorphic cycle as is the case within many poly - deformational orogenic belts i.e. the Ubendian (Ring, 1993) and Kaoko Belts (Durr & Dingerly, 1996). Evidence such as relict mineral assemblages and / or fabrics within low strain zones or as inclusions within the cores of prograde metamorphic porphyroblasts have yet to be identified within the Ophiolite Terrane. It is unclear as to the cause of such an extended tectonic hiatus (*c.* 800 Ma) within this terrane.

7.4.2 *Geodynamic evolution of the Chewore Inliers.*

Figure 7.3 illustrates the major, radiometrically dated tectonic events within the various Chewore Inlier terranes, i.e. the Zambezi, Quartzite and Granulite Terranes (based on Goscombe *et al.*, 1998) and the Ophiolite Terrane (this study).

There is no age constraint for the protoliths of the Granulite or Zambezi Terranes. The oldest radiometric age data is for an intrusive orthogneiss unit which is U / Pb SHRIMP dated at 1071 ± 8 Ma and 1083 ± 8 Ma for the Zambezi and Granulite Terranes respectively (Goscombe *et al.*, 1998) thus suggesting that the two terranes were perhaps amalgamated at this time. From *c.* 1100 Ma both terranes display a similar tectonic history (Fig 7.3). Metamorphic zircons from the Granulite Terrane have been SHRIMP dated by Goscombe *et al.*, (1998) at 943 ± 34 Ma and are interpreted to represent peak metamorphism (M_1) within this terrane. M_1 metamorphism is characterised by high *T*, low *P*, granulite facies with an anticlockwise *PT* path and is responsible for the near anhydrous mineral assemblages within the

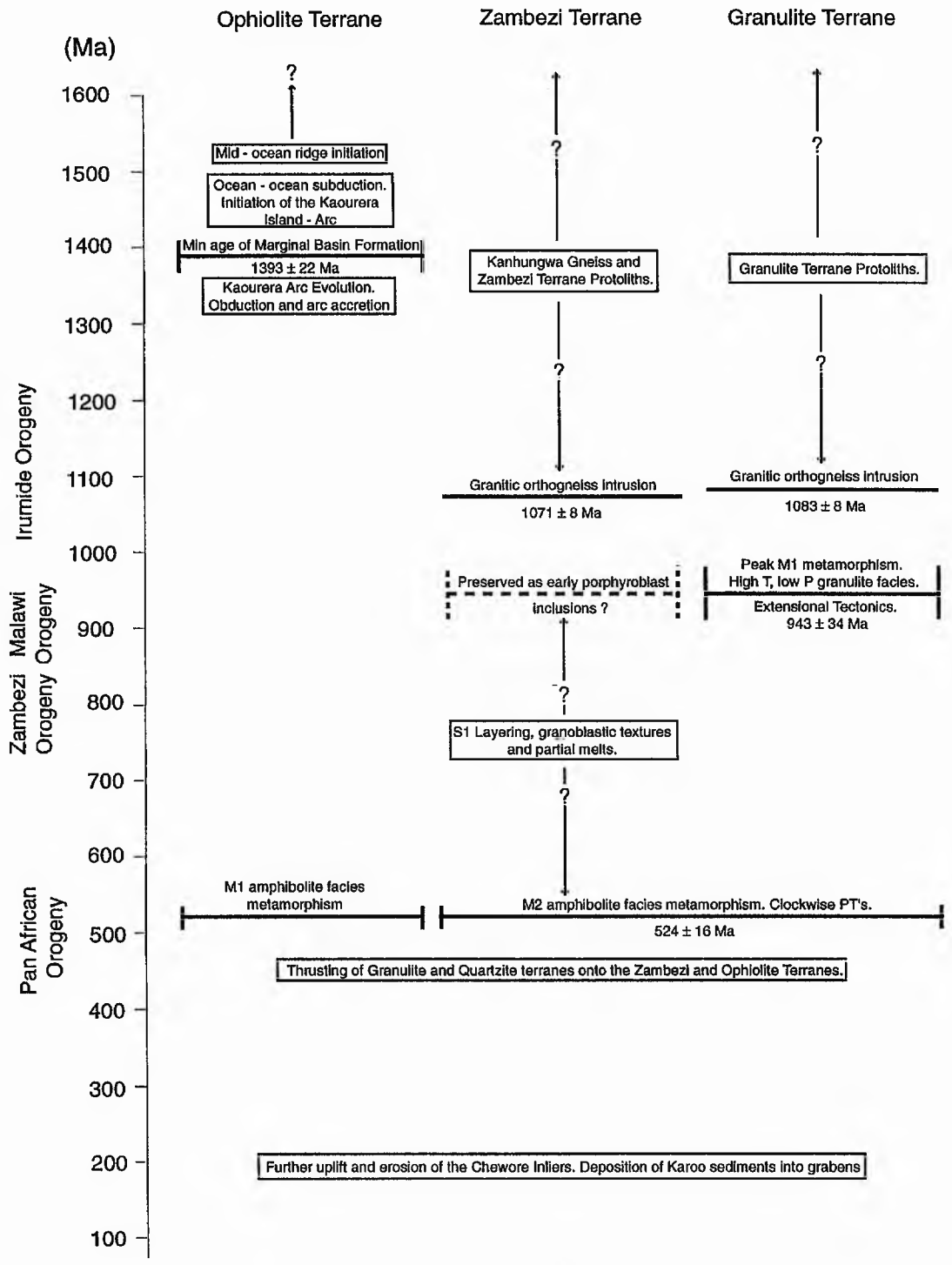

Fig. 7.3 Diagram illustrating the geodynamic evolution of the various Chewore Inlier terranes. Data compiled from this study and Goscombe *et al.*, (1994, 1997, 1998).

Granulite Terrane. Sillimanite and hercynite inclusions within the cores of early M_2 porphyroblasts within the Zambezi Terrane is evidence that this terrane experienced the M_1 metamorphic cycle. High *T*, low - moderate *P* granulites and associated anticlockwise *PT* paths have been interpreted by many authors (Sandiford & Powell, 1986; Appel *et al.*, 1997; Gibson & Ireland, 1995) to indicate extensional tectonics within continental plates. The lack of evidence for granulite facies and / or high *T* metamorphism (M_1) within the Ophiolite Terrane suggests that this terrane was separated from the Zambezi and Granulite Terranes at this time. The Zambezi and Granulite Terranes, therefore underwent a period of extensional tectonics at *c.* 943 ± 34 Ma which might be related to the breakup of the supercontinent of Rodinia (Oliver *et al.*, 1998).

The parallelism of D_2 deformation fabrics within the Ophiolite, Zambezi and Granulite Terranes indicate that juxtaposition occurred during D_2. The M_2 (M_1 within the Ophiolite Terrane) metamorphic cycle peaked within the amphibolite facies (section 4.3.1) and is associated with a clockwise *PT*t path constant with that of a collisional, crustal thickening tectonic event. Peak M_2 (M_1 within the Ophiolite Terrane) metamorphism has possibly been dated by Goscombe *et al.*, (1998), from zircon overgrowths in the Granulite Terrane at 524 ± 16 Ma. The high *P*, moderate *T* metamorphism of the Kadunguri Whiteschists are somewhat inconsistent with both the M_1 and M_2 cycle. Peak metamorphic *PT*'s suggest a minimum geothermal gradient of 10°C / km which is similar to subduction zones. It is possible that this high *P*, moderate *T* metamorphism is related to subduction of the lithospheric plate under the island - arc system. These rocks may have remained buried at such depth until their exhumation during the M_2 (M_1 within the Ophiolite Terrane) cycle within a crustal scale shear zone.

Thrusting during the M_2 (M_1 within the Ophiolite Terrane) metamorphic cycle is responsible for the uplift and erosion of the Chewore

Inliers. Further uplift and erosion was caused by brittle, extensional tectonics during the Permian period and the deposition of Karoo sandstones into graben basins (Fig. 7.3).

7.4.3 *Regional Synthesis*

The presence of the marginal basin crust and island - arc complex within the Chewore Inliers is direct evidence for the full oceanic separation of the Zimbabwe and Congo Cratons at 1393 ± 22 Ma. Such an arrangement is also supported by Rogers (1996) who indicates that both the Zimbabwe and Kalahari Cratons were part of a separate continent entitled "Ur". Figure 7.4 illustrates the spatial distribution of the main deformation events within the tectonic belts of central southern Africa. It is evident that the belts associated with Grenvillian aged orogenesis (1.2 - 1.0 Ga) or the break up of the Rodinia supercontinent occur to the north (i.e., within the Congo Craton) of the Ophiolite Terrane (Andreoli, 1984; Sacchi *et al.*, 1984; Hanson *et al.*, 1988; Rumvegeri, 1991; Goscombe *et al.*, 1994; Kampunzu, 1997). The Ophiolite - Zambezi Terrane boundary marks the southernmost limit to this deformation event. No Grenvillian aged tectonism is evident within the Zimbabwe Craton indicating that the Congo and Zimbabwe Cratons were still separate at this time .

The Zambezi Belt in northern Zimbabwe and Zambia (i.e., south of the Ophiolite Terrane) displays a major orogenic episode at *c.* 860 Ma (Munyanyiwa & Blenkinsop, 1994; Hanson *et al.*, 1988, 1993, 1994; Barton *et al.*, 1993; Dirks *et al.*, 1997; Sithole *et al.*, 1997; Vinyu *et al.*, 1997) which is not recorded within any other belt. It is unclear as to the nature of this orogenic cycle which is characterised by high grade amphibolite and granulite facies metamorphism and intense ductile fabrics. Dirks *et al.*, (1997) suggest that this belt represents a crustal scale shear zone which is associated with earliest amalgamation of the Gondwana supercontinent and thus the suturing

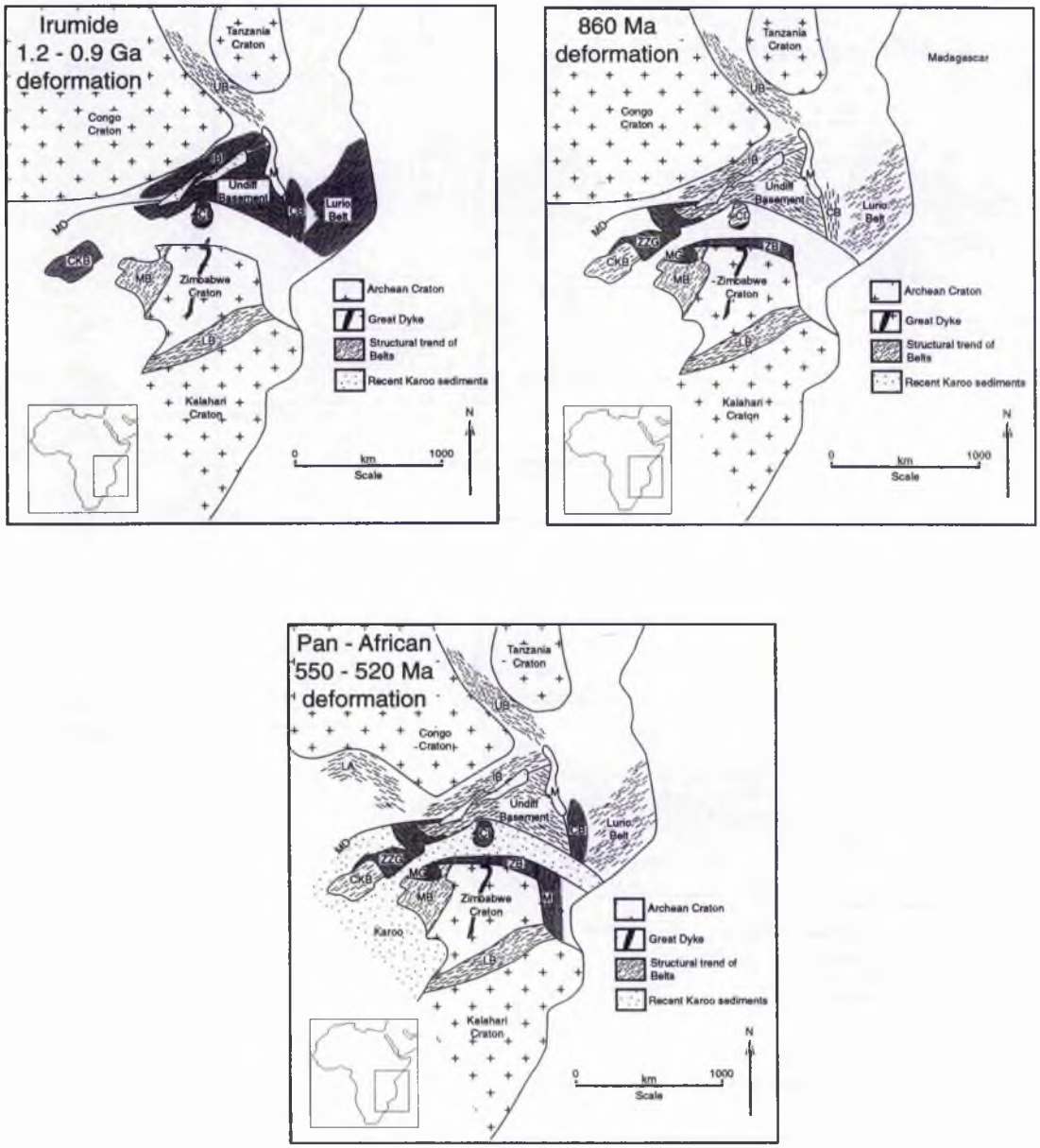

Fig. 7.4 The spatial distribution of the main deformational events within the tectonic belts of central southern Africa. The darkly shaded regions indicate deformation within the associated time period. Abbreviations used are :-CB = Coube Belt; CKB = Choma Kalomo Block; CI = Chewore Inliers; IB = Irumide Belt; LA = Lufillian Arc; LB = Limpopo Belt; LM = Lake Malawi; M = Manica Belt; MB = Magondi Belt; MD = Mwembeshi Dislocation; MG = Makuti Group; ZZG = Zambian Zambezi Group.

together of the Zimbabwe and Congo Cratons. However, the apparent lack of any pre M_2 (M_1 within the Ophiolite Terrane) metamorphic fabrics or minerals within the Ophiolite Terrane and post M_1 / pre M_2 fabrics or minerals within the Granulite and Zambezi Terranes suggests that the Chewore Inliers did not experience this *c.* 860 Ma tectonic event and thus the Zimbabwe and Congo Cratons could not have been sutured at this time. This *c.* 860 Ma event represents a major orogenic episode within the northern margin of the Zimbabwe Craton; however, it is still unclear as to its regional significance.

A plethora of U / Pb zircon ages within the 550 - 520 Ma range (Hanson *et al.*, 1998; Vinyu *et al.*, 1997; Goscombe *et al.*, 1998; Meert *et al.*, 1995; Li & McPowell, 1993; Shackleton, 1996) occur within all belts throughout this region and records the amalgamation of the supercontinent of Gondwanaland. In northern Zimbabwe this event is recorded by resetting of Rb / Sr ages (Barton *et al.*, 1991); ^{40}Ar / ^{39}Ar hornblende cooling ages (Hanson *et al.*, 1998 and Vinyu *et al.*, 1997); syn - tectonic, magmatic zircons (Vinyu *et al.*, 1997) and related deformation. ^{40}Ar / ^{39}Ar cooling ages of 539 ± 6 Ma, are also evident within the Zambian segment of the Zambezi Belt (Hanson *et al.*, 1990). The main M_2 (M_1 within the Ophiolite Terrane) tectonothermal event within the Chewore Inliers is U / Pb SHRIMP dated at 524 ± 16 Ma (Goscombe *et al.*, 1998). The coincidence of all these dates throughout the region, indicates that the Zimbabwe and Congo Cratons were sutured together at this time and is related to the amalgamation of East and West Gondwana (Fig. 7.5). The juxtaposition of the Zimbabwe and Congo Cratons at this time indicates that West Gondwana was divided into a north and south component with a complex, east to west striking suture zone running through the Chewore Inliers (Fig. 7.6) where it is represented by the

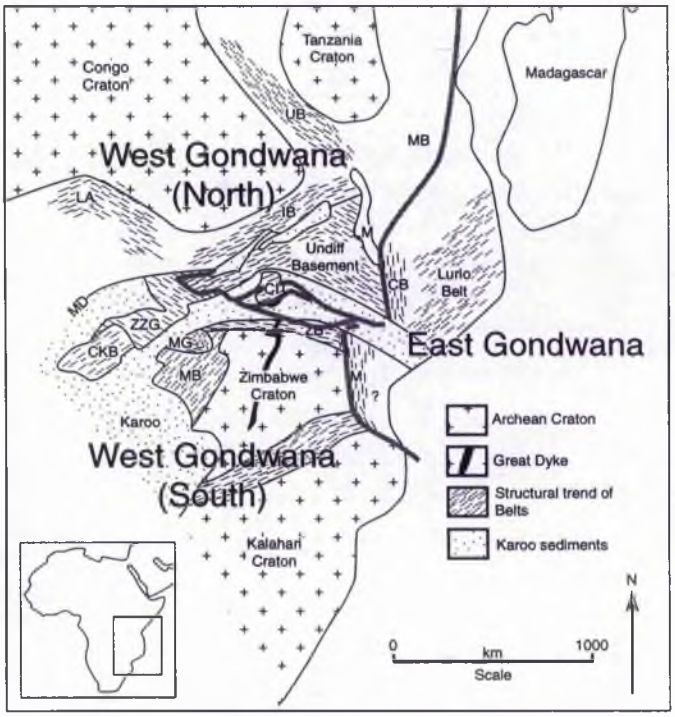

Fig.7.5 Location of the major Gondwana sutures and the position of the east - west trending suture in the Zambezi Belt (dark grey lines) which disects West Gondwana into a north and south component. Abbreviations :- MB - Mozambique Belt; CB - Coube Belt; CI - Chewore Inliers; MD - Mwembeshi Dislocation; LA - Lufilian Arc; ZZG - Zambian Zambezi Group; CKB - Choma Kalomo Block; MG - Makuti Group; MB - Magondi Belt; M - Manica Belt; ZB - Zambezi Belt.

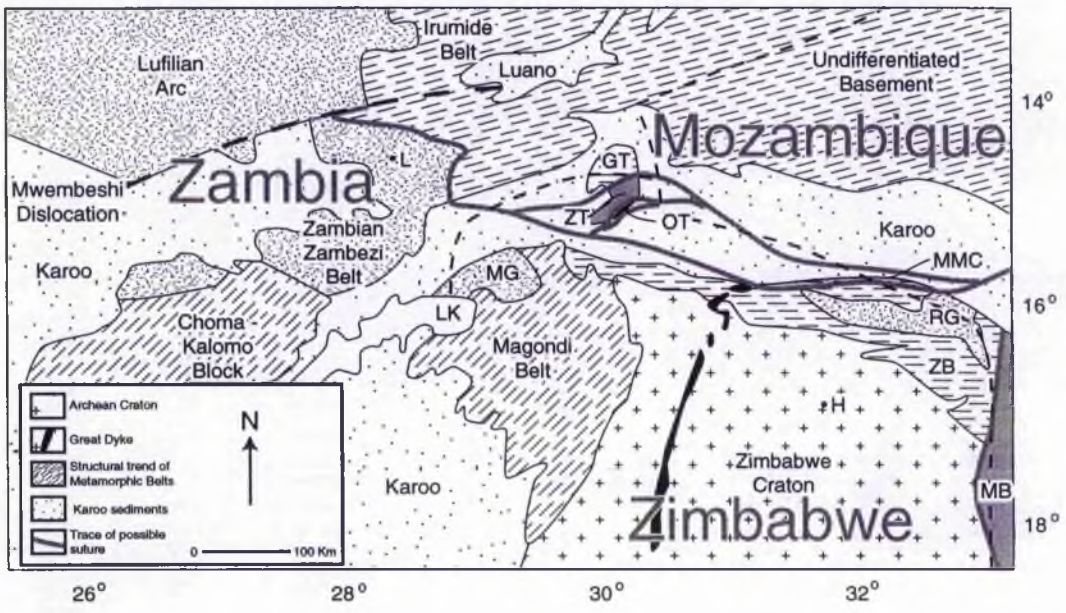

Fig. 7.6 Location of the complex suture zone which divides West Gondwana into a north and south component. Key :- GT, ZT and OT are the components within the Southern Chewore Inliers. LK - Lake Kariba; MG - Makuti Group; MMC - Mavhuradonna Metamorphic Complex; RG - Rushinga Group; ZB - Zambezi Belt; MB - Manica Belt; H - Harare and L - Lusaka.

juxtaposition of the different Chewore terranes. The southern limit to this zone is represented by the juxtaposition of the Mavhuradonha Complex (MMC in Fig. 7.6) with the Zambezi Belt in northern Zimbabwe where Barton *et al.*, (1991) interpret it to be allocthonous to the rest of the Zambezi Belt. The westward continuation of this suture in Zambia is a 200 km long, ultra - high pressure belt characterised by trains of eclogitic and possible ophiolitic fragments (Vrána *et al.*, 1975) which terminate or are displaced by the Mwembeshi Dislocation (Fig 7.6). This suture zone indicates that the Zimbabwe and Congo Cratons were separated at this time by an ocean of unknown extent. Pan - African aged lithologies with ophiolitic affinities have possibly been identified within the Zambian segment of the Zambezi Belt (Vrána *et al.*, 1975); however, their whole rock major element, *REE* and isotope geochemistryhave yet to be validated.

7.4.4 *Conclusions*.

It is concluded that the Zimbabwe / Kalahari and Congo Cratons were juxtaposed and sutured together during the Pan - African amalgamation of the Neoproterozoic supercontinent called Pannotia between 550 and 520 Ma (Dalziel, 1997). The Chewore Inliers represent part of a complex, east - west trending suture, terminating at the Mwembeshi Dislocation, that divides West Gondwana into a northern and southern component indicating oceanic separation prior to the Pan - African suturing.

7.5 Conclusions.

It is concluded that :-

1) The Maunde Ophiolite Group represents a relict, tectonically dismembered ophiolite complex that formed at 1393 ± 22 Ma, within a marginal basin environment. This is apparently the oldest dated ophiolite (*senso stricto*) in Africa.

2) The Kaourera Island - Arc Group represents the relict, tectonically excised island - arc counterpart to the marginal basin. Some basalts within this group indicate the presence of a relict seamount.

3) The Kadunguri Whiteschists are apparently the largest outcrop of whiteschist anywhere in the world and contains the second occurrence of the mineral yoderite. Geochemical analysis suggests that the protolith to this group is metasomatised, island - arc type basalt, similar to those within the Kaourera Island - Arc Group.

4) The Ophiolite Terrane underwent a single period of shear dominated, crustal thickening during the Pan - African Orogeny. Associated metamorphism peaked in the lower and upper amphibolite facies.

5) The mosaic nature of terranes within the Chewore Inliers and surrounding regions suggests that they represent an east to west trending crustal scale suture zone which divides West Gondwana into a northern and southern component, indicating that prior to the Pan - African amalgamation of Gondwanaland the Zimbabwe and Congo cratons were separated by an ocean of unknown extent.

7.6 Future Work.

Future work required as a result of this study include :-

1) Further mapping to refine formation contacts.

2) Geochemical analysis of *REE* and isotopes to re - enforce the geochemical interpretations.

3) Radiometric age dating, particularly U / Pb zircon for dating the Chewore protoliths and ^{40}Ar / ^{39}Ar for dating the amphibolite facies metamorphism.

4) Field investigation of the surrounding terranes, especially the Zambian Segment of the Zambezi Belt to identify Pan - African aged ophiolitic remnants.

References

Abazlov, M. Z. 1998. Chrome - spinels in gabbro - wehrlite intrusions of the Pechenga area, Kola Penninsular, Russia : emphasis on alteration features. *Lithos* **43**, 109 - 134.

Abu - Eid, R. M., Langer, K. & Seifert, F., 1978. Optical absorption and Mössbauer spectra of purple and green yoderite, a kyanite - related mineral. *Physics and Chemistry of Minerals* **3**, 271 - 289.

Andreoli, M. A. G. 1984. Petrochemistry, tectonic evolution and metasomatic mineralisations of Mozambique Belt granulites from south Malawi and Tete (Mozambique). *Precambrian Research* **25**, 16 - 186.

Appel, P., Moller, A. & Schenk, V. 1998. High-pressure granulite facies metamorphism in the Pan-African belt of eastern Tanzania: P-T-t evidence against granulite formation by continent collision. *Journal of Metamorphic Geology* **16**, 491 - 509.

Anonymous, 1972. Penrose field conference on ophiolites : *Geotimes* **17**, 24 25.

Anonymous, 1989. Topographic maps : 1 : 50, 000 sheet nos 1530 C3, "Chimonje". *Department of the Surveyor General, Harare, Zimbabwe.*

Anonymous, 1992. Aeromagnetic maps: 1 : 50,000 sheet nos. 1529 D4 - AM, 1530 C3 - AM, 1629 B2 - AM & 1630 A1 - AM. *Geological Survey of Zimbabwe.*

Baker, P. E. 1973. Volcanism at destructive plate margins. *Journal of Earth Sciences of Leeds* **8**, 183 - 195.

Barton, C. M., Carney, J. N., Crow, M. J., Dunkley, P. N. & Simango, S. 1991. The geology of the country around Rushinga and Nyamapanda. *Zimbabwe Geological Survey Bulletin* **92.**

Barton, C. M., Evans, J. A., Carney, J. N., Crow, M. J. & Simango, S. 1993. Geological and structural framework of the Zambezi Belt, northeastern Zimbabwe. *Gondwana Eight, Findlay, Unrug, Banks & Veevers (eds)* 55 - 68.

Basaltic Volcanism Study Project, 1981. *Basaltic Volcanism on the Terrestrial Planets.* New York : Pergamon Press.

Berman, R. G. 1990. Mixing properties of Ca - Mg - Fe - Mn garnets. *American Mineralogist* **75**, 328 - 344.

Bickle, M. J., Nisbet, E. G. & Martin, A. 1994. Archean Greenstone Belts are not oceanic crust. *Journal of Geology* **102**, 121 - 138.

Bodenlos, A.J., 1955. Magnesite deposits of the Serra das Èquas, Brumado, Bahia, Brazil. *U.S. Geological Survey Bulletin* **975**, 87 - 170.

Both, F. 1991. The geology of the Chewore Inliers (Mid - Zambezi Valley) - a preliminary report. *ANNALS of the Zimbabwe Geological Survey* **XV**, 6 - 10.

Both, F. 1992. A further report on the geology of the Chewore Inliers (Mid - Zambezi Valley). *ANNALS of the Zimbabwe Geological Survey* **XVI**, 6 - 9.

Brekke, H., Furnes, H., Nordås, J. & Hertogen, J. 1984. Lower Palaeozoic convergent plate margin volcanism on Bømlo, SW Norway, and its bearing on the tectonic environments of the Norwegian Caledonides. *Journal of the Geological Society of London* **141**, 1015 - 1032.

Brouxel, M., Lecuyer, C., & Lapierre, H. 1989. Diversity of magma types in the lower Paleozoic island arc - marginal basin system (Eastern Klamath Mountains, California, U.S.A). *Chemical Geology* **77**, 251 - 264.

Canbis, B. & Lecolle, M. 1989. Le diagramme La / 10 - Y / 15 - Nb / 8 : un outil pour la discrimination des series volcaniques et la mise un des processus de melange et / ou de contamination crustale. *C. R. Acad. Sci. Ser II*, **309**, 2023 - 2029.

Carmichael, I. S. E., 1964. The petrology of Thingmuli, a Tertiary volcano in eastern Iceland. *Journal of Petrology* **5**, 435 - 460.

Coleman, R. G. 1977. Ophiolites. *Springer - Verlag Berlin, Heidelberg.*

Curtis C. D. & Brown P.E., 1969. The metasomatic development of zoned ultrabasic bodies in Unst, Shetland. *Contributions to Mineralogy and Petrology* **24**, 275-292.

Daly, M. C & Coward, M. P. 1984. Crustal lineaments and shear zones in Africa - their relationship to plate movements. *Precambrian research* **24**, 24 -45.

Dalziel, I. W. D. 1997. Neoproterozoic-Paleozoic geography and tectonics: Review, hypothesis, environmental speculation. *Geological Society of America Bulletin* **109**, 16 - 42.

Deer, W. A., Howie, R. A & Zussman, J. 1992. An introduction to the rock forming minerals. *Longman.*

Dickenson, M. P & Hewitt, D. 1986. A garnet - chlorite geothermometer. *Geological Society of America Abstracts* **18**, 584.

Dirks, P. G. M., Kroner, A., Jelsma, H. A. & Vinyu, M. L. 1997. The Makuti Group (NW Zimbabwe): a suture zone in the Zambezi Belt. *Abstract.*

Intraplate magmatism and tectonics of southern Africa conference, Harare, Sept. 1997. 12 - 13.

Dirks, P. G. M. & Jelsma, H. A. 1998. Horizontal accretion and stabilisation of the Archean Zimbabwe Craton. *Geology* **26**, 11 - 14.

Dodson, M. H., Compston, W., Williams, I. S. and Wilson, J. F. 1988. A search for anchient detrital zircons in Zimbabwean sediments. *Journal of the Geological Society of London* **145**, 977 - 983.

Durr, S. B. & Dingerly, D. P. 1996. The Kaoko belt (Namibia): part of a late Neoproterozoic continental - scale strike - slip system. *Geology* **24**, 505 - 506.

Elthon, D. 1991. Geochemical evidence for formation of the Bay of Islands Ophiolite above a subduction zone. *Nature* **354**, 140 - 143.

Ferry, J. M. & Spear, F. S. 1978. Experimental calibration of the partitioning of Fe and Mg between biotite and garnet. *Contributions to Mineralogy and Petrology* **66**, 113 - 117.

Fockenberg, T. & Schreyer, W., 1991. Yoderite, a mineral with essential ferric iron: its lack of occurrence in the system MgO - Al_2O_3 - SiO_2 - H_2O. *American Mineralogist* **76**, 1052 - 1060.

Fockenberg, T. & Schreyer, W., 1994. Stability of yoderite in the absence and in the presence of quartz: an experimental study in the system MgO - Al_2O_3 - Fe_2O_3 - SiO_2 - H_2O. *Journal of Petrology* **35**, 1341 - 1375.

Furlong,K. P., Chapman, D. S. & Alfeld, P. W. 1982. Thermal modelling of the geometry of subduction with implications for the tectonics of the overriding plate. *Journal of Geophysical Reviews* **87**, 1786 - 1802.

Furman, T., Frey, F. & Park, K. H. 1995. The scale of source heterogeneity beneath the eastern neovolcanic zone, iceland. *Journal of the Geological Society of London* **152**, 997- 1002.

Ganguly, J. & Saxena, S. K. 1984. Mixing properties of aluminosilicate garnets : constrains from natural and experimental data and implications to geothermo - barometry. *American Mineralogist* **69**, 88 - 97.

Geological Survey Department Nicosia, 1987. Field excursion guidebook. *symposium, Troodos 1987, Ophiolites and Oceanic Lithosphere, Nicosia, Cyprus, 4 - 10 October, 1987.*

Gerlach, D. C., Leeman, W. P. & Lallemant, H. G. 1981. Petrology and geochemistry of plagiogranite in the Canyon Mountain Ophiolite, Oregon. *Contributions to Mineralogy and Petrology* **77**, 82 - 92.

Gibson, G. M. & Ireland, T. R. 1995. Granulite formation during continental extension in Fjordland, New Zealand. *Nature* **375**, 479 - 482.

Goscombe, B., Fey, P. & Both, F., 1994. Structural evolution of the Chewore Inliers, Zambezi Mobile Belt, Zimbabwe. *Journal of African Earth Sciences* **19**, 199 - 224.

Goscombe, B., Armstrong, R., Barton, J. M. 1997. Partial re- equilibration of high grade basement during the Zambezi / Mozambique orogeny and new SHRIMP data from the Chewore Inliers, Zimbabwe. *Abstract. Intraplate magmatism and tectonics of southern Africa conference, Harare, Sept. 1997.* p16.

Goscombe, B., Armstrong, R., Barton, J. M., 1998. Tectonometamorphic evolution of the Chewore Inliers : partial re- equilibration of high grade basement during the Pan - African Orogeny. *Journal of Petrology* **39**, 1347 - 1384.

Graham, C. M. & Powell, R., 1984. A garnet - hornblende geothermometer: calibration, testing and application to the Pelona Schist, Southern California. *Journal of Metamorphic Petrology* **2**, 13 -21.

Grew, E . S., Pertsev, N. N., Vrána, S., Yates, M. G., Shearer, C. K. & Wiedenbeck, M., 1998. Kornerupine paragenesis in whiteschists and other magnesian rocks: is kornerupine + talc a high - pressure assemblage equivalent to tourmaline + orthoamphibole? *Contributions to Mineralogy and Petrology* **131**, 22 - 38.

Gribble, R. F., Stern, R. J., Newman, S., Bloomer, S. H. & O'Hern, T. 1998. Chemical and isotopic composition of lavas from the Northern Mariana Trough : implications for magmagenesis in back - arc basins. *Journal of Petrology* **39**, 125 - 154.

Hanson, R. E., Wilson, T. J., Bruekner, H. K., Onstott, T. C., Wardlaw, M. S., Johns, C. C., Hardcastle, K. C., 1988. Recconnaissance geochronology, tectono - thermal evolution and regional significance of the Middle Proterozoic Choma - Kalomo block, southern Zambia. *Precambrian Research* **42**, 39 - 61.

Hanson, R. E., Wilson, T. J., Wardlaw, M. S. & Onstott, T. C. 1990. Nature and timing of depositional and orogenic events in the Late Proterozoic (Pan - African) Zambezi belt, Zambia. *Abstracts Geological Society of America Programmes* **22**, A264.

Hanson, R. E., Wardlaw, M. S., Wilson, T. J.& Mwale, G. 1993. U - Pb zircon ages from the Hook granite massif and Mwembeshi dislocation : constraints on Pan - African deformation plutonism and transcurrent shearing in central Zambia. *Precambrian Research* **63**, 189 - 209.

Hanson, R. E., Wilson, T. J., Munyanyiwa, H., 1994. Geologic evolution of the Neoproterozoic Zambezi Orogenic Belt in Zambia. *Journal of African Earth Sciences* **18**, 135 - 150.

Harte, B. & Graham, C. M. 1975. The graphical analysis of greenschist to amphibolite facies mineral assemblages in metabasites. *Journal of Petrology* **16**, 347 - 370.

Hawkins, J. W., Lonsdale, P. F., Macdougall, J. D. & Volpe, A. M. 1990. Petrology of the axial ridge of the Mariana Trough backarc spreading center. *Earth and Planetary Science Letters* **100**, 226 - 250.

Hey, M. H. 1954. A new review of the chlorites. *Mineralogical Magazine* **30**, 277.

Higgins. J. C., Ribbe, P. H. & Nakajima. Y., 1982. An ordering model for the commensurate antiphase structure of yoderite. *American Mineralogist* **67**, 76 - 84.

Hodges, K. V. & Crowley, P. D. 1985. Error estimation and empirical geothermobarometry for pelitic systems. *American Mineralogist* **70**, 702 - 709.

Hodges. K. V. & Spear, F. S. 1982. Geothermometry, geobarometry and the Al_2SiO_5 triple point at Mt. Moosilauke, New Hampshire. *American Mineralogist* **67**, 1118 - 1134.

Hoisch, T. D. 1990. Empirical calibration of six geobarometers for the mineral assemblage quartz + muscovite + biotite + plagioclase + garnet. *Contributions to Mineralogy and Petrology* **104**, 225 - 234.

Humphris, S. E. & Thompson, G. 1977. Hydrothermal alteration of oceanic basalts by seawater. *Geochemica Cosmichemica Acta* **42**, 107 -125.

Hunter, M. A., Bickle, M. J., Nisbet, E. G., Martin, A. & Chapman, H. J. 1998. Continental extensional setting for the Archean Belingwe Greenstone Belt, Zimbabwe. *Geology* **26**, 883 - 886.

Irvine, T. N. & Baragar, W. R. A. 1971. A guide to the chemical classification of the common volcanic rocks. *Canadian Journal of Earth Sciences* **8**, 523 - 548.

Johnson, S. P. & Oliver, G. J. H., 1998. A second natural occurrence of yoderite. *Journal of Metamorphic Geology* **16**, 809 - 818.

Kamona, A. F. 1997. Pan - African orogenesis and metallogeny in the Damara - Luffilian fold belt: Lead isotopic evidence from carbonate hosted deposits. *Abstract. Intraplate magmatism and tectonics of southern Africa conference, Harare, Sept. 1997.* p25.

Kampanzu, A. B. 1997. The Kibaran orogenic cycle (ca. 1400 - 100 Ma): review and new perspectives in the framework of Rodinia reconstruction. *Abstract. Intraplate magmatism and tectonics of southern Africa conference, Harare, Sept. 1997.* p25.

Karig, D. E. 1971. Origin and development of marginal basins in the western Pacific. *Journal of Geophysical Research* **76**, 2542 - 2561.

Kohn, M. J. & Spear, F. S. 1989. Empirical calibration of geobarometers for the assemblage garnet + hornblende + plagioclase + quartz. *American Mineralogist* **74**, 77 - 84.

Kohn, M. J. & Spear, F. S., 1990. Two new barometers for garnet amphibolites with applications to eastern Vermont. *American Mineralogist* **75**, 89 - 96.

Kohn, M. J. & Spear, F. S. 1996. Thermobarometry, Version 2.0. A computer program for the analysis of geothermobarometry.

Kontinen, A. 1987. An early Proterozoic ophiolite - the Jormua mafic - ultramafic complex, northern Finland. *Precambrian Research* **35**, 313 - 341.

Korzhinskii, D. S., 1959. *Physiochemical basis of the analysis of the petrogenesis of minerals. Consultants Bureau*, New York.

Kulke, H. G. & Schreyer, W., 1973. Kyanite - talc schist from Sar e Sang, Afghanistan. *Earth and Planetary Science Letters* **18**, 324- 328.

Kusky, T. M. & Kidd, W. S. F. 1992. Remnants of an Archean oceanic plateau, Belingwe greenstone belt, Zimbabwe. *Geology* **20**, 43, - 46.

Le Maitre, R. W. 1989 (Ed.) A classification of igneous rocks and glossary of terms, *Blackwell, Oxford.*

Laird, J. 1988. Chlorites : Metamorphic Petrology. *Reviews in Mineralogy* **19**, 405 - 454.

Laird, J & Albee, A. L. 1981. High pressure metamorphism in mafic schist from northern Vermont. *American Journal of Science* **281**, 97 - 126.

Leake, B. E. 1978. Nomenclature of amphiboles. *American Mineralogist* **63**, 1023 - 1052.

Li, Z. X., & Mc Powell, C. 1993. Late Proterozoic to early Palaeozoic palaoemagnetism and the formation of Gondwanaland. In : *Gondwana Eight* (Edited by Findlay, R. H., Unrug, R., Banks, M. R, & Veevers, J. J.) Balkema, Rotterdam.

Massonne, H. J., 1989. The upper thermal stability of chlorite + quartz : an experimental study in the system MgO - Al_2O_3 - SiO_2 - H_2O. *Journal of Metamorphic Geology* **7**, 567 - 581.

Mahoney, J. J., Jones, W. B., Frey, F. A., Salters, V. J. M., Pyle, D. G., Davies, H. L. 1995. Geochemical characteristics of lavas from Broken Ridge, the Naturaliste Plateau and southernmost Kerguelen Plateau : Cretaceous plateau volcanism in the southeast Indian Ocean. *Chemical Geology* **120**, 315 - 345.

McDonough, W. F. & Sun, S. -S. 1995. The composition of the Earth. *Chemical Geology* **120**, 223 - 253.

McKie, D., 1959. Yoderite, a new hydrous magnesium iron alumino - silicate from Mautia Hill, Tanganyika. *Mineralogical Magazine* **32**, 282 - 307.

McKie, D. & Bradshaw, J., 1966. A green variety of yoderite. *Nature* **210**, 1148.

Meert, J. G., van der Voo, R, & Ayub, S. 1995. Paleomagnetic investigation of the Neoproterozoic Gagwe Lavas and Mbozi complex, Tanzania and the assembly of Gondwana. *Precambrian Research* **74**, 225 - 244.

Meisel, T., Melcher, F., Tomascak, K., Dingeldey, C. & Koller, F. 1997. Re - Os isotopes in orogenic peridotite massifs in the Eastern Alps, Austria. *Chemical Geology*. **143**, 217 - 229.

Meschende, M., 1986. A method of discriminating between different types of mid - ocean ridge basalts and continental tholeiites with the Nb - Zr - Y diagram. *Chemical Geology* **56**, 207 - 218.

Middlemost, E. A. K. 1975. The basalt clan. *Earth Science Reviews* **11**, 337 - 364.

Middlemost, E. A. K. 1985. Magmas and magmatic rocks. *Wiley, New York.*

Moorbath, S., Taylor, P. N., Orpen, J. L., Treolar, P. & Wilson, J. F. 1987. First direct radiometric dating of Archean stromatolitic limestone. *Nature* **326**, 865 - 867.

Mrurma, A. H. & Basu, N. K., 1987. Petrology of the talc - kyanite - yoderite - quartz schist and associated rocks of Mautia Hill, Mpwapwa District, Tanzania. *Journal of African Earth Sciences* **6**, 301 - 311.

Mullen, E. D. 1983. MnO / TiO_2 / P_2O_5 : a minor element discrimination diagram for basaltic rocks of oceanic environments and its implications for petrology. *Earth and Planetary Science Letters* **62**, 53 - 62.

Munyanyiwa, H. & Blenkinsop, T. G. 1994. Pan - African structures and metamorophism in the Makuti Group, north - west Zimbabwe. *Journal of African Earth Sciences* **19**, 185 - 198.

O'Conner, J. T. 1965. A classification of quartz - rich igneous rocks based on feldspar ratios. *U.S. Geological Survey Prof. Paper* **525B**, B 79 - B 84.

Oliver, G. J. H., Johnson, S. P., Williams, I. S. & Herd, D. A., 1998. Relict 1.4 Ga oceanic crust in the Zambezi Valley, northern Zimbabwe: evidence for Mid - Proterozoic supercontinental fragmentation. *Geology*. **26**, 571 - 573.

Passchier, C. W. & Simpson, C. 1986. Porphyroclast systems as kinematic indicators. *Journal of Structural Geology* **8**, 831 - 843.

Pearce, J. A. 1976. Statistical analysis of major element patterns in basalts. *Journal of Petrology* **17**, 15 - 43.

Pearce, J. A. 1982. Trace element characteristics of lavas from destructive plate boundaries. 525 - 548 in Thorpe, R. S. (Ed.), *Andesites*, John Wiley & Sons. Chichester.

Pearce, J. A. 1983. Role of the sub - continental lithosphere in magama genesis at active continental margins. In Hawksworth, C. J. & Norry, M. J. (eds) *Continental basalts and mantle xenoliths*, Shiva, Nantwich pp 230 - 249.

Pearce, J. A. & Cann, J. R. 1973. Tectonic setting of basic volcanic rocks determined using trace elements analyses. *Earth and Planetary Science Letters* **19**, 290 - 300.

Pearce, J. A. & Norry, M. J. 1979. Petrogenetic implications of Ti, Zr, Y and Nb variations in volcanic rocks. *Contributions to Mineralogy and Petrology* **69**, 33 - 47.

Pearce, T. H., Gorman, B. E. & Birkett, T. C. 1977. The relation between major element data and tectonic environment of basaltic and intrusive volcanic rocks. *Earth and Planetary Science Letters* **36**, 121 - 132.

Percival, J. A., Stern, R. A., Skulski, T., Card, K. D., Mortensen, J. K. and Bégin, N. J. 1994. Minto Block, Superior Province: missing link in deciphering assembly of the craton at 2.7 Ga. *Geology* **22**, 839 - 842.

Ramsay, J. G. & Huber, M, I. 1987. The techniques of modern structural geology. Volume 2 : Folds and fractures. *Academic Press, London*.

Ring, U. 1993. Aspects of the kinematic history and mechanisms of superposition of Proterozoic mobile belts of eastern Central Africa (northern Malawi and southern Tanzania). *Precambrian Research* **62**, 207 - 226.

Robinson, P., Spear, F. S., Schumacher, J. C., Laird, J., Klein, C., Evans, B. W. & Doolan, B. L. 1981. Phase relations of metamorphic amphiboles : natural occurrence and theory. *Reviews in Mineralogy* **9B**, 1 - 228.

Rogers, J. J. W., 1996. A history of continents in the past three billion years. *Journal of Geology* **104**, 91 - 107.

Rollinson, H. 1993. Using geochemical data : evaluation, presentation, interpretation. *Longman, Singapore.*

Rumble, D. III. 1971. Chloritiod - staurolite quartzites from the Moosilauke Quadrangle, New Hampshire. *Carnegie Institute of Washington Annula Report Director of Geophysical Laboratories 1969 - 1970* 290 - 294.

Rumvegeri, B. T. 1991. Tectonic significance of Kibaran structures in Central and Eastern Africa. *Journal of African Earth Sciences* **13**, 267 - 276.

Sacchi , R., Marques, J., Costa, M. & Casati, C. 1984. Kibaran events in the southernmost Mozambique Belt. *Precambrian Research* **25**, 141 - 159.

Sandiford, M. & Powell, R. 1986. Deep crustal metamorphism during continental extension : modern and ancient examples. *Earth and Planetary Science Letters* **79**, 151 - 158.

Saunders, A. D. & Tarney, J. 1979. The geochemistry of basalts from a back arc spreading centre in the east Scotia Sea. *Geochemica Cosmichemica Acta* **43**, 555 - 572.

Saunders, A. D., Tarney, J., Marsh, N. G. & Wood, D. A. 1979. Ophiolites as oceanic crust or marginal basin crust : A geochemical approach. In Panayiotou, A. (ed) *Ophiolites : Proceedings International Ophiolite Symposium Cyprus 1979* pp 193 - 204.

Schilling, J. G., Zajac, M., Evans, R., Johnston, T., White, W., Devine, J. D. & Kingsley, R. 1983. Petrology and geochemical variations along the Mid - Atlantic Ridge from 29°N to 73°N. *American Journal of Science* **283**, 510 - 586.

Schreyer, W. 1973. Whiteschist : a high pressure rock and its geologic significance. *Journal of geology* **81**, 735 - 739.

Schreyer, W., 1977. Whiteschists: their compositions and pressure - temperature regimes based on experimental, field, and petrographic evidence. *Tectonophysics* **43**, 127 - 144.

Schreyer, W., 1988. Experimental studies on metamorphism of crustal rocks under mantle pressures. *Mineralogical Magazine* **52**, 1 - 26.

Schreyer, W. & Seifert, F., 1969a. Compatibility relations of the aluminium silicates in the system MgO - Al_2O_3 - SiO_2 - H_2O and K_2O - MgO - Al_2O_3 - SiO_2 - H_2O at high pressures. *American Journal of Science* **267**, 371 - 388.

Schreyer, W. & Seifert, F., 1969b. High pressure phases in the system MgO - Al_2O_3 - SiO_2 - H_2O. *American Journal of Science* **267 - A**, 407 - 443.

Schreyer, W. & Yoder, H. S., 1968. Yoderite: synthesis, stability and interpretation of its natural occurrence. *Carnegie Institute Washington Yearbook* **66**, 376 - 380.

Shackleton, R. M., 1996. The final collision zone between East and West Gondwana : where is it ? *Journal of African Earth Sciences* **23**, 271 - 287.

Simpson, J. G., 1962. The geology of the Mwembeshi river area; explanation of degree sheet 1527, NE. *Quarter of the Geological Survey of Northern Rhodesia* **11**, p29.

Shelly, D. 1983. Igneous and metamorphic rocks under the microscope. *Chapman and Hall.*

Simpson, C. & Schmid, S. M. 1983. An evaluation of criteria to deduce the sense of movement in sheared rocks. *Geological Society of America Bulletin* **94**, 1281 - 1288.

Sithole, T. A., Dirks, P., & Passchier, C. W. 1997. The Makuti Group - A Neoproterozoic supracrustal sequence or a crustal scale shear zone within the Zambezi Belt. *Abstract. Intraplate magmatism and tectonics of southern Africa conference, Harare, Sept. 1997.* p47.

Smith, A. G. 1993. Tectonic significance of the Hellenic - Dinaric ophiolites. In Prichard, H. M., Alabaster, T., Harris, N. B. W. & Neary. C. R. (eds) *Magmatic Processes and Plate Tectonics : Geological Society Special Publication* No 76. pp 213 - 244.

Spear, F. S. 1993. Metamorphic phase equilibria and pressure - temperature - time paths. *Mineralogical Society of America Monograph*, New York.

Spear, F. S. & Cheney, J. T. 1989. A petrogenetic grid for pelitic schists in the system SiO_2 - Al_2O_3 - FeO - MgO - K_2O - H_2O. *Contributions to Mineralogy and Petrology* **101**, 149 - 164.

Suen, C. J., Frey, F. A. & Malpas, J. 1979. Bay of Islands Ophiolite suite, Newfoundland : petrologic and geochemical characteristics with emphasis on rare earth element geochemistry. *Earth and Planetry Science Letters* **45**, 337 - 348.

Taylor, R. N., Murton, B. J. & Nesbitt, R. W. 1992. Chemical transects scross intra - oceanic arcs : implications for the tectonic setting of ophiolites. In Parson, L. M., Murton, B. J. & Browning, P. (eds) *Ophiolites and their Modern Oceanic Analogues : Geological Society Special Publication* No 60. pp117 - 132.

Thompson, R. N. 1982. Magmatism of the British Tertiary Volcanic Province. *Scottish Journal of Geology* **18**, 49 - 107.

Tilley, C. E. 1939. Kyanite - gedrite paragenses. Geological Magazine. **76**, 326 - 330.

Tuttle, O. F. & Bowen, N. L. 1958. Origin of granite in the light of experimental studies in the $NaAlSi_3O_8$ - $KAlSi_3O_8$ - SiO_2 - H_2O. *Geological Society of America Memoir* **74.**

van der Pluijm, B. A. & Marshak, S. 1997. Earth Structure : an introduction to structural geology and tectonics. *McGraw - Hill.*

Vinyu. M. L., Martin, M. W., Bowring, S., Hanson, R., Jelsma, H. A., Dirks, P., 1997. Tectonothermal evolution of the polymetamorphic Zambezi Belt in NE Zimbabwe : constraints from U - Pb single grain zircon data. *Abstract. Intraplate magmatism and tectonics of southern Africa conference, Harare, Sept. 1997.* p52.

Vrána, S., 1975. Magnesian - aluminous rocks, the associated ore mineralisation and the problem of magnesium - iron metasomatism. *Krystalinikum* **11**, 101 - 114.

Vrána, S., 1975. Magnesian - aluminous rocks, the associated ore mineralisation and the problem of magnesium - iron metasomatism. *Krystalinikum* **11**, 101 - 114.

Vrána, S. & Barr M. W. C., 1972. Talc - kyanite - quartz schist and other high pressure assemblages from Zambia. *Mineralogical Magazine* **38**, 837 - 846.

Vrána, S., Prasad, R. & Fediuková, E. 1975. Metamorphic kyanite eclogites in the Lufilian Arc of Zambia. *Contributions to Mineralogy and Petrology* **51**, 139 - 160.

West, H. B., Garcia, M. O., Gerlach, D. C. & Romano, J. 1992. Geochemistry of tholeiites from Lanai, Hawaii. *Contributions to mineralogy and Petrology* **112**, 520 - 542.

Whittaker, A., Cope, J. C. W., Cowie, J. W., Gibbons, W., Hailwood, E. A., House, M. R., Jenkins, D. G., Rawson, P. F., Rushton, A. W. A., Smith, D. G., Thomas, A. T. & Wimbledon, W. A. 1994. A guide to

stratigraphical proceedure. *Journal of the Geological Society of London* **148**, 813 - 824.

Williams, I. S., & Claesson, S., 1987. Isotopic evidence for the Precambrian provenance and Caledonian metamorphism of high - grade paragneisses from the Seve nappes, Scandinavian Caledonides : 2. Ion microprobe zircon U - Th - Pb. *Contributions to Mineralogy and Petrology* **97**, 205 - 217.

Wilson, J. F. 1981. The granite - greenstone shield, Zimbabwe. In D. R. Hunter (Ed.), *Precambrian of the Southern Hemisphere* (454 - 488). Amsterdam : Elsevier.

Wilson, M. 1989. Igneous Petrogenesis. *Chapman & Hall, New York.*

Windley, B., 1995. The Evolving Continents. 3rd Edition *New York, Wiley*

Yardley, B. W. D. 1989. Introduction to metamorphic petrology. *Longman, Harlow.*

Yoder, H. S., 1952. The MgO - Al_2O_3 - SiO_2 - H_2O system and related metamorphic facies. *American Journal of Science* **Bowen Vol**, 569 - 627.

APPENDIX A.

Sample localities and sample descriptions.

This appendix comprises a list of samples collected by the author which are used in this study. Each sample has a unique sample number (prefixed by SJ). The appendix gives a map reference for each sample, gives the specimen a lithological name and indicates its mapping group, formation and member classification. A cross in the TS (thin section), PS (probed section) or XRF (whole rock analysis) donates the use of that sample for thin section, electron microprobe and / or XRF analysis.

Hand samples, thin sections, probe sections and rock powders are held in the Department of Geography and Geosciences, University of St Andrews.

Sample No prefix [SJ...]	Loc	MR	Sample description	Group	Formation	Member	TS	PS	XRF	Tectonic environment
2	2	8505 3662	musc gneiss	Kanhungwa Gneiss	-	-	X	-	-	-
5	5	8512 3676	calc silicate	Kanhungwa Gneiss	-	-	X	-	-	-
10	10	8420 3653	amphibolite	Kaourera	Kamuyu	Banded	X	-	X	OIB
11	11	8432 3655	epidote amphibolite	Kaourera	Kamuyu	Banded	X	-	-	-
22	22	8580 3675	aplite	Kanhungwa Gneiss	-	-	X	-	-	-
24	24	8645 3580	augen gneiss	Kanhungwa Gneiss	-	-	X	-	-	-
25	25	8650 3550	augen gneiss	Kanhungwa Gneiss	-	-	X	-	-	-
27	27	8655 3525	biotite schist	Kanhungwa Gneiss	-	-	X	-	-	-
48	48	8970 3455	garnet mica schist	Kanhungwa Gneiss	-	-	X	-	-	-
62	62	9020 3230	amphibolite	Kaourera	Kamuyu	Banded	X	-	X	OIB
67	67	8985 3305	garnet amphibolite	Kaourera	Kamuyu	Banded	X	X	X	OIB
72	72	9025 3325	amphibolite	Kaourera	Kamuyu	Banded	-	-	-	-
73	73	9055 3310	amphibolite	Kaourera	Kamuyu	Banded	X	-	-	-
77	77	8845 3265	augen gneiss	Kanhungwa Gneiss	-	-	X	-	-	-
78	78	3345 3275	biotite gneiss	Kanhungwa Gneiss	-	-	-	-	-	-
82	82	8810 3300	amphibolite	Kaourera	Kamuyu	Banded	X	-	-	-
94	94	8790 3370	epidote rich granitic gneiss	Kanhungwa Gneiss	-	-	X	-	-	-
95	95	8825 3225	garnet amphibolite	Kaourera	Kamuyu	Banded	X	X	X	OIB
96	96	8875 3330	amphibolite	Kaourera	Kamuyu	Banded	X	-	-	-
100.1	202	9167 3763	semi pelite	Maunde	Nzou	Grey	X	-	-	-
100.2	202	9167 3763	biotite schist	Maunde	Nzou	Dark	X	-	-	-
100.3	203	9165 3766	amphibolite pillow core	Maunde	Mvuu	Pillowed	X	-	X	Marginal Basin
100.4	203	9165 3766	amphibolite pillow rim	Maunde	Mvuu	Pillowed	X	-	X	Marginal Basin
100.5	203	9165 3766	serpentenite	Maunde	-	podiform rock	X	-	-	-
101.1	208	9147 3780	amphibolite	Maunde	Mbizi	Non - amygdaloidal	X	-	-	-
105.1	213 a	9116 3766	serpentenite	Maunde	Ngwena	Pale	X	-	-	-
105.2	213 c	9115 3766	serpentenite	Maunde	Ngwena	Layered	X	-	-	-
105.3	213 f	9114 3768	serpentenite	Maunde	Ngwena	Blue	X	-	-	-
105.4	213 Hb	9113 3771	meta - gabbro	Maunde	Twiza	Massive	X	-	-	-
105.5	213 Ha	9113 3771	hornblendite	Maunde	Ingwe	-	X	-	-	-
106	215	9110 3771	plagiogranite dyke	Maunde	Twiza	plagiogranite dyke	X	-	-	-
107	215.f	9106 3771	ultramyolinite gneiss	Kanhungwa Gneiss	-	-	X	-	-	-
108	217	9166 3651	amphibolite	Kaourera	Nhema	Biotite	-	-	X	Island arc
109	220	9163 3642	banded dacite	Kaourera	Mharapara	-	X	-	X	Island arc

Sample No prefix [SJ...]	Loc	MR	Sample description	Group	Formation	Member	TS	PS	XRF	Tectonic environment
110	222	9159 3731	garnet amphibolite	Kaourera	Nhema	Biotite	X	X	X	Island arc
115.1	229	9141 3714	dacite pillow rim	Kaourera	Gora	-	X	-	X	Island arc
115.2	229	9141 3714	dacite pillow core	Kaourera	Gora	-	-	-	X	Island arc
124	261	9695 3522	Quartz W'schist (Fol)	Kadunguri W'Schists	-	-	X	-	X	-
125	400	9662 3471	Gedrite Whiteschist	Kadunguri W'Schists	-	-	X	X	-	-
126	400	9662 3471	Gedrite Whiteschist	Kadunguri W'Schists	-	-	X	X	X	-
127	425	9642 3471	Gedrite Whiteschist	Kadunguri W'Schists	-	-	X	-	-	-
128	420	9664 3494	Yoderite Whiteschist	Kadunguri W'Schists	-	-	X	X	X	-
129	464	9676 3599	Quartz W'schist (Fol)	Kadunguri W'Schists	-	-	X	-	-	-
130	263	9677 3510	Quartz W'schist (Fol)	Kadunguri W'Schists	-	-	X	-	-	-
132	float		amphibolite	Kaourera	Kamuyu	Banded	X	-	X	Within Plate
133	133	8220 3635	augen gneiss	Kanhungwa Gneiss	-	-	X	-	X	-
134	134	8225 3650	calc silicate	Kaourera	Kamuyu	Calc Silicate	X	X	X	-
135	135	8222 3657	amphibolite	Kaourera	Kamuyu	Banded	X	-	X	Marginal Basin
141	141	8215 3762	dacite	Kaourera	Kamuyu	Banded	X	-	X	Island arc
144.1	144	8165 3650	augen gneiss	Kanhungwa Gneiss	-	-	X	-	X	-
144.2	144	8157 3665	amphibolite	Kaourera	Kamuyu	Banded	X	-	X	OIB
144.3	144	8162 3660	augen gneiss	Kanhungwa Gneiss	-	-	X	-	X	-
144.4	144	8099 3732	augen gneiss	Kanhungwa Gneiss	-	-	X	-	X	-
144.5	144	8105 3742	augen gneiss	Kanhungwa Gneiss	-	-	X	-	X	-
147	147	8099 3732	amphibolite	Kaourera	Kamuyu	Banded	X	-	X	OIB
148.1	148	8105 3748	dacite	Kaourera	Kamuyu	Banded	X	-	X	Island arc
148.2	148	8105 3748	dacite	Kaourera	Kamuyu	Banded	X	-	X	Island arc
152	152	8175 3855	Tonalite gneiss	Kanhungwa Gneiss	-	-	X	-	X	-
156	156	8175 3710	amphibolite	Kaourera	Kamuyu	Banded	X	-	X	Marginal Basin
162.1	162	8505 3748	banded quartz ironstone	Kaourera	-	-	-	-	-	-
162.2	162	8505 3748	banded quartz ironstone	Kaourera	-	-	-	-	-	-
163	163	8478 3745	amphibolite	Kaourera	Kamuyu	Banded	X	-	X	OIB
165	165	8463 3718	amphibolite	Kaourera	Kamuyu	Banded	X	-	X	Marginal Basin

Sample No prefix [SJ...]	Loc	MR	Sample description	Group	Formation	Member	TS	PS	XRF	Tectonic environment
202	202	9167 3763	biotite schist	Maunde	Nzou	Dark	X	-	-	
203	203	9165 3766	amphibolite	Maunde	Mvuu	Massive	X	-	X	Marginal Basin
205	205	9158 3775	amphibolite	Maunde	Mvuu	Massive	X	-	X	Marginal Basin
206	206	9157 3780	amphibolite	Maunde	Mvuu	Massive	X	-	X	Marginal Basin
208.1	208	9151 3781	amygdaloidal amphibolite	Maunde	Mbizi	Amygdaloidal	X	-	X	Marginal Basin
208.2	208	9148 3780	amygdaloidal amphibolite	Maunde	Mbizi	Amygdaloidal	X	-	X	Marginal Basin
209	209	9140 3778	amphibolite	Maunde	Mbizi	Non - Amygdaloidal	X	-	X	Marginal Basin
210	210	9136 3775	amphibolite	Maunde	Mbizi	Non - Amygdaloidal	X	-	X	Marginal Basin
211a	211a	9132 3769	amphibolite	Kaourera	Nhema	Biotite	X	-	X	Island arc
211b	211b	9131 3767	dacite	Kaourera	Gora	-	X	-	X	Island arc
211c	211c	9131 3767	amphibolite	Kaourera	Nhema	Biotite	X	-	X	Island arc
211e	211e	9131 3767	amphibolite	Kaourera	Nhema	Biotite	X	-	X	Island arc
211g	211g	9130 3766	amphibolite	Kaourera	Nhema	Biotite	X	-	X	Island arc
211j	211j	9130 3766	amphibolite breccia	Kaourera	Nhema	Biotite	X	-	-	-
211k	211k	9128 3762	dacite	Kaourera	Gondo	-	X	-	X	Island arc
211m	211m	9127 3762	dacite	Kaourera	Gondo	-	X	-	X	Island arc
211n	211n	9126 3761	dacite	Kaourera	Gondo	-	-	-	X	Island arc
213a	213a	9116 3765	serpentenite	Maunde	Ngwena	Pale	X	-	X	-
213b	213b	9116 3766	serpentenite	Maunde	Ngwena	Pale	-	-	X	-
213c	213c	9115 3766	serpentenite	Maunde	Ngwena	Layered	X	X	X	-
213f	213f	9115 3767	serpentenite	Maunde	Ngwena	Blue	X	X	X	-
213g	213g	9115 3767	serpentenite	Maunde	Ngwena	Blue Member	-	-	-	-
213Ha	213Ha	9114 3768	hornblendite	Maunde	Ingwe	-	X	-	X	-
213Hb	213Hb	9114 3768	meta - gabbro	Maunde	Twiza	Massive	X	-	X	-
213Hc	213Hc	9113 3770	meta - gabbro	Maunde	Twiza	Massive	X	-	X	-
213Hd	213Hd	9113 3770	hornblendite	Maunde	Ingwe	-	X	X	X	-
214e	214e	9112 3770	meta - gabbro	Maunde	Twiza	Massive	X	-	X	-
214f	214f	9112 3771	hornblendite	Maunde	Ingwe	-	-	-	X	-
215b	215b	9109 3771	meta - gabbro	Maunde	Twiza	High Strain	X	-	X	-
215f	215f	9106 3771	meta - gabbro	Maunde	Twiza	High Strain	X	-	X	-
215g	215g	9106 3771	meta - gabbro	Maunde	Twiza	High Strain	-	-	X	-

Sample No prefix [SJ...]	Loc	MR	Sample description	Group	Formation	Member	TS	PS	XRF	Tectonic environment
218b	218	9164 3746	amphibolite	Kaourera	Nhema	Biotite	-	-	X	Island arc
219	219	9162 3743	amphibolite	Kaourera	Nhema	Biotite	-	-	X	Island arc
220	220	9163 3741	dacite	Kaourera	Fura	-	-	-	X	Island arc
222A	222	9159 3731	amphibolite	Kaourera	Gondo	-	-	-	X	Island arc
222BI	222	9159 3731	rhyolite	Kaourera	Gondo	-	-	-	X	Island arc
222BII	222	9159 3731	amphibolite	Kaourera	Nhema	Biotite	-	-	X	Island arc
223	223	9159 3717	amphibolite	Kaourera	Nhema	Biotite	-	-	X	Island arc
224	224	9165 3710	amphibolite	Kaourera	Nhema	Biotite	-	-	X	Island arc
226	226	9156 3695	dacite	Kaourera	Gondo	-	X	-	X	Island arc
228	228	9145 3712	amphibolite	Kaourera	Nhema	Biotite	-	-	X	Island arc
229	229	9142 3714	dacite	Kaourera	Gora	-	X	-	X	Island arc
234	234	9133 3723	amphibolite	Kaourera	Nhema	Biotite	-	-	X	Island arc
236	236	9121 3729	granular amphibolite	Kaourera	Nhema	Granular	X	-	X	Island arc
237	237	9115 3724	dacite	Kaourera	Gondo	-	X	-	X	Island arc
240	240	9096 3723	amphibolite	Kaourera	Nhema	Biotite	-	-	X	Island arc
241	241	9081 3710	amphibolite	Kaourera	Nhema	Biotite	-	-	X	Island arc
248	248	9050 3715	dacite	Kaourera	Gondo	-	-	-	X	Island arc
250	250	9044 3717	amphibolite	Kaourera	Nhema	Biotite	-	-	X	Island arc
253	253	9032 3798	amphibolite	Kaourera	Nhema	Biotite	-	-	X	Island arc
256	256	9020 3689	amphibolite	Kaourera	Nhema	Biotite	-	-	X	Island arc
281	281	9149 3750	amphibolite	Kaourera	Nhema	Biotite	-	-	X	Island arc
285	285	9127 3740	epidote amphibolite	Kaourera	Bere	-	X	-	X	Island arc
286	286	9121 3741	amphibolite	Kaourera	Bere	-	-	-	X	Island arc
287.1	287	9121 3741	amphibolite	Kaourera	Nhema	Biotite	-	-	X	Island arc
287.2	287	9114 3741	granular amphibolite	Kaourera	Bere	-	X	-	X	Island arc
289	289	9056 3733	amphibolite	Kaourera	Nhema	Biotite	-	-	X	Island arc
328	328	9082 3761	amphibolite	Kaourera	Nhema	Biotite	-	-	X	Island arc
370	370	9292 3892	gnt - musc schist	Kaourera	Bhumi	Coarse	X	X	-	-
373	373	9247 3930	amphibolite	Kaourera	Nhema	Biotite	-	-	X	Island arc
378	378	9360 3955	gnt - musc schist	Kaourera	Bhumi	Fine	X	-	-	-
382	382	9170 3776	dacite	Kaourera	Gondo	-	-	-	X	Island arc
394	394	9673 3473	Gedrite Whiteschist	Kadunguri W'Schists	-	-	X	-	-	-
426	426	9638 3510	qtz - hematite Sheets	Kadunguri W'Schists	-	-	X	-	-	-
435	435	9620 3532	Phlogopite W'schist	Kadunguri W'Schists	-	-	X	-	-	-
467	467	9655 3520	Quartz Whiteschist (Fol)	Kadunguri W'Schists	-	-	X	-	-	-

Sample No prefix [SJ...]	Loc	MR		Sample description	Group	Formation	Member	TS	PS	XRF	Tectonic environment
474	474	9685	3538	Phlogopite W'schist	Kadunguri W'Schists	-	-	X	-	-	-
479	479	9606	3515	Phlogopite W'schist	Kadunguri W'Schists	-	-	X	-	-	-
482	482	9605	3482	Quartz Whiteschist (Unfol)	Kadunguri W'Schists	-	-	X	-	-	-
497	497	9582	3672	amphibolite	Kaourera	Kamuyu	-	-	-	X	Island arc
498	498	9500	3788	amphibolite	Kaourera	Kamuyu	-	-	-	X	Island arc
499	499	9392	3328	radial gedrite rock	Kadunguri W'Schists	-	-	X	-	-	-

APPENDIX B.

Thin section analyses

This appendix presents the mineralogy of the collected samples from thin section analyses. Map references for all samples are given in Appendix A.

Key to Abbreviations :-

anth - anthophyllite
bi - biotite
chl - chlorite
cr - chromite
cte - calcite
dr - dravite
ep - epidote
gd - gedrite
gn - garnet
hem - hematite
hb - hornblende
ks - K - feldspar
ky - kyanite
mu - muscovite
op - opaques
phl - phlogopite
pl - plagioclase
q - quartz
serp - serpentine
sp - sphene
tl - tourmaline
tlc - talc
tr - tremolite
yod - yoderite

Appendix B.1 Mafic and volcanic Samples

Sample	hb	pl	q	gn	bi	mu	ep	ks	sp	chl	op
10	x	x	x				x				x
11	x	x	x				x				x
62	x	x	x		x		x				x
67	x	x	x	x			x				x
73	x	x	x				x			x	x
82	x	x	x		x						
95	x	x	x	x			x				x
96	x		x				x			x	
100.3	x	x	x				x				
100.4	x	x	x				x		x		
101.1	x	x	x				x		x		x
105.4	x	x									
105.5	x	x									
109		x	x			x	x				x
110		x	x	x	x	x	x		x	x	x
115.1	x	x	x				x				
132	x	x	x				x		x		x
134	x	x	x	x			x	x		x	x
135	x	x	x				x				x
141		x	x	x	x		x				x
144.2	x	x	x				x				x
147	x	x	x		x		x				x
148.1		x	x		x	x	x		x		x
148.2		x	x		x	x	x		x		x
156	x	x	x				x	x			x
163	x	x	x				x	x			x
165	x	x	x				x				
203	x	x	x				x		x		
205	x	x	x				x		x		
206	x	x	x		x		x		x		
208.1	x	x	x				x		x		x
208.2	x	x	x				x		x		x
209	x	x	x				x		x		
210	x	x	x				x		x		
211a	x	x	x				x		x		x
211b	x	x	x				x	x	x		
211c	x	x	x				x		x		
211e	x	x	x				x				
211g	x	x	x				x		x		x
211j		x	x		x		x	x			
211k		x	x		x	x	x				
211m		x	x		x	x	x				
213Ha	x	x									
213Hb	x	x									
213Hc	x	x	x				x				
213Hd	x	x									x
214e	x	x									
215b	x	x	x				x				x
215f	x	x	x				x		x		x

Sample	hb	pl	q	gn	bi	mu	ep	ks	sp	chl	op
226		x	x		x		x				
229		x	x		x		x				
236	x	x	x				x		x		
237		x	x		x	x	x				x
285	x	x	x				x				
287.2	x	x	x				x		x		

Appendix B.2 Granitic and Pelitic Samples

Sample	pl	q	ks	gn	bi	mu	ep	hb	sp	chl	op	tl	cte
2		x			x	x	x		x	x			
5	x	x	x				x	x	x				
22	x	x	x		x	x							
24		x				x	x						
25		x					x						
27		x			x					x			
48		x		x	x	x	x						
77	x	x				x					x		
78													
94		x			x		x						
100.1	x	x			x	x	x		x				x
100.2		x			x	x				x			x
106	x	x			x								
107	x	x	x	x	x							x	
152	x	x					x	x	x				
370		x		x		x				x			
378		x		x		x				x			

Appendix B.3 Ultramafics and Whiteschists

Sample	tr	serp	cr	chl	q	ky	tlc	gd	anth	hem	yod	dr	cte	phlog
100.5	x	x	x	x			x							
105.1			x	x	x		x							
105.2	x		x	x			x							
105.3	x		x				x							
124					x	x	x			x		x		
125					x	x		x		x		x		
126					x	x		x	x	x		x		
127				x	x	x	x			x		x		
128				x		x	x			x	x	x		
129				x	x	x	x			x		x		
130				x	x	x	x			x		x		
213a	x		x	x										
213c	x		x	x										
213f	x	x	x	x			x						x	
394					x	x		x		x		x		
435				x	x	x	x			x		x		x
467				x	x	x	x			x		x		
474				x			x			x		x		x
479				x		x	x			x		x		x
482				x	x	x	x			x		x		
499				x	x	x		x		x		x		
Q + Ky					x	x				x				

APPENDIX C.

Whole rock, major and trace element data

This appendix presents the results of whole rock major and trace element XRF analyses of the samples illustrated in Appendix A.

Samples were jaw crushed and then powdered in a tungsten carbide tema. The resulting powder was used for XRF analyses. The major elements were analyses from fused discs and the trace elements from pressed powder pellets. The analyses were carried out by Mr. A. Calder at the University of St Andrews using a Phillips PW1450/20 XRF spectrometer with a Rh X - ray tube. This had been calibrated using international rock standards.

The precision of the trace element data is presented here (Calder, *pers. comm.*).

Nb	±2	ppm
Zr	±10	ppm
Y	±3	ppm
Sr	±3	ppm
U	±3>5	ppm
Rb	±5	ppm
Th	±5	ppm
Pb	±5	ppm
Ga	±3	ppm
Zn	±3	ppm
Cu	±5	ppm
Ni	±3	ppm
Cr	±5	ppm
Ce	±15	ppm
Sc	±5	ppm
V	±5	ppm
Ba	±30	ppm
La	±10	ppm

Appendix C.1 Maunde Ophiolite Group Meta - basalts

Mvuu Meta - Mafic Volcanic Formation

NAME	SiO2	TiO2	Al2O3	Fe2O3	MnO	MgO	CaO	Na2O	K2O	P2O5	P.LOSS	TOTAL
100.3	40.05	0.83	18.97	14.27	0.2	3.76	19.99	0.22	0.09	0.1	1.55	100.03
100.4	49.33	0.93	16.03	11.4	0.19	7.43	9.65	3.75	0.38	0.11	1	100.20
203.1	48.60	0.78	14.66	11.33	0.22	10.50	9.35	2.99	0.32	0.09	2.00	100.84
205.1	54.51	0.99	15.32	10.14	0.15	5.43	9.36	3.60	0.54	0.13	0.80	100.97
206.1	47.48	0.74	17.00	10.93	0.24	8.47	8.65	2.51	2.66	0.13	1.90	100.71

NAME	Nb	Zr	Y	Sr	U	Rb	Th	Pb	Ga	Zn	Cu	Ni	Cr	Ce	Sc	V	Ba	La
100.3	2	51	21	1024	0	1	2	22	26	62	151	97	118	10	45	265	31	2
100.4	2	50	19	374	0	10	1	8	16	115	15	239	121	11	38	190	167	3
203.1	1	33	16	273	0	10	0	6	15	154	24	270	700	5	42	245	133	1
205.1	4	98	22	280	1	13	5	16	16	92	52	95	136	28	30	249	121	10
206.1	1	46	17	223	0	123	0	45	16	232	26	211	184	9	30	211	831	2

Mbizi Sheeted Dyke Formation

NAME	SiO2	TiO2	Al2O3	Fe2O3	MnO	MgO	CaO	Na2O	K2O	P2O5	P.LOSS	TOTAL
208/1	48.06	1.90	14.00	17.41	0.23	6.01	8.85	1.82	0.99	0.19	1.00	100.46
208/2	47.55	0.80	17.93	11.77	0.16	7.72	9.59	3.07	0.61	0.10	1.30	100.60
209/1	50.35	1.01	13.83	11.85	0.20	9.31	9.88	2.61	0.53	0.14	0.80	100.51
210.00	52.39	1.06	14.51	10.54	0.18	7.47	10.03	2.96	0.34	0.14	0.90	100.52

NAME	Nb	Zr	Y	Sr	U	Rb	Th	Pb	Ga	Zn	Cu	Ni	Cr	Ce	Sc	V	Ba	La
208/1	9	90	30	114	0	35	1	9	21	183	182	73	49	20	44	433	205	4
208/2	1	42	18	313	1	27	1	28	17	101	106	151	77	13	31	200	189	2
209/1	4	93	21	229	0	15	3	2	15	116	108	252	550	31	35	274	126	14
210.00	4	103	21	300	0	5	2	5	16	97	37	149	364	25	38	259	80	10

Appendix C. 2 Maunde Ophiolite Group meta - gabbros, mafic - cumulates and ultramafics

Ingwe Meta - Mafic Cumulate Formation

NAME	SiO2	TiO2	Al2O3	Fe2O3	MnO	MgO	CaO	Na2O	K2O	P2O5	P.LOSS	TOTAL
213HA	46.77	0.70	11.80	9.84	0.23	15.17	12.86	1.27	0.34	0.04	1.40	100.42
213HD	40.99	4.82	9.40	17.89	0.33	13.40	10.69	1.17	0.26	0.05	1.20	100.20
214F	47.36	0.53	10.64	7.66	0.16	17.91	12.44	1.10	0.18	0.03	2.40	100.41

NAME	Nb	Zr	Y	Sr	U	Rb	Th	Pb	Ga	Zn	Cu	Ni	Cr	Ce	Sc	V	Ba	La
213HA	1	13	5	28	0	2	1	0	10	110	16	542	1410	4	51	204	30	0
213HD	7	36	10	27	1	1	0	0	14	100	322	422	515	9	50	948	33	1
214F	1	11	2	26	1	1	0	0	9	86	113	530	1870	3	54	226	27	1

Twiza Meta - Gabbro Formation

NAME	SiO2	TiO2	Al2O3	Fe2O3	MnO	MgO	CaO	Na2O	K2O	P2O5	P.LOSS	TOTAL
215B	43.31	3.89	13.10	15.93	0.18	7.70	12.41	2.09	0.29	0.47	1.20	100.57
215F	46.97	2.27	12.89	13.97	0.22	9.47	11.23	1.95	0.40	0.05	1.00	100.42
215G	45.24	0.72	13.48	14.03	0.23	11.11	12.41	1.38	0.64	0.03	1.10	100.37
213Hc	49.27	0.96	15.95	11.53	0.18	7.08	9.53	3.35	0.66	0.12	2.00	100.63
214E	46.58	0.52	15.59	6.06	0.14	11.79	17.39	0.59	0.12	0.04	1.80	100.62
213Hb	46.34	0.51	16.68	6.68	0.13	10.53	17.60	0.58	0.20	0.03	1.10	100.38
106.1	76.72	0.12	12.99	0.85	0.03	0.32	0.76	6.8	0.14	0.02	1	99.72

NAME	Nb	Zr	Y	Sr	U	Rb	Th	Pb	Ga	Zn	Cu	Ni	Cr	Ce	Sc	V	Ba	La
215B	3	18	11	160	0	8	1	0	19	76	204	73	272	10	50	500	68	1
215F	2	20	7	127	1	12	0	0	19	95	27	200	700	5	42	423	151	1
215G	0	8	11	111	0	35	0	0	15	95	14	224	644	3	56	421	122	0
213Hc	3	79	21	300	1	33	1	1	16	86	72	168	163	20	37	274	85	7
214E	1	10	2	387	0	1	0	2	14	58	34	427	840	4	47	148	30	0
213HB	2	15	3	548	0	5	1	3	14	58	25	365	1045	7	55	183	56	1
106.1	9	72	2	123	0	7	2	2	10	7	5	9	2	27	1	11	44	12

CIPW NORM for SJ 106.1 qtz = 36% alb= 58% an= 4%

Ngwena Ultramafic Formation

NAME	SiO2	TiO2	Al2O3	Fe2O3	MnO	MgO	CaO	Na2O	K2O	P2O5	P.LOSS	TOTAL
105.3	41.1	0.22	2.69	14.29	0.13	30.57	2.09	0.01	0	0	8.6	99.7
213A	44.64	0.33	3.88	14.20	0.17	24.42	8.10	0.01	0.01	0.03	3.80	99.59
213B	42.89	0.41	2.88	11.68	0.17	29.99	3.85	0.01	0.02	0.02	8.00	99.92
213C	42.24	0.27	2.70	21.89	0.15	21.11	8.12	0.02	0.02	0.02	3.50	100.04
213F	38.29	0.30	3.05	12.05	0.14	30.87	3.21	0.01	0.02	0.03	11.70	99.67

NAME	Nb	Zr	Y	Sr	U	Rb	Th	Pb	Ga	Zn	Cu	Ni	Cr	Ce	Sc	V	Ba	La
105.3	0	4	2	1	0	0	1	1	5	113	187	1739	3239	5	13	94	12	3
213A	1	8	1	5	0	1	1	0	9	80	275	980	3970	1	22	110	10	1
213B	1	9	2	4	0	0	1	0	5	89	143	1630	2450	1	17	105	15	0
213C	2	4	2	6	1	0	0	0	8	81	69	722	5000	0	25	157	5	0
213F	1	6	1	10	1	0	0	0	6	100	164	1620	2750	1	16	85	15	1

Appendix C. 3 Kaourera Island - Arc Group.

Bere Amphibolite Formation

NAME	SiO2	TiO2	Al2O3	Fe2O3	MnO	MgO	CaO	Na2O	K2O	P2O5	P.LOSS	TOTAL
285	49.52	1.53	13.90	12.64	0.26	2.97	####	0.13	0.12	0.26	1.70	0.00
286	49.73	0.68	15.20	10.78	0.21	8.64	9.70	3.39	0.23	0.05	2.10	100.28
287.2	48.09	0.66	16.54	11.10	0.18	8.20	####	2.75	0.27	0.07	1.80	100.71
497	44.85	0.82	15.70	16.45	0.20	7.95	####	1.61	0.34	0.07	1.30	100.46
498	45.41	4.44	11.66	20.84	0.28	4.74	9.38	2.21	0.68	0.21	1.20	100.49

NAME	Nb	Zr	Y	Sr	U	Rb	Th	Pb	Ga	Zn	Cu	Ni	Cr	Ce	Sc	V	Ba	La
285	9	150	33	1585	2	1	7	16	29	87	17	50	40	49	38	333	85	23
286	2	31	15	296	2	2	1	0	9	125	10	237	199	6	38	167	72	2
287.2	2	32	16	216	1	5	0	1	14	88	11	206	177	10	36	230	91	3
497	3	43	16	187	1	2	1	0	15	126	72	309	362	9	32	235	58	3
498	7	93	30	144	1	19	4	3	21	180	127	9	19	25	46	463	130	7

Gondo Meta - Felsic Volcanic Formation (Mharapara Member)

NAME	SiO2	TiO2	Al2O3	Fe2O3	MnO	MgO	CaO	Na2O	K2O	P2O5	P.LOSS	TOTAL
211K	69.86	0.92	12.85	4.45	0.08	0.90	2.46	3.25	3.71	0.26	0.90	99.64
211N	69.44	0.95	12.34	5.52	0.07	0.80	2.96	2.38	3.69	0.25	1.40	99.80
222A	63.21	1.65	11.92	11.33	0.29	3.20	2.64	1.76	2.55	0.35	1.10	100.00
222BI	78.89	0.65	8.94	3.73	0.05	1.01	2.16	0.11	2.44	0.24	2.00	100.22
226.00	66.51	0.99	12.81	6.58	0.13	1.53	4.42	4.61	1.06	0.26	1.20	100.10
237.00	69.08	0.91	12.85	6.03	0.06	0.81	2.32	3.39	3.77	0.22	0.65	100.09
248.00	64.60	1.22	12.51	10.20	0.16	1.75	2.60	2.47	2.98	0.41	1.60	100.50
382.00	60.66	1.88	12.86	8.40	0.09	0.13	####	0.05	0.07	0.30	1.30	99.37
211M	68.11	0.93	12.90	6.01	0.09	0.93	3.51	2.98	3.03	0.26	1.20	99.95

NAME	Nb	Zr	Y	Sr	U	Rb	Th	Pb	Ga	Zn	Cu	Ni	Cr	Ce	Sc	V	Ba	La
211K	18	262	40	97	4	157	23	6	20	31	5	11	11	82	10	55	785	40
211N	19	267	41	172	6	117	22	7	18	41	3	8	11	82	12	54	592	40
222A	18	313	53	73	1	141	15	3	24	185	95	9	7	82	18	139	643	39
222BI	25	463	67	26	2	115	18	2	16	23	222	7	4	118	7	29	625	52
226.00	29	518	83	148	7	52	19	1	22	85	56	7	4	95	7	25	643	43
237.00	18	269	43	128	5	157	21	5	17	38	5	9	9	87	10	50	724	45
248.00	22	442	63	213	4	75	17	1	22	262	53	2	3	95	13	29	523	42
382.00	16	295	49	774	4	1	19	16	21	14	11	5	10	93	33	140	84	46
211M	19	269	44	162	6	117	25	12	21	48	8	9	12	87	15	61	493	46

Gora Member

NAME	SiO2	TiO2	Al2O3	Fe2O3	MnO	MgO	CaO	Na2O	K2O	P2O5	P.LOSS	TOTAL
211B	59.42	0.70	15.22	7.51	0.12	2.17	9.32	3.26	1.00	0.16	1.10	99.98
229.00	65.82	0.71	13.32	6.52	0.13	0.08	####	0.23	0.56	0.18	1.30	99.95
115.1	69.93	0.80	13.57	4.81	0.12	0.51	6.22	3.26	0.16	0.19	0.90	100.46

NAME	Nb	Zr	Y	Sr	U	Rb	Th	Pb	Ga	Zn	Cu	Ni	Cr	Ce	Sc	V	Ba	La
211B	13	180	33	337	5	12	13	9	29	50	63	29	63	59	19	178	280	30
229.00	22	492	65	1260	4	12	26	17	23	16	45	5	2	106	14	10	576	51
115.1	3.42	4.32	23	476	70	628	4	7	28	13	18	32	88	10	133	115	11	45

Fura Member

NAME	SiO2	TiO2	Al2O3	Fe2O3	MnO	MgO	CaO	Na2O	K2O	P2O5	P.LOSS	TOTAL
220A	66.14	3.00	15.92	1.96	0.05	0.23	3.05	8.35	0.24	0.46	1.00	100.40

NAME	Nb	Zr	Y	Sr	U	Rb	Th	Pb	Ga	Zn	Cu	Ni	Cr	Ce	Sc	V	Ba	La
220A	24	413	84	61	5	6	14	3	9	14	69	8	11	24	13	224	414	4

Appendix C. 4 Kaourera Island - Arc Group, Nhema Amphibolite Formation

NAME	SiO2	TiO2	Al2O3	Fe2O3	MnO	MgO	CaO	Na2O	K2O	P2O5	P.LOSS	TOTAL
108.1	55.06	2.45	13.16	16.10	0.35	2.39	1.50	2.88	1.46	0.33	4.20	99.85
110.1	46.33	1.01	17.86	15.74	0.21	7.09	1.82	0.91	6.76	0.12	2.70	100.53
211A	54.45	0.97	16.00	8.12	0.17	6.52	7.11	4.38	1.16	0.15	0.70	99.73
211C	64.43	0.64	14.08	6.35	0.12	1.91	7.05	3.45	0.62	0.17	1.20	100.02
211E	48.85	0.81	16.59	10.39	0.18	7.16	8.49	2.65	1.99	0.12	2.80	100.03
218B	54.39	2.51	11.73	15.69	0.29	4.35	1.95	3.00	0.92	0.34	4.90	100.07
219A	48.91	1.05	18.72	10.96	0.11	5.93	2.51	3.44	4.26	0.09	4.20	100.18
222BII	59.62	1.71	10.33	14.07	0.15	4.73	2.68	0.09	3.29	0.22	2.90	99.79
223A	61.29	1.60	11.02	13.39	0.19	4.05	2.50	0.14	3.67	0.40	1.80	100.05
224A	60.85	1.80	12.60	11.90	0.22	1.93	3.48	3.22	2.20	-0.52	1.30	100.02
228	68.48	0.84	12.86	7.32	0.08	1.17	2.29	5.25	1.33	0.23	1.00	100.85
234	44.99	2.39	12.43	18.71	0.26	6.52	11.62	1.77	0.55	0.10	1.40	100.74
236	48.51	0.70	16.75	11.13	0.19	8.55	10.87	2.58	0.43	0.10	0.90	100.71
240	53.32	2.00	13.13	15.32	0.21	3.88	7.10	3.10	1.47	0.25	1.00	100.78
241	53.53	1.59	13.84	12.93	0.18	4.44	7.47	3.66	1.24	0.22	1.00	100.10
253	59.47	1.22	14.07	9.50	0.15	3.12	6.92	2.32	2.36	0.22	1.20	100.55
256	52.15	1.25	14.11	11.25	0.17	8.11	8.82	3.09	0.44	0.14	1.00	100.53
281	50.93	1.06	14.88	11.55	0.19	7.37	11.35	1.19	0.32	0.10	1.30	100.24
287.10	55.96	1.79	13.62	10.35	0.14	3.99	12.30	0.52	0.14	0.24	1.00	100.05
328	55.77	2.06	14.31	11.59	0.16	2.34	7.04	2.47	2.46	0.26	1.30	99.76
351	51.36	0.56	16.21	9.56	0.16	6.73	11.66	2.37	0.37	0.08	1.70	100.76
373	42.49	2.08	14.19	18.98	0.30	8.84	10.48	1.83	0.61	0.06	0.60	100.46
211G	54.80	1.42	14.14	11.27	0.16	5.19	9.02	2.41	0.37	0.21	1.00	99.99
289	48.16	0.76	13.84	11.19	0.19	11.54	10.68	2.37	0.26	0.02	1.70	100.71

NAME	Nb	Zr	Y	Sr	U	Rb	Th	Pb	Ga	Zn	Cu	Ni	Cr	Ce	Sc	V	Ba	La
108.1	4.33	14.49	13	214	36	106	2	64	9	3	23	395	62	17	75	54	36	279
110.1	7.67	14.16	2	49	19	39	0	344	0	0	23	155	94	138	283	7	18	194
211A	20	141	24	325	1	53	8	16	12	110	33	84	64	52	38	235	213	19
211C	10	160	27	315	4	19	9	14	22	50	18	30	66	51	18	183	233	25
211E	2	49	20	231	1	82	2	5	13	105	50	217	195	10	39	243	885	3
218B	12	230	35	116	2	47	7	3	22	222	83	20	21	44	41	272	420	15
219A	1	46	21	149	1	245	0	2	18	101	74	119	110	16	26	204	1370	3
222BII	11	190	40	17	1	232	5	1	21	71	202	32	20	26	24	343	500	9
223A	19	334	59	24	1	235	13	1	18	41	54	9	7	106	17	54	426	45
224A	21	347	63	159	3	99	15	5	22	246	19	6	5	101	20	38	616	52
228	28	478	81	218	4	43	18	10	21	67	51	13	7	97	15	68	478	45
234	2	51	17	140	1	10	2	3	21	157	312	37	53	9	51	1060	162	2
236	1	36	17	172	0	17	0	1	15	81	29	204	174	10	40	235	192	1
240	10	177	36	213	2	65	6	2	21	112	149	48	40	37	33	485	507	13
241	9	157	35	223	1	47	7	5	19	101	200	56	38	34	35	335	526	12
253	12	198	33	211	2	108	8	5	18	109	39	28	20	54	21	239	766	27
256	4	81	20	303	1	13	0	2	17	87	41	160	453	24	35	277	65	7
281	5	90	24	195	2	6	3	2	18	75	132	175	284	24	43	274	148	9
287.10	10	189	38	343	2	0	4	4	18	64	243	61	50	54	35	355	241	24
328	18	282	52	313	3	112	17	10	20	114	5	13	13	80	25	221	555	32
351	3	56	16	220	1	13	4	8	17	73	134	124	37	17	40	177	200	7
373	3	14	14	67	2	23	1	2	21	98	83	88	343	9	51	705	33	3
211G	9	155	33	248	1	6	7	11	21	75	61	60	68	45	36	303	147	18
289	1	25	16	109	1	6	0	0	15	111	10	381	744	5	43	220	35	1

Appendix C. 5 Kaourera Island - Arc Group, Kamuyu Amphibolite Formation.

NAME	SiO2	TiO2	Al2O3	Fe2O3	MnO	MgO	CaO	Na2O	K2O	P2O5	P.LOSS	TOTAL
10	42.46	3.24	13.20	22.80	0.21	5.82	10.52	1.31	0.41	0.08	1.00	101.04
62	48.57	1.01	15.19	11.78	0.22	8.29	12.01	2.32	0.39	0.05	0.90	100.70
67	49.11	2.98	12.52	18.28	0.25	4.97	9.30	1.35	0.46	0.40	1.20	100.79
72	48.06	3.12	11.93	19.18	0.27	4.66	8.72	1.43	0.70	0.38	1.30	99.73
73	49.60	2.73	13.38	16.79	0.23	4.93	8.78	2.27	0.41	0.20	0.90	100.19
75	47.51	2.94	12.61	19.27	0.27	4.17	9.23	2.17	0.90	0.60	1.10	100.76
82.1	50.20	0.78	16.36	11.05	0.20	8.46	6.65	4.27	1.26	0.10	1.00	100.30
82.2	50.11	0.80	16.34	10.55	0.17	8.58	6.35	4.12	1.56	0.09	1.40	100.05
95	49.48	2.54	12.63	18.01	0.25	4.37	9.16	1.33	0.54	0.32	1.90	100.50
132	49.50	2.24	17.63	10.94	0.15	3.89	8.05	3.78	1.13	0.31	2.70	100.30
135	50.97	1.24	14.01	13.48	0.20	7.02	10.97	1.77	0.46	0.11	0.70	100.92
141	68.26	0.96	12.54	7.17	0.14	1.25	2.30	3.50	2.22	0.23	0.90	99.44
144.2	50.65	1.94	13.08	15.48	0.22	5.28	9.84	1.95	0.54	0.19	0.70	99.84
147.1	53.99	2.26	12.65	15.38	0.23	5.05	4.97	3.13	1.64	0.27	0.30	99.84
148.1	66.87	1.09	12.54	7.50	0.10	1.28	2.20	3.16	3.19	0.24	1.10	99.25
148.2	63.30	1.21	12.86	8.96	0.09	3.26	2.11	2.84	3.95	0.23	1.25	100.04
156	48.46	1.33	14.30	17.01	0.29	5.68	9.51	2.59	0.58	0.12	0.40	100.24
165	49.70	1.02	15.17	11.81	0.25	7.47	10.19	2.68	0.52	0.12	1.00	99.90

NAME	Nb	Zr	Y	Sr	U	Rb	Th	Pb	Ga	Zn	Cu	Ni	Cr	Ce	Sc	V	Ba	La
10	2	57	19	159	0	12	2	5	24	141	403	130	112	13	45	1376	172	1
62	2	29	14	213	0	7	1	7	15	127	98	119	271	9	46	295	252	2
67	15	166	48	103	0	5	4	2	21	142	87	39	127	42	40	416	170	16
72	12	141	44	169	0	10	5	4	23	153	154	49	95	34	44	551	185	9
73	8	134	31	207	0	2	4	5	21	118	164	49	143	32	36	479	98	14
75	16	138	46	257	1	23	3	9	24	175	40	29	127	58	37	303	258	17
82.1	2	45	37	122	0	98	0	4	23	109	28	197	301	22	31	243	172	15
82.2	2	47	26	124	0	129	2	5	20	99	9	199	271	16	31	239	188	8
95	13	161	51	156	0	4	5	3	21	132	203	40	161	50	40	451	165	36
132	33	232	28	541	0	30	7	12	24	57	47	79	222	72	24	226	335	29
135	2	62	23	144	0	7	1	6	19	120	53	83	294	17	47	393	76	4
141	17	227	40	178	4	92	21	7	16	425	2	9	119	103	14	48	685	45
144.2	8	118	34	280	0	5	3	3	21	112	324	56	134	29	42	481	119	8
147.1	15	253	55	90	0	56	10	2	20	198	14	13	86	70	32	307	262	33
148.1	19	255	47	192	4	119	23	5	20	60	88	11	156	90	13	86	443	43
148.2	15	214	48	68	2	168	18	3	18	62	6	21	158	96	14	172	592	49
156	3	89	28	217	0	7	3	4	19	145	286	65	127	26	41	424	130	4
165	4	92	24	216	0	10	2	5	16	176	18	125	326	27	39	278	108	8

Appendix C.6 Kadunguri Whiteschists

NAME	SiO2	TiO2	Al2O3	Fe2O3	MnO	MgO	CaO	Na2O	K2O	P2O5	P.LOSS	TOTAL
Foliated	51.95	1.15	15.50	2.29	0.00	18.99	0.11	0.10	0.02	0.07	10.60	100.78
Random	56.37	1.38	16.07	7.59	0.03	16.24	0.02	0.40	0.01	0.06	1.80	99.95
Yoderite	35.46	0.27	23.80	12.97	0.02	20.35	0.18	0.33	0.00	0.05	6.80	100.23
Gedrite	57.16	1.78	15.96	8.66	0.02	13.88	0.06	0.27	0.04	0.08	2.80	100.73

NAME	Nb	Zr	Y	Sr	U	Rb	Th	Pb	Ga	Zn	Cu	Ni	Cr	Ce	Sc	V	Ba	La
Foliated	9	131	12	4	0	1	7	1	6	4	0	54	92	6	9	29	14	2
Random	16	164	29	2	0	1	10	0	25	8	8	128	132	22	27	25	66	9
Yoderite	1	26	2	5	2	0	0	0	52	4	8	69	105	4	29	64	36	1
Gedrite	17	188	21	5	0	2	2	0	5	4	9	50	174	5	20	19	101	1

Appendix C.7 Kanhungwa Gneisses

NAME	SiO2	TiO2	Al2O3	Fe2O3	MnO	MgO	CaO	Na2O	K2O	P2O5	P.LOSS	TOTAL
144.1	75.15	0.18	12.37	1.79	0.05	0.14	0.70	2.17	6.41	0.05	0.50	99.50
144.3	75.67	0.17	12.25	1.35	0.04	0.19	0.69	2.08	6.37	0.05	0.90	99.75
144.4	69.80	0.71	13.59	4.41	0.09	0.83	2.31	2.57	4.73	0.18	0.90	100.11
152.1	63.74	1.08	16.61	2.83	0.04	1.56	6.53	5.65	0.27	0.31	0.00	98.60
166.1	74.19	0.41	12.54	2.68	0.03	0.53	0.58	3.55	4.41	0.10	0.70	99.71
173.1	76.66	0.21	10.97	1.85	0.03	0.12	0.02	0.35	8.45	0.01	0.80	99.46
1.2	63.20	1.11	17.85	2.21	0.03	4.65	0.33	0.33	6.43	0.33	3.20	99.67
1.5	67.31	0.96	14.06	3.64	0.05	1.07	5.52	6.14	0.25	0.28	1.00	100.28
133.0	74.37	0.55	12.27	2.28	0.02	0.81	1.02	3.11	3.98	0.16	1.00	99.57
134.0	37.71	1.35	24.40	13.12	0.18	1.72	18.91	0.22	0.41	0.36	2.00	100.38

NAME	Nb	Zr	Y	Sr	U	Rb	Th	Pb	Ga	Zn	Cu	Ni	Cr	Ce	Sc	V	Ba	La
144.1	4	102	25	77	2	290	79	40	13	22	2	6	155	127	1	15	365	34
144.3	5	115	30	135	3	203	86	34	12	15	14	7	188	120	0	14	713	38
144.4	17	215	50	149	3	223	31	27	16	40	7	13	182	61	7	65	717	38
152.1	29	341	80	500	3	1	37	6	20	10	1	13	114	174	18	83	67	78
166.1	13	164	43	71	6	245	41	13	17	15	1	10	162	133	4	33	400	68
173.1	20	189	15	29	0	549	22	17	10	23	6	8	178	17	0	17	1549	2
1.2	27	350	62	34	4	242	66	3	11	25	70	7	13	35	6	33	556	13
1.5	23	315	76	360	10	2	45	8	20	19	0	10	13	132	15	64	35	81
133.0	20	238	62	121	12	239	57	23	16	19	1	9	9	140	4	38	455	78
134.0	26	440	85	2207	12	19	58	66	42	46	30	22	77	192	38	330	190	95

APPENDIX D.

Microprobe data.

The following appendix presents the results of major element electron microprobe analyses. The analyses were made using a JEOL © JCXA - 733 Superprobe at the University of St Andrews. The operating conditions were :-

Accelerating Voltage	15Kv
Probe current	20nA
Beam diameter	1 - 2μm except for Na plagioclase where the beam was de- focused to 10 μm.

Map references for samples are given in Appendix A.

A, B, C and T for amphibole analyses refer to the atomic sites within the generalised amphibole formula which may be written as :-
$A_{0\text{-}1}B_2C_5T_8O_{22}(OH,F)_2$ (Deer *et al.*, 1992).

Appendix D.1 Maunde Ophiolite Group, Ngwena Ultramafic Formation

Layered Member [SJ 213 C]

	Chromite			Tremolite	Chlorite
	Core	Rim	Core		
SiO2	0.219	0.428	0.245	59.443	31.832
TiO2	0.424	0.040	0.496	0.048	0.044
Al2O3	0.094	0.000	0.046	0.057	13.664
Cr2O3	19.012	4.495	15.388	0.047	0.428
FeO	30.823	30.698	30.555	2.986	3.982
Fe2O3	49.301	62.917	52.046		1.335
MnO	0.798	0.134	0.822	0.153	0.010
NiO	0.150	0.115	0.199	0.045	0.101
MgO	0.421	0.236	0.331	24.724	32.537
CaO	0.000	0.124	0.022	12.490	0.055
Na2O	0.000	0.000	0.000	0.000	0.018
K2O	0.000	0.000	0.000	0.011	0.034
Total	101.242	99.187	100.15	100	84.04
Si	0.07	0.13	0.07	7.93	6.28
Ti	0.10	0.01	0.11	0.01	0.01
Al	0.03	0.00	0.02	0.01	3.18
Cr	4.51	1.10	3.70	0.01	0.07
Fe3+	11.13	14.62	11.91	0.10	0.20
Fe2+	7.74	7.93	7.77	0.23	0.66
Mn	0.20	0.04	0.21	0.02	0.00
Mg	0.19	0.11	0.15	4.92	9.57
Ca	0.00	0.04	0.01	1.79	0.01
Ni	0.04	0.03	0.05	0.01	0.02
Na	0.00	0.00	0.00	0.00	0.01
K	0.00	0.00	0.00	0.00	0.01
Tot	24	24	24	15	20
O2	32	32	32	23	28
			Mg/(Mg+Fe2+)	0.955	

Appendix D.2 Maunde Ophiolite Group, Ngwena Ultramafic Formation

Blue Member [SJ 213 F]

	Chromite									Serpentine			Amphibole		
			2		3			4							
	Core	Rim	Core	Rim	Core	Core	Rim	Core	Rim						
SiO2	0.167	0.174	0.157	0.129	0.296	0.234	0.247	0.134	0.141	40.631	41.203	40.701	59.948	58.018	57.553
TiO2	0.083	0.083	0.246	0.100	0.693	0.859	0.050	0.501	0.038	0.033	0.029	0.000	0.070	0.019	0.000
Al2O3	0.000	0.060	0.082	0.004	0.123	0.226	0.000	0.102	0.004	3.994	4.023	3.985	0.040	0.012	0.003
Cr2O3	5.848	2.215	12.959	2.435	16.309	20.368	1.915	15.654	2.322	0.450	0.411	0.268	0.052	0.000	0.013
FeO	31.020	31.569	30.545	31.080	31.297	46.085	65.858	52.890	66.582	6.356	5.952	6.150	2.483	2.384	2.536
Fe2O3	62.439	67.108	55.380	67.447	51.297	30.648	30.696	29.580	31.197	0.083	0.126	0.061	0.160	0.179	0.208
MnO	0.115	0.046	0.616	0.115	0.669	0.968	0.035	0.719	0.099	-	-	-	-	-	-
NiO	0.240	0.053	0.202	0.089	0.225	0.161	0.089	0.192	0.178	0.159	0.077	0.145	0.038	0.015	0.000
MgO	0.000	0.040	0.253	0.000	0.279	0.467	0.000	0.358	0.000	35.780	35.660	36.521	24.595	23.993	23.695
CaO	0.004	0.000	0.000	0.025	0.007	0.007	0.052	0.144	0.000	0.013	0.020	0.000	11.965	12.349	12.801
Na2O	0.000	0.000	0.000	0.118	0.000	0.000	0.010	0.166	0.000	0.000	0.000	0.000	0.004	0.014	0.022
K2O	0.016	0.026	0.023	0.000	0.000	0.000	0.000	0.051	0.000	0.000	0.032	0.028	0.040	0.015	0.009
Total	99.932	101.374	100.463	101.542	101.195	100.023	98.952	100.491	100.561	87.582	87.659	87.920	99.395	96.998	96.840
Si	0.05	0.05	0.05	0.04	0.09	0.07	0.08	0.04	0.04	Si 1.93	1.94	1.92	Si 8.02	7.97	7.93
Ti	0.02	0.02	0.06	0.02	0.16	0.20	0.01	0.11	0.01	Al 0.07	0.06	0.08	Al 0.00	0.00	0.00
Al	0.00	0.02	0.03	0.00	0.04	0.08	0.00	0.04	0.00	Al 0.15	0.16	0.14	Ti 0.00	0.00	0.00
Cr	1.42	0.53	3.11	0.58	3.87	4.88	0.47	3.74	0.56	Cr 0.02	0.02	0.01	Fe3+ 0.00	0.03	0.07
Fe3+	14.44	15.32	12.66	15.36	11.59	10.51	15.36	12.03	15.33	Fe2+ 0.25	0.24	0.24	Fe3+ 0.00	0.01	0.07
Fe2+	7.97	8.01	7.76	7.89	7.90	7.77	8.03	7.48	7.98	Ni 0.01	0.00	0.01	Mg 4.91	4.91	4.86
Mn	0.03	0.01	0.16	0.03	0.17	0.25	0.01	0.18	0.03	Mn 0.00	0.01	0.00	Fe2+ 0.09	0.10	0.07
Mg	0.00	0.02	0.12	0.00	0.12	0.21	0.00	0.16	0.00	Mg 2.53	2.51	2.57	Fe2+ 0.19	0.13	0.08
Ca	0.00	0.00	0.00	0.01	0.00	0.00	0.02	0.05	0.00	Ca 0.00	0.00	0.00	Mn 0.02	0.02	0.03
Ni	0.06	0.01	0.05	0.02	0.05	0.04	0.02	0.05	0.04	Na 0.00	0.00	0.00	Ca 1.72	1.82	1.89
Na	0.00	0.00	0.00	0.07	0.00	0.00	0.01	0.10	0.00	K 0.00	0.00	0.00	Na 0.00	0.00	0.01
K	0.01	0.01	0.02	0.00	0.00	0.00	0.00	0.02	0.00				K 0.01	0.00	0.00
Tot	24.00	24.00	24.00	24.00	24.00	24.00	24.00	24.00	24.00	5	5	5	15	15	15
O2	32	32	32	32	32	32	32	32	32	7	7	7	23	23	23
													(Ca+Na)B 1.720	1.820	1.890

Appendix D.3 Maunde Ophiolite Group, Ingwe Meta - Mafic Cumulate Formation

Sample [SJ 213 Hd]

		Amphibole							Chlorite	Ilmenite
		1		2	3		4	5		
		Rim	Core	Rim	Rim	Core	Core	Matrix		
SiO2		45.157	45.763	50.346	50.298	45.631	44.465	44.867	27.086	0.124
TiO2		0.388	0.491	0.199	0.293	0.378	0.421	0.430	0.049	50.248
Al2O3		9.576	10.225	6.361	6.484	10.737	11.200	11.261	20.827	0.000
FeO		14.104	11.775	9.565	9.426	11.745	11.427	12.143	13.576	45.926
MnO		0.177	0.185	0.166	0.233	0.143	0.210	0.235	0.196	1.456
MgO		12.843	13.931	16.573	16.741	13.719	13.439	13.661	23.586	0.370
CaO		12.465	11.335	12.302	11.835	11.976	12.218	12.177	0.109	0.030
Na2O		1.444	1.619	1.076	1.026	1.645	1.753	1.544	0.000	0.000
K2O		0.319	0.292	0.113	0.145	0.278	0.313	0.451	0.019	0.000
Total		96.473	95.616	96.701	96.481	96.252	95.446	96.769	85.560	98.394
	Si	6.75	6.79	7.27	7.26	6.74	6.64	6.62	**Si** 5.50	0.01
T	**Al**	1.25	1.21	0.73	0.74	1.26	1.36	1.38	**Ti** 0.01	1.94
	Al	0.44	0.58	0.35	0.37	0.60	0.61	0.58	**Al** 4.96	0.00
	Ti	0.04	0.05	0.02	0.03	0.04	0.05	0.05	**Fe3+** 0.01	0.12
C	**Fe3+**	-	-	-					**Fe2+** 2.30	1.85
	Mg	2.86	3.08	3.57	3.60	3.02	2.99	3.01	**Mg** 0.03	0.03
	Fe2+	1.66	1.29	1.07	1.00	1.34	1.36	1.37	**Mn** 7.14	0.06
	Fe2+	0.10	0.18	0.09	0.14	0.12	0.07	0.13	**Ca** 0.02	0.00
B	**Mn**	0.02	0.02	0.02	0.03	0.02	0.03	0.03	**Na** 0.00	0.00
	Ca	1.88	1.80	1.89	1.83	1.87	1.90	1.84	**K** 0.01	0.00
	Ca	0.12	0.00	0.01	0.00	0.03	0.05	0.09		
A	**Na**	0.42	0.47	0.30	0.29	0.47	0.51	0.44	**Tot** 19.97	4.00
	K	0.06	0.06	0.02	0.03	0.05	0.06	0.08		
		15.60	15.52	15.33	15.31	15.55	15.62	15.61		
(Ca+Na)B		1.880	1.800	1.891	1.830	1.867	1.904	1.837		
Mg/(Mg+Fe2+)		0.619	0.678	0.755	0.760	0.676	0.677	0.667		
(Na+K)A		0.479	0.521	0.322	0.314	0.523	0.567	0.527		

Appendix D.4 Kaourera Island - Arc Group, Kamuyu Amphibolite Formation

Sample [SJ 8.67]

	Garnet					Amphibole				Plagioclase		
	A rim	B rim	B core			A rim	B rim	B core		A rim	B rim	B core
SiO2	38.237	37.884	37.539			41.474	41.397	41.355		60.571	60.966	61.031
TiO2	0.068	0.109	0.042			0.455	0.633	0.644		0.000	0.000	0.000
Al2O3	21.756	21.685	21.521			15.899	15.935	15.056		24.640	24.375	25.661
FeO	26.655	26.158	25.141			18.866	18.618	18.063		0.086	0.057	0.198
MnO	3.685	3.465	4.162			0.186	0.251	0.213		0.000	0.003	0.039
MgO	1.939	1.991	1.844			7.078	7.253	7.338		0.007	0.000	0.000
CaO	9.525	9.618	9.531			11.142	11.442	11.014		5.891	5.547	6.215
Na2O	0.000	0.039	0.000			1.708	1.725	1.518		9.412	9.194	9.332
K2O	0.009	0.007	0.000			0.590	0.625	0.567		0.049	0.074	0.077
Total	101.874	100.956	99.780			97.398	97.879	95.768		100.656	100.216	102.553
Si	5.98	5.97	5.98		Si	6.27	6.23	6.33	Si	10.75	10.84	10.65
Al	0.02	0.03	0.02	T	Al	1.73	1.77	1.67	Al	5.16	5.11	5.28
-					Al	1.10	1.06	1.05				
Al	3.98	3.99	4.02		Ti	0.05	0.07	0.07				
Ti	0.01	0.01	0.01	C	Fe3+	-	-	-	Ti	0.00	0.00	0.00
-					Mg	1.59	1.63	1.68				
Fe	3.48	3.44	3.35		Fe2+	2.25	2.24	2.20	Fe2+	0.01	0.01	0.03
Mn	0.49	0.46	0.56		Fe2+	0.13	0.10	0.11	Mg	0.00	0.00	0.01
Mg	0.45	0.47	0.44	B	Mn	0.02	0.03	0.03	Mn	0.00	0.00	0.00
Ca	1.59	1.62	1.63		Ca	1.80	1.85	1.81	Ca	1.12	1.06	1.16
Na	0.00	0.01	0.00		Ca	-	-	-	Na	3.24	3.17	3.16
K	0.00	0.00	0.00	A	Na	0.50	0.51	0.45	K	0.01	0.02	0.02
-					K	0.11	0.12	0.11				
Tot	16.01	16.01	16.00			15.57	15.61	15.51		20.29	20.20	20.30
Xpyr	0.075	0.078	0.073	(Ca+Na)B		1.800	1.850	1.810	Xan	0.256	0.249	0.268
Xalm	0.579	0.574	0.560	Mg/(Mg+Fe2+)		0.401	0.410	0.420	Xab	0.741	0.747	0.728
Xsps	0.081	0.077	0.094	(Na+K)A		0.610	0.630	0.560				
Xgrs	0.265	0.271	0.272									

Appendix D.5 Kaourera Island - Arc Group, Kamuyu Amphibolite Formation

Sample [SJ 10.95]

	Garnet					Amphibole				Plagioclase		
	A rim	A rim	B rim			A rim	A rim	B rim		A rim	A rim	B rim
SiO2	38.301	38.275	37.958			40.909	40.926	41.266		60.564	62.091	61.491
TiO2	0.100	0.107	0.124			0.429	0.499	0.367		0.000	0.008	0.125
Al2O3	21.502	21.459	21.962			16.761	15.554	15.019		24.552	24.558	24.022
FeO	26.121	25.646	26.983			20.100	19.455	20.713		0.135	0.258	0.234
MnO	2.900	3.112	3.038			0.278	0.221	0.247		0.055	0.023	0.023
MgO	1.845	1.840	1.872			5.928	6.357	6.555		0.000	0.000	0.000
CaO	9.154	9.755	9.935			11.202	11.133	11.209		5.802	5.265	5.392
Na2O	0.000	0.000	0.000			1.519	1.626	1.781		9.189	9.502	8.925
K2O	0.000	0.000	0.024			0.752	0.653	0.652		0.074	0.049	0.067
Total	99.923	100.194	101.626			97.878	96.424	97.809		100.371	101.754	100.279
Si	6.06	6.05	5.95		Si	6.19	6.28	6.28	Si	10.78	10.87	10.91
Al	0.00	0.00	0.05	T	Al	1.81	1.72	1.72	Al	5.15	5.07	5.02
-					Al	1.18	1.09	0.97	Ti	0.00	0.00	0.02
Al	4.07	4.04	3.96		Ti	0.05	0.06	0.04	Fe2+	0.02	0.04	0.03
Ti	0.01	0.01	0.01	C	Fe3+	-	-	-	Mn	0.01	0.00	0.00
-					Mg	1.34	1.45	1.49	Mg	0.00	0.00	0.00
Fe2+	3.46	3.39	3.54		Fe2+	2.43	2.40	2.50	Ca	1.11	0.99	1.03
Mn	0.29	0.42	0.40		Fe2+	0.12	0.10	0.14	Na	3.17	3.23	3.07
Mg	0.44	0.43	0.44	B	Mn	0.04	0.03	0.03	K	0.02	0.01	0.02
Ca	1.55	1.65	1.67		Ca	1.82	1.83	1.83				
Na	0.00	0.00	0.00		Ca	-	-	-		20.24	20.21	20.10
K	0.00	0.00	0.00	A	Na	0.45	0.48	0.53				
-					K	0.15	0.13	0.13	Xan	0.258	0.234	0.249
Tot	15.92	15.94	16.03			15.56	15.57	15.66	Xab	0.738	0.764	0.747
Xpyr	0.075	0.074	0.072	(Ca+Na)B		1.820	1.830	1.830				
Xalm	0.593	0.575	0.585	Mg/(Mg+Fe2+)		0.344	0.368	0.360				
Xsps	0.067	0.071	0.067	(Na+K)A		0.600	0.612	0.652				
Xgrs	0.266	0.280	0.276									

Appendix D.6 Kaourera Island - Arc Group, Kamuyu Amphibolite Formation

Sample [SJ 14.134]

	Garnet					Amphibole			Plagioclase		K - Spar	Epidote	
	A rim	B rim	B core			A rim	B rim	B core	A rim	B core	Rim	core	
SiO2	38.868	38.889	38.268			40.086	40.610	41.357	49.056	45.522	65.623	38.256	
TiO2	0.000	0.011	0.108			0.209	0.171	0.430	0.075	0.027	0.116	0.090	
Al2O3	21.849	21.896	21.323			18.397	18.163	17.398	32.949	34.527	19.627	27.029	
FeO	30.312	29.866	30.625			19.287	20.591	19.278	0.225	0.160	0.031	8.286	
MnO	1.860	0.729	0.809			0.154	0.242	0.246	0.038	0.003	0.000	0.069	
MgO	3.648	4.020	2.732			6.418	5.375	6.880	0.000	0.029	0.000	0.049	
CaO	5.336	6.189	7.138			11.682	11.304	11.375	15.476	17.461	0.011	23.329	
Na2O	0.000	0.000	0.000			1.092	1.054	1.202	2.687	1.438	0.288	0.000	
K2O	0.000	0.045	0.012			0.525	0.485	0.394	0.047	0.023	15.583	0.000	
Total	101.873	101.645	101.015			97.850	97.995	98.560	100.553	99.190	101.278	97.108	
Si	6.04	6.03	6.03		Si	6.04	6.13	6.17	Si 8.92	8.45	11.91	Si	2.99
Al	0.00	0.00	0.00	T	Al	1.96	1.87	1.84	Al 7.06	7.55	4.20	Al	0.02
-					Al	1.30	1.36	1.22					
Al	4.04	4.03	3.98		Ti	0.02	0.02	0.05				Al	2.47
Ti	0.00	0.00	0.01	C	Fe3+	-	-	-	Ti 0.01	0.00	0.02	Ti	0.01
-					Mg	1.44	1.21	1.53					
tot Fe	3.94	3.87	4.03		Fe2+	2.24	2.41	2.20	Fe2+ 0.03	0.02	0.01	Fe2	0.54
Mn	0.24	0.10	0.11		Fe2+	0.19	0.19	0.20	Mn 0.01	0.00	-	Mn	-
Mg	0.85	0.93	0.64	B	Mn	0.02	0.03	0.03	Mg 0.00	0.01	-	Mg	0.01
Ca	0.89	1.03	1.20		Ca	1.79	1.78	1.77	Ca 3.02	3.47	-	Ca	1.95
Na	0.00	0.00	0.00		Ca	0.10	0.05	0.05	Na 0.95	0.52	0.10	Na	-
K	0.00	0.01	0.00	A	Na	0.32	0.31	0.35	K 0.01	0.01	3.60	K	-
-					K	0.10	0.09	0.08					
Tot	15.96	15.97	15.98			15.52	15.45	15.47	20.01	20.03	19.83		9.02
Xpyr	0.143	0.157	0.107	(Ca+Na)B		1.790	1.780	1.770	Xan 0.759	0.869	Xor 0.973	Ps	18
Xalm	0.666	0.654	0.674	Mg/(Mg+Fe2+)		0.372	0.317	0.389	Xab 0.238	0.130	Xan 0.000	Cz	82
Xsps	0.041	0.016	0.018	(Na+K)A		0.420	0.400	0.422			Xab 0.027		
Xgrs	0.150	0.174	0.201										

Appendix D.7 Kaourera Island - Arc Group, Nhema Amphibolite Formation

Sample [SJ 12.110]

	Garnet				Biotite				Plagioclase				Muscovite		Epidote
	A Core	A Rim	B Rim		A Core	A rim	B Rim		A Core	A Rim	B Rim				
SiO2	37.867	38.128	38.171		36.589	36.653	36.248		59.646	60.863	63.053		47.690		38.266
TiO2	0.100	0.022	0.032		1.486	1.236	1.807		0.045	0.002	0.002		0.378		0.133
Al2O3	21.345	21.816	21.692		18.246	18.819	18.272		25.732	24.732	24.219		34.817		24.851
FeO	26.697	32.202	30.476		18.689	17.675	18.377		0.085	0.060	0.189		2.144		10.428
MnO	5.399	0.543	0.822		0.080	0.106	0.053		0.000	0.039	0.076		0.026		0.351
MgO	1.861	3.205	2.895		11.227	10.933	10.929		0.000	0.000	0.021		1.220		0.021
CaO	6.694	5.091	5.040		0.000	0.000	0.006		7.128	5.893	4.305		0.000		23.048
Na2O	0.000	0.000	0.000		0.177	0.017	0.111		8.726	9.697	8.399		0.641		0.000
K2O	0.000	0.000	0.040		9.835	9.228	9.422		0.079	0.076	1.919		10.186		0.024
Total	99.963	101.007	99.168		96.329	94.667	95.225		101.451	101.362	102.183		97.103		97.100
Si	6.04	6.00	6.08	Si	5.49	5.54	5.48	Si	10.54	10.74	11.01		6.23	Si	3.01
Al	0.00	0.00	0.00	Al	2.50	2.45	2.51	Al	5.35	5.14	4.98		5.36	Al	2.31
-				Al	0.72	0.89	0.75								
Al	4.05	4.04	4.15	Ti	0.16	0.14	0.20							Al	0.00
Ti	0.01	0.00	0.00	tot Fe	2.34	2.23	2.32	Ti	0.00	0.00	0.00		0.03	Ti	0.00
-				Mn	0.01	0.01	0.00								
tot Fe	3.56	4.24	4.06	Mg	2.51	2.46	2.47	tot Fe	0.12	0.00	0.03		0.23	Fe2	0.68
Mn	0.73	0.07	0.11	Ca	0.00	0.00	0.00	Mn	0.00	0.00	0.01		0.00	Mn	0.02
Mg	0.44	0.75	0.68	Na	0.05	0.00	0.03	Mg	0.00	0.00	0.01		0.24	Mg	0.00
Ca	1.14	0.85	0.86	K	1.88	1.78	1.81	Ca	1.35	1.11	0.80		0.00	Ca	1.95
Na	0.00	0.00	0.00	Tot	15.69	15.53	15.60	Na	2.99	3.32	2.84		0.16	Na	-
K	0.00	0.00	0.00					K	0.01	0.02	0.42		1.70	K	-
-				Xann	0.408	0.389	0.405								
Tot	15.94	15.97	15.88	Xph	0.437	0.429	0.429		20.28	20.35	20.13		13.95		7.97
Xpyr	0.143	0.127	0.107					Xan	0.310	0.250	0.197	Xmu	0.700	Ps	22
Xalm	0.666	0.716	0.674					Xab	0.685	0.745	0.697	Xpa	0.070	Cz	77
Xsps	0.041	0.012	0.018									Xph	0.260		
Xgrs	0.150	0.145	0.201												

Appendix D.8 Kaourera Island - Arc Group, Bhumi Semi - Pelite Formation

Sample [SJ 370]

	Garnet		Chlorite		Muscovite	
	A Rim	B Rim	A Rim	B rim		
SiO2	37.584	36.521	26.548	24.275	47.129	47.353
TiO2	0.040	0.120	0.067	0.037	0.202	0.272
Al2O3	21.751	21.494	23.385	22.610	37.196	35.834
FeO	37.250	35.851	25.202	23.924	1.299	1.008
MnO	0.383	0.244	0.000	0.000	0.080	0.000
MgO	2.720	3.681	14.154	14.204	0.527	0.706
CaO	1.182	1.039	0.191	0.000	0.000	0.000
Na2O	0.000	0.063	0.041	0.000	1.421	1.300
K2O	0.027	0.000	0.251	0.024	8.189	8.436
Total	100.937	99.013	89.831	85.074	96.043	94.909
Si	5.994	5.920	5.422	5.238	6.140	6.238
Al	0.006	0.080	2.578	2.762	1.860	1.762
-						
Al	4.082	4.026	3.050	2.987	3.852	3.802
Ti	0.005	0.015	0.010	0.006	0.020	0.027
-						
tot Fe	4.967	4.859	4.303	4.316	0.009	0.000
Mn	0.052	0.033	0.000	0.000	0.102	0.139
Mg	0.647	0.890	4.308	4.568	4.124	4.078
Ca	0.202	0.180	0.042	0.000	0.000	0.000
Na	0.000	0.020	0.016	0.000	0.359	0.332
K	0.005	0.000	0.065	0.007	1.361	1.418
-						
Tot	15.96	16.02	19.794	19.884	13.844	13.828
Xpyr	0.110	0.149			**Xmu** 0.690	0.704
Xalm	0.847	0.815			**Xpa** 0.182	0.165
Xsps	0.009	0.006				
Xgrs	0.034	0.030				

Appendix D.9 Garnet Profile for [SJ 12.110]

SiO2	38.545	38.159	37.687	38.373	38.229	37.772	37.635	37.786	37.617	37.976	37.862	37.682	37.873	37.530	37.452	37.840	37.604	37.840	37.914
TiO2	0.114	0.191	0.129	0.132	0.155	0.189	0.124	0.226	0.186	0.093	0.235	0.117	0.244	0.185	0.125	0.152	0.100	0.088	0.059
Al2O3	21.745	21.694	21.352	21.586	21.556	21.007	21.213	21.258	21.014	21.516	21.553	21.068	21.518	21.414	21.166	21.470	21.099	21.315	21.474
FeO	31.962	32.756	29.760	30.514	28.886	24.876	28.157	26.969	25.667	28.334	28.541	29.400	30.159	30.889	30.297	31.015	32.808	32.426	31.843
MnO	0.984	0.914	3.073	3.298	4.601	6.920	5.662	6.075	6.587	5.949	4.337	3.662	3.483	2.564	1.783	1.213	1.026	0.793	1.272
MgO	2.622	2.930	2.239	2.203	1.979	1.700	1.627	1.704	1.606	1.828	2.004	2.030	2.137	2.132	2.397	2.672	2.846	2.967	2.659
CaO	5.969	5.240	6.477	5.970	5.779	6.264	6.002	7.090	6.550	5.975	6.119	6.225	6.097	6.158	5.757	5.700	5.060	5.243	5.256
Na2O	0.000	0.000	0.000	0.000	0.000	0.000	0.006	0.000	0.000	0.000	0.169	0.028	0.000	0.000	0.000	0.002	0.000	0.000	0.000
K2O	0.039	0.027	0.000	0.000	0.000	0.000	0.000	0.000	0.000	0.000	0.104	0.022	0.000	0.000	0.031	0.027	0.000	0.049	0.020
Total	101.980	101.911	100.717	102.076	101.185	98.728	100.426	101.108	99.227	101.671	100.924	100.234	101.511	100.872	99.008	100.091	100.543	100.721	100.497
Si	6.02	5.98	5.99	6.02	6.04	6.09	6.02	5.99	6.05	6.00	6.00	6.02	5.98	5.97	6.03	6.02	5.99	6.00	6.02
Al	0.00	0.02	0.01	0.00	0.00	0.00	0.00	0.01	0.00	0.00	0.00	0.00	0.02	0.03	0.00	0.00	0.01	0.00	0.00
-																			
Al	4.03	3.99	3.98	4.00	4.05	4.08	4.01	3.97	4.04	4.00	4.02	3.99	3.98	3.98	4.04	4.04	3.95	3.98	4.04
Ti	0.01	0.02	0.02	0.02	0.02	0.02	0.01	0.03	0.02	0.01	0.03	0.01	0.03	0.02	0.02	0.02	0.01	0.01	0.01
-																			
Fe	4.18	4.29	3.95	4.00	3.81	3.35	3.76	3.58	3.45	3.74	3.78	3.93	3.98	4.11	4.08	4.12	4.37	4.30	4.23
Mn	0.13	0.12	0.41	0.44	0.62	0.94	0.77	0.82	0.90	0.80	0.58	0.50	0.47	0.35	0.24	0.16	0.14	0.11	0.17
Mg	0.61	0.68	0.53	0.51	0.47	0.41	0.39	0.40	0.39	0.43	0.47	0.48	0.50	0.51	0.58	0.63	0.68	0.70	0.63
Ca	1.00	0.88	1.10	1.00	0.98	1.08	1.03	1.20	1.13	1.01	1.04	1.07	1.03	1.05	0.99	0.97	0.86	0.89	0.89
Na	0.00	0.00	0.00	0.00	0.00	0.00	0.00	0.00	0.00	0.00	0.05	0.01	0.00	0.00	0.00	0.00	0.00	0.00	0.00
K	0.01	0.01	0.00	0.00	0.00	0.00	0.00	0.00	0.00	0.00	0.02	0.00	0.00	0.00	0.01	0.01	0.00	0.01	0.00
-																			
Tot	15.97	16.00	16.00	15.97	15.94	15.89	15.97	15.99	15.93	15.99	16.00	15.99	15.99	16.01	15.95	15.96	16.02	16.00	15.97
position=	14.144	14.004	13.275	13.039	12.675	12.371	11.647	10.401	9.972	9.540	8.962	8.775	8.651	8.290	7.957	7.691	7.444	7.242	6.983
Xpyr	0.103	0.115	0.088	0.086	0.079	0.071	0.065	0.067	0.066	0.072	0.081	0.081	0.084	0.084	0.098	0.108	0.112	0.117	0.106
Xalm	0.706	0.718	0.659	0.672	0.649	0.579	0.633	0.596	0.589	0.626	0.644	0.658	0.666	0.684	0.692	0.700	0.723	0.717	0.714
Xsps	0.022	0.020	0.069	0.074	0.105	0.163	0.129	0.136	0.153	0.133	0.099	0.083	0.078	0.057	0.041	0.028	0.023	0.018	0.029
Xgrs	0.169	0.147	0.184	0.168	0.166	0.187	0.173	0.201	0.193	0.169	0.177	0.178	0.172	0.175	0.169	0.165	0.143	0.148	0.151

Appendix D.10 Garnet Profile for [SJ 14.134]

SiO2	38.437	38.353	37.933	37.749	37.535	38.064	38.044	38.065
TiO2	0.000	0.078	0.052	0.051	0.024	0.143	0.000	0.008
Al2O3	21.669	21.460	21.484	21.428	21.158	21.618	21.706	21.727
FeO	29.008	30.929	28.085	27.428	30.051	30.949	29.287	28.914
MnO	0.786	0.902	2.337	3.095	1.353	0.785	0.845	0.620
MgO	4.302	3.023	1.377	1.433	1.715	2.425	3.523	4.880
CaO	6.067	6.711	9.378	9.602	8.174	7.970	6.618	5.681
Na2O	0.064	0.002	0.000	0.000	0.000	0.000	0.000	0.000
K2O	0.028	0.000	0.000	0.013	0.004	0.022	0.022	0.015
Total	100.361	101.458	100.646	100.799	100.014	101.976	100.045	99.910
Si	6.026	6.013	6.010	5.982	6.002	5.960	6.006	5.986
Al	0.000	0.000	0.000	0.018	0.000	0.040	0.000	0.014
-								
Al	4.029	3.978	4.021	3.984	3.989	3.950	4.045	4.012
Ti	0.000	0.009	0.006	0.006	0.003	0.017	0.000	0.001
-								
Fe	3.803	4.055	3.721	3.635	4.018	4.052	3.866	3.802
Mn	0.104	0.120	0.314	0.415	0.183	0.104	0.113	0.083
Mg	1.005	0.707	0.325	0.339	0.409	0.566	0.829	1.144
Ca	1.019	1.127	1.592	1.630	1.400	1.337	1.119	0.957
Na	0.019	0.001	0.000	0.000	0.000	0.000	0.000	0.000
K	0.006	0.000	0.000	0.003	0.001	0.004	0.004	0.003
-								
Tot	15.985	15.996	15.978	16.012	16.002	16.030	15.977	16.002
position=	13.866	13.298	12.298	11.953	11.519	11.071	10.522	10.240
Xpyr	0.170	0.118	0.055	0.056	0.068	0.093	0.140	0.191
Xalm	0.641	0.675	0.625	0.604	0.669	0.669	0.652	0.635
Xsps	0.018	0.020	0.053	0.069	0.030	0.017	0.019	0.014
Xgrs	0.172	0.188	0.267	0.271	0.233	0.221	0.189	0.160

Appendix D.11 Garnet Profile for [SJ 370]

SiO2	37.043	37.508	37.433	37.474	37.366	37.347	37.401	37.194	37.545	37.286	36.807	36.910	37.298	37.280	36.759	36.859	37.063	37.125	37.366	37.314	36.915	37.418	37.228	36.064	36.800
TiO2	0.009	0.106	0.009	0.051	0.046	0.048	0.059	0.054	0.084	0.056	0.036	0.000	0.030	0.082	0.032	0.094	0.004	0.091	0.087	0.077	0.074	0.036	0.016	0.091	0.059
Al2O3	21.129	21.441	21.393	21.481	21.499	21.222	21.324	21.390	21.383	21.373	21.274	21.440	21.288	21.263	21.237	21.414	21.486	21.277	21.284	21.242	21.507	21.505	21.090	21.413	21.227
FeO	35.885	36.888	36.547	35.506	35.971	35.662	36.248	36.580	37.015	36.997	36.184	36.851	36.843	36.874	36.791	37.327	37.198	36.869	37.715	36.977	37.279	36.769	36.759	36.628	36.653
MnO	0.259	0.263	0.250	0.291	0.275	0.210	0.247	0.272	0.216	0.232	0.241	0.235	0.250	0.256	0.185	0.241	0.241	0.340	0.302	0.213	0.256	0.297	0.278	0.265	0.213
MgO	3.237	3.439	3.527	3.543	3.362	3.482	3.385	3.465	3.431	3.264	3.119	3.085	3.074	3.000	3.066	2.903	3.063	2.945	2.918	2.835	2.830	2.899	3.068	3.036	3.021
CaO	1.247	1.242	0.960	0.972	1.116	1.112	1.148	1.043	1.028	0.848	1.160	0.953	1.168	1.119	0.977	1.093	1.090	1.036	1.194	1.091	1.132	1.232	1.149	1.078	1.145
Na2O	0.000	0.007	0.143	0.000	0.007	0.000	0.000	0.000	0.000	0.000	0.000	0.000	0.037	0.000	0.000	0.015	0.000	0.000	0.022	0.000	0.029	0.000	0.000	0.010	0.000
K2O	0.028	0.000	0.000	0.000	0.004	0.000	0.046	0.000	0.009	0.000	0.003	0.001	0.000	0.030	0.000	0.025	0.000	0.000	0.000	0.000	0.000	0.007	0.000	0.003	0.010
Total	98.837	100.894	100.262	99.318	99.646	99.083	99.858	99.998	100.711	100.056	98.824	99.475	99.988	99.904	99.047	99.971	100.145	99.683	100.888	99.749	100.022	100.163	99.588	98.588	99.128
Si	6.01	5.98	5.99	6.03	6.01	6.03	6.01	5.98	5.99	5.99	5.98	5.97	6.00	6.00	5.98	5.95	5.96	6.00	5.98	6.02	5.95	6.00	6.02	5.90	5.98
Al	0.00	0.02	0.01	0.00	0.00	0.00	0.00	0.02	0.01	0.01	0.02	0.03	0.00	0.00	0.02	0.05	0.04	0.00	0.02	0.00	0.05	0.00	0.00	0.10	0.02
-																									
Al	4.05	4.00	4.03	4.10	4.08	4.07	4.04	4.03	4.01	4.04	4.06	4.06	4.04	4.04	4.04	4.02	4.04	4.04	4.00	4.06	4.04	4.07	4.03	4.03	4.04
Ti	0.00	0.01	0.00	0.01	0.01	0.01	0.01	0.01	0.01	0.01	0.00	0.00	0.00	0.01	0.00	0.01	0.00	0.01	0.01	0.01	0.01	0.00	0.00	0.01	0.01
-																									
Fe2+	4.87	4.92	4.89	4.77	4.83	4.81	4.87	4.91	4.94	4.97	4.92	4.98	4.96	4.97	5.00	5.04	5.00	4.98	5.05	4.99	5.03	4.93	4.97	5.01	4.98
Mn	0.04	0.04	0.03	0.04	0.04	0.03	0.03	0.04	0.03	0.03	0.03	0.03	0.03	0.03	0.03	0.03	0.03	0.05	0.04	0.03	0.03	0.04	0.04	0.04	0.03
Mg	0.78	0.82	0.84	0.85	0.81	0.84	0.81	0.83	0.82	0.78	0.76	0.74	0.74	0.72	0.74	0.70	0.73	0.71	0.70	0.68	0.68	0.69	0.74	0.74	0.73
Ca	0.22	0.21	0.16	0.17	0.19	0.19	0.20	0.18	0.18	0.15	0.20	0.17	0.20	0.19	0.17	0.19	0.19	0.18	0.20	0.19	0.20	0.21	0.20	0.19	0.20
Na	0.00	0.00	0.04	0.00	0.00	0.00	0.00	0.00	0.00	0.00	0.00	0.00	0.01	0.00	0.00	0.00	0.00	0.00	0.01	0.00	0.01	0.00	0.00	0.00	0.00
K	0.01	0.00	0.00	0.00	0.00	0.00	0.01	0.00	0.00	0.00	0.00	0.00	0.00	0.01	0.00	0.01	0.00	0.00	0.00	0.00	0.00	0.00	0.00	0.00	0.00
-																									
Tot	15.97	16.00	16.01	15.93	15.95	15.95	15.97	15.99	15.99	15.98	15.97	15.99	15.98	15.97	15.99	16.01	16.00	15.97	16.00	15.95	16.00	15.96	15.98	16.02	15.99
position=	27.325	27.182	27.037	26.992	26.876	26.770	26.693	26.604	26.496	26.406	26.248	26.120	26.000	25.833	25.755	25.672	25.556	25.351	25.073	24.881	24.685	23.696	22.915	22.537	21.893
Xpyr	0.133	0.137	0.142	0.146	0.137	0.143	0.137	0.139	0.137	0.132	0.128	0.126	0.124	0.122	0.125	0.117	0.123	0.120	0.116	0.116	0.115	0.118	0.124	0.124	0.123
Xalm	0.825	0.822	0.825	0.819	0.824	0.820	0.824	0.824	0.829	0.838	0.832	0.841	0.836	0.840	0.842	0.846	0.840	0.842	0.843	0.847	0.847	0.839	0.836	0.838	0.838
Xsps	0.006	0.006	0.006	0.007	0.006	0.005	0.006	0.006	0.005	0.005	0.006	0.005	0.006	0.006	0.004	0.006	0.006	0.008	0.007	0.005	0.006	0.007	0.006	0.006	0.005
Xgrs	0.037	0.035	0.028	0.029	0.033	0.033	0.033	0.030	0.029	0.025	0.034	0.028	0.034	0.033	0.029	0.032	0.032	0.030	0.034	0.032	0.033	0.036	0.033	0.032	0.034

Appendix D.12 Orthoamphibole analysis from the Gedrite Whiteschist, Kadunguri Whiteschists.

		Gedrite												Anthophyllite	
	SiO2	50.490	50.599	49.933	50.220	49.107	50.541	49.095	47.295	49.432	49.266	48.233	47.436	55.858	56.814
	TiO2	0.146	0.168	0.129	0.165	0.130	0.113	0.120	0.167	0.000	0.163	0.090	0.100	0.000	0.000
	Al2O3	14.373	15.026	14.077	14.772	15.909	13.984	15.559	17.706	15.690	15.276	16.482	15.871	4.850	4.427
	FeO	1.699	1.438	1.466	1.784	1.596	1.185	1.600	1.748	1.376	1.609	1.680	1.550	1.532	1.161
	MnO	0.034	0.000	0.000	0.000	0.000	0.042	0.000	0.000	0.046	0.097	0.003	0.009	0.046	0.000
	MgO	29.467	29.536	28.518	28.867	28.810	29.569	28.939	27.786	28.953	28.951	27.841	27.280	37.388	38.115
	CaO	0.027	0.029	0.155	0.041	0.033	0.057	0.021	0.046	0.000	0.045	0.086	0.000	0.000	0.016
	Na2O	1.419	1.503	1.329	1.347	1.526	1.264	1.701	2.070	1.820	1.689	1.779	1.654	0.000	0.000
	K2O	0.018	0.010	0.039	0.014	0.000	0.022	0.012	0.019	0.000	0.022	0.006	0.023	0.000	0.013
	Total	97.673	98.308	95.640	97.160	97.110	96.777	97.058	96.837	97.318	97.119	96.199	93.928	99.674	100.545
	Si	6.70	6.66	6.75	6.69	6.55	6.75	6.56	6.36	6.58	6.58	6.51	6.55	7.25	7.29
T	Al IV	1.30	1.34	1.25	1.31	1.45	1.26	1.44	1.64	1.42	1.42	1.49	1.45	0.74	0.67
	Al	0.95	0.99	0.99	1.01	1.06	0.94	1.02	1.16	1.05	0.99	1.13	1.13	0.00	0.00
C	Ti	0.02	0.02	0.01	0.02	0.01	0.01	0.01	0.02	0.00	0.02	0.01	0.01	0.00	0.00
	Mg	4.04	3.99	4.00	3.98	3.93	4.05	3.97	3.82	3.96	3.99	3.86	3.86	5.00	5.00
	Mg	1.79	1.80	1.76	1.76	1.80	1.84	1.80	1.75	1.79	1.78	1.74	1.75	2.00	2.00
B	Fe2+	0.19	0.16	0.17	0.20	0.18	0.13	0.18	0.20	0.15	0.18	0.19	0.18	0.00	0.00
	Na	0.03	0.04	0.08	0.05	0.02	0.03	0.03	0.06	0.06	0.04	0.07	0.07	0.00	0.00
A	Na	0.34	0.34	0.27	0.30	0.37	0.30	0.42	0.48	0.42	0.39	0.39	0.37	0.00	0.00
	Tot	15.34	15.34	15.27	15.30	15.37	15.30	15.42	15.48	15.42	15.39	15.39	15.37	14.99	14.96
	(Ca+Na)B	0.03	0.04	0.08	0.05	0.02	0.03	0.026	0.056	0.055	0.042	0.073	0.072	0	0
	Mg/(Mg+Fe)	0.969	0.973	0.972	0.966	0.970	0.978	0.970	0.966	0.974	0.970	0.967	0.969	0.978	0.983

Appendix D.13 Microprobe Analyses of Yoderite and Associated minerals within the Kadunguri Whiteschists.

		Yoderite					Associated Minerals						
		Chewore Hills			Mautia Hill								
Weight %		Mean of 2C analyses	Std deviation	Fe3+ elevated	Green*	Purple**	Penninite	Sheridanite	Talc	Hematite	Dravite	Kyanite	rutile
	SiO2	37.11	0.24	36.75	36.05	36.70	33.63	30.12	58.71	0.31	37.19	37.17	0.13
	TiO2	0.03	0.02	0.10	0.10	0.00	0.04	0.00	0.01	0.78	0.29	BD	89.62
	Al2O3	45.12	0.23	45.25	43.46	43.16	22.90	22.99	2.46	0.24	32.13	62.33	0.03
	FeO	0.00	0.00	0.00	0.00	0.00	12.31	0.64	0.21	0.00	0.00	0.00	0.00
	Fe2O3	3.43	0.14	4.93	3.85	3.56	0.05	0.00	0.00	98.71	3.49	0.59	2.51
	MnO	0.02	0.02	0.00	<0.01	1.80	BD	0.02	BD	BD	BD	BD	BD
	MgO	12.43	0.17	12.78	12.25	12.16	19.10	32.84	28.80	0.13	10.20	BD	BD
	CaO	0.01	0.01	BD	<0.01	BD	0.16	0.02	0.01	0.02	0.28	BD	BD
	Na2O	0.01	0.01	BD	BD	BD	0.02	0.01	0.18	BD	2.18	BD	BD
	K2O	0.01	0.01	0.01	BD	BD	0.02	0.01	0.02	BD	0.06	BD	BD
	Total	98.17	0.40	99.31	95.71	97.38	88.23	86.65	90.39	100.19	85.81	100.09	92.29
Cation Proportion	Si	4.00	0.02	3.92	3.93	4.01	3.21	2.81	3.91	0.01	5.95	4.02	0.00
	Ti	0.00	0.00	0.01	0.01	0.00	0.00	0.00	0.00	0.02	0.04	0.00	0.97
	Al	5.73	0.02	5.68	5.58	5.56	2.58	2.52	0.19	0.01	6.05	7.94	0.00
	Fe2+	0.00	0.00	0.00	0.16	0.00	0.98	0.05	0.01	0.00	0.00	0.00	0.00
	Fe3+	0.28	0.01	0.40	0.32	0.29	0.00	0.00	0.00	1.96	0.42	0.05	0.03
	Mn3+	0.00	0.00	0.00	0.00	0.15	0.00	0.00	0.00	0.01	0.00	0.00	0.00
	Mg	2.00	0.03	2.03	1.99	1.98	2.72	4.56	2.86	0.00	2.43	0.00	0.00
	Ca	0.00	0.00	0.00	0.00	0.00	0.02	0.00	0.00	0.00	0.05	0.00	0.00
	Na	0.00	0.00	0.00	0.00	0.00	0.00	0.00	0.02	0.00	0.68	0.00	0.00
	K	0.00	0.00	0.00	0.00	0.00	0.00	0.00	0.00	0.00	0.01	0.00	0.00
	Cation total	12.00	0.01	12.04	11.99	11.99	9.51	9.94	7.02	1.99	15.62	12.01	1.00
No of oxygens		19		19	19	19	14	14	11	32	24.5	20	2

Explanation : BD = Below detection.
*Analysis taken from McKie & Bradshaw (1966).
**Analysis taken from Fockenburg & Schreyer (1993), Table 1, analysis number 3.

Relict 1.4 Ga oceanic crust in the Zambezi Valley, northern Zimbabwe: Evidence for Mesoproterozoic supercontinental fragmentation

G. J. H. Oliver, S. P. Johnson — Crustal Geodynamics Group, School of Geography and Geosciences, University of St. Andrews, Fife, Scotland, KY16 9ST, United Kingdom
I. S. Williams — Research School of Earth Sciences, Australian National University, Canberra, ACT 0200, Australia
D. A. Herd — Crustal Geodynamics Group, School of Geography and Geosciences, University of St. Andrews, Fife, Scotland, KY16 9ST, United Kingdom

ABSTRACT

The Archean cratons of southern Africa are separated from one another by younger orogenic belts. It is widely believed that these deformation belts developed entirely within continental crust, but in the Zambezi belt of northern Zimbabwe, relict oceanic crust, i.e., ophiolite, has now been discovered. The zircon age of a plagiogranite dike within the ophiolite—1393 ± 22 Ma—makes this the oldest dated remnant of oceanic crust in Africa. Presence of the ophiolite is direct evidence for the rifting and/or assembly of continental fragments within Africa. The age of the ophiolite is consistent with its being a remnant of sea floor formed during the episode of continental fragmentation that immediately preceded the Grenville orogeny, the global event that marked the coalescence of the Late Proterozoic supercontinent of Rodinia.

INTRODUCTION

Most of the orogenic belts that border African cratons (Kennedy, 1964; Fig. 1) appear to be of Pan-African age (750–550 Ma; Clifford, 1967); a few, e.g., the Limpopo, the Eburnian and the Kibaran-Irumide-Namaqua-Natal belts, are known to be Mesoproterozoic to Neoproterozoic or older (Windley, 1995). Debate continues over whether these belts are largely ensialic, i.e., formed on continental crust (Kröner, 1991; Hanson et al., 1994), or ensimatic, i.e., formed by continental rifting, growth and destruction of oceanic crust, and continental collision (Burke and Dewey, 1972; Windley, 1995). Dating remnants of oceanic crust (ophiolite) within these orogens provides valuable information on the nature of Precambrian supercontinents and how, where, and when they became fragmented and amalgamated.

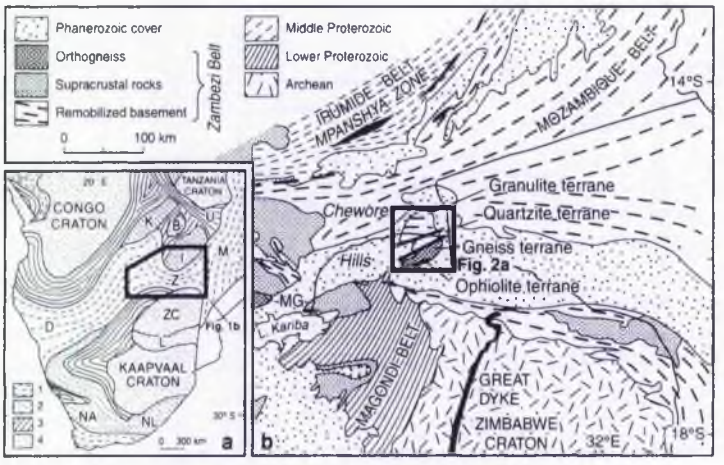

Figure 1. a: Main tectonic provinces of sub-Saharan Africa. 1—Pan-African mobile belts, 2—Late Proterozoic mobile belts, 3—Early Proterozoic mobile belts, 4—Archean cratons, B—Bangweula block, D—Damara belt, I—Irumide belt, K—Kibaran belt, L—Limpopo belt, M—Mozambique belt, NA—Namaqua belt, NL—Natal belt, U—Ubendian belt, Z—Zambezi belt, ZC—Zimbabwe craton (Thomas et al., 1994). b: Geologic map (modified after Goscombe et al., 1994) showing southern Chewore Hills in relationship to four main terranes of Zambezi belt and surrounding mobile belts. MG—Mpande Gneiss.

THE CHEWORE OPHIOLITE

Essential elements of an ophiolite are, in stratigraphic order from bottom to top, (1) serpentinite-peridotite; (2) gabbro and ultramafic cumulates; (3) a mafic sheeted dike unit with plagiogranite screens; (4) a mafic massive and pillowed sediment-free lava sequence; and (5) argillite, pelagic limestones, and chert, all in an allochthonous tectonic setting (Anonymous, 1972; Windley, 1995). All these elements have now been recognized in the Chewore Hills, northern Zimbabwe, in a section of the Zambezi belt, which separates the Congo and Zimbabwe cratons (Figs. 1b, 2a, 2b). We interpret the 5.5-km-long "discontinuous train of conformable pods of hornblende-chlorite schist and serpentine-talc rock" (Goscombe et al., 1994) as the remains of an ophiolite (here named the Chewore ophiolite). Along a well-exposed 1.5 km section of the Maunde River are found (1) altered peridotites, as sheared clinopyroxene-chromite serpentinites (?wehrlite), some with intergrown clinopyroxene + plagioclase pseudomorphs of orthopyroxene (?harzburgite), sheared talc-chromite serpentinites, and sheared serpentinites (?dunite); (2) massive and layered hornblende gabbros and cumulate hornblendite; (3) sheeted (~50 cm wide) dolerite dikes with recrystallized chilled margins, gabbro dikes, and rare ~1-m-thick plagiogranite dikes (some cutting, and some parallel to, the dolerite dikes); and (4) yoderite whiteschists, metapelites, imbricated graywacke and calc-silicate distal turbidites, pillow basalts with relict chilled pillow margins and minor jasper matrix, massive amygdaloidal basalt lava, and interbasalt chert. Younging indicators in the sedimentary units, pillow lavas, and layered gabbro are all toward the southeast, which places serpentinite at the "bottom" of the section. Each unit is bounded by oblique sinistal strike-slip ductile shear zones (faults) that dismember the ophiolite into ~100-m-thick slivers. Metamorphism is garnet-amphibolite grade.

Analyses[1] of metalava and sheeted dikes (Fig. 3) reveal two groups of basalts, one whose composition is similar to modern-day normal mid-ocean-ridge basalt (N-MORB), the other resembling basalt from modern-day island arcs. The latter range from calc-alkalic basalt to high-potassium calc-alkalic dacite. There is a lack of andesite, suggesting a primitive island-arc setting. The Chewore ophiolite is not a tectonized greenstone belt. Greenstone belts typically contain thick MORB pillow-basalt sequences with subordinate komatiites, mafic and ultramafic layered intrusive bodies, andesites, rhyolites, and thick conglomerates and banded iron formations (Windley, 1995). The Chewore ophiolite terrane conspicuously lacks all of these. Furthermore, plagiogranite sheets are common late intrusive bodies in ophiolite suites, but not in greenstone belts (Windley, 1995).

[1]GSA Data Repository item 9862, tables of whole rock geochemical data and zircon spot analyses, is available from Documents Secretary, GSA, P.O. Box 9140, Boulder, CO 80301. E-mail: editing@geosociety.org.

Data Repository item 9862 contains additional material related to this article.

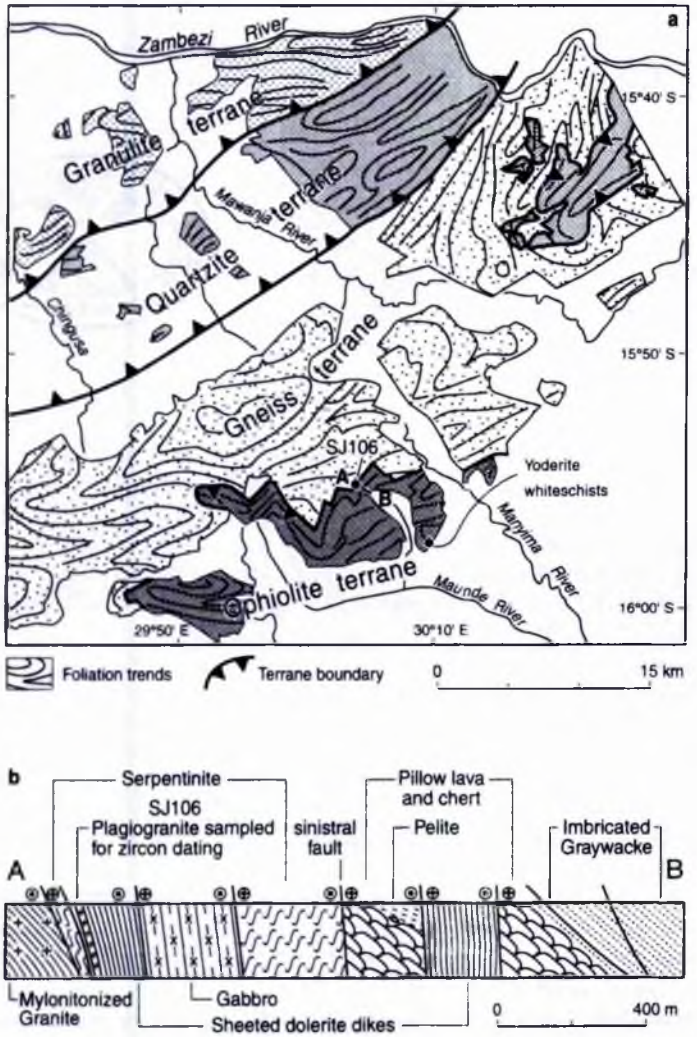

Figure 2. a: Geologic map of Chewore Hills (modified after Goscombe et al., 1993) showing Chewore ophiolite in relation to other thrust-bounded terranes, plus locations of yoderite whiteschists and plagiogranite sample SJ106. Gneiss terrane is made up of metamorphosed megacrystic granite and gneissic amphibolite facies pelites and calcsilicates; amphibolite facies Quartzite terrane is thrust over this; Granulite terrrane is composed of pelites and basic protoliths. b: Geologic cross section along Maunde River (location A–B in part a) of Chewore ophiolite and structural location of dated plagiogranite dike. Note how each unit is bounded by oblique sinistral strike faults that dismember ophiolite into ~100-m-thick slivers.

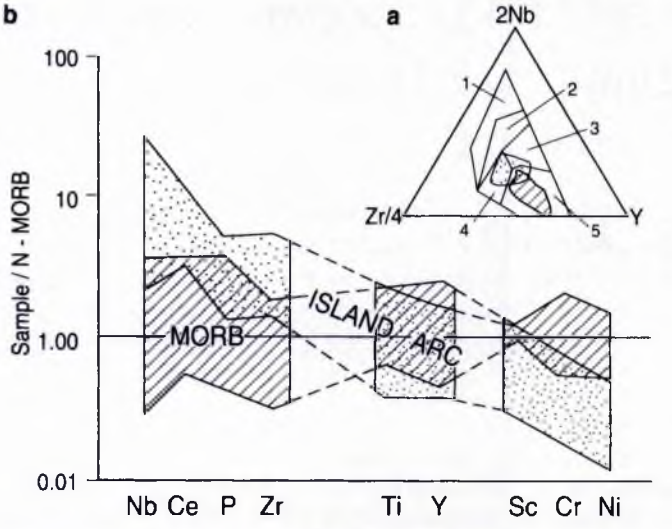

Figure 3. a: Triangular diagram of 2Nb, Zr/4, and Y contents (X-ray fluorescence [XRF] analyses, see footnote 1) showing Chewore ophiolite basalts plotting as two distinct groups, in island arc basalt (dots) and normal mid-ocean-ridge basalt (N-MORB, stripes). Numbered fields: 1—within-plate alkali basalt, 2—within-plate alkali and tholeiite basalt, 3—plume-derived MORB, 4—island-arc basalt, 5—N-MORB or island-arc basalt (Meschede, 1986). b: Trace element spider plot showing XRF analyses of Chewore ophiolite basalt (see footnote 1) normalized to N-MORB (Pearce, 1983). The island-arc group (dots) shows relative enrichment in incompatible elements and depletion in compatible elements as found in modern day island arcs. N-MORB group (stripes), in contrast, shows a flat pattern like modern-day MORB.

Lenticular serpentinite at the base of the ophiolite is in contact with megacrystic K-feldspar granite, now mylonitized augen gneiss. This granite is separate: It does not cut the ophiolite, nor do any amphibolites of the ophiolite cut it. Tectonic imbrications of ophiolite slices and granite augen gneiss form a complicated suture zone up to 3 km thick that can be traced for more than 60 km as a northeast-trending magnetic lineament (Anonymous, 1992) beneath Permian Karoo sedimentary cover (Fig. 2b). Rocks in the suture zone have strong ductile L-S fabrics that have transposed early structures. Most kinematic indicators (e.g., asymmetric augen with quartz tails, rotated porphyroclasts, shear bands, and C-S fabrics) show that the southeast side moved obliquely upward to the north and northeast. Quartz-free yoderite whiteschist (Fig. 2a) is unique. Yoderite has the composition SiO_2 = 37.11, Al_2O_3 = 45.12, Fe_2O_3 = 3.43, MgO = 12.43, MnO = 0.02 wt%. The assemblage yoderite + talc + kyanite + chlorite + dravite + hematite indicates high pressures between 1.3 and 2.1 GPa, but moderate temperatures between 590 and 650 °C (Fockenburg and Schreyer, 1994), such as might have existed in an active suture zone with a large vertical component of motion.

AGE OF THE OPHIOLITE

Zircon from a plagiogranite dike was separated for dating by the SHRIMP (sensitive high-resolution ion microprobe) U-Pb method (Williams and Claesson, 1987). The ~1-m-wide dike can be traced between, and parallel to, sheeted metadolerite dikes up the side of a gorge and is not a xenolith. It shares the same stuctural elements as the metadolerite dikes, so it must be of similar age to them. We conclude that the plagiogranite dike was intruded at the time of ophiolite formation, a common relationship in Phanerozoic ophiolites (Pitcher, 1993). The plagiogranite zircon forms large (>200 μm diameter), simply zoned prisms without cores (Fig. 4), suggesting zircon growth only at the time of plagiogranite magma crystallization. This interpretation is confirmed by the analyses (Fig. 5; see footnote 1); 10 analyses from various parts of 7 crystals show consistently low U (<120 ppm) and low Th (<75 ppm) and the same concordant U-Pb isotopic composition within analytical uncertainty, yielding a mean age of 1393 ± 22 Ma (95% confidence). This ophiolite is the oldest dated ophiolite in Africa, having formed at the same time as the initiation of the Irumide orogeny in Africa, and of the Grenville orogeny in North America (Tack et al., 1994; Gower et al., 1990). The Chewore megacrystic granite might be analogous to neighboring 1100 Ma Zambian augen gneiss inliers (e.g., the Mpande Gneiss, Fig. 1b; Hanson et al., 1988). Mineral cooling ages from elsewhere in the Zambezi belt are 600–450 Ma (Hanson et al., 1994), reflecting Pan-African tectonism.

IMPLICATIONS FOR SUPERCONTINENT FRAGMENTATION

Considering Phanerozoic plate motions (Dalziel, 1997), it is unlikely that the Chewore "ocean" simply opened and closed, rejoining the original continental block. The Bangweula block (Fig. 1a) acted as the foreland to the Irumide fold and thrust belt in northern Zambia (Daly, 1986). However, there is no evidence to place the Zimbabwe craton on the other side of the Chewore ophiolite at 1.4 Ga. Indeed, at 1.5 Ga, the Zimbabwe craton, with its distinctive granite-greenstone terranes, is thought to have been linked to Madagascar, northern India, and eastern Australia as part of an entirely sep-

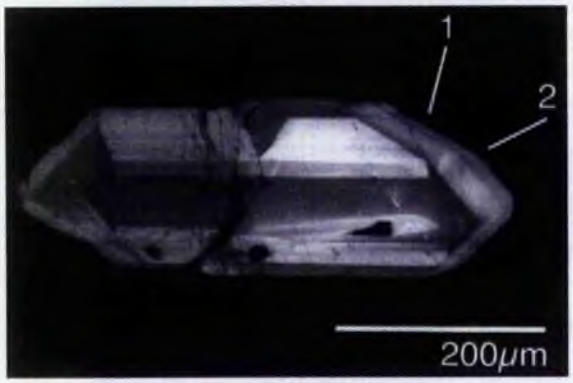

Figure 4. Scanning electron microscope cathodoluminescence image of zircon grain 6 showing the very simple euhedral growth zoning and intense fracturing typical of the zircon crystals from plagiogranite SJ-106. This grain is one of the few in which the zoning pattern suggests the possible presence of a younger overgrowth, but SHRIMP analyses of the center and overgrowth (elliptical pits 1 and 2) show no significant difference in age (Fig. 5).

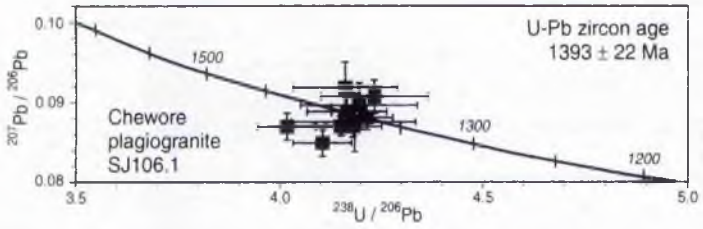

Figure 5. Concordia plot of SHRIMP zircon U-Pb isotopic analyses (see footnote 1) from Chewore ophiolite plagiogranite dike SJ-106. Analytical uncertainties = 1 standard error. All radiogenic $^{238}U/^{206}Pb$ measurements are the same within analytical uncertainty, yielding a weighted mean age of 1393 ± 22 Ma (95% confidence).

arate continent (Rogers, 1996). Thus, the discovery of the 1.4 Ga Chewore ophiolite cannot readily be interpreted within the currently preferred concept of Proterozoic supercontinent fragmentation and amalgamation.

The ~400-km-long Mpanshya zone of mafic and ultramafic rocks in Zambia (Fig. 1b) has been proposed as an Irumide suture zone (Daly, 1986). It is possible that the Chewore and Mpanshya zones are equivalent in age and origin, in which case the Irimide mobile belt cannot be ensialic. Thus the nature of other African mobile belts needs to be reassessed, as do Proterozoic continental reconstructions based on the ensialic mobile belt model (Rogers, 1996).

The accretion of the Laurentia supercontinent was largely completed by 1.6 Ga (Hoffman, 1989). A dearth of tectonism and plutonism between 1.6 and 1.3 Ga reflects stability within that continent (Hoffman, 1989), despite its amalgamation with Greenland, Siberia, Baltica, and East Antarctica by 1.5 Ga to form the supercontinent of NENA (northern Europe and North America) (Gower, 1990). Africa had a similar period of quiescence from 1.75 to 1.42 Ga (Fig. 24.1 in Cahen et al., 1984). By analogy with NENA, this quiescence probably reflects the stabilization of a supercontinent which, given the coincidence in time, might have been part of NENA itself, creating a supercontinent of Pangean size (Super-NENA). The 1.4 Ga Chewore ophiolite might be the remains of sea floor formed during the initial disaggregation of Super-NENA, the first stirrings in Africa of the worldwide 1.35–0.9 Ga Grenville orogeny (Gower et al., 1990), and the cascade of continental collisions that subsequently constructed the supercontinent of Rodinia.

ACKNOWLEDGMENTS

We thank the Universities of Harare and St. Andrews and the Chewore National Safari Park for funding and logistical support, I. W. D. Dalziel, R. L. Gibson, and C. Passchier for constructive reviews, and Mary Eberle for editing. The staff of the ANU EMU and N. Gabbitas kindly assisted with the cathodoluminescence imaging.

REFERENCES CITED

Anonymous, 1972, Penrose field conference on ophiolites: Geotimes, v. 17, p. 24–25.

Anonymous, 1992, Aeromagnetic maps: Geological Survey of Zimbabwe, sheets 1529 D4-AM, 1530 C3-AM, 1629 B2-AM, and 1630 A1-AM, scale 1:50000.

Burke, K. C., and Dewey, J. F., 1972, Orogeny in Africa, *in* Dessauuvagie, T. F. L., and Whiteman, A. J., eds., Orogeny in Africa: Ibadan, Nigeria, University of Ibadan, p. 583–608.

Cahen, L., Snelling, N. L., Delhal, J., and Vail, J. R., 1984, The geochronology and evolution of Africa: Oxford, Clarendon Press, 512 p.

Clifford, T., 1967, The Damaran episode in the Upper Proterozoic–Lower Palaeozoic structural history of southern Africa: Geological Society of America Special Paper 92, 100 p.

Daly, M. C., 1986, The intracratonic Irumide belt of Zambia and its bearing on collision orogeny during the Proterozoic of Africa, *in* Coward, M. P., and Ries, A. C., eds., Collision tectonics: Geological Society [London] Special Publication 19, p. 321–328.

Dalziel, I. W. D., 1997, Neoproterozoic-Paleozoic geography and tectonics: Review, hypothesis, environmental speculation: Geological Society of America Bulletin, v. 109, p. 16–42.

Fockenburg, T., and Schreyer, W., 1994, Stability of yoderite in the absence and in the presence of quartz: An experimental study in the system MgO-Al_2O_3-SiO_2-H_2O: Journal of Petrology, v. 35, p. 1341–1375.

Goscombe, B., Fey, P., and Both, F., 1994, Structural evolution of the Chewore Inliers, Zambezi Mobile Belt, Zimbabwe: Journal of African Earth Sciences, v. 19, p. 199–224.

Gower, C. F., Ryan, A. B., and Rivers, T., 1990, Mid-Proterozoic Laurentia-Baltica: Geological Association of Canada Special Paper 38, p. 1–20 .

Hanson, R. E., Wilson, T. J., Bruekner, H. K., Onstott, T. C., Wardlaw, M. S., Johns, C. C., and Hardcastle, K. C., 1988, Recconnaissance geochronology, tectonothermal evolution and regional significance of the Middle Proterozoic Choma-Kamomo block, southern Zambia: Precambrian Research, v. 42, p. 39–61.

Hanson, R. E, Wilson, T. J., and Munyanyiwa, H., 1994, Geologic evolution of the Neoproterozoic Zambezi orogenic belt in Zambia: Journal of African Earth Sciences, v. 18, p. 135–150.

Hoffman, P. K., 1989, Precambrian geology and tectonic history of North America, *in* Bally, A. W., and Palmer, A. R., eds., The geology of North America—An overview: Boulder, Colorado, Geological Society of America, Geology of North America, v. A, p. 447–512.

Kennedy, W. Q., 1964, The structural differentiation of Africa in the Pan-African tectonic episode: Leeds University Institute of African Geology 8th Annual Report, p. 48–49.

Kröner, A., 1991, Tectonic evolution in the Archean and Proterozoic: Tectonophysics, v. 187, p. 393–410.

Meschede, M., 1986, A method of discriminating between different types of mid-ocean ridge basalts and continental tholeiites with the Nb-Zr-Y diagram: Chemical Geology, v. 56, p. 207–218.

Pitcher, W. S., 1993, The nature and origin of granite: Padstow, United Kingdom, T J Press, 321 p.

Pearce, J. A., 1983, Role of the sub-continental lithosphere in magma genesis at active continental margins, *in* Hawkesworth, C. J., and Norry, M. J., eds., Continental basalts and mantle xenoliths: Nantwich, Shiva, p. 230–249.

Rogers, J. J. W., 1996, A history of continents in the past three billion years: Journal of Geology, v. 104, p. 91–107.

Tack, L., Liégeeois, J. P., Deblond, A., and Duchesene, J. C., 1994, Kibaran A-type granitoids and mafic rocks generated by two mantle sources in a late orogenic setting (Burundi): Precambrian Research, v. 68, p. 323–356.

Thomas, R. J., Agenbacht, A. L. D., Cornell, D. H., and Moore, J. M., 1994, The late Kibaran of Southern Africa: Tectonic evolution and metallogeny: Ore Geology Reviews, v. 9, p. 131–160.

Windley, B., 1995, The evolving continents: New York, Wiley, 526 p.

Williams, I. S., and Claesson, S., 1987, Isotopic evidence for the Precambrian provenance and Caledonian metamorphism of high-grade paragneisses from the Seve nappes, Scandinavian Caledonides: 2. Ion microprobe zircon U-Th-Pb: Contributions to Mineralogy and Petrology, v. 97, p. 205–217.

Manuscript received October 27, 1997
Revised manuscript received February 23, 1998
Manuscript accepted March 3, 1998

Seismic reflections from subvertical diabase dikes in an Archean terrane: Comment and Reply

COMMENT

David K. Smythe
Department of Geology and Applied Geology, University of Glasgow, Glasgow G12 8QQ, United Kingdom

The demonstration by Zaleski et al. (1997) that bright subhorizontal reflectors apparently at 1–3 km depth are actually sideswipe from dikes trending subparallel to the seismic line is salutary. They have provided a valuable warning of the possible dangers of over-enthusiastic geological interpretation of two-dimensional seismic reflection profiles over crystalline terrane.

However, their claim to have published the first data set in which reflections are "unambiguously correlated with dikes" is unfounded. Seismic reflection observations were made as long ago as 1969 of some of the well-known Tertiary (Paleocene) tholeiitic dikes of northwest Britain inferred from geophysical methods. The Loch Ewe dike in the North Minch west of Scotland is the best documented example (McQuillin et al., 1979, fig. 7/22; Chesher et al., 1983). It is about 500 m wide, with its top about 1 km below sea level, and it shows up prominently as a reflected refraction event on all the seismic reflection sections that cross it. It dies out to the southeast at the mainland coastline and does not reach the surface anywhere (Ofoegbu and Bott, 1985). The Loch Ewe dike and others of the same swarm were also noted (although not explicitly discussed) on the well-known BIRPS deep seismic profiles from offshore northwest Scotland (Brewer and Smythe, 1986; Klemperer and Hobbs, 1991). Members of the swarm can be traced to the southeast off the eastern coast of England, where they are identified on industry multichannel seismic reflection lines, correlating with aeromagnetic anomalies (Kirton and Donato, 1985; Brown et al., 1994).

I have compiled geophysical evidence for the Late Carboniferous quartz dolerite dike swarm of northern Britain (Smythe, 1994; Smythe et al., 1995). Aeromagnetic data in the North Sea show that onshore dike anomalies can be traced up to 200 km east from the United Kingdom coast. Individual dikes, which are generally up to 30 m wide onshore, attain widths of well over 1 km offshore. Thus they are at least as wide as any known dikes. This swarm is probably as extensive and voluminous as the well-known and better-exposed Paleocene tholeiitic swarm of northwest Britain. The easterly extensions offshore of dikes at Dunbar are seen on industry multichannel seismic reflection sections, coincident with the location of the positive linear magnetic anomalies. The dikes are revealed by prominent diffraction patterns, which are probably reflected refractions (Day and Edwards, 1983). The closely spaced Dunbar dike sub-group has a cumulative width of 2–3 km over its length of 200 km, which makes it as large, volumetrically, as any intracontinental dike discovered to date. In comparison, the Great Abitibi dike on the Canadian Shield is 600 km long and 250 m wide (Ernst et al., 1987). The Great Dyke of Nova Scotia (also known as the Shelburne dike) is up to 200 km long, and 60–180 m wide (Papezik and Barr, 1981). Gravity modeling of the Great Dyke of Zimbabwe shows that it is bell shaped, with the main feeder about 1 km wide (Podmore and Wilson, 1987). This dike is 550 km long.

What can we learn from this? First, many more ultrawide dikes may be discovered if we look for them. We can reprocess existing seismic reflection data to enhance reflected refractions, and thereby identify dikes, rather than to filter them out, as is normally the aim in conventional processing (e.g., Larner et al., 1983; Tsai, 1984, 1985). Second, such reprocessing methods may prove to be fruitful on data shot over oceanic crust, to enhance and possibly image the dikes of oceanic layer 2. Third, those of us interested in seismic imaging of the crystalline upper crust should employ three-dimensional (3-D) methods to avoid the pitfall of misleading out-of-plane reflections such as those demonstrated by Zaleski et al. (1997). This is especially important where the primary aim of the survey is to image sub-horizontal reflections at deep crustal boreholes where igneous intrusives or extrusives are known to be present; obviously, such sills and basalts are usually fed by dikes. As a minimum precaution, intersecting 2-D lines must be surveyed, as over the Swedish Siljan Ring structure (Juhlin, 1990). A better strategy is to augment a 2-D profile with some limited 3-D coverage, as was done at the Kola (Russia) SG-3 superdeep well (Smythe et al., 1994). But the best strategy is to obtain full 3-D seismic coverage, as was done at the German KTB superdeep well (Harjes et al., 1997). In conclusion, the future of crystalline crustal seismic reflection profiling lies in using some kind of 3-D method, as is already routine in hydrocarbon exploration and production.

REFERENCES CITED

Brewer, J. A., and Smythe, D. K., 1986, Deep structure of the foreland to the Caledonian orogen, NW Scotland: Results of the BIRPS WINCH profile: Tectonics, v. 5, p. 171–194.
Brown, G., Platt, N. H., and McGrandle, A., 1994, The geophysical expression of Tertiary dykes in the southern North Sea: First Break, v. 12, p. 137–146.
Chesher, J. A., Smythe, D. K., and Bishop, P., 1983, The geology of the Minches, Inner Sound, and Sound of Raasay: Report of the [UK] Institute of Geological Sciences 83-6, 29 p.
Day, G. A., and Edwards, J. W. F., 1983, Reflected refracted events on seismic sections: First Break, v. 1, p. 14–17.
Ernst, R. E., Bell, K., Ranalli, G., and Halls, H. C., 1987, The Great Abitibi Dyke, southeastern Superior Province, Canada, *in* Halls, H. C and Fahrig, W. F., eds., Mafic dyke swarms: Geological Association of Canada Special Paper 34, p. 123–135.
Harjes, H.-P., Bram, K., Dürbaum, H.-J., Gebrande, H., Hirschmann, G., Janik, M., Klöckners, M., Lüschen, E., Rabbel, W., Simon, M., Thomas, R., Tormann, J., and Wenzel, F., 1997, Origin and nature of crustal reflections: Results from integrated seismic measurements at the KTB superdeep drilling site: Journal of Geophysical Research, v. 102, p. 18267–18288.
Juhlin, C., 1990, Interpretation of reflections in the Siljan Ring area based on results from the Gravberg-1 borehole: Tectonophysics, v. 173, p. 345–360.
Kirton, S. R., and Donato, J. A., 1985, Some buried Tertiary dykes of Britain and surrounding waters deduced by magnetic modelling and seismic reflection methods: Journal of the Geological Society of London, v. 142, p. 1047–1057.
Klemperer, S., and Hobbs, R., 1991, The BIRPS atlas, deep seismic reflection profiles around the British Isles: Cambridge University Press, 124 p.
Larner, K., Chambers, R., Yang, M., Lynn, W., and Wai, W., 1983, Coherent noise in marine seismic data: Geophysics, v. 48, p. 854–886.
McQuillin, R., Bacon, M., and Barclay, W., 1979, An introduction to seismic interpretation: London, Graham and Trotman, 199 p.
Ofoegbu, C. O., and Bott, M. H. P., 1985, Interpretation of the Minch linear magnetic anomaly and of a similar feature on the shelf north of Lewis by non-linear optimization: Journal of the Geological Society of London, v. 142, p. 1077–1087.
Papezik, V. S., and Barr, S. M., 1981, The Shelburne dyke, an early Mesozoic diabase dike in Nova Scotia: Mineralogy, chemistry, and regional significance: Canadian Journal of Earth Science, v. 18, p. 1346–1355.
Podmore, F., and Wilson, A. H., 1987, A reappraisal of the structure, geology and emplacement of the Great Dyke, Zimbabwe, *in* Halls, H. C., and Fahrig, W. F., eds., Mafic dyke swarms: Geological Association of Canada Special Paper 34, p. 317–330.
Smythe, D. K., 1994, Geophysical evidence for ultrawide dykes of the late Carboniferous quartz-dolerite swarm of northern Britain: Geophysical Journal International, v. 119, p. 20–30.
Smythe, D. K., Smithson, S. B., Gillen, C., Humphreys, C., Kristoffersen, Y., Karaev, N. A., Garipov, V. Z., Pavlenkova, N. I., and the Kola-92 Working Group, 1994, Project images crust, collects seismic data in world's largest borehole: Eos (Transactions, American Geophysical Union), v. 75, p. 473–476.
Smythe, D. K., Russell, M. J., and Skuce, A. G., 1995, Intra-continental rifting inferred from the major Late Carboniferous quartz-dolerite dyke swarm of NW Europe: Scottish Journal of Geology, v. 31, p. 151–162.
Tsai, C. J., 1984, An analysis leading to the reduction of scattered noise on deep marine records: Geophysics, v. 49, p. 17–26.
Tsai, C. J., 1985, A method to analyze and verify deep crustal reflections offshore Costa Rica: Geophysics, v. 50, p. 196–206.
Zaleski, E., Eaton, D. W., Milkereit, B., Roberts, B., Salisbury, M., and Petrie, L., 1997, Seismic reflections from subvertical diabase dykes in an Archean terrane: Geology, v. 25, p.

REPLY

Eva Zaleski
Geological Survey of Canada, Ottawa, Ontario K1A 0E8, Canada
David W. Eaton
Department of Earth Sciences, University of Western Ontario, London, Ontario N6H 3C6, Canada
Bernd Milkereit
Institute of Geophysics, Christian Albrechts University, 24098 Kiel, Germany
Brian Roberts
Geological Survey of Canada, Ottawa, Ontario K1A 0E8, Canada

J. metamorphic Geol., 1998, **16**, 809–818

A second natural occurrence of yoderite

S. P. JOHNSON AND G. J. H. OLIVER*
Crustal Geodynamics Group, School of Geography and Geosciences, Purdie Building, The University, St Andrews, Fife, KY16 9ST, UK

ABSTRACT A second example of yoderite has been discovered in whiteschists from the Southern Chewore Hills of northern Zimbabwe. The mineral is pale green in colour and occurs in an equilibrium assemblage with talc + chlorite + kyanite + dravite + hematite. There is no quartz present. Recalculated microprobe analyses give a structural formula of $Mg_2Al_{5.7}Fe_{0.3}Si_4O_{18}(OH)_2$, similar to that obtained for the type locality at Mautia Hill, Tanzania, i.e. $Mg_2Al_{5.6}Fe_{0.4}Si_4O_{18}(OH)_2$. Textural relationships and relative proportions of minerals suggest that the yoderite was formed by reaction between talc, chlorite, kyanite and hematite. Experimental evidence suggests high-water-pressure metamorphic conditions at temperatures exceeding a reaction curve that extends between 13 kbar at 590 °C and 21 kbar at 650 °C. The yoderite-bearing whiteschist is associated with a 1.4 Ga dismembered ophiolite. It is proposed that this yoderite occurrence is associated with a relict subduction/suture zone.

Key words: Chewore Hills; high pressure; natural yoderite, whiteschist.

INTRODUCTION

Until now the only known occurrence of yoderite is from a 5 m thick talc + kyanite + quartz 'whiteschist' in the Usagaran Complex, exposed in Mautia Hill, Tanzania (McKie, 1959; Mruma & Basu, 1987). Nd model ages give 2.7 Ga for the protolith of the yoderite-bearing schist; whole-rock Rb/Sr ages date metamorphism at 2.0 Ga (Möller *et al.*, 1998). Yoderite-bearing schists from this locality are interlayered with dolomitic marble, biotite gneiss, piedmontite quartzite and kyanite schist. McKie (1959) named the mineral in honour of H. S. Yoder, who was the first to experimentally investigate the reactions and phases in the central part of the $MgO–Al_2O_3–SiO_2–H_2O$ (MASH) system (Yoder, 1952). Schreyer & Yoder (1968) first synthesized yoderite at pressures between 10 and 25 kbar at temperatures ranging from 700 to 850 °C. Detailed studies on the synthesis, occurrence and crystal structure of this mineral were undertaken by Fleet & Megaw (1962), McKie & Bradshaw (1966), Schreyer & Seifert (1969a), Schreyer & Seifert (1969b), Abu-Eid *et al.* (1978), Higgins *et al.* (1982), Mrurma & Basu (1987), Schreyer (1988) and Fockenberg & Schreyer (1991, 1993, 1994). Yoderite is important as a metamorphic indicator of moderate to high pressure (> 6 kbar) and moderate to high temperature (590–790 °C). We report a second natural occurrence of yoderite from a whiteschist in the Southern Chewore Hills in northern Zimbabwe.

*Corresponding author (email: gjho@st-and.ac.uk)

GEOLOGICAL SETTING

The Southern Chewore Hills are a group of isolated horsts within the Zambezi Valley, consisting of granulite, quartzite, gneissic (Goscombe *et al.*, 1994) and ophiolite terranes (Oliver *et al.*, 1998), (Fig. 1). Zircon from a plagiogranite dyke of the Ophiolite Complex was dated with a SHRIMP at 1393 ± 22 Ma and used to postulate the presence of a suture zone of Grenvillian age (Oliver *et al.*, 1998). These terranes have undergone unknown amounts of Pan-African tectonic overprinting. The single yoderite-bearing rock (sample SJ 13.128) (sheet name 'Chimonje', number 1530 C3, grid reference ST 9662 3494; latitude 30° 10′ 10″ E, longitude 15° 57′ 42″ S; Figs 1, 2 & 3) is a coarse-grained talc + kyanite + chlorite + hematite + dravite + yoderite pod (12 × 3 m), which was discovered in a whiteschist outcrop, 6 × 3 km in size (here named the Kadunguri Whiteschist Formation after the nearby Kadunguri Hill, grid reference ST 9619 3497). Aeromagnetic maps at 1 : 50 000 scale (Anon., 1992) indicate that the whiteschists continue underneath the unconformable Karoo sandstone cover sequence giving a total area of 10 × 3 km. The contact between the Kadunguri Whiteschist Formation and the Ophiolite terrane to the north is poorly exposed. It is interpreted to be tectonic since it is parallel to foliation and to outcropping north-west-directed thrusts, which themselves are parallel to foliation in the Ophiolite terrane.

Lithologies of the Ophiolite terrane include amphibolite of island-arc chemistry interbanded with muscovite-bearing quartzite and garnet muscovite schist, MORB-type garnet amphibolite (with deformed pillow structures), serpentinite, metagabbro and cumulate hornblendite (Oliver *et al.*, 1998).

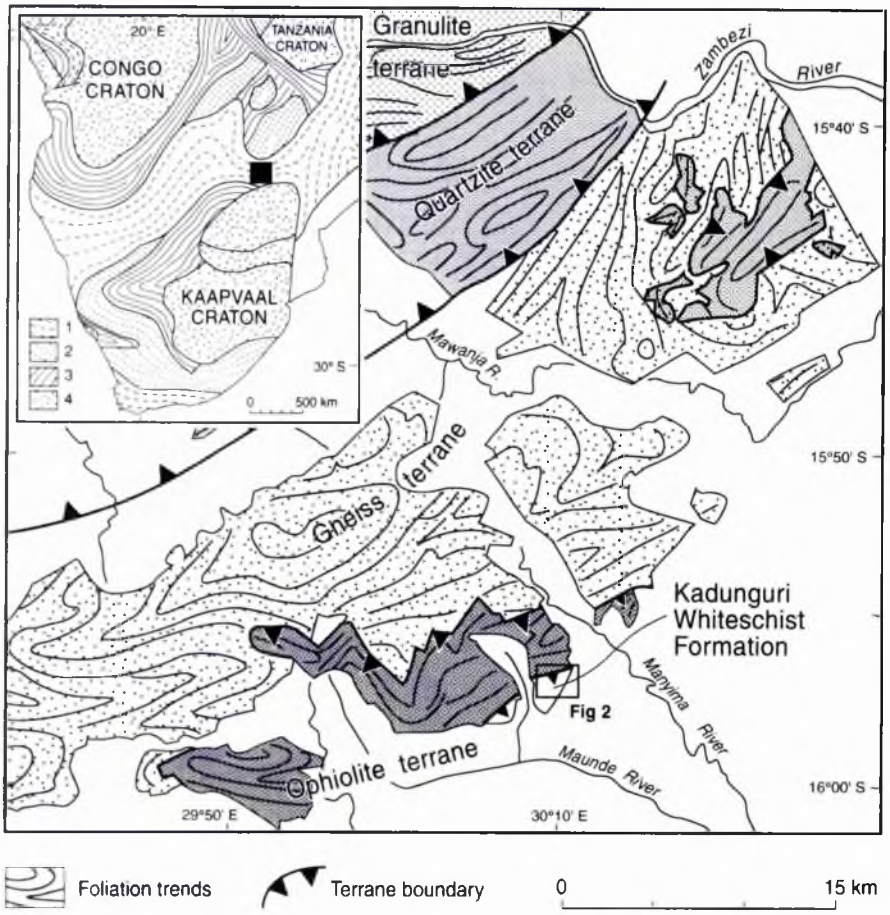

Fig. 1. Geological map of the Chewore Inliers (modified from Goscombe *et al.*, 1994) showing the location of the Kadunguri Whiteschist Formation. The inset is a geological map of southern Africa showing the location of the Chewore Inliers with respect to the surrounding orogenic belts. 1 = Pan African; 2 = Irumide; 3 = Ubendian; 4 = Archean.

PETROGRAPHY

The yoderite-bearing whiteschist pod in the Southern Chewore Hills consists of a randomly oriented assemblage of chlorite (40%) + kyanite (30%) + tourmaline (dravite) (10%) + hematite (10%) + yoderite (5%) and talc (5%). There is no quartz in the rock. The surrounding whiteschists are comprised of talc + kyanite + quartz + hematite and dravite without chlorite. To the north-east of the pod the whiteschists have a strong tectonic fabric (i.e. with foliation, lineation and crenulation), which grades into random fabrics some 5–10 m to the south-west of the pod. These oriented tectonic fabrics indicate a zone of higher strain to the north-east. The southern margin of this zone is marked by a 1–5 m thick band that surrounds the pod and is composed of fine-grained (<0.5 mm), randomly oriented quartz + hematite + kyanite rock. It contains parallel-sided hematite + quartz veins (>1 cm wide, >40 cm long), giving the rock a banded appearance. The banding is steep and parallel to both the margin of the high-strain zone and the long axis of the yoderite-bearing pod (Figs 2 & 3). Exposure in the critical area (where the various rock units are juxtaposed) is unfortunately poor, and direct contact between the units is never seen. The yoderite-bearing rock crops out as many small (<35 cm), scattered, *in situ* blocks within a 12 × 3 m area, roughly defining the shape of an ellipsoid pod. *In situ* outcrops of fine-grained quartz + hematite + kyanite rock are rare, but a small exposure on the southern margin pinpoints the boundary with the pod to within 20 cm. Neither unit changes in character towards this contact, and the examination of nearby float suggests that the yoderite-bearing rock is a discrete unit surrounded by the fine-grained quartz + hematite + kyanite banded rock. A sharp break in slope on either side of these units is interpreted as the boundary to the surrounding whiteschists (Fig. 3).

Mineral phases within the yoderite-bearing rock are coarse grained and randomly oriented. Chlorite is predominant in the assemblage as a primary matrix mineral and surrounds all other phases. Minor talc laths (*c.* 5%) are intergrown with the chlorite matrix. Contacts between the two are sharp and straight and

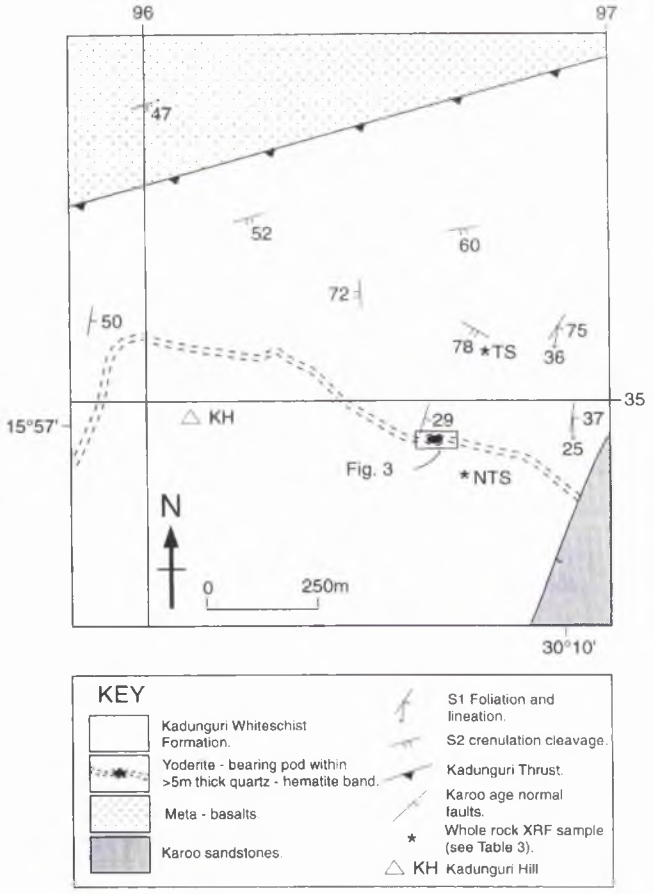

Fig. 2. Geological map of the area around the yoderite-bearing locality. The Kadunguri Whiteschist Formation is in thrust contact with metabasalts of the Ophiolite terrane to the north and faulted against Karoo sandstones to the south-east. TS and NTS are the localities of samples collected for whole-rock XRF analysis.

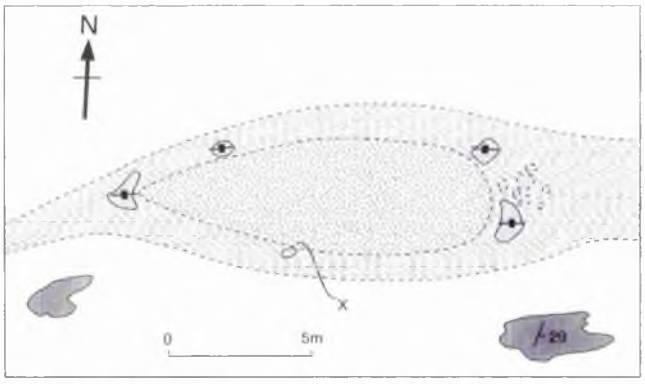

Fig. 3. Geological map of the yoderite-bearing pod and surrounding lithologies. The yoderite-bearing rock occurs as many small (< 35cm) scattered blocks situated within the outlined ellipsoidal region. Position X marks a small exposure where the boundary between the yoderite-bearing pod and quartz + hematite + kyanite band can be pinpointed to within 20 cm. Sample SJ 13.128 was collected from the centre of the pod.

suggest an equilibrium relationship (Fig. 4). Kyanite crystals are arranged in radiating masses, often > 4 cm long, surrounded by matrix chlorite and talc, and occasionally occur in direct contact with yoderite. Dravite is present as both a coarse-grained phase (> 15 mm diameter) in contact with all other minerals and as inclusions within kyanite and hematite. It is a common phase within other whiteschist occurrences such as the Sar e Sang example in Afghanistan, (Kulke & Schreyer, 1973). Hematite forms large (> 2.5 cm), euhedral, tabular to hexagonal crystals which aggregate together into randomly oriented clusters of up to 5 cm in diameter.

The yoderite crystals are generally 1–5 mm long, 1 mm wide, anhedral and either surrounded by chlorite or in sharp contact with kyanite or more rarely hematite. Minor fractures within the yoderite crystals contain chlorite and kyanite without quartz. In hand specimen the yoderite is pale green with a glassy lustre. In thin-section the mineral is colourless, has high relief (Fig. 5) and one strong cleavage (010) with a maximum extinction angle of 29°. The absence of a strong purple

Fig. 4. Electron back-scattered image showing talc laths (bright) intergrown with the chlorite (sheridanite) matrix (dark). The contacts are sharp and straight, suggesting equilibrium. Width of view is 2.5 mm.

colour suggests that the manganese chromophore group (Mn^{2+}–O–Mn^{3+}) is not present (Abu-Eid *et al.*, 1978); this has been confirmed by microprobe analysis (Table 1). The α/β sections display a birefringence of 0.002 (low first-order grey), whereas the α/γ sections display a birefringence of 0.013 (upper first-order red), similar to synthetic phases recorded by Higgins *et al.*

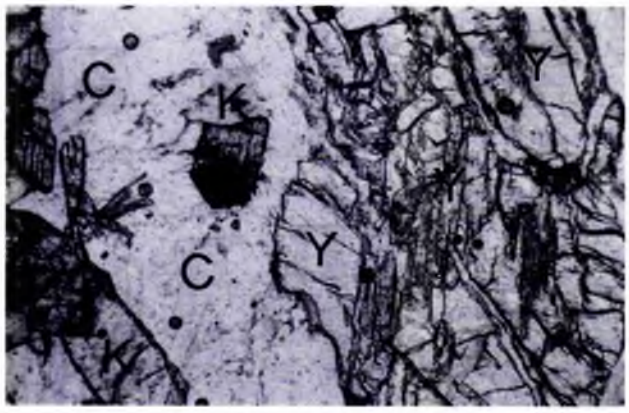

Fig. 5. Photomicrograph of sample SJ 13.128. Note (1) high-relief yoderite (Y) on the right-hand side surrounded by primary chlorite (C); (2) the single crystal of kyanite (K) surrounded by primary chlorite in the centre; (3) the kyanite–chlorite contact on the left-hand side; (4) inclusions within the yoderite were analysed as chlorite and kyanite but not quartz. Outside the field of view, coarse-grained talc and chlorite (as in Fig. 4) are in contact with yoderite. Width of view is 3.5 mm.

(1982) and Fockenberg & Schreyer (1991). The mineral is monoclinic and positive with a $2V\gamma \sim 30°$.

Compared to Chewore green yoderite, the optical properties of Mautia Hill green yoderite are very similar, e.g. α/β sections birefringence = 0.002, α/γ sections birefringence = 0.021 (all $\pm$ 0.003) and $2V\gamma = 30°$. Yoderite at Mautia Hill forms coronas around kyanite (unlike the Chewore Hill example) and is set in a matrix of talc and quartz; chlorite is not reported, yet it is an essential phase in the Chewore yoderite-bearing rock. Despite the strong purple colouration, its mineralogical and optical properties are similar to the green variety, e.g. α/β sections birefringence = 0.002, α/γ sections birefringence = 0.026 (all $\pm$ 0.002), is monoclinic and positive with a $2V\gamma = 25°$ (McKie, 1959). It is possible that high-relief, colourless yoderite has been overlooked from other whiteschist occurrences around the world.

CHEMISTRY AND STRUCTURE

Yoderite crystals from sample SJ 13.128 were analysed using electron microprobe and XRD techniques. Table 1 shows the mean and standard deviation of 20 microprobe spot analyses of four different unzoned crystals of yoderite. The range of composition between grains is within analytical error. The formula is $Mg_2Al_{5.7}Fe_{0.3}Si_4O_{18}(OH)_2$, with a little less Fe than in the green yoderite reported by Higgins *et al.* (1982), $Mg_2Al_{5.6}Fe_{0.4}Si_4O_{18}(OH)_2$, or in purple yoderite $Mg_{1.98}Al_{5.63}Fe_{0.4}Mn_{0.09}Si_{3.92}O_{18.06}(OH)_{1.94}$ reported by McKie & Bradshaw (1966) for the Mautia Hill examples. The difference in molar proportion of Fe^{3+} and Al^{3+} suggests that minor substitution of Al^{3+} for Fe^{3+} occurs within the A (3) site of the crystal structure (Higgins *et al.*, 1982). Although the ideal formula can be written as $Mg_2(Al,Fe)_6Si_4O_{18}(OH)_2$, the amount of Fe^{3+} in the structure appears to lie within the range 0.2–0.4 per formula unit (pfu) as calculated by Fockenburg & Schreyer (1991). Saturation of Fe^{3+} (up to 0.7 pfu) in synthetic yoderite occurs when the mineral is in equilibrium with hematite (Fockenburg & Schreyer, 1991). In the Chewore Hills sample, only yoderite that is in direct contact with hematite displays rims slightly elevated in Fe^{3+}, up to but not beyond 0.4 pfu (see Table 1). Microprobe analysis of the accompanying metamorphic assemblage confirms the presence of sheridanite + chlorite + dravite + hematite + kyanite + talc. Hematite encloses needles of rutile. Representative analyses are given in Table 1.

Results of XRD determinations on the yoderite crystals correspond well with the results for the Tanzanian example (Anon., 1993) (Table 2). The superlattice reflections described by Higgins *et al.* (1982) are present, suggesting that the yoderite is in the ordered, lower-temperature form (< 800 °C).

PROTOLITH

The protoliths of the Kadunguri Whiteschist Formation, including the yoderite-bearing rock, must be rather exceptional since they belong to the simple $MF^{3+}ASH$ system (plus some Na and B). The Mg–Al-rich, alkali-poor chemistry of whiteschists has been explained in other localities by the following situations:

1 mudstones associated with evaporite deposits producing talc, kyanite and scapolite (Kulke & Schreyer, 1973; Fockenberg & Schreyer, 1994);

2 *in situ* weathering and metamorphism of saponitic bentonites (McKie, 1959);

3 hydrothermal alteration of metabasic volcanics producing talc and kyanite (Vrána & Barr, 1972; Vrána, 1975);

4 interaction of hydrothermal fluids with dolomite and quartzite producing talc, kyanite and magnesite (Bodenlos, 1955);

5 metasomatism of peridotite and serpentinite producing talc and chlorite (Curtis & Brown, 1969).

The large size of the Kadunguri Whiteschist Formation (6 × 3 km) makes it one of the largest single continuous outcrops of talc + kyanite + quartz rock recorded anywhere in the world. This alone suggests that its precursor was homogeneous on a kilometre scale, and this would therefore seem to exclude a localized evaporite or a bentonite origin. The lack of any recognizable sedimentary features and/or any magnesite/scapolite mineralization also seems to indicate a non-sedimentary source. A large homogeneous body of the size and composition indicated is likely to have an igneous origin. The trace-element geochemistry of the Kadunguri Whiteschist Formation is similar to that of MORB-type amphibolites exposed along the Maunde River (latitude 30° 07′ 00′ E, longitude 15° 56′ 20′ S) within the adjacent Ophiolite terrane (unpublished data). It is envisaged that the whiteschists are

Table 1. Electron microprobe data of the minerals within the yoderite-bearing rock (SJ 13.128) from the Chewore Hills and both green and purple yoderite from Mautia Hill, Tanzania.

		Yoderite					Associated minerals						
		Chewore Hills			Mautia Hill								
Weight %		Mean of 20 analyses	Std deviation	Fe^{3+} elevated	Green*	Purple**	Penninite	Sheridanite	Talc	Hematite	Dravite	Kyanite	Rutile
	SiO_2	37.11	0.24	36.75	36.05	36.70	33.63	30.12	58.71	0.31	37.19	37.17	0.13
	TiO_2	0.03	0.02	0.10	0.10	0.00	0.04	0.00	0.01	0.78	0.29	BD	89.62
	Al_2O_3	45.12	0.23	45.25	43.46	43.16	22.90	22.99	2.46	0.24	32.13	62.33	0.03
	FeO	0.00	0.00	0.00	0.00	0.00	12.31	0.64	0.21	0.00	0.00	0.00	0.00
	Fe_2O_3	3.43	0.14	4.93	3.85	3.56	0.05	0.00	0.00	98.71	3.49	0.59	2.51
	MnO	0.02	0.02	0.00	<0.01	1.80	BD	0.02	BD	BD	BD	BD	BD
	MgO	12.43	0.17	12.78	12.25	12.16	19.10	32.84	28.80	0.13	10.20	BD	BD
	CaO	0.01	0.01	BD	<0.01	BD	0.16	0.02	0.01	0.02	0.28	BD	BD
	Na_2O	0.01	0.01	BD	BD	BD	0.02	0.01	0.18	BD	2.18	BD	BD
	K_2O	0.01	0.01	0.01	BD	BD	0.02	0.01	0.02	BD	0.06	BD	BD
	Total	98.17	0.40	99.31	95.72	97.38	88.23	86.65	90.39	100.19	85.81	100.09	92.29
Cation	Si	4.00	0.02	3.92	3.93	4.01	3.21	2.81	3.91	0.01	5.95	4.02	0.00
Proportion	Ti	0.00	0.00	0.01	0.01	0.00	0.00	0.00	0.00	0.02	0.04	0.00	0.97
	Al	5.73	0.02	5.68	5.58	5.56	2.58	2.52	0.19	0.01	6.05	7.94	0.00
	Fe^{2+}	0.00	0.00	0.00	0.16	0.00	0.98	0.05	0.01	0.00	0.00	0.00	0.00
	Fe^{3+}	0.28	0.01	0.40	0.32	0.29	0.00	0.00	0.00	1.96	0.42	0.05	0.03
	Mn^{3+}	0.00	0.00	0.00	0.00	0.15	0.00	0.00	0.00	0.01	0.00	0.00	0.00
	Mg	2.00	0.03	2.03	1.99	1.98	2.72	4.56	2.86	0.00	2.43	0.00	0.00
	Ca	0.00	0.00	0.00	0.00	0.00	0.02	0.00	0.00	0.00	0.05	0.00	0.00
	Na	0.00	0.00	0.00	0.00	0.00	0.00	0.00	0.02	0.00	0.68	0.00	0.00
	K	0.00	0.00	0.00	0.00	0.00	0.00	0.00	0.00	0.00	0.01	0.00	0.00
Cation total	12.00	0.01	12.04	11.99	11.99	9.51	9.94	7.02	1.99	15.62	12.01	1.00	
No of oxygens		19		19	19	19	14	14	11	32	24.5	20	2

Notes: BD = below detection.

* Analysis taken from McKie & Bradshaw (1966).

** Analysis taken from Fockenberg & Schreyer (1993), Table 1, analysis number 3.

Table 2. Powder X-ray diffraction data for the Chewore Hills yoderite compared with Mautia Hill, Tanzania, given in McKie (1959).

d Spacing standard (Å) Mautia Hill	*d* Spacing measured (Å) Chewore Hills	Intensity standard Mautia Hill	Intensity measured Chewore Hills	hkl value
4·18	4·18	5	11	−111
3·87	3·87	10	7	−201
3·83*	3·83*	10	17	
3·63	3·63	20	18	111
3·50	3·50	100	100	002
3·34*	3·35*	5	20	
3·23	3·22	50	34	210
3·19*	3·19*	50	36	
3·07	3·07	10	14	201
3·03	3·03	80	56	−112
2·91	2·90	50	30	102
2·72	2·72	10	11	120
2·68	2·68	40	37	−301
2·65*	2·65*	10	11	
2·61	2·61	60	47	−121
2·58	2·58	50	30	300
2·46	2·46	50	26	121
2·41	2·41	5	8	−103
2·39*	2·39*	30	26	
2·36	2·36	20	18	310
2·32	2·32	20	14	220
2·27	2·27	10	11	−122
2·24	2·24	50	32	−312
2·16	2·15	10	9	013
2·11	2·11	10	9	−421
2·06	2·06	5	6	−422
2·00*	2·00*	60	37	−502
1·97	1·97	40	22	322
1·89*	1·89*	20	12	330

* Superlattice reflection

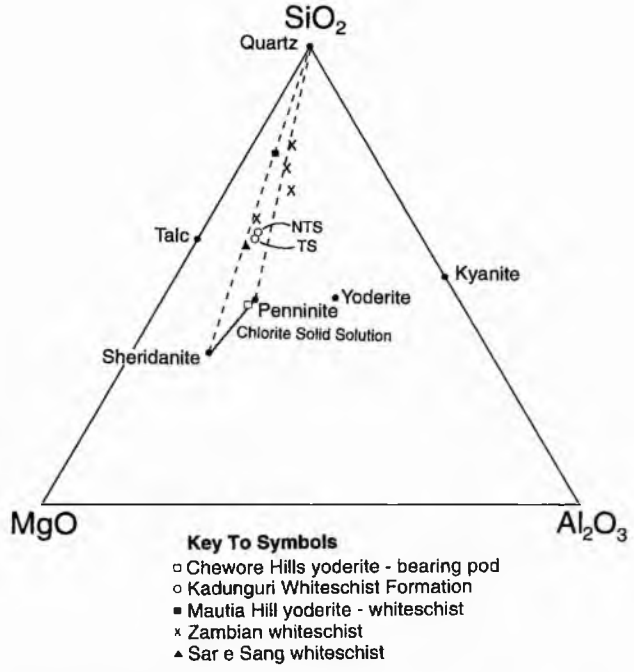

Fig. 6. SiO_2, MgO, Al_2O_3 (mol.%) triangular compatibility diagram (in the presence of excess H_2O, FeO and Fe_2O_3) showing the positions of the coexisting phases and whole-rock major-element analyses for various whiteschist examples (see Fig. 2 for Chewore Hills localities and Table 3 for geochemical analyses). Note that the whole-rock compositions are concentrated within or close to a two-phase field of chlorite solid solutions and quartz. Refer to Fig. 2 for the locality and Table 3 for the whole-rock major-element analysis of samples TS and NTS.

perhaps metasomatized metabasalts similar to those described by Vrána & Barr (1972) and Vrána (1975) in Zambia. The closest of these crops out 90 km to the north-west.

PETROGENESIS

As we have yet to discover all the mineral assemblages in the Kadunguri Whiteschists we can only make some preliminary comments on their petrogenesis. The presence of yoderite and the relatively large (centimetre) grain size of all phases in the yoderite-bearing pod compared to the surrounding whiteschist suggest that fluid with a high water activity was involved in the metamorphic evolution of the rock (Fockenberg & Schreyer, 1994). Assuming that the seven components MgO, Fe_2O_3, Al_2O_3, SiO_2, Na_2O, H_2O and B_2O_3 define the system and that the latter three are mobile, then this leaves four inert components (C_i). According to the Korzhinskii Phase Rule (Korzhinskii, 1959), assuming that the degrees of freedom are P–T, then the number of solid phases (P_s) equals C_i, i.e. in this case four. Actually, P_s equals six, i.e. yoderite + kyanite + talc + chlorite + dravite + hematite. If H_2O was the only mobile component and Na_2O and B_2O_3 are considered as inert then $C_i = 6 = P_s$, thus obeying the Korzhinskii Phase Rule. This indicates that dravite might have been initially present, possibly as a product of hydrothermal/metasomatic alteration of the protolith and that yoderite formation proceeded isochemically during further progressive metamorphism.

The positions of the coexisting phases and whole-rock major element analyses of various whiteschist examples are plotted in Fig. 6. Schreyer (1977) indicates that 'most of the components present within whiteschists can theoretically be represented by the assemblage Mg-chlorite plus quartz', since 'the projection points of major element analysis onto a SiO_2–MgO–Al_2O_3 triangular diagram are concentrated within a two-phase field of chlorite solid solutions with quartz'. Samples from the Kadunguri Whiteschist Formation also plot within or lie close to this two-phase field (Fig. 6): the pod rock plots below the kyanite + talc tie-line and the country rocks plot above this (for analyses see Table 3). In fact, Fe-rich chlorite [penninite, with a formula $Mg_3Al_{2.5}Fe_1Si_{3.2}O_{10}(OH)_8$] is preserved as inclusions within the cores of kyanite and hematite crystals (see Table 1 for analyses). According to the experiments of Massonne (1989), with increasing P–T, chlorite and quartz become unstable to form talc and kyanite. However, in the Chewore Hills example, hematite is

present. This suggests a reaction

(1) $100\ Mg_3Al_{2.5}Fe_1Si_{3.2}O_{10}(OH)_8$ (penninite) $+205\ SiO_2+32.5\ O_2=100\ Mg_3Si_4O_{10}(OH)_2$ (quartz, oxygen, talc) $+125\ Al_2SiO_5+50\ Fe_2O_3+300\ H_2O$ (kyanite, hematite, water)

[note that reactions (1)–(6) use mineral formulae from the Chewore Hills analyses (Table 1)]. Reaction (1) is a redox reaction and therefore high oxygen fugacity (f_{O2}) is a prerequisite. The chlorite that comprises the coarse-grained matrix (40% of the rock) is actually Fe-poor, Mg-rich sheridanite [$Mg_{4.5}Al_{2.5}Fe_{0.05}\ Si_{2.8}O_{10}(OH)_8$; see Table 1]. If the fO_2 remains high and all the quartz becomes exhausted by reaction (1), then sheridanite might be produced via a second reaction:

(2) $500\ Mg_3Al_{2.5}Fe_1Si_{3.2}O_{10}(OH)_8$ (penninite) $+173.5\ O_2=230\ Mg_{4.5}Al_{2.5}Fe_{0.05}Si_{2.8}O_{10}(OH)_8$ (oxygen, sheridanite) $+155\ Mg_3Si_4O_{10}(OH)_2+338\ Al_2SiO_5$ (talc, kyanite) $+244\ Fe_2O_3+925\ H_2O$ (hematite, water)

Note the positions of the two chlorite compositions in Fig. 6: one for penninite and the other for sheridanite. As penninite and sheridanite form a solid solution, these two invariant points may become one, as shown in Fig. 7. Experimental work by Fockenburg & Schreyer (1994) indicates a variety of possible yoderite-forming reactions in the MgO–Fe_2O_3–Al_2O_3–SiO_2–H_2O (MFASH) system. Two potential reactions are worth considering for the Chewore Hills yoderite:

(3) $54.2\ Mg_3Si_4O_{10}(OH)_2$ (talc) $+120\ Mg_{4.5}Al_{2.5}Fe_{0.05}Si_{2.8}O_{10}(OH)_8+848\ Al_2SiO_5$ (sheridanite, kyanite) $+50\ Fe_2O_3=350\ Mg_2Al_{5.7}Fe_{0.3}Si_4O_{18}(OH)_2$ (hematite, yoderite) $+183.4\ H_2O$ (water)

(4) $2.22\ Mg_{4.5}Al_{2.5}Fe_{0.05}Si_{2.8}O_{10}(OH)_8$ (sheridanite) $+11.47\ Al_2SiO_5+2\ SiO_2+0.7\ Fe_2O_3$ (kyanite, quartz, hematite) $=5\ Mg_2Al_{5.7}Fe_{0.3}Si_4O_{18}(OH)_2+3.9\ H_2O$ (yoderite, water)

The *P–T* stability field of yoderite (after Fig. 11 in Fockenburg & Schreyer, 1994) and the approximate *P–T* conditions for both the Chewore Hills and Mautia Hill assemblages and their associated mineral parageneses are illustrated in Fig. 7. Two possible *P–T* paths for the Kadunguri Whiteschist Formation (including the yoderite-bearing pod) are indicated in this diagram. Both *P–T* paths (medium and higher pressure) will end in the identical yoderite without quartz field. If metamorphism proceeded via the medium-pressure path, yoderite would initially be produced in *all* of the Kadunguri Whiteschist Formation rocks as a result of reaction (4). Further progressive metamorphism is via

Table 3. Whole-rock major-element compositions of the Kadunguri Whiteschist Formation (including the yoderite-bearing rock) and other whiteschist occurrences. Refer to Figs 2 & 3 for the locality of the Kadunguri Whiteschist samples.

	Chewore Hills			Mautia Hill	Zambia				Sar e Sang
Weight %	TS	NTS	Yoderite Pod	T*	Z157*	Z159*	Z161*	Z234*	A42*
SiO_2	51.95	56.37	35.46	74.54	61.20	67.00	71.40	57.20	56.20
TiO_2	1.15	1.38	0.27	0.27	1.14	1.51	1.22	1.18	0.30
Al_2O_3	15.50	16.07	23.80	8.13	13.40	13.10	10.70	16.20	16.00
B_2O_3				n.rep	0.01	0.01	0.02	0.13	0.34
Fe_2O_3	2.29	7.59	12.97	1.92	0.10	4.40	5.10	5.20	0.30
FeO	0.00	0.00	0.00	0.90	0.30	0.30	0.30	0.70	0.10
MnO	0.00	0.03	0.02	0.11	0.00	0.00	0.00	0.00	<0.01
MgO	18.99	16.24	20.35	12.33	20.00	11.50	9.60	11.40	22.90
CaO	0.11	0.02	0.18	trace	0.10	0.10	0.10	0.20	0.10
Na_2O	0.10	0.40	0.33	0.14	0.30	0.20	0.10	5.30	0.60
K_2O	0.02	0.01	0.00	0.03	0.10	0.10	0.10	0.70	0.20
P_2O_5	0.07	0.06	0.05	trace	0.02	0.27	0.00	0.04	<0.02
LOI	10.60	1.80	6.80 H_2O	1.87	3.90	2.00	1.70	2.30	3.50
Total	100.78	99.95	100.23	100.24	100.57	100.49	100.34	100.55	100.54

Notes: n.rep = not reported.
* Analyses taken from Schreyer (1977).

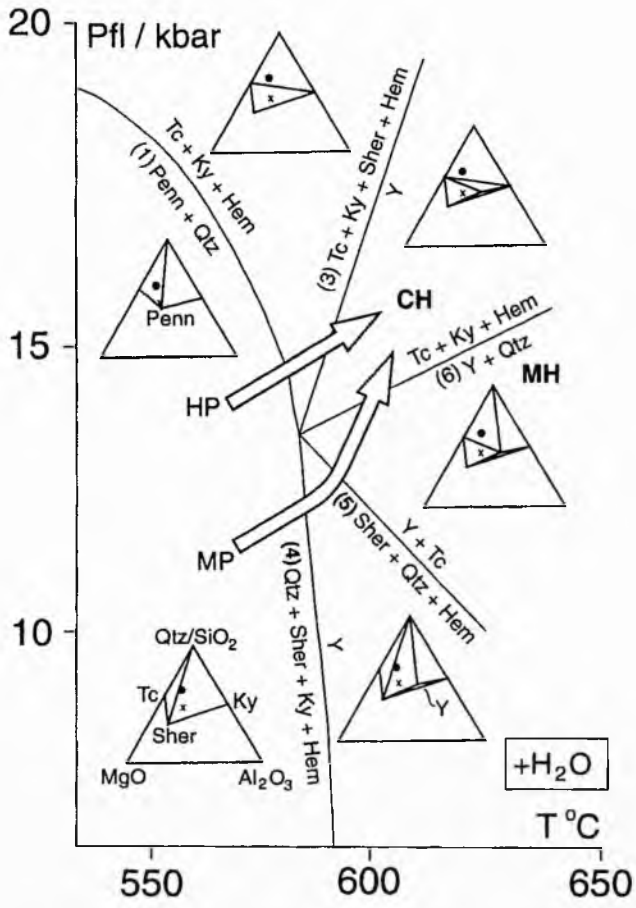

Fig. 7. *P–T* diagram showing the stability of yoderite-forming reactions in the $MgO–Al_2O_3–SiO_2–H_2O$ (MASH) system and associated mineral parageneses based on the experiments of Fockenburg & Schreyer (1994). The chlorite + quartz = talc + kyanite reaction curve (1) is from Massonne (1989). Reaction curve numbers refer to reactions (1)–(6) discussed in the text. MH are the approximate *P–T* conditions for the Mautia Hill quartz + yoderite locality (from Fig. 13 in Fockenburg & Schreyer, 1994) and CH are the approximate *P–T* conditions for quartz-free yoderite at Chewore Hills. The arrows represent theoretical *P–T* paths for the Chewore Hills yoderite-bearing pod (HP indicates the high-pressure path and MP indicates the medium-pressure path; refer to text for discussion). On the triangular plots the crosses represent Mg-rich whole-rock compositions and the dots represent Si-rich compositions. Note how Si-rich whiteschists will produce Qtz + Ky + Tc assemblages and how Mg-rich whiteschists will produce Tc + Ky + Chl + Y assemblages at > 13 kbar and 590 °C. Mineral abbreviations are as follows: Hem = hematite; Ky = kyanite; Penn = penninite; Sher = sheridanite; Tc = talc; Qtz = quartz and Y = yoderite.

the following reactions:

$$(5)\quad 33.1\ \underset{\text{sheridanite}}{Mg_{4.5}Al_{2.5}Fe_{0.05}Si_{2.8}O_{10}(OH)_8} + 124\ \underset{\text{quartz}}{SiO_2} + 1.3\ \underset{\text{hematite}}{Fe_2O_3} = 40\ \underset{\text{talc}}{Mg_3Si_4O_{10}(OH)_2} + 14.5\ \underset{\text{yoderite}}{Mg_2Al_{5.7}Fe_{0.3}Si_4O_{18}(OH)_2} + 78\ \underset{\text{water}}{H_2O}$$

$$(6)\quad 15\ \underset{\text{yoderite}}{Mg_2Al_{5.7}Fe_{0.3}Si_4O_{18}(OH)_2} + 22.8\ \underset{\text{quartz}}{SiO_2} = 10\ \underset{\text{talc}}{Mg_3Si_4O_{10}(OH)_2} + 42.8\ \underset{\text{kyanite}}{Al_2SiO_5} + 2.3\ \underset{\text{hematite}}{Fe_2O_3} + 5\ \underset{\text{water}}{H_2O}$$

Thus reactions (4) and (5) produce yoderite in silica-rich whiteschists. Reaction (6) produces talc + chlorite + kyanite + yoderite in Mg-rich compositions (i.e. the yoderite-bearing pod) and talc + kyanite + quartz *without* chlorite or yoderite in the Si-rich whiteschists (Fig. 7).

If metamorphism proceeded via the higher-pressure path then these whiteschists would evolve via reaction (1) and/or reaction (2) so that chlorite and quartz become mutually exclusive. Yoderite will be produced in chlorite + talc + kyanite assemblages *without* quartz through reaction (3). Thus the quartz-bearing whiteschists that surround the yoderite-bearing pod will never have contained yoderite (in contrast to the medium-pressure path).

The higher-pressure path of metamorphism for the Kadunguri Whiteschist Formation is supported by textural evidence, i.e. there is a notable lack of relict quartz inclusions within yoderite crystals in the pod and an absence of relict yoderite crystals or inclusions within the surrounding quartz-bearing whiteschists. There is no textural evidence for reactions (4), (5) or (6), which might have been expected to leave behind some relict inclusions.

Experimental stability conditions for a quartz-free yoderite assemblage in the MFASH system where a_{H2O} and f_{O2} are high are at a minimum pressure of 13 kbar at 590 °C and a maximum pressure of 21 kbar at 650 °C (Fig. 7) (if staurolite is not involved; see details in Fig. 11 of Fockenburg & Schreyer, 1994).

In common with the Mautia Hill occurrence, this yoderite petrogenesis has a near absence of Fe^{2+} in any of the mineral phases, and any ferromagnesian phases approach their Mg-end-members. Note, however, that Fe_2O_3 is present in excess, so many of the reactions become redox ones. The stabilities of the reactions will be dependent on the fugacity of O_2. Since chlorite has mainly Fe^{2+}, the $f_{O2}–T$ relations for the yoderite-forming reactions become complex. The *P–T* stability can be affected by the partitioning of Fe^{2+} and Fe^{3+} among the phases (e.g. chlorite and yoderite). Hence the *P–T* estimate for the yoderite-bearing rock and surrounding whiteschists may be somewhat lower than indicated. However, since chlorite has only 0.05 pfu Fe^{2+} and yoderite has 0.3 pfu Fe^{3+}, this effect may not be significant. The consequence of including Na + B components (forming dravite) in the $MF^{3+}ASH$ system are unknown, although it is to be expected that reaction temperatures might be raised slightly, especially if Na and/or B enter a phase of the

yoderite-forming reaction (Grew *et al.*, 1998). This increase in reaction temperature is also likely to be negligible since the Na content of talc is so small (0.02 pfu Na in talc, see Table 1).

Minor chlorite and kyanite, but not quartz, occur within fractures in yoderite crystals. If quartz were present then it may be interpreted that this assemblage represents a retrogressive metamorphic event via reaction (4) (see Fig. 7). However, detailed microprobe analyses of mineral phases within these fractures reveal that this chlorite has a composition identical to the matrix phase (see Table 1). The lack of quartz and the primary nature of the mineral phases suggest that this is not indicative of a retrogressive event.

Thus quartz free chlorite + yoderite + kyanite + talc whiteschists are indicative of high-pressure and medium- to high-temperature metamorphism. Assuming that the geothermal gradient was linear, these *P–T* conditions indicate a gradient of *c.* 10 °C km^{-1}, which is typical of subduction zone metamorphism.

Preliminary thermobarometric studies (using the unpublished computer program THERMOBAROMETRY of Kohn & Spear, version 2.0, 1996) of garnet amphibolites from the neighbouring Ophiolite terrane have yielded estimates of maximum *P–T* values for garnet cores of 9.5 ± 0.5 kbar and 625 °C ± 25 °C (using the Tschermakite–Mg calibration of Kohn & Spear, 1990 and the calibration of Graham & Powell, 1984). Minimum *P–T* values for garnet rims are 10.5 ± 0.5 kbar at 700 ± 25 °C. As yet no higher *P–T* mineral inclusions have been discovered within the garnet-bearing amphibolites or pelites. These results are outside the experimentally determined *P–T* range of the yoderite without quartz assemblages studied by Fockenburg & Schreyer (1994). Since the two terranes are most probably in tectonic contact it is possible that the two were metamorphosed either at different times and different *P–T*, or contemporaneously but at different *P–T* conditions. Further work is in progress.

CONCLUSIONS

The Kadunguri Whiteschist Formation is one of the largest recorded outcrops of talc + kyanite + quartz rock and contains the second known natural occurrence of yoderite. The lack of the intense purple colouration that is associated with the type locality in Tanzania suggests that colourless/pale green yoderite may have been overlooked at other whiteschist localities.

Preliminary results of trace-element analyses of these whiteschists suggest they were formed from hydrothermally altered/metasomatized metabasalts comparable to metabasalts within the adjacent Ophiolite terrane. A similar origin for whiteschist occurrences some 90 km to the north-west in Zambia has been suggested by Vrána & Barr (1972) and Vrána (1975).

From textural and mineralogical observations it is suggested that yoderite formed as a result of reactions between talc, chlorite, kyanite and hematite. Experimental evidence suggests a minimum of 13 kbar and 590 °C for this reaction (Fockenburg & Schreyer, 1994), indicating a depth of burial of at least 50 km and a possible minimum geothermal gradient of *c.* 10 °C km^{-1}.

The Kadunguri Whiteschist Formation is most probably in tectonic contact with the 1393 ± 22 Ma Chewore Ophiolite Complex. The similarity in trace-element geochemistry between these whiteschists and the ophiolite amphibolite metabasalts and the high-pressure, moderate-temperature nature of the whiteschist metamorphism (with its yoderite-bearing pod) suggest the two terranes may be related in a complex relict subduction/suture zone of possible Grenvillian age.

ACKNOWLEDGEMENTS

This research was funded by a scholarship to St Andrews University, grants from the Irvine and Welch Bequests to St Andrews University and a grant from Elsevier. Field assistance from R. Chaukura, E. Dzingira, S. Chikwangwani and J. Ndlovu from the Chewore National Safari Park is gratefully acknowledged. D. Herd and A. Calder carried out the microprobe and XRD analyses and P. Bowden kindly donated a sample of Mautia Hill yoderite schist. Constructive reviews by K. Bucher, E. Grew, J. G. Liou, W. Schreyer and J. C. Schumacher greatly improved the manuscript.

REFERENCES

Abu-Eid, R. M., Langer, K. & Seifert, F., 1978. Optical absorption and Mössbauer spectra of purple and green yoderite, a kyanite-related mineral. *Physics and Chemistry of Minerals*, **3**, 271–289.

Anon., 1992. *Aeromagnetic maps*, 1:50,000 sheet nos. 1529 D4 – AM, 1530 C3 – AM, 1629 B2 – AM and 1630 A1 – AM. Geological Survey of Zimbabwe.

Anon., 1993. *International Centre for Diffraction Data*, sets 1–42, PDF1 Mineral Subfile – 12–625.

Bodenlos, A. J., 1955. Magnesite deposits of the Serra das Èquas, Brumado, Bahia, Brazil. *US Geological Survey Bulletin*, **975**, 87–170.

Curtis, C. D. & Brown, P. E., 1969. The metasomatic development of zoned ultrabasic bodies in Unst, Shetland. *Contributions to Mineralogy and Petrology*, **24**, 275–292.

Fleet, S. G. & Megaw, H. D., 1962. The crystal structure of yoderite. *Acta Crytallographica*, **15**, 721–728.

Fockenberg, T. & Schreyer, W., 1991. Yoderite, a mineral with essential ferric iron: its lack of occurrence in the system MgO–Al_2O_3–SiO_2–H_2O. *American Mineralogist*, **76**, 1052–1060.

Fockenberg, T. & Schreyer, W., 1993. Synthesis and properties of Mn-bearing yoderite and of Mn-bearing kornerupine as a by-product. *Mineralogy and Petrology*, **48**, 115–128.

Fockenberg, T. & Schreyer, W., 1994. Stability of yoderite in the absence and in the presence of quartz: an experimental study in the system MgO–Al_2O_3–Fe_2O_3–SiO_2–H_2O. *Journal of Petrology*, **35**, 1341–1375.

Goscombe, B., Fey, P. & Both, F., 1994. Structural evolution of the Chewore Inliers, Zambezi Mobile Belt, Zimbabwe. *Journal of African Earth Sciences*, **19**, 199–224.

Graham, C. M. & Powell, R., 1984. A garnet–hornblende

geothermometer: calibration, testing and application to the Pelona Schist, Southern California. *Journal of Metamorphic Petrology*, **2**, 13–21.

Grew, E. S., Pertsev, N. N., Vrána, S., Yates, M. G., Shearer, C. K. & Wiedenbeck, M., 1998. Kornerupine paragenesis in whiteschists and other magnesian rocks: is kornerupine + talc a high-pressure assemblage equivalent to tourmaline + orthoamphibole? *Contributions to Mineralogy and Petrology*, **131**, 22–38.

Higgins, J. C., Ribbe, P. H. & Nakajima, Y., 1982. An ordering model for the commensurate antiphase structure of yoderite. *American Mineralogist*, **67**, 76–84.

Kohn, M. J. & Spear, F. S., 1990. Two new barometers for garnet amphibolites with applications to eastern Vermont. *American Mineralogist*, **75**, 89–96.

Korzhinskii, D. S., 1959. *Physiochemical basis of the analysis of the petrogenesis of minerals*. Consultants Bureau, New York.

Kulke, H. G. & Schreyer, W., 1973. Kyanite–talc schist from Sar e Sang, Afghanistan. *Earth and Planetary Science Letters*, **18**, 324–328.

Massonne, H. J., 1989. The upper thermal stability of chlorite + quartz: an experimental study in the system MgO-Al_2O_3-SiO_2-H_2O. *Journal of Metamorphic Geology*, **7**, 567–581.

McKie, D., 1959. Yoderite, a new hydrous magnesium iron alumino-silicate from Mautia Hill, Tanganyika. *Mineralogical Magazine*, **32**, 282–307.

McKie, D. & Bradshaw, J., 1966. A green variety of yoderite. *Nature*, **210**, 1148.

Möller, A., Mezger, K. & Schenk, V., 1998. Crustal age domains and the evolution of the continental crust in the Mozambique Belt of Tanzania: combined Sm–Nd, Rb–Sr, and Pb–Pb isotopic evidence. *Journal of Petrology*, **39**, 749–783.

Mrurma, A. H. & Basu, N. K., 1987. Petrology of the talc–kyanite–yoderite–quartz schist and associated rocks of Mautia Hill, Mpwapwa District, Tanzania. *Journal of African Earth Sciences*, **6**, 301–311.

Oliver, G. J. H., Johnson, S. P., Williams, I. S. & Herd, D. A., 1998. Relict 1.4 Ga oceanic crust in the Zambezi Valley, northern Zimbabwe: evidence for Mid-Proterozoic supercontinental fragmentation. *Geology*, **26**, 571.

Schreyer, W., 1977. Whiteschists: their compositions and pressure–temperature regimes based on experimental, field, and petrographic evidence. *Tectonophysics*, **43**, 127–144.

Schreyer, W., 1988. Experimental studies on metamorphism of crustal rocks under mantle pressures. *Mineralogical Magazine*, **52**, 1–26.

Schreyer, W. & Seifert, F., 1969a. Compatibility relations of the aluminium silicates in the system MgO–Al_2O_3–SiO_2–H_2O and K_2O–MgO-Al_2O_3–SiO_2–H_2O at high pressures. *American Journal of Science*, **267**, 371–388.

Schreyer, W. & Seifert, F., 1969b. High pressure phases in the system MgO–Al_2O_3–SiO_2–H_2O. *American Journal of Science*, **267A**, 407–443.

Schreyer, W. & Yoder, H. S., 1968. Yoderite: synthesis, stability and interpretation of its natural occurrence. *Carnegie Institute Washington Yearbook*, **66**, 376–380.

Vrána, S., 1975. Magnesian–aluminous rocks, the associated ore mineralisation and the problem of magnesium–iron metasomatism. *Krystalinikum*, **11**, 101–114.

Vrána, S. & Barr, M. W. C., 1972. Talc–kyanite–quartz schist and other high pressure assemblages from Zambia. *Mineralogical Magazine*, **38**, 837–846.

Yoder, H. S., 1952. The MgO–Al_2O_3–SiO_2–H_2O system and related metamorphic facies. *American Journal of Science*, **Bowen Vol.**, 569–627.

Received 10 October 1997; revision accepted 18 May 1998.

Map 1a. 1 : 25 000 scale locality map of the Southern Chewore Hills.

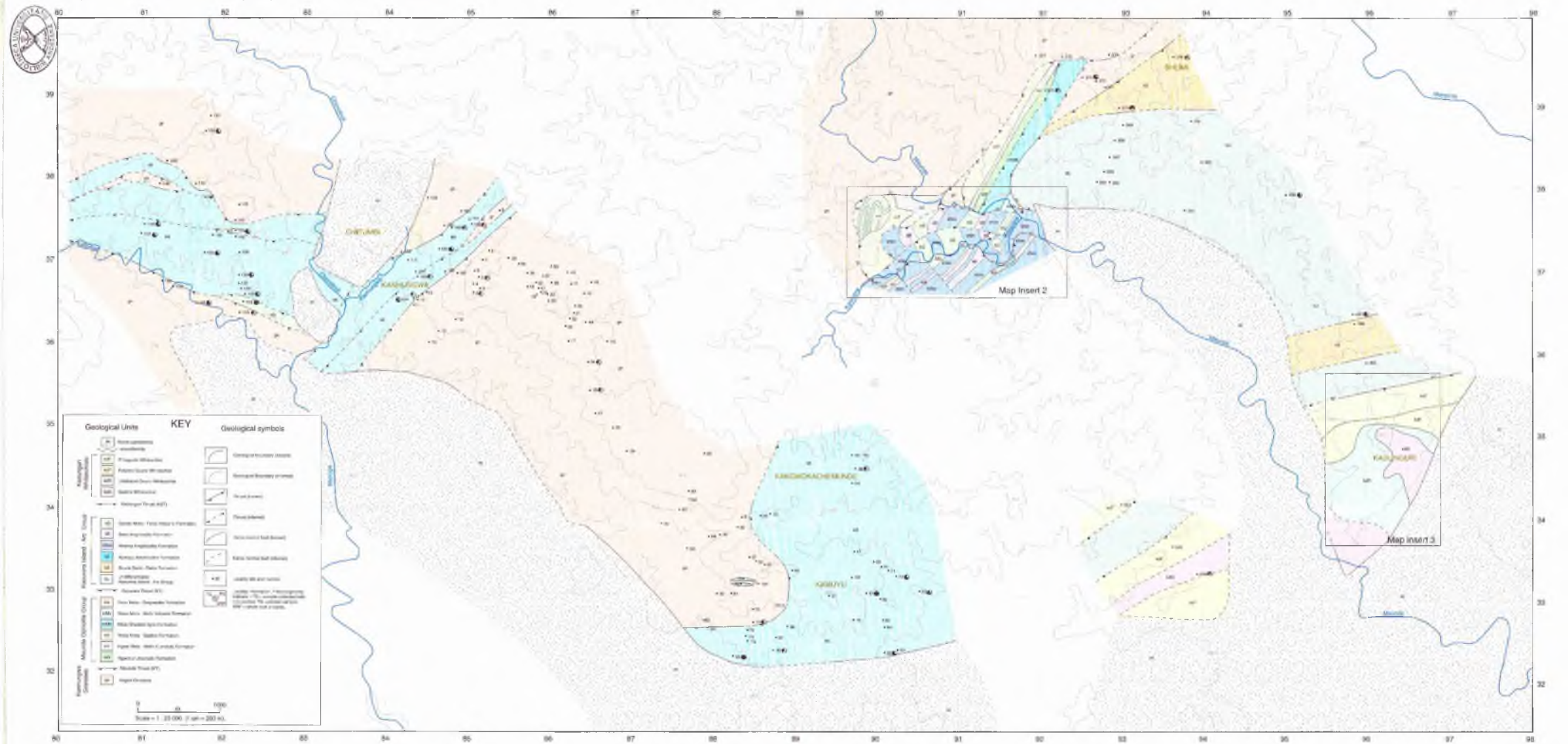

Map 1b. 1 : 25 000 scale structural map of the Southern Chewore Hills.

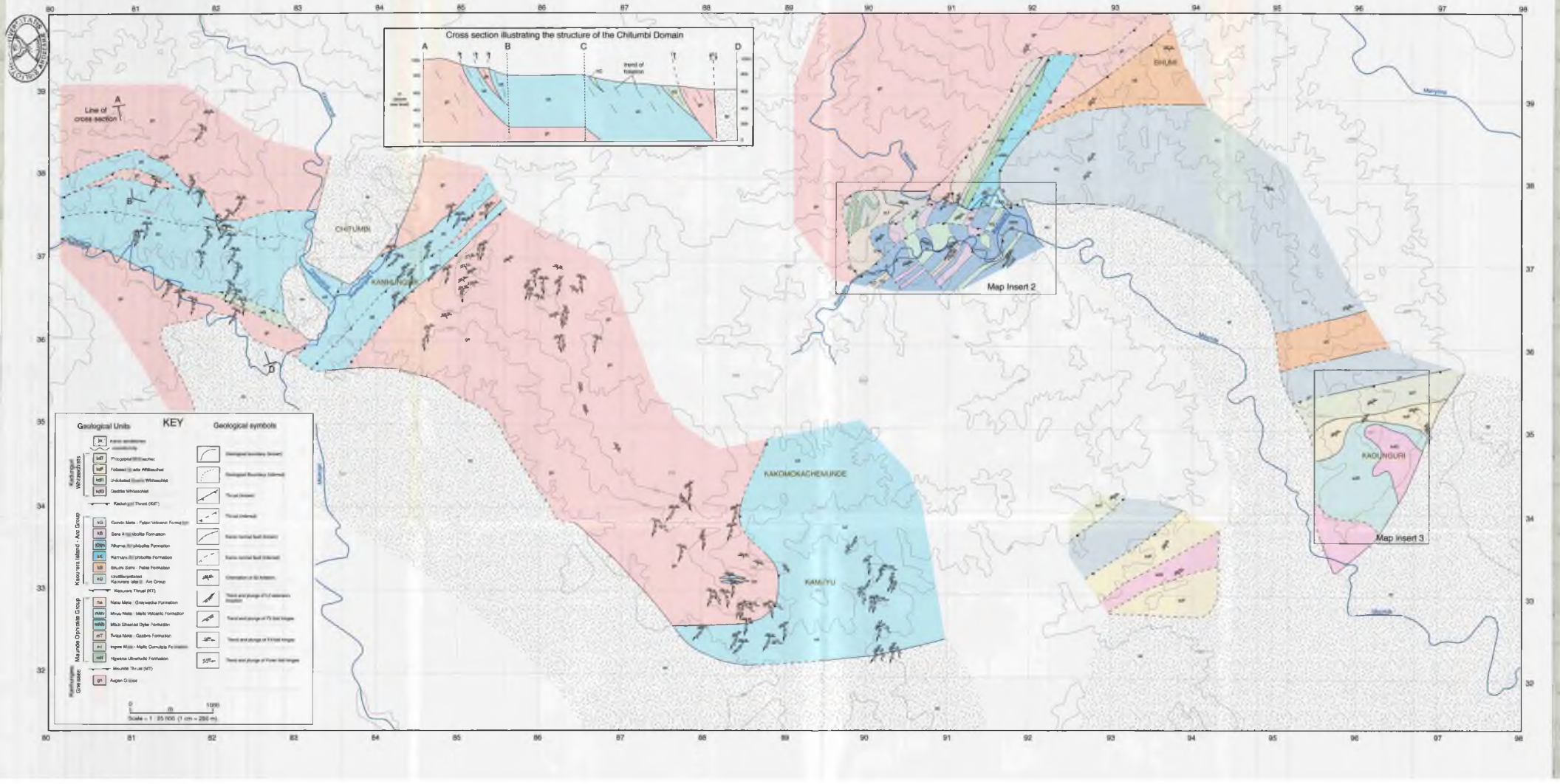

Map 2a. 1 : 5 000 scale locality map of the Maunde Domain.

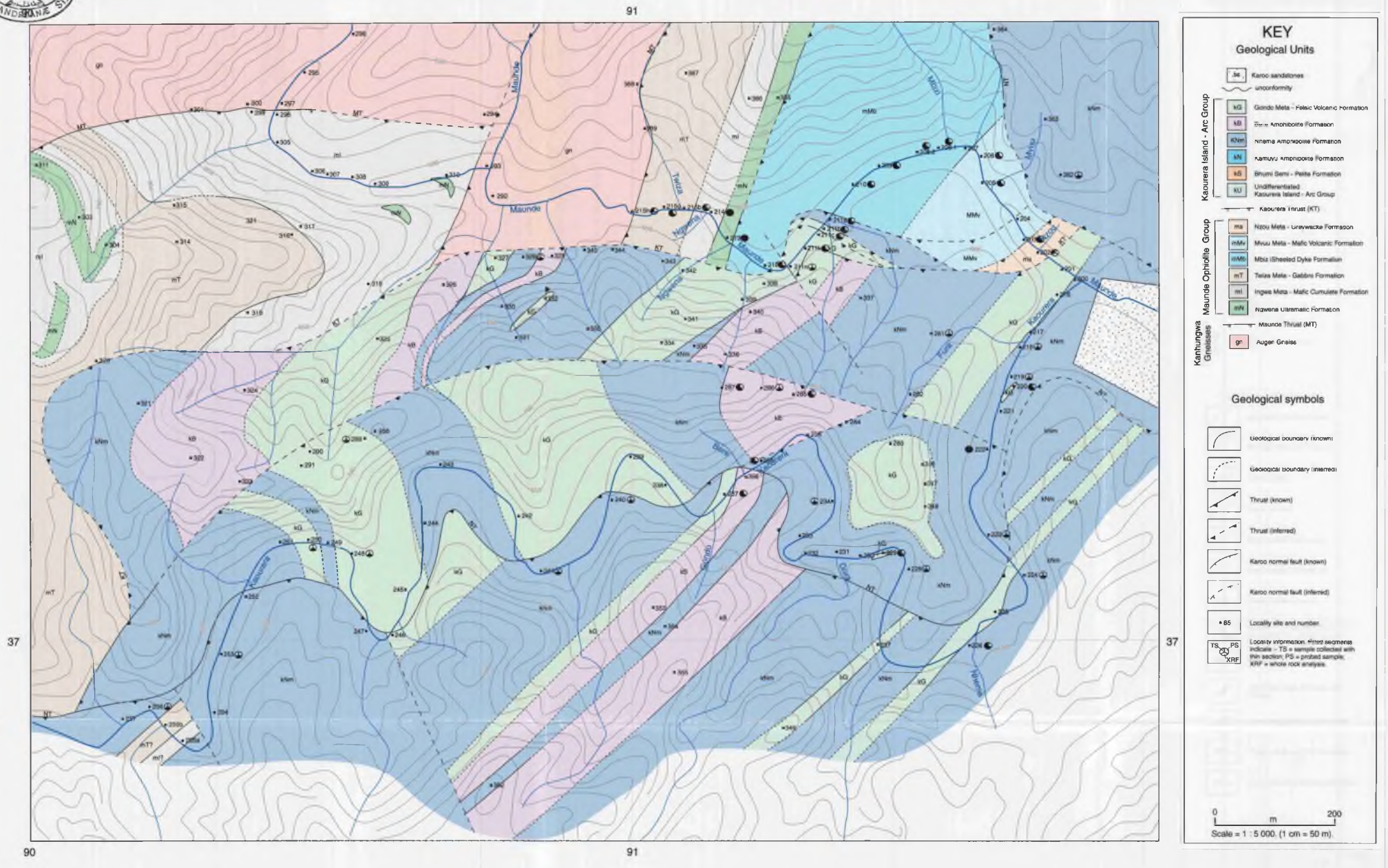

Map 2b. 1 : 5 000 scale structural map of the Maunde Domain.

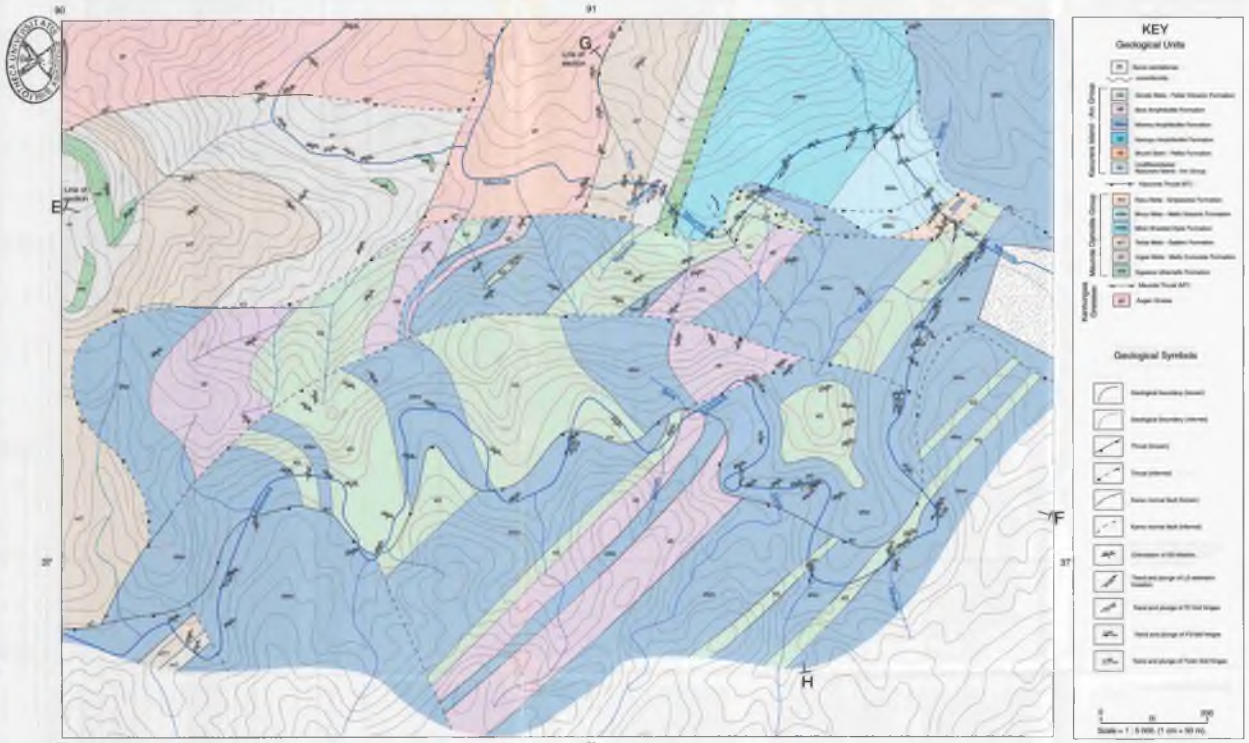

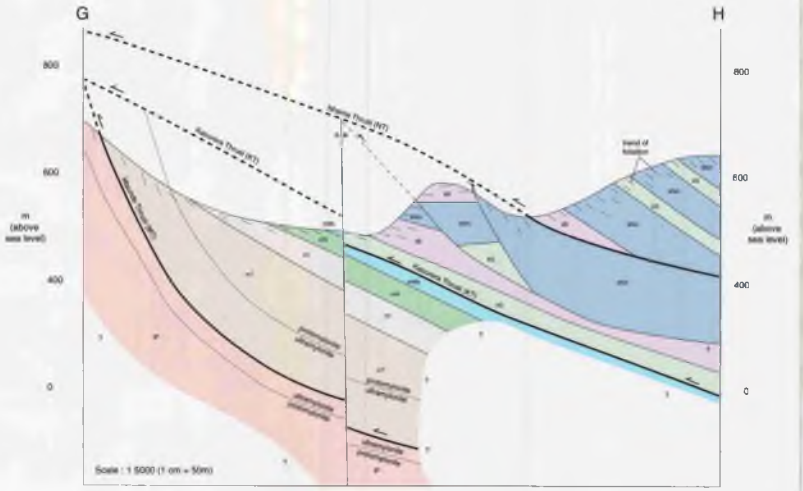

E Cross Section E to F Illustrated in Map Insert 2b. F

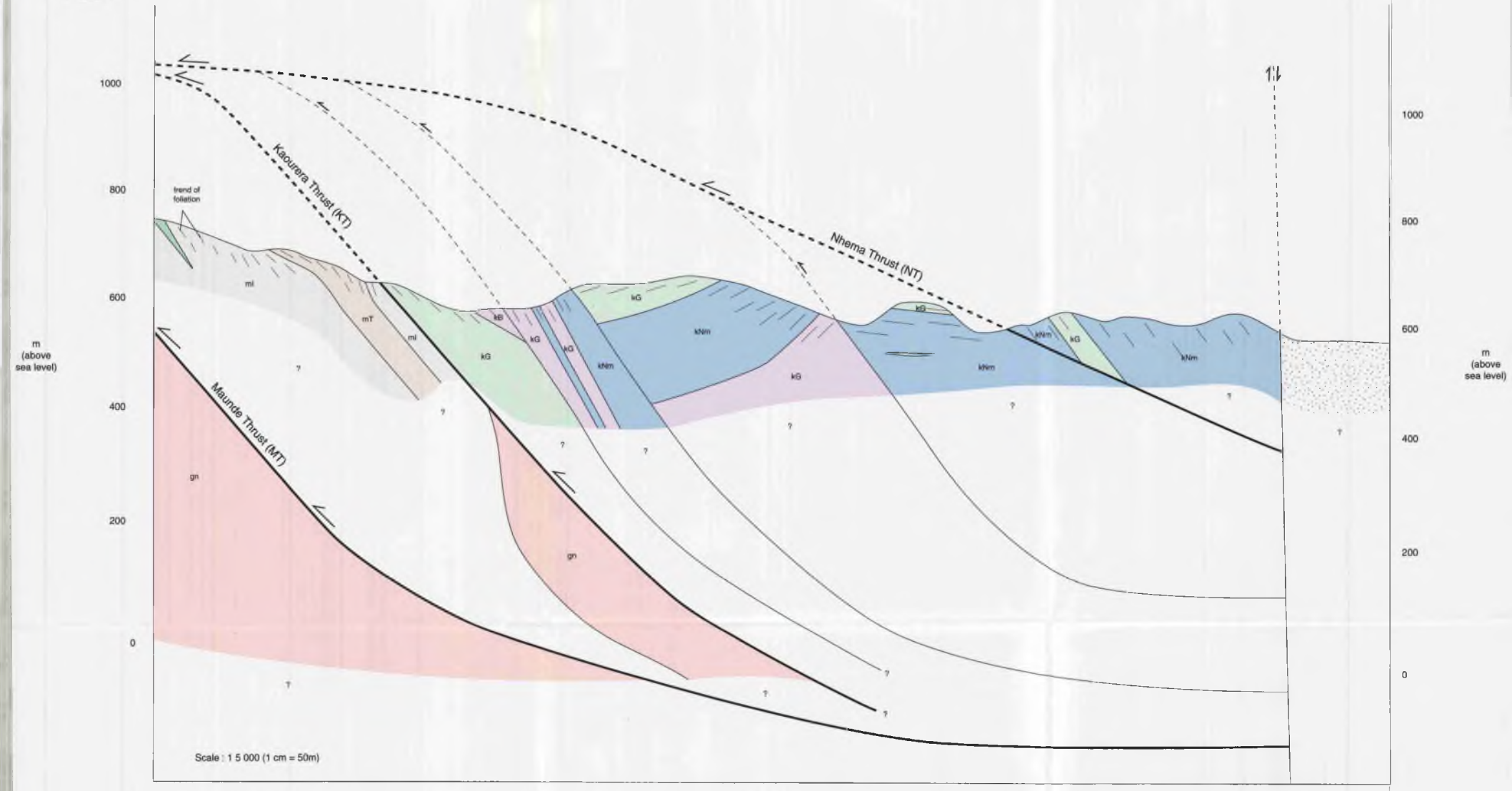

Map 3a. 1 : 5 000 scale locality map of the Kadunguri Domain.

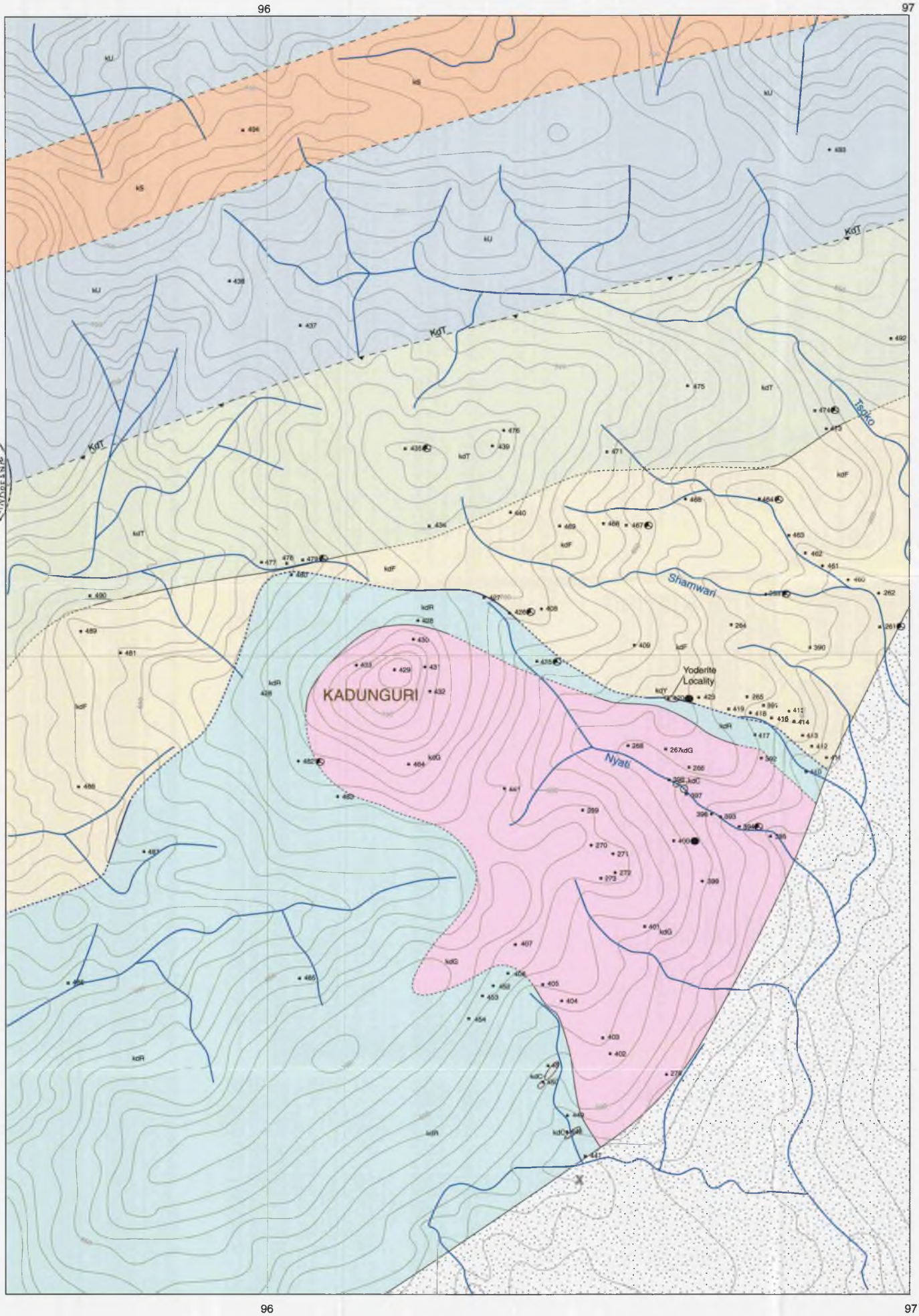

Map 3b. 1 : 5 000 scale structural map of the Kadunguri Domain.

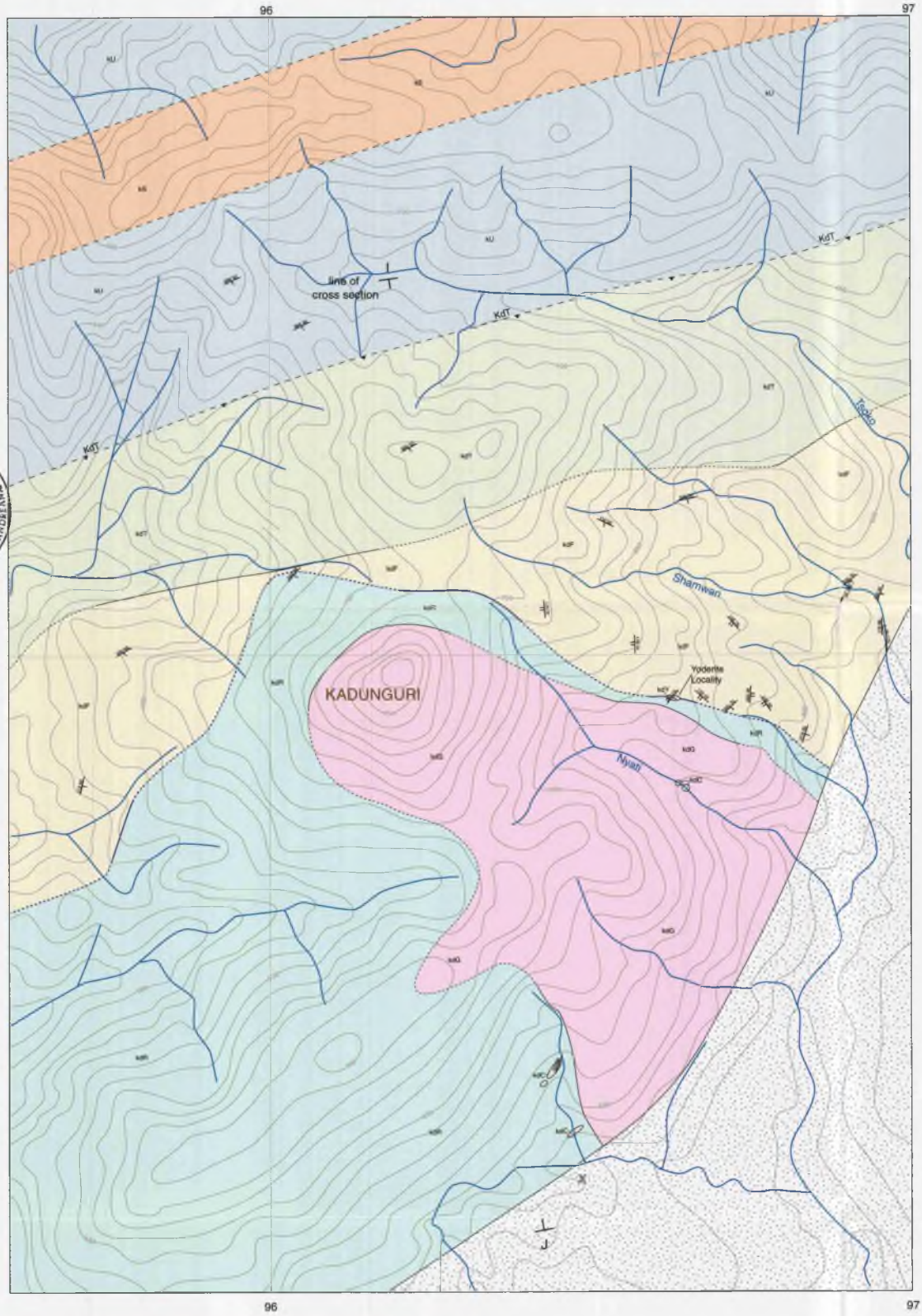

KEY

Geological Units

- Karoo sandstones
- unconformity
- Kadunguri Whiteschists
  - kdT Phlogopite Whiteschist
  - kdF Foliated Quartz Whiteschist
  - kdR Unfoliated Quartz Whiteschist
  - kdY YodentaWhiteschist
  - Quartz - Hematite Sheets
  - kdC Quartz - Diopside Sheets
  - kdG Gedrite Whiteschist
- Kadunguri Thrust (KdT)
- Kasurera Island - Arc Group
  - kS Bhuiri Semi - Pelite Formation
  - kU Undifferentiated Kasurera Island - Arc Group

Geological Symbols

- Geological boundary (known)
- Geological Boundary (inferred)
- Thrust (known)
- Thrust (inferred)
- Karoo normal fault (known)
- Karoo normal fault (inferred)
- Orientation of S2 foliation.
- Trend and plunge of L2 extension lineation.
- Orientation of Foran cleavage

0 m 200

Scale = 1 : 5 000. (1 cm = 50 m).

Cross section illustrating the structure of the Kadunguri Domain